An X-Ray and Neutron Diffraction Investigation into Engineering Hydrogen Bonding Interactions in Molecular Complexes

András Arnold Kállay

Doctor of Philosophy Degree in Chemistry

School of Chemistry
University of Glasgow

Declaration

This thesis has been written in accordance with the University of Glasgow regulations and all work presented here is original and performed by the author unless otherwise stated and referenced in the text.

András Arnold Kállay, October 2011

Abstract

The main focus of this research was to examine the molecular complexes formed by the proton sponge material DMAN [1,8-bis(dimethylamino)naphthalene]. It is well known that DMAN will readily protonate – forming the $DMANH^+$ – leaving the second molecule in a DMAN complex negatively charged. In addition to the preparation of materials by crystallisation techniques, full characterisation was carried out using X-ray diffraction of the single crystal samples obtained. Neutron diffraction was also carried out on some of the samples for which the hydrogen atom information was most important to obtain, though this was restricted by the amount of beamtime available on the central facilities used.

Several families of DMAN complexes were studied, including DMAN : benzoic acid (chapter 4), DMAN with a wide series of halo-substituted benzoic acids (Chapter 4), DMAN with hydroxyl-, nitro- and methyl- substituted benzoic acids (Chapter 5), and its complexes with a selection of other organic acids (Chapter 6). Several general patterns are found in this work, including the following:

- The DMAN is usually protonated ($DMANH^+$), with the hydrogen atom held in a short N–H···N intramolecular hydrogen bond, as observed previously;
- The carboxylic acids tend to form dimers, but with a carboxyl and a deprotonated carboxylate group involved, these $DIMER^-$ units are formed through a single, very short, strong, charge-assisted O–H···O hydrogen bond;
- a wide range of C–H···O and C–H···π weaker hydrogen bonds are present, together with consistent stacking of the DMAN rings, including π···π interactions, but with additional stacking at a range of interplanar distances;
- the overall packing in several complexes includes chains or sheets of $DIMER^-$ units with $DMANH^+$ included in pockets in the structure.

There are some exceptions to these patterns, for example

- varying stoichiometry, resulting in the first example of the occurrence of both protonated ($DMANH^+$) and unprotonated DMAN in a single complex
- the inclusion of solvent water in some hydrated complex, which interrupts some of the patterns of intermolecular interactions

In addition to the studies of DMAN, a ternary hydrogen bonded complex was studied using X-ray and neutron diffraction and the new molecular porous material 4-phenoxyphenol, containing a range of solvents, was fully characterised using these diffraction techniques as well as the thermal methods TGA and DSC.

Acknowledgments

I would firstly like to thank my supervisor Professor Chick Wilson for giving me the opportunity to work in his group and for his guidance and encouragement throughout my PhD. I will be always grateful for his support during this project and for his unique enthusiasm which has always been highly motivating.

I also would like to say thank you to Lynne for her help and patience over the years of this work. Her help and patience guided me through the wonders of crystallography and I will be always thankful for this.

I cannot be more thankful to Professor Luminița Silaghi-Dumitrescu and Professor Majdik Cornelia who persuaded me to undertake work in science, without their guiding hands it would be unlikely that I would have submitted a PhD thesis.

Thanks also goes to the present and past members of chicklets for all the fun and entertainment over these years spent in the group from the Friday wine through to Chick's gardening parties and long nights of the conferences.

I would like to thank my friends for all the support and encouragement they have given me through every part of my life. In particular, I would like to thank Lóri and Oli who's encouragement inspired me to pursue a scientific career which played an undeniable part in my PhD.

Last but not least thank you to Réka for her patience and support, especially coping with me during my write up.

TABLE OF CONTENTS

List of figures

List of tables

List of abreviations

23DOHBA	2,3-dihydroxybenzoic acid
24DOHBA	2,4-dihydroxybenzoic acid
26DOHBA	2,6-dihydroxybenzoic acid
2BBA	2-bromobenzoic acid
2CBA	2-chlorobenzoic acid
2FBA	2-fluorobenzoic acid
2IBA	2-iodobenzoic acid
35DNBA	3,5-dinitrobenzoic acid
3BBA	3-bromobenzoic acid
3CBA	3-chlorobenzoic acid
3FBA	3-fluorobenzoic acid
3IBA	3-iodobenzoic acid
3NBA	3-nitrobenzoic acid
3OHBA	3-hydroxybenzoic acid
3TOLA	3-toluic acid
4BBA	4-bromobenzoic acid
4CBA	4-chlorobenzoic acid
4DABA	4-(dimethylamino)benzoic acid
4FBA	4-fluorobenzoic acid
4IBA	4-iodobenzoic acid
4OHBA	4-hydroxybenzoic acid
4TOLA	4-toluic acid
BA	benzoic acid
BIPY	4,4'-bipyridyl
BrA	bromanilic acid
CA	chloranilic acid
DMAN	N,N,N′,N′-tetramethyl-1,8-naphthalenediamine
OA	oxalic acid

Chapter 1

1. Crystal engineering

1.1 Introduction

Understanding intermolecular hydrogen bonding is very important for a range of structural and functional reasons. Structurally, hydrogen bonds are among the most important types of intermolecular interactions, playing a role in defining the structure of a wide range of materials. These interactions play an essential role in forming anisotropic interactions in condensed systems, which in addition to their structural implications, have an effect on the function of many materials. For example, hydrogen transfer through hydrogen bonds between the molecules enables energy and charge transfer in solid chemical and biological systems[1], with widespread implications for issues as diverse as ferroelectrics, electrochemical processes and enzyme action. Many recent investigations have been carried out aimed at understanding the variation of hydrogen-bonded structures in the solid state by changing external variables such as temperature and pressure[2-7].

The aims of this work include elements of both of these aspects. A particular focus of this work is in examining molecular systems and molecular complexes in which proton transfer or migration is significant and often observed. These effects, often associated with the occurrence of short, strong hydrogen bonds, can often have a significant effect on tuning molecular properties. The presence of potentially dominant hydrogen bond motifs also allows the possibility of a systematic examination of the effects of these hydrogen bonds on the structure and packing of the complexes investigated. Ideally, these systematics may lead to the identification of potentially predictable structural patterns, and the use of crystal engineering in designing further systems containing these patterns.

The principles of crystal engineering are to identify likely intermolecular interactions between molecular components in a crystal structure, through identification and rationalisation of regularly occurring motifs. These motifs are often linked through hydrogen bonds, and if these are sufficiently well understood to allow for their prediction and use in rational design of intermolecular interactions, molecular associations in the solid state (crystal packing) then this is getting towards the ability to engineer crystals. Engineering crystals begins with strong predictable interactions as short strong hydrogen bonds motifs or predictable, strongly directional medium strength hydrogen bond interactions representing the molecular building blocks of the structure. This is then followed by attempting to understand the role of weaker intermolecular interactions, such as weaker hydrogen bonds and halogen-halogen interactions, which, although less directional, often play a very significant role by holding together these building blocks. Through a better understanding of these interactions from strong towards to weaker interactions it might open the possibility towards to the design of well-defined systems with tuneable properties such as melting point, solubility, optical properties, etc, as well as self-assembly structural characteristics such as porosity.

1.2 Hydrogen bonding

"*Without hydrogen bonds, all wooden structures would collapse, cement would crumble, oceans would vaporize, and all living things living things would disintegrate in to inanimate matter*" quoted from George A. Jeffrey[8].

Hydrogen bonding is one of the most important intermolecular interactions. It has been studied extensively over the last 90 years and has no decline in its interest. Hourly, new papers on hydrogen bonds are indexed in SciFinder[9-10]and even these days chemists are redefining its meaning[10].

The IUPAC gold book definition of hydrogen bonding from 1994[11] is:

"*A form of association between an electronegative atom and a hydrogen atom attached to a second, relatively electronegative atom. It is best considered as*

an electrostatic interaction, heightened by the small size of hydrogen, which permits proximity of the interacting dipoles or charges. Both electronegative atoms are usually (but not necessarily) from the first row of the Periodic Table, i.e. N, O or F. Hydrogen bonds may be inter-molecular or intramolecular. With a few exceptions, usually involving fluorine, the associated energies are less than 20-25 kJ mol^{-1} (5-6 kcal mol^{-1})".

However, since the last definition from the IUPAC, further investigations of the nature of the interaction have led to changes in our understanding and use of the term, and the preamble from the most recent proposed definition is:

"*the hydrogen bond is an attractive interaction between a hydrogen atom from a molecule or a molecular fragment X–H in which X is more electronegative than H, and an atom or a group of atoms in the same or different molecule, in which there is evidence of bond formation*"[12].

To cover comprehensively all aspects of the matter is quite challenging and given the limited space, here will be covered only those aspects related to the work presented, including a few examples for each related research area.

Hydrogen bonding is a donor(D) - acceptor(A) interaction specifically involving hydrogen atoms. They are formed when the electronegativity of D relative to H in a D—H covalent bond is such as to withdraw electrons and leave the proton partially unshielded. To interact with this donor D—H bond, the acceptor A must have a lone-pair of electrons or polarisable π electrons. Very strong hydrogen bonds can resemble covalent bonds in directionality and strength, while the very weak hydrogen bonds are closer in nature to van der Waals forces. The majority of hydrogen bonds are between these extremes[8].

Hydrogen bonds are normally classified into three groups. Strong hydrogen bonds have an energy between 15-40 kcal/mol and a bond length (D···A) between 2.2-2.5 Å. Moderate hydrogen bonds have an energy between 4-15 kcal/mol and their bond lengths are between 2.5-3.2 Å. Weak hydrogen bonds have an energy < 4 kcal/mol and their bond lengths are between 3.2 and 4.0 Å[8]. Moderate and weak hydrogen bonds have a stretching and bonding force constant an order of

magnitude less than is found for covalent bonds. Strong hydrogen bonds are often formed in groups in which there is a deficiency of electron density in the donor group or an excess of electron density in the acceptor group, these are sometimes called ionic or charge-assisted hydrogen bonds[13]. Strong hydrogen bonds can also occur when the molecular configuration is such as to force the neutral donor and acceptor groups closer together than in normal hydrogen bonded contact. These are known as forced strong hydrogen bonds. Moderate hydrogen bonds are formed generally by neutral donor and acceptor groups, in which donor atoms are electronegative relative to the hydrogen atoms and the acceptor atoms have a lone-pair of unshared electrons. Weak hydrogen bonds are formed when the hydrogen is bonded covalently to a slightly more electroneutral atom and the acceptor has no lone-pairs but has π electrons.

It is useful here also to provide some additional basic definitions used in describing hydrogen bonds: *intermolecular*, when the donor and the acceptor groups are in different molecules; *intramolecular*, when the donor and the acceptor groups are in the same molecule; *homonuclear*, when the donor and the acceptor are the same; and *heteronuclear* when the donor and the acceptor groups are different. There are many examples in the literature focusing on the determination of accurate hydrogen positions in intramolecular and intermolecular hydrogen bonds and their symmetry or asymmetry in the bonding[14-23].

To define the geometry of a hydrogen bond it is necessary to use three scalar quantities. The D—H covalent bond length, the H····A hydrogen bond length and the D····A hydrogen bond distance. These three quantities can define the D—H····A hydrogen bond angle and only in the strong hydrogen bond is this angle ~180°; for moderate hydrogen bonds, this angle is usually significantly different from linearity. It follows that it is reliable to use the D····A distance as a full description of the hydrogen bond geometry for strong hydrogen bonds. Since many of the systems discussed in this work involve strong hydrogen bonds as an important part of their structure, these will be discussed in more detail here.

1.2.1 Strong hydrogen bonds

Four types of short strong ($2.50 \leq d(D\cdots A) \leq 2.65$ Å) and very strong ($d(D\cdots A) \leq 2.50$ Å) hydrogen bonds are classified in chemical classes, which are known from accurate X-ray and neutron diffraction studies[24-25]:

- double charge assisted hydrogen bond *(±)CAHB* occurs when the donor and acceptor have very similar pKa values as in the case of the complex formed between pyridine-*N*-oxide (p*K*a = 0.79) and trichloroacetic acid (p*K*a = 0.66)[26].

- negative charge-assisted hydrogen bond *(–)CAHB*, of which examples can be found between the acid complexes of organic or inorganic acids as hydrogen-difluoride[27].

- positive charge assisted hydrogen bond *(+)CAHB*, which occurs usually when a proton is donated by an acid and two molecules are bridged together as in the complex of hydrogen–bis(dimethyl-sulphoxide)[28].

- resonance assisted hydrogen bond *RAHB*, where there is no charge transfer between the donor and acceptor but there is an increased resonance in the energy. Good examples of systems showing RAHB are carboxylic acid dimers and ß-diketo enols[29].

In the most general semi empirical model the energy of the hydrogen bond, E_{HB} is the sum of three terms, $E_{HB} = E_{COV} + E_{EL} + E_{REP}$. E_{COV} is the covalent energy term, E_{EL} is the electrostatic attraction term and E_{REP} is the repulsion energy term.

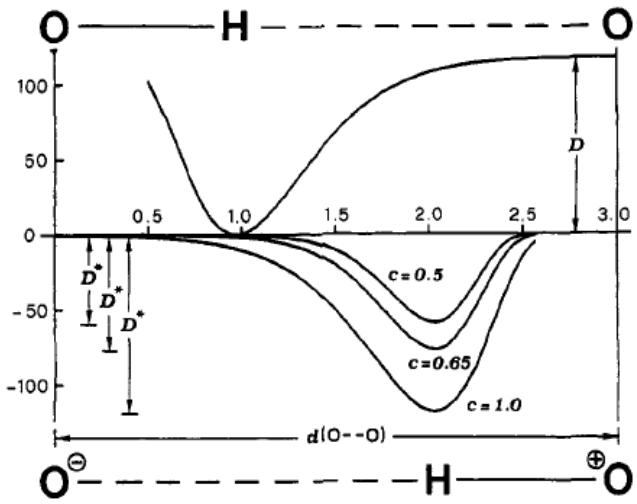

Figure 1-1. The form I (upper curve) and form II (lower curve) of O-H and H-O$^+$ bond with bond dissociation energies D and D - cD, respectively[24]. The plot is of potential energy V(r) against bond distance, r.*

Using the definition of the O—H "covalent" bond dissociation energy D, and the dissociation energy of the "non-covalent" H—O$^+$ bond D* where the H atom has been transferred from the donor to the acceptor atom. This dissociation energy is lower than D caused by the destabilization induced by the positive charge, and it can be written that D* = cD (*Figure 1-1*). The empirical parameter c takes a value between 0 and 1. For a relatively weak hydrogen bond in water, c = 0.65, which is increased to 1 in the case of the strongest hydrogen bond. The value of c strongly affects the calculated value of E_{COV} (*Figure 1-2*). This figure shows E_{EL} and E_{REP} as a function of the d(O····O) distance.

A hypothesis that has been proposed to allow for estimating the strength of hydrogen bonding is the use of proton affinity PA, or pK_a matching. It has been introduced as a relatively inexpensive way for the determination of the hydrogen bond strength. The pK_a matching principle states that the strength of a hydrogen bond increases with decreasing ΔpK_a = pK_a(donor) − pK_a(acceptor) with a maximum at ΔpK_a = 0. One major drawback with this simple method is that since the pK_a is measured in the gas phase or solution, when hydrogen bonds are studied in the solid state there are many other interactions involved as well, but it can be used as an approximate and quick evaluation of these bonds[30].

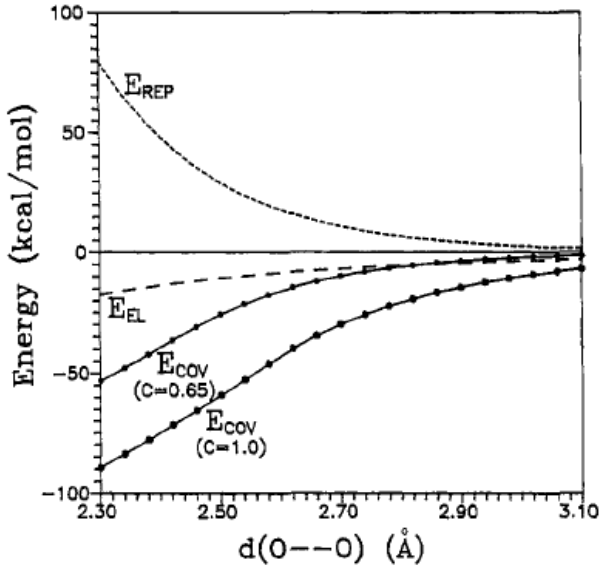

Figure 1-2. Energy components of the linear O—H····O hydrogen bond, calculated as a function of O····O distance. The E_{COV} is calculated for two different values of c, an empirical parameter related to the different dissociation energies of the two O–H interactions in the hydrogen bond[24].

1.2.2 Moderate hydrogen bonds

While amongst the studies of hydrogen bonds it is well agreed that hydrogen bonds with a length less than 2.5-2.55 Å (O–H···O; ~2.55-2.6 Å (N–H···N) are SSHBs, the border between strong and moderate hydrogen bond is not as clear. As has been described the length of moderate (or medium strength) hydrogen bonds are between ~2.5 Å and 3.2 Å, their energy is between 4-15 kcal/mol and their bonding angles range from 180° to 140° defined by Jeffrey[8]. These bonds form usually between a neutral donor to which the hydrogen atom is closely located with a well-defined potential energy surface and neutral atoms containing lone pairs of electrons, with some exceptions such as $O{=}C^-$ or NH_4^+. Most common examples involve nitrogen or oxygen as donor and acceptor atoms and these bonds often can have influence or determine the final packing of the structure and are particularly important in both small and macro-molecules of biological systems. However, since this definition has been described and discussed in more detail, there has been much debate around the definition of a moderate strength hydrogen bond both by their energy and their bond length.

Some of the latest definitions set different bond length limit restrictions between different types of hydrogen bonds depending on the hydrogen bond description. The moderate type of hydrogen bond has been described as an electrostatic interaction which becomes, with the shortening of the bond, more covalent in nature[25, 31-32]. It also has been described as an electrostatic interaction with a continuous variuation, becoming more covalent in nature with shortening of the bond length, and going towards to van der Waals nature with increasing bond length[10, 33], although there no clear definition on their length and energy has been agreed.

As there is no well defined border of the moderate hydrogen bonds, these have been defined in varying ways in their minimum and maximum length and energies involved in the hydrogen bonding. In this work, hydrogen bonds involving nitrogen and oxygen atoms as donor or acceptor, with lengths between 2.5 Å and 3.0 Å will be referred to as moderate hydrogen bonds.

1.2.3 Weak hydrogen bonds

If the moderate hydrogen bond were not clearly classified in their length or their strength, in the case of the weak hydrogen bonds this definition is even more ill-defined across the scientific community. Weak hydrogen bonds have been defined by Jeffrey to have energies up to ~4 kcal/mol and D···A bond lengths between 3.2 and 4.0 Å[8]. However, as in the case of moderate hydrogen bonds there is no clear definition on their bond length or strength. Over the past decades the nature of the weak hydrogen bond has been extensively studied, and have been defined as hydrogen bonds formed between two structural moieties when one or both of them are of moderate to low electronegativity[25, 33-36]. Examples can include bonds between weak donor and strong acceptor (C–H···O, C–H···N, etc.), strong donor and weak acceptor (O–H···π, N–H···π, etc.) and weak donor and weak acceptor (C–H···F, C–H···π, etc.). Problem occurs with the definition of an interaction as a weak hydrogen bond as opposed to van der Waals interactions, with the increase of the bond length. There have been many investigations over the years to overcome this problem, however, the electrostatic interactions do not have an arbitrary threshold limit, to become a

purely van der Waals interactions[10, 25, 34]. Therefore the C–H···O, C–H···π interactions, repeatedly occurring in the discussion the structures in this work, will be referred to as weak hydrogen bonds when their lengths are within sum of the van der Waals radii if the donor and acceptor atoms.

1.3 Hydrogen disorder

Hydrogen disorder is an unusual behaviour of the hydrogen atom in a linear strong hydrogen bond, where the hydrogen atom can show a positional disorder across the bond. This effect is often seen in the pair of O–H···O bonds linking dimers of carboxylic acids, and can be identified in refinements that include only a single H atom position by its typical appearance with a very elongated anisotropic displacement parameter[24,37].

The commonly used method to study behaviour of hydrogen atoms in crystal structures is by the visualisation of the bond through difference Fourier maps[38-39]. Fourier maps are a visual representation of the electron density in a chosen plane of the structure (see Chapter 2). The difference Fourier map is a representation in the difference of the electron density map between the electron density maps calculated from the observed structure factors and that from the generated structure factors. In order to visualise the electron density of the hydrogen atom, this atom is previously removed from the list of atoms used to generate the map of the calculated electron density of the structure (*Figure 1-3*). The method is the same for neutron diffraction except the visualised map is a representation of the nuclear density rather than the electron density.

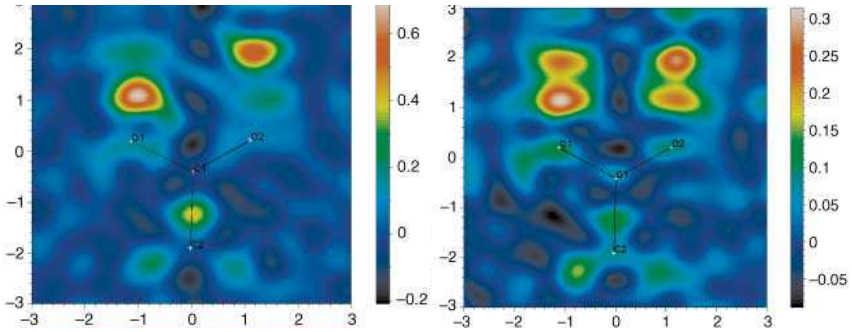

Figure 1-3. The difference Fourier maps of the electron density in the structure of 2,4,6-trimethylbenzoic acid, calculated in the plane of the hydrogen bonds between the carboxylic acid dimers with the hydrogen removed from the calculated map. The map at 100K (left) shows a single well defined electron density peak, while at 290K (right) there is a clear split electron density of the hydrogen atom across two positions[38].

One of the first examples in which the temperature dependent hydrogen disorder was studied is in the structure of fluoro-malonic acid, where the electron density difference synthesis showed a split electron density of the hydrogen atom at ambient temperature while by cooling down the sample the split tendency disappears[40]. The determination of the crystal structure was carried out by single crystal X-ray diffraction experiment, hence it cannot give a full definition of the hydrogen disorder due to the limitations of the method for determining hydrogen positions[41]. The occupancies of the two sites of the hydrogen atom can be refined using X-ray data but for a clear determination of the disordered hydrogen atom within such a hydrogen bond, a neutron diffraction experiment is normally required.

In some cases when using X-ray data alone, the difference Fourier maps do not show the hydrogen atom position due to the low completeness of the data set, as found in the case of the 5,5'-dibromo-3-dimethylaminomethyl-2,2'-biphenol N-oxide[42]. In this case FT-IR spectroscopy measurements were used to complement the diffraction measurements. In this structure there is a very strong intramolecular O–H···O hydrogen bond between the hydroxyl group and the N-oxide, but the hydrogen atom electron density could not be located from the X-ray measurement. A broad peak appears in the FT-IR spectra at around

2000 cm^{-1}. The results are compared with previous NMR and IR spectroscopic measurements in solution[43], and a fast fluctuation of the proton in the hydrogen bond suggested by the authors. While these methods are good to complement the diffraction data, they are still ambiguous when it comes to determining accurate hydrogen positions.

The unambiguously determined hydrogen positions using a multiple temperature neutron diffraction experiment on the crystal structure of benzoic acid is a good example of determining accurately intermolecular hydrogen bonding and the effect of temperature on the disorder of the hydrogen position within this[44]. The structure has been investigated with variable temperature X-ray and neutron diffraction methods at 20, 50, 100 and 175 K. The disorder of the hydrogen can be clearly seen from the anisotropic thermal displacement parameters in a model with a single H position, and this position can be well modelled across two sites (*Figure 1-4*). The O···O distance of the O–H···O hydrogen bond is 2.629 Å at a temperature of 175 K.

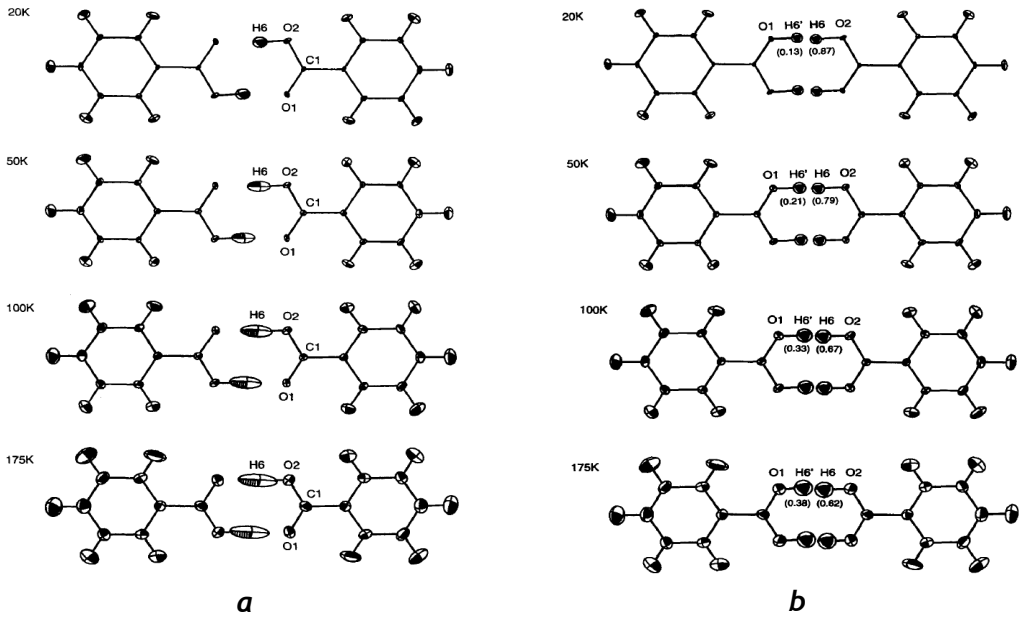

Figure 1-4. The likely presence of disorder of hydrogen atoms in the carboxylic acid dimer in benzoic acid indicated by increasingly elongated anisotropic thermal vibration ellipsoids a, and the disorder modelled with the two possible site occupancy of hydrogen atom position, b[44].

The hydrogen atom, when refined with a single site, shows an anomalous very elongated thermal vibration across the hydrogen bond, which is modelled as a disorder between two refined positions. The occupancy ratio between the two positions increases as a function of temperature from ~87:13% at the lowest temperature to ~62:38% at 175 K. This effect has been studied later by other methods, investigating the potential energy surface of the disordered hydrogen bond. The representation of these hydrogen bonds in terms of simple potential surfaces is well used and a sensible approach in such systems[45-46]. When the energy surface potential shows a flat bottomed surface the hydrogen atom has the same energy when it occupies any of the positions, and can be envisaged either oscillating across the single broad potential well or having an essentially continuous static disorder across the well, while in the other two cases where the two wells are separated by an energy barrier between them, the hydrogen atoms can be statically disordered between the two positions with the two wells having the same (isoenergetic double-well) or different (double-well) energy minimum (*Figure 1-5*).

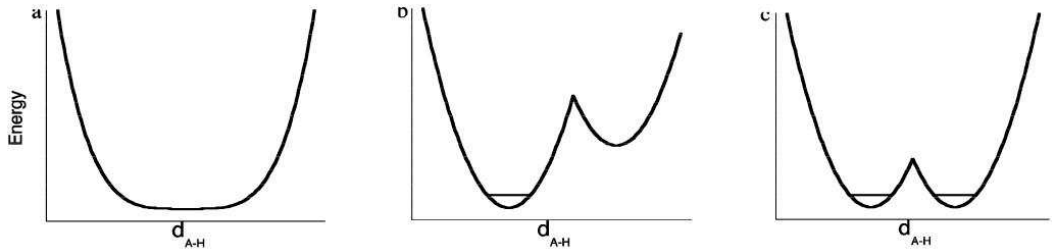

Figure 1-5. The hydrogen energy potential surface within the hydrogen bond with a broad single well potential (left), double well (centre) and isoenergetic double well (right)[46].

Quasi-elastic neutron scattering, NMR and NMR relaxometry[47-49] studies have shown that while in the structures measured above 20 K the proton correlation rate between the two minima of the potential energy surface is dominated by thermally activated processes, below this temperature the proton motion is determined by one-phonon transition between the energy levels. Since the first proton disorder were found and investigated in this detailed manner, there are other examples of research focusing on the understanding of the hydrogen disorder in short strong hydrogen bonds in intermolecular[38] and

intramolecular[50,51] situations using variable temperature measurements and computational methods[52,53]. However, a full understanding and the ability to predict such behaviour has not yet been attained.

1.4 Hydrogen migration

Hydrogen migration, also referred to as proton migration, is an expression sometimes used with different meaning by researchers working in different fields of chemistry. The expression used in the work herein describes the hydrogen atom's subtle positional movement across an inter- or intramolecular hydrogen bond with a change of an external condition such as temperature or pressure.

The first example where tuned proton migration in a hydrogen bond is referred to explicitly appears in the molecular complex of pentachlorophenol and 4-methylpyridine[54].

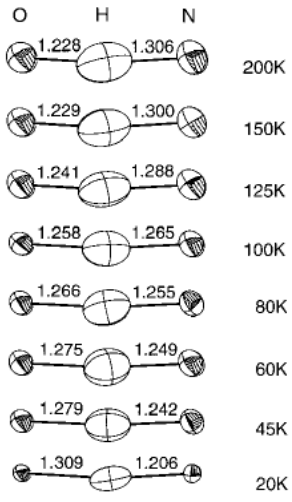

Figure 1-6. The hydrogen bond in 4-methylpyridine : pentachlorophenol as observed by neutron diffraction at eight different temperatures; displacement ellipsoids are drawn at the 50% probability level. The equidistant (centred) H atom position occurs at around 90 K[54].

The structure was studied first by X-ray diffraction at room temperature and at 80 K. At the two different temperatures the position of the hydrogen within the hydrogen bond has a different position. To investigate this further, variable temperature neutron diffraction data were collected on the complex at 8 temperatures between 20 and 200 K (*Figure 1-6*). The hydrogen atom position in the O-H-N hydrogen bond at lower temperature is located closer to the nitrogen atom, but with the increase of temperature this atom migrates towards the oxygen atom. The research does not define fully whether the change is in the hydrogen potential surface itself or the thermal population of the constant unsymmetrical hydrogen-bond potential but the small vibration of the hydrogen atom along the hydrogen bond suggests a potential with a well-defined single minimum.

A variable temperature X-ray study has been used to compare two molecular complexes of N,N,N',N'-Tetramethyl-1,8-naphthalenediamine (dimethylamino-naphthalene; DMAN) with 4,5-dichlorophthalic acid (dCPA) and 3,4-furandicarboxylic acid (FdCA)[39]. In this case there is proton transfer into the "proton sponge" material DMAN (see below); DMAN is thus protonated ($DMANH^+$) and the carboxylic acids deprotonated ($dCPA^-$, $FdCA^-$). Both complexes have an $[O{-}H{\cdots}O]^-$ and an $[N{-}H{\cdots}N]^+$ intramolecular hydrogen bond in their structure, but while in the structure of $DMANH^+.dCPA^-$ the intramolecular hydrogen bond of the $DMANH^+$ has shown a proton migration within the $[N{-}H{\cdots}N]^+$ as a function of temperature, in the complex of $DMANH^+.FdCA^-$ this behaviour was not present. Two possible explanations have been developed to explain the unusual behaviour of the hydrogen atom. The first explanation involves the changing of the potential surface with temperature, where with the increase of the temperature the double well hydrogen bond energy barrier decreases to produce a broad single well but this would not explain why the other structure does not show any change in the same hydrogen bond. The second explains it with the evolution of the local environment as, while the expansion of the cells is approximately linear, the local contact distance lengthenings are different as the temperature changes. This affects the intermolecular interaction of the nitrogen atoms on the naphthalene and as a consequence it will affect the hydrogen bond within the $DMANH^+$ and makes possible the observed behaviour of the hydrogen atom.

Another piece of research in this area shows temperature dependent proton migration in the complex of urea-phosphoric acid (UPA)[55]. In this case the variable temperature X-ray diffraction data has been compared with neutron diffraction data collected in an earlier study of the same system[56]. In the very short intermolecular O–H···O hydrogen bridge in UPA at lower temperature the hydrogen atom is closer to the urea and with the increase of the temperature this atom becomes more centred in the hydrogen bond. In this work it has been also pointed out that the migration is much more pronounced from the X-ray data (~0.1 Å) than from the neutron data (~0.04 Å) (*Figure 1-7)* due to the asphericity effect in the bonding, but none the less this example illustrated the use of X-diffraction measurements for qualitative examination of such proton behaviour.

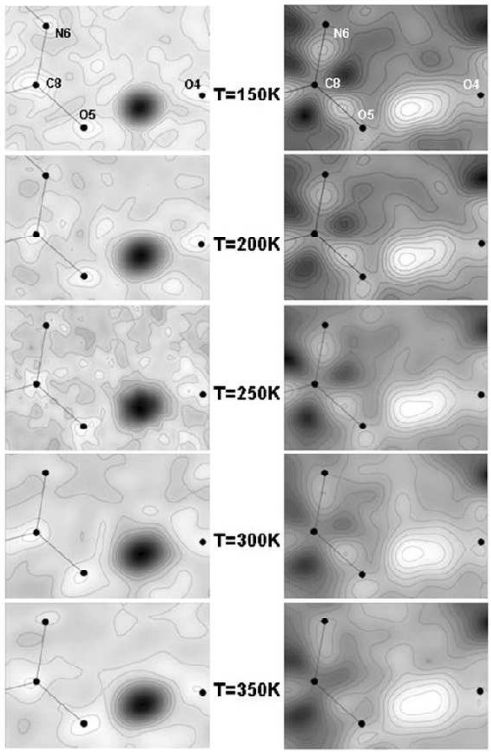

Figure 1-7. Difference Fourier maps (Fo–Fc) obtained at temperatures of 150, 200, 250, 300 and 350 K from both neutron (left) and X-ray (right) diffraction data. The maps were calculated in the plane of the hydrogen bond through atoms C8, O4 and O5, with contours plotted at consistent intervals throughout the neutron and X-ray maps. Note that hydrogen peaks are negative in neutron diffraction. The atoms are labelled on the 150 K map[55].

Temperature dependent proton migration has also been identified in very short N–H···O hydrogen bonds[57], studied by a deuterated sample, where a significant increase in the migration of the hydrogen atom across the bond has been observed[58]. High pressure X-ray[59] and neutron[60] diffraction experiments have been carried out on the crystal structure of oxalic acid dihydrate complemented with DFT calculations. Migration of the hydrogen from the hydroxyl group to the water molecule has been observed, in good agreement with the calculations, and it has been suggested that similar behaviour could appear in other hydrogen bonded systems containing functional groups such as carboxylic acid groups.

The examples quoted here show that there is strong evidence of proton mobility in hydrogen bonds in crystal structures, but that this has not been widely studied yet and there are still many questions unanswered. One aim of this work is that by engineering of such complexes with very short hydrogen bonds and studying them by variable temperature diffraction could lead to a deeper understanding in the matter.

1.5 Hydrogen transfer

Hydrogen transfer plays important role in many areas of structural chemistry, from small molecules where the transfer often creates building blocks[61-62] of structures, to proteins[63], where hydrogen transfer can drive changes in the structure of the protein itself. It is a more widely studied behaviour of the hydrogen atom in molecular complexes compared to migration or disorder. When an organic base is co-crystallised with an organic acid as illustrated in Equation 1.1 the hydrogen is often transferred from the acid to the base molecule and an organic salt is formed. The complexes with proton transfer occurring in a particular crystal structure are correctly called “salts” and those complexes where there is no proton transfer in the structure are often called “co-crystals”; both types of material are more often called molecular complexes, which is the nomenclature used here. While some researchers use extensively these denominations as a differentiation between these structures[64-65] there is debate and inconsistency in use of the terms. In the work herein these expressions will

not be used as differentiation between the proton "transferred" and "not transferred" structures.

Equation 1.1 $$A-H+B \xrightarrow{co-crystallisation} A^{-}\cdots H-B^{+}$$

To predict the outcome of the crystallisation of a two compoment system such as that illustrated is very difficult even when using well-known functional groups, well-known supramolecular synthons, and controlling the environment and location of the other functionalities[66-68]. Sometimes the inclusion of a slightly different substituent can change the whole solid phase by altering the proton transfer characteristics. Using benzoic acid and substituted 2-aminopyrimidines, for example, led to different hydrogen behaviour in the two complexes 2-amino-4-methyl-6-phenylpyrimidine : benzoic acid (complex 1) and 2-amino-4,6-dimethylpyrimidine : benzoic acid (complex 2)[13]. In the asymmetric unit of complex 1 a proton transfers from the benzoic acid carboxyl group to the nitrogen atom of 2-amino-4-methyl-6-phenylpyrimidine which causes changes in the charge of the pyrimidine molecule and therefore prevents the self dimerisation motif that appears in complex 2. Extensive research has been done on complexes of derivatives of cyanophenols and nitrophenols (hydrogen bond donors) with substituted pyridines (hydrogen bond acceptors)[69]. In this work, 22 different crystal structures are presented and compared to determine the relationship between the proton transfer occurring in the structure and the pK_a values of the starting materials. Structures with a pK_a difference in their components equal or greater then 2.95 have been found to have proton transfer in their complex while the structures with a lower difference have no proton transfer in their complexes. The same results have been found in the structure of 4,4'-bipyridine (bipy) and 1,4,5,6-tetrahydro-5,6-dioxo-2,3-pyrazinedi-carbonitrile (H2tdpd) [70]. In this case a proton is transferred from the H2tdpd to the bipy creating a negatively charged $Htdpd^{-}$ and a positively charged $bipyH^{+}$. The two molecules are assembled through strong intermolecular hydrogen bonding between the hydrogen atom of the $Htdpd^{-}$ and the nitrogen atom of the $bipyH^{+}$ on one side and a bifurcated hydrogen bond between the $bipyH^{+}$ hydrogen atom and the two oxygen atoms of the $Htdpd^{-}$ on the other, assembled into a

layer (*Figure 1-8*). The proton transfer is explained by the difference between the pK_a values of the assembling molecules (H2tdpd: pK_a ~ 3.84; bipy: pK_a ~ 7.05). However, as noted above, using pK_a differences to explain proton transfer in the solid state can give guidance but do not always offer a definitive explanation.

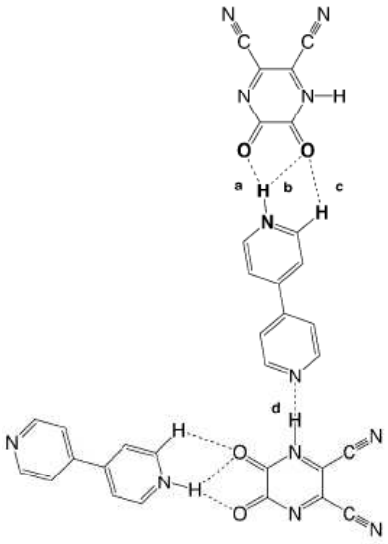

Figure 1-8. The hydrogen bonding scheme between the 4,4'-bipyridine (bipy) and 1,4,5,6-tetrahydro-5,6-dioxo-2,3-pyrazinedicarbonitrile (H2tdpd)[70].

In further work examining the possibility of using pK_a matching in predicting proton transfer, a series of pentachlorophenol (PCP) complexes with dimethylpyridines (lutidines) have been investigated[71]. The pK_a rule outlined above was found to predict the hydrogen transfer in the complexes of 1:1 stoichiometric ratio, but the situation in the 2:1 PCP:lutidine complexes is different. One hydrogen is transferred from the PCP to the lutidine but the pentachlorophenolate ion is stabilised by strong hydrogen bonding either directly or through a water molecule to the second PCP , and the pK_a rule has not been found to be fully applicable (*Figure 1-9*).

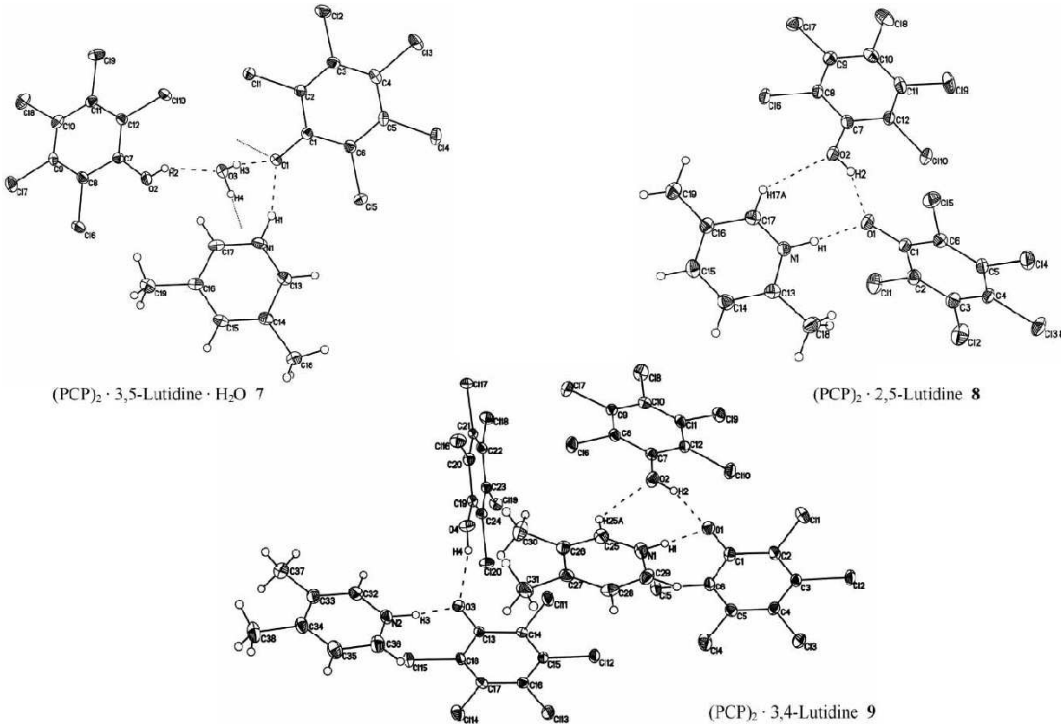

Figure 1-9. Hydrogen bonding between the PCP : lutidine molecules in the (2:1) complexes[71].

Hydrogen transfer sometimes produces interesting behaviour of molecules in molecular complexes. One example can be found in complexes of maleic acid. The structure of maleic acid itself contains an intermolecular and an intramolecular hydrogen bond[72]. The co-crystallisation of maleic acid with (*E*)-2(1*H*)-6-methyl-pyridiniminium (MP) results in a molecular complex of 2:1 ratio, where a hydrogen is transferred from the carboxyl group of the maleic acid to the nitrogen of the MP[73].

While the unprotonated maleic acid keeps the original planar conformation and its intramolecular hydrogen bond, in the other maleic acid the intramolecular hydrogen bond breaks up and bonds to the carboxylate group of the unprotonated maleic acid (*Figure 1-10*). In an attempt at generalising this finding, the authors also note that when a monoacid base (B) is co-crystallised with a dibasic acid (H_2A) this may result in the formation of B_2A, BHA, BH_3A_2 or $B_2H_4A_3$ molecular complexes. While the B_2A and BHA complexes are very common, the formation of other forms is not common, and in the cases they are formed this appears to be serendipitous rather than predictable.

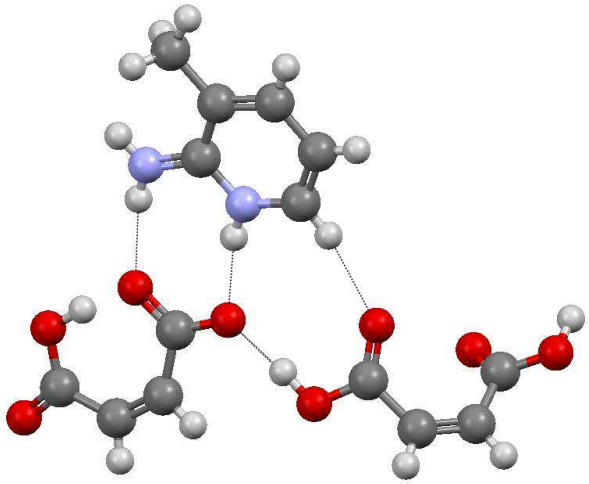

Figure 1-10. The hydrogen bonding between maleic acid, hydrogen maleate and (E)-2(1H)-6-methyl-pyridiniminium in the 2:1 molecular complex, showing the maleic acid with no intramolecular hydrogen bonding (right), and the maleate with intramolecular hydrogen bond (left) [73].

Temperature dependent hydrogen transfer in the structure of the chloranilic acid : 1,2-diazine molecular complex has been studied by NMR combined with NQR. A significant change is found in the spectrum as the hydrogen is transferred from the chloranilic acid to the 1,2-diazine[74]. Later research has confirmed the hydrogen transfer in this complex by dielectric response and IR absorption spectrum[75].

1.6 Halogen interactions

Non hydrogen-bonded intermolecular interactions such as halogen bonding interactions can also play an important role in the formation of a crystal structure. These non-covalent interactions are not just the next important interaction after the hydrogen bond but can be an important tool in the assembly of the supramolecular synthon and have a significant role even in the presence of very strong hydrogen bonds in crystal structures[76]. One of the earliest descriptions of the diversity and importance of the halogen interactions in the solid state interactions is from 1968, describing the halogen atoms

involved in intermolecular interactions as playing the role both of an electron donor and of an electron acceptor in halogen-halogen interactions[77]. Since then there have been many examples of studies focusing on halogen interactions, trying to determine their nature and role in crystal structures, both by comparison of the experimental studies of structures found in the CSD research[78] and through theoretical calculations[79].

As this project has mostly focused on the halogen-halogen type interactions, those will be discussed in greater detail. An extensive CSD[80] search shows that the halogen-halogen interactions may be represented as specific attractive forces between the halogens, by comparing the ratio of X···X to X···C and X···H contacts. By comparing the number of halogen-halogen contacts to the number of halogen-hydrogen contacts the attractive nature of the halogen-halogen interaction has been concluded, through knowing the $\delta^{-}\cdots\delta^{+}$ nature of halogen-hydrogen contacts. In general, the number of Cl···Cl and Cl···H contacts are nearly similar, while as the polarizability of the halogen increases (Cl<Br<I) the number of halogen-halogen contacts increases compared to the number of halogen-hydrogen contacts present. While this conclusion stands in the case of the Cl, Br and I atoms, the case of F····F interactions is different. Due to the strongly dipolar character of the F····H interaction this appears in a significantly greater number, suggesting the conclusion that the F···F interaction has no additional stabilising role in close packing. These attractive forces have been studied by natural bond order calculations analysis[79] on the CF_3X molecule, where X represents F, Cl, Br or I. The calculations showed that in the case of X= Cl, Br or I, the molecules have an approximate $s^2 p_x^2 p_y^2 p_z^1$ configuration, where the three unshared electrons produce a ring of negative electrostatic potential around the central part of the halogen and a positive potential on the outermost part of the halogen along the R-X bond called "σ-hole"(*Figure 1-11*). In the case where X=F, the combination of the fluorine atom's high electronegativity and the *sp* hybridization neutralizes this effect and hence the σ-hole is not present in the case of this molecule.

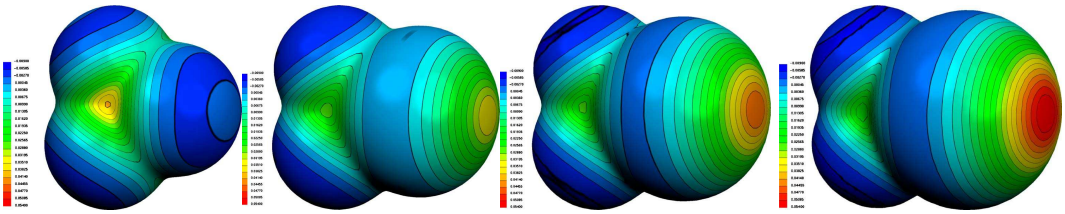

Figure 1-11. The molecular electrostatic potential of CF_3X where X represents, from left to right, F, Cl, Br and I[79].

The halogen-halogen bonds are also classified by the two C-X····X angles in the C–X····X–C unit and can be split into two classes: type I, $\theta_1 = \theta_2$; type II, $\theta_1 \approx 180^\circ$ and $\theta_2 \approx 90^\circ$ (*Figure 1-12*)[81].

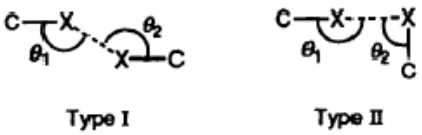

Figure 1-12. The two types of halogen-halogen interactions classified by their θ angles[81].

The possibility of separation of these two classes of halogen-halogen interactions was indicated by the analysis of these two fragment types from CSD results[81]. There is evidence of clustering, but while type I and type II are well demarcated for I····I, this separation is more unclear in Br····Br and there is no gap evident for Cl····Cl. A new type of contact, the quasi-type I, was introduced to bridge the gap between the type I and type II contacts; in this class, $|\theta_1 - \theta_2| < 20^\circ$. These contacts are prominent for Cl····Cl. not observed for the I····I while the Br····Br contacts are intermediate. The presence of quasi-type I contacts for Cl····Cl and their absence for I····I suggests that while polarisation effects are important in the case of the I····I, other effects such as anisotropy are important for Cl····Cl.

Halogen bonding has also been described as a competing interaction with hydrogen bonding[82] in some recent structural investigations in which it plays an essential role in the assembly of the crystal structure. In these cases, mixing an equimolar amount of halogen bond and hydrogen bond donor in solution with an

electron donating bipyridine derivative resulted in crystals being formed with the halogen bond donors and the hydrogen donors left in the solution, suggesting that in these systems the halogen bonding seems to be more effective in the control of construction in the supramolecular architecture than the hydrogen bonding[83]. Hydrogen bonding and halogen bonding can in many cases coexist in crystal structures and can be used as crystal engineering tool with some level of predictability for assembly of molecular complexes. The 4-nitrobenzoic acid : 4-iodopyridine and 3,5-dinitrobenzoic acid : 4-iodopyridine co-crystals have a molecular tape like structure connected through hydrogen bonding O–H····N and C–I····O halogen interactions[84]. In both molecular structures the acid····pyridine and iodo····nitro synthons are present and are preferred pairing when these four synthons are present in a crystal structure (*Figure 1-13*).

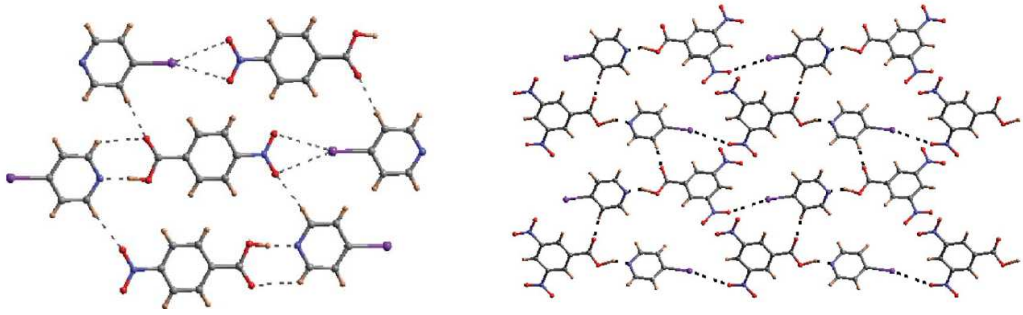

Figure 1-13. The structure of 4-nitrobenzoic acid : 4-iodopyridine(left) and 3,5-dinitrobenzoic acid : 4-iodopyridine(right) showing the acid····pyridine and iodo····nitro synthons.

While as a crystal engineering tool these synthons have been used, their selectivity is still not understood. In the molecular complex of 4-iodoanilinium : 2-carboxy-6-nitrobenzoate there is a N–H···O interaction between the molecules and a halogen···halogen interaction between the two 4-iodoanilinium molecules, but there is no iodo···nitro interaction[85]. The case of the 3-cyanopyridine : 2-chloro-4-nitrobenzoic acid molecular complex is very similar with the N···H–O motif between the molecules but there is no halogen···nitro[86], as in the complexes of 2-chloro-4-nitro-benzoic acid and 2-chloro-5-nitro-benzoic acid crystallised with pyrazine[87]; this could be caused by the chlorine atom's lower polarizability.

1.7 π···π interactions

The strength of π interactions are defined by attractive forces such as electrostatic, dispersion, inductive, or repulsive such as repulsive exchange forces[88-89]. The differences between the different type π interactions have been widely studied mostly with computational methods as these interactions usually appear in complexes as secondary interactions according to their strength[90-91]. There are two main type of π interactions, the sandwiched π···π stacking also called face-to-face (D) which also can have the parallel displaced (PD) arrangement, and the T shaped (T)[92] with several variations of these depending on the nature of the interacting aromatic π systems[88].

The first computational π···π interaction study showing there are four energy components that have to be accounted for (electrostatic, inductive, dispersion and repulsive exchange forces) in a π···π interaction was that on porphyrin systems by Hunter and Saunders in their much cited paper[93]. More comprehensive quantitative energy analyses have been undertaken using quantum mechanical calculations of these various π interactions, calculating the electrostatic, dispersion and induction energies of these systems. It has been shown that the π···π(D) / π···π(T) interactions in systems involving benzene, toluene and benzonitrile, the most dominant of the energy components are the dispersion energy with energies of ~67/59%, the electrostatic with energies ~26/32% and the lowest the induction components with energies of ~7/9%, respectively. It also has been demonstrated that the exchange repulsion forces increase with the increasing contacting area between the two benzene rings[94].

1.8 Materials

1.8.1 DMAN

Proton sponges are known for their very high proton affinity, low nucleophilicity, slow protonation/deprotonation and they form very stable ionic complexes with

mineral and organic acids often containing low barrier intramolecular $[N\cdots H\cdots N]^+$ hydrogen bonds.

1,8-bis(dimethylamino)naphthalene (DMAN) was first synthesised in 1968 and recognised by its very high basicity[95]. The N-H···N intramolecular hydrogen bond distance in the protonated DMAN ($DMANH^+$) can be tuned by varying the substituent on the naphthalene ring[96]. 30 years after its discovery there were already 30 different naphthalene-based proton sponges[97]. Infrared and NMR studies have been carried out on protonated naphthalene proton sponges[98], showing a correlation between the substituent on the naphthalene ring and the length of the hydrogen bridges which causes an increase in the chemical shift. DFT calculation of the basicity of organic bases has shown that in the case of intramolecular hydrogen bonds these methods are satisfactory, but are less accurate than conclusions from measurements of the Gibbs free energies and often fail in the case of the proton affinity measurement, due to the lack of the entropy term in the calculations[99]. Since there are derivatives known with orders of magnitude higher basicity[100], these proton sponge materials are widely used, not just in crystallisation of complexes through proton transfer, but also in synthetic chemistry[101-104].

More recent investigations have reported the charge density distribution in a series of ionic complexes of DMAN with a selection of different organic acids[105]. The $DMANH^+$ cations in the complexes studied show the consistent effect of asymmetric protonation. The proton in the $[N\text{-}H\cdots N]^+$ hydrogen bridge is found to be very sensitive to local interactions. In the $DMANH^+$ complex with the 1,2,4,5-benzene-tetracarboxylic acid anion, the electron density associated with this proton is shared between the two nitrogen atoms, while it is clearly separated from the valence shell charge concentration of the acceptor N(1) atoms in the other three complexes studied (*Figure 1-14*). In all of the cations, there is a noticeable polarization of the lone electron pair of the acceptor N(1) atom. This is one example demonstrating the presence of very interesting behaviour of the hydrogen bonds in DMAN complexes.

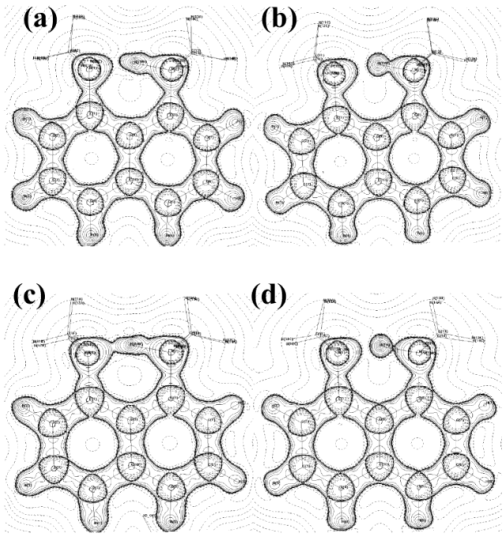

Figure 1-14. Valence shell concentration and depletion of electron density in $DMANH^+$ cations taken from (a) dicyanoimidazole , (b) 4,5-dichlorophthalic acid, (c) 1,2,4,5-benzenetetracarboxylic acid and (d) o-benzoic sulfimide dihydrate[105].

A variable temperature single crystal X-ray diffraction study of a small selection of ionic complexes of protonated DMAN with the anions of a series of acids showed interesting behaviour of the hydrogen bond at several temperatures[39]. The reason for structural changes of the $DMANH^+$ cation is the interaction between the H-bonded fragment and the nearest counterion in the crystal lattice. By varying the anion it is thus possible to generate changes in hydrogen bonding in the $DMANH^+$ complexes, which will in turn change the electron density distribution in the molecule. An example of this phenomenon is seen in the material $DMANH^+$: 4,5-dichlorophthalic acid, in which three possible temperature-dependent hydrogen bond evolution effects are indicated from the X-ray diffraction data: the disorder and migration in the N-H···N intermolecular hydrogen bond in the $DMANH^+$ moiety, possible proton migration in the intermolecular hydrogen bond of the dichlorophthalic acid molecule and evidence of cooperativity of this migration with the evolution of intermolecular hydrogen bonding between $DMANH^+$ and dichlorophthalic acid as this expands asymmetrically with the lattice expansion. Another investigation in this series that shows interesting hydrogen bond behaviour, results from the crystallisation of $DMANH^+$ with 1,8-diamino-2,4,5,7-tetranitronaphthalene (DATNN). This structure crystallises in the triclinic system and studies by X-ray crystallography

and by IR spectroscopic studies show that the intramolecular NHN^+ hydrogen bonding in the $DMANH^+$ is symmetric, while the NHN^- intramolecular hydrogen bonding in the DATNN is asymmetric[106].

Other X-ray and IR spectroscopic studies of a substituted 2,7-dichloro-$DMANH^+$ complexed with the acid HBr indicate the same symmetric protonation, but in this case the twisting of the methyl groups is slightly less than in the case of the unsubstituted DMAN molecule. This is because the main factor in the structure determining the conformation remains the repulsion of the nitrogen lone electron pairs. A series of other X-ray and IR structural studies have been reported on $DMANH^+$ and substituted $DMANH^+$ complexes with a centrally localized hydrogen between the two nitrogen atoms[107,108,109] . However, to have a full description of the hydrogen bonding, and obtain the properties of the hydrogen bond, neutron diffraction is required[110]. The first low-temperature, high resolution X-ray and neutron diffraction study of uncomplexed DMAN was reported in 1999[111] . In this work a full description of the uncomplexed DMAN molecule is compared with its protonated ($DMANH^+$) form in molecular complexes. A minor asymmetry is found in the naphthalene group of the uncomplexed molecule, induced by the weak intermolecular interaction, while this asymmetry is more conspicuous in $DMANH^+$. Compared with its protonated form, the neutral DMAN molecule shows a difference in atomic charges and in structural parameters such as bond lengths. The largest difference is in the monopole charges of the nitrogen, which are less negative in the protonated DMAN. The other significant difference between the two structures is in bond lengths; on average the C–C bond lengths are shorter while the C–N bond lengths are longer in the structure of $DMANH^+$ than in the neutral, uncomplexed form of DMAN.

The aim in studies of DMAN complexes to be undertaken in this work is to identify any interesting systems using X-ray diffraction and then go on to investigate more fully hydrogen positions in some of these complexes using neutron diffraction.

A search of the CSD[161] yields 182 hits of DMAN and substituted DMAN complexes, and there are still new complexes being discovered, studied and compared by

charge density[112], spectroscopy (IR, NMR)[113], theoretical calculations[114], etc, trying to explain the behaviour of the intramolecular hydrogen bond in its structure.

1.8.2 Benzoic acids

Carboxylic acids are one of the most extensively studied compounds in crystal engineering as they have convenient hydrogen bond donor and hydrogen acceptor capabilities[8]. Benzoic acids are the simplest aromatic carboxylic acids and are well studied by crystallography, with a CSD search[115] showing well over 4000 molecular complexes containing benzoic acids and derivatives. In the early stage of crystal engineering it has been recognised that molecular synthons based on the common carboxylic acid hydrogen bonding motifs is a good tool in the design of molecular complexes[116]. The common synthons of monocarboxylic acids exist in two forms. The *dimer* motif where the two carboxylic acids are connected through two hydrogen bonds in an $R_2^2(8)$ motif and the *catemer* motif where successive carboxylic acids are connected through a single hydrogen bond and form open chain catemers[117-118](*Figure 1-15*). While both forms have two hydrogen bonds per carboxylic acid group the dimer motif is more common than the catemer form. Around one third of all molecular complexes of carboxylic acids found in the CSD are identified with hydrogen bonds between the carboxyl functions from which the majority are dimers (85%) and just a fraction (15%) of these form non-cyclic arrangements[119].

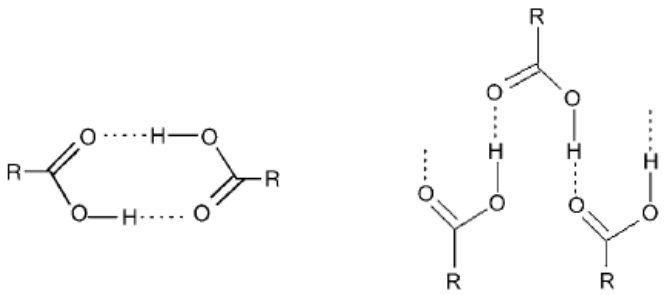

Figure 1-15. hydrogen bond motifs between carboxylic acids in the dimer (left) and catemer (right) configurations[117].

Dimers of benzoic acids have been studied before by neutron and X-ray diffraction methods as the hydrogen bonding between the benzoic acid dimers shows the possibility of disorder (Section 1.4 above). These hydrogen bonds however, are in the range of ~2.65Å, which is usually regarded as representing medium strength, but could be arguably in the range of short hydrogen bonds given the definition by Gilli and Gilli[25]. However, it is certainly out of the range of the very short strong hydrogen bonds (D···A ≤ 2.5Å). In the CSD[120] there are 1306 entries of benzoic acids connected through at least one hydrogen bond of which there are 1134 dimers. A restriction of hydrogen bond length (D···A ≤ 2.5Å) reveals that just 156 of these hydrogen bonds between benzoic acids are shorter than 2.5Å (in the short, strong hydrogen bond range) , and only one of these hits is double hydrogen-bonded, though in this case there is some doubt as to the validity of the deposited structure. One third of the very short hydrogen bonded complexes are metal-organic complexes, where the oxygen is deprotonated and coordinated to the metal. The remaining two thirds of the complexes are molecular complexes of benzoic acid derivatives and metal ions or other organic molecules. All of these organic complexes with very short hydrogen bond between the carboxylic acids involve charge assisted hydrogen bonds. Most of these cases are presented as brief structure reports but there are a small number of research groups which have studied in a more conscious way these short strong hydrogen bonds, comparing similar structures. One of the most relevant examples of research in this area studied four different substituted tetraalkylammonium (R = Me, Et, n-Pr and n-Bu) complexes with four carboxylic acid derivatives, resulting in a selection of nine different molecular complexes, of which five are hydrates[121]. Of these nine complexes, seven are assembled through very short hydrogen bonds between the carboxylic acids, with one of the carboxylic acid being deprotonated by the tetraalkylammonium salt and hydrogen bonded to another neutral carboxylic acid. In the case of the 5-nitroisophthalic acid, all four tetraalkylammonium salts have been successfully co-crystallised, and these systematic results could lead to a better comparison on the effect of the counterion volumes. There are two types of supramolecular organization of these four complexes. For the two smallest cations (R = Me, Et) the 5-nitroisophthalic acids have a very similar hydrogen bonding pattern where the units of carboxy-carboxylate dimers are connected through a short hydrogen bond from the other carboxylic group of the 5-nitroisophthalic acid. This defines

a tetrameric unit with a 24 membered ring with a large cavity in a layered structure and between these layers are sandwiched the ammonium molecules. The cavity is empty but the aliphatic groups on the ammonium group are below or above them. In the case of the two larger ammonium molecules (R = n-Pr, n-Bu) the supramolecular units are influenced by the size of the cations and instead of the tetrameric layer arrangement, crinkled layers are found in repeating hexameric units. It is concluded from the two types of supramolecular arrangements that the hydrogen bonds between the carboxyl-carboxylate units have a small range of tolerance for empty space in the crystal lattice before a rearrangement to a more stable packing occurs. The other structures presented in this research all have slightly different patterns and due to the variation of both cation and anion the comparison is more difficult then of those structures presented above. However the authors agree that a final conclusion can be drawn, supported also by theoretical study of these compounds, that the single hydrogen bonded dimer of the carboxyl-carboxylate seems to be a more robust building unit in crystal engineering than the typical homodimeric units so often seen between the carboxylic acids.

Further research in this area has investigated the complexes of mellitate anions ($[C_6(COO)_6H_{6-n}]^{n-}$, where n is the deprotonation number) with pyridine derivatives, where the mellitates are anions and are connected through single hydrogen bonds, showing a strong self organising ability due to the strong hydrogen bonding in the complexes studied[122]. It is also noted that this ability of the coordination in the self organisation depends on the deprotonation state of the mellitate. Similar work has been done on the mellitate and phosphonium molecular complexes[123].

Chapter 2

2. Theory

2.1 Crystallography

In the development of new materials in chemistry, one of the most important basic knowledge requirements is the structure of the matter being developed. Structural determination of a material to atomic level is essential for a better understanding of the chemical and physical properties of the particular material. There are many methods used to investigate the structure of the materials including mass spectrometry, IR spectroscopy, NMR spectroscopy, solid-state NMR and electron microscopy, but because of their technical limitation they are no match to crystallographic techniques when it comes to three dimensional structure determination to atomic resolution. In order to obtain accurate and precise structural descriptions including the atomic average motion, X-ray and neutron diffraction are the techniques of choice. Both have their advantages and disadvantages but one feature in common is that they both require crystalline samples of the material to be studied.

X-rays are a form of electromagnetic radiation and so interact with the electron density of the materials being studied. Hence it is not generally very accurate when it comes to the determination of hydrogen atom positions, since hydrogen has just one electron, but it is a relatively cheap and fast method requiring "just" a laboratory diffractometer. Neutrons (Section 2.8), on the other hand, interacts with the nuclei of the atoms and the scattering factor of each individual atom is not proportional with the size of its nucleus. The scattering power of a hydrogen nucleus is of the same order as for other atoms, hence neutron diffraction is very accurate in the determination of hydrogen atom positions. However, it does require a large facility to produce the neutron beams, which makes it a very expensive method for structure determination[124]. Electron diffraction is the third but less common method for structure determination by diffraction. Since the electrons interact with the material far stronger than X-rays, there are many challenges of this technique[125]. In

summary, for three dimensional structure determination to atomic level, diffraction techniques remain the best methods available.

2.2 Unit cell and the crystal lattice

The *crystal* is a structure built up from a regular repeated pattern of small units (unit cells)[124]. The basic unit in a crystal structure is not (necessarily) a single molecule from the crystallographic view but a motif that is repeated periodically to generate the whole structure. In a crystal structure, if the motif is represented by a single point the overall crystal shows a regular array of points. The identical points are related to each other by translational symmetry and this array of points is called the lattice of the structure. The parallelepiped enclosed by eight lattice points at its corners is called the unit cell, which is the smallest regularly repeating unit in the crystal structure. The three dimensional unit cell has three sides (*a,b,c*) and three angles (*α, β, γ*) between these pairs of sides; in general the cell edges have different lengths and angles from each other. Within the unit cell, sets of lattice planes are defined, described by the Miller indices: *h, k, l*. These are defined with reference to the intercepts of the plane with the *a*, *b* and *c* axes, respectively defining the intercept along a as *a*/*h*, along *b* as b/ *k* and along *c* as c/*l* (*Figure 2-1*). It can be seen from this definition that the unit cell is bounded by the planes (100), (010) and (001).

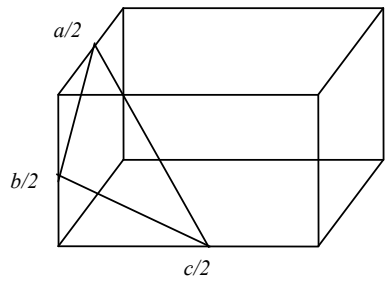

Figure 2-1. The lattice planes and the definition of the Miller indices. In this case the intercepts are at (a/2, b/2, c/2)=(a/h, b/k, c/l), so this is a (222) plane.

2.3 Crystal symmetry

There are seven types of crystal systems uniquely defined by the six parameters of the unit cell, the three lengths of its sides (*a*,*b*,*c*) and three angles between these (*α, β, γ*)) (*Table 2-1*), where the unit cell is generally the smallest volume which can be replicated along the three spatial axes to form the crystal.

Table 2-1. Unit cell types, defined through relationships and constraints involving the unit cell dimensions

Triclinic	a ≠ b ≠ c	α ≠ β ≠ γ ≠ 90°
Monoclinic	a ≠ b ≠ c	α = γ = 90°, β > 90°
Orthorhombic	a ≠ b ≠ c	α = β = γ = 90°
Tetragonal	a = b ≠ c	α = β = γ = 90°
Cubic	a = b = c	α = β = γ = 90°
Trigonal	a = b ≠ c	α = β = 90°, γ = 120°
or	a = b = c	α = β = γ = 90° < 120°
Hexagonal	a = b ≠ c	α = β = 90°, γ = 120°

The unit cell can be *primitive*, when it contains one lattice point, denoted a *P* type lattice. If the lattice has more than one lattice point it is described as a non-primitive unit cell. A non-primitive three dimensional unit cell could have three kinds of additional lattice points: *C-centered*, has an extra lattice point centered in each of two opposing faces of the cell; *face-centered (F)*, an extra lattice point is centered in every face of the cell; *body-centered (I)*, an extra lattice point is centered in the exact middle of the cell. This internal constitutions introduce another additional seven lattice types; in total 14 types of lattices exist, which are called *Bravais* lattices.

Other internal symmetry can exist within the unit cell, building the unit cell contents from the unique structural component of the crystal (termed the asymmetric unit). This symmetry, additional to that involving the lattice points can include rotation, reflection and combinations of these with translation. There are four types of these symmetry elements: *mirror plane*, *glide plane*,

rotation axis (2-, 3-, 4-, or 6-fold), *screw axis* (Figure 2-2), and also elements including rotation and inversion (centres of symmetry).

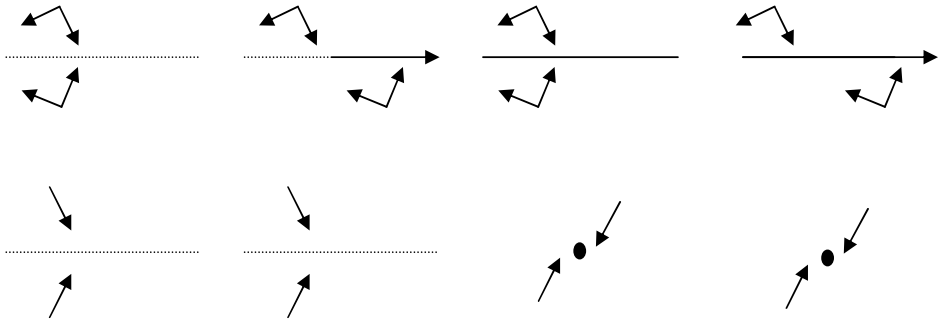

Figure 2-2. The representation of internal unit cell symmetry elements in elevation (top) and projection (bottom), from left to right: mirror plane, glide-plane, two-fold rotation axis and two-fold screw axis[124].

With the combination of these symmetry elements with lattice types, there are a total of 32 point groups (the group of symmetry operations which describes the symmetry of discrete objects, with no translational elements) and 230 space groups which describe all possible distributions of the motifs in the lattice to produce the entire unit cell contents that that build up the three-dimensional crystal through translational symmetry. More detailed description of unit cell symmetry, and crystal lattices can be found in the *International Tables for Crystallography, Volume A*[126].

2.4 Diffraction pattern

2.4.1 Laue equations

Diffraction occurs when a crystal is positioned in the path of an incident X-ray beam with appropriate wavelength. Every atom in the crystal scatters the beam in every direction and these beams interfere constructively and destructively, with just the constructive interference defining the geometry of the diffraction

pattern which reveals the size and the shape of the crystal lattice. This information, together with the intensities of the diffraction spots (reflecting the electron density) can be used in determining the unit cell contents – ultimately determining and refining the type, position and other information about each atom in the structure. The symmetry of the diffraction pattern has an impact on both the geometry and the intensities of the diffraction.

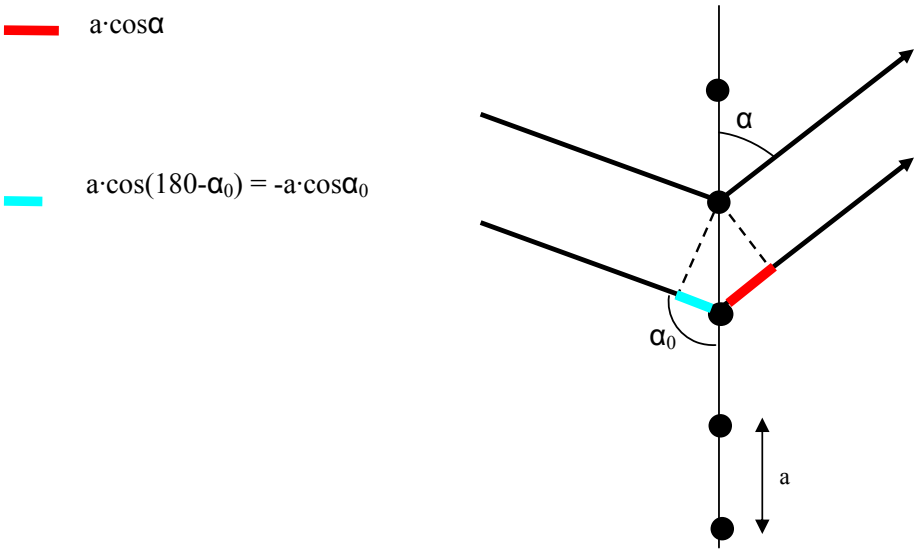

Figure 2-3. Representation of the diffraction for a 1-D array of atoms[127].

If it is considered that the atoms are positioned similarly spaced in a single row, then the scattered X-ray beam from each individual atom travels different distances and the path length between them must equal an integer multiple of the wavelength in order for constructive interference to arise (*Figure 2-3*). The path length difference between atoms separated by distance *a* can be calculated from the geometry of the incident and the diffracted beam (*Equation 2.1*).

Equation 2.1 *path difference* $= a \cdot \cos\alpha - a \cdot \cos\alpha_0 = h\lambda$

where α and α_0 are the angles of the diffracted and the incident beam with respect to the 1-D row of atoms. When the beam is scattered in the direction in which the geometry required for complete constructive interference is satisfied,

diffraction occurs, whereas in any other case the intensity of the scattered beam diminishes away. Similarly, in the case of a three dimensional lattice, three similar equations must be satisfied simultaneously in order for diffraction to occur. These are the Laue equations (*Equation 2.2, Equation 2.3, Equation 2.4*).

Equation 2.2 $$a(\cos\alpha - \cos\alpha_0) = h\lambda$$

Equation 2.3 $$b(\cos\beta - \cos\beta_0) = k\lambda$$

Equation 2.4 $$c(\cos\gamma - \cos\gamma_0) = l\lambda$$

The Laue equations contain the interatomic spacings *a, b* and *c*, three different integers *h,k* and *l* and the wavelength, λ. While the Laue equations define the required geometry of the incoming and the diffracted beams, a simpler interpretation of diffraction geometry in terms of lattice spacings is usually used, as it is easier to understand and apply – this is Bragg's Law.

2.4.2 Bragg's law

In this more intuitive way to describe the diffraction pattern, the diffraction is considered as reflection from sets of parallel planes within the crystal. Between the incident beam and the diffracted beam is a path difference, which according to *Bragg's law*, must be an integer number of wavelengths for constructive interference to occur. The path difference between the two beams can be calculated from geometrical considerations (*Equation 2.5, Figure 2-4*)[124].

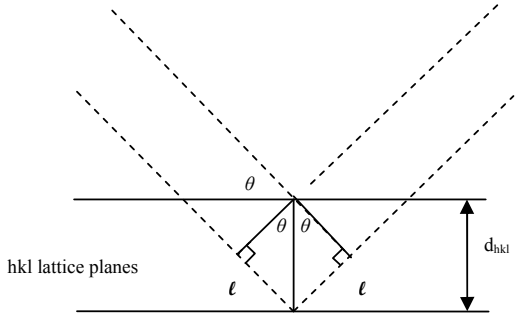

Figure 2-4. Demonstration of Bragg's law [124].

Equation 2.5 $$l + l = 2d_{hkl} \cdot \sin\theta_{hkl}$$

where d_{hkl} is the separation between the *hkl* lattice planes and θ is the angle the incident X-ray beam makes with this set of lattice planes. The path difference between the incident and diffracted beams has to be an integer multiple of the wavelength for constructive interference; consequently $l + l = n\lambda$ where λ is the wavelength, thus,

Equation 2.6 $$n \cdot \lambda = 2d_{hkl} \cdot \sin\theta_{hkl}$$

where *n* is an integer. The d_{hkl} is the spacing between the neighbouring lattice planes with *hkl* indices and is a function of the *a*, *b*, *c* and *α*, *β*, *γ* unit cell parameters. Bragg's Law also implies that the incident and diffracted beam as well as the normal to the lattice planes must lie in the same plane.

2.4.3 The reciprocal lattice

The orientation of the crystal can be defined using Bragg's law and the direction of the normal to the set of the *hkl* lattice planes. Quantities required for a description of the d_{hkl} lattice planes are the direction of the normal and the length of a vector in this direction magnitude. These two quantities describe each reflection in the diffraction pattern and can be referred to as scattering vectors. As these two quantities are derived from the *hkl* lattice planes and the lattice planes are defined by the relative position to the unit cell, the direction of the scattering vector is well defined with respect to the unit cell for every lattice plane. The magnitude of the vector is related to d_{hkl} since the diffraction angle is proportional to $1/d_{hkl}$ as seen from the rearrangement of the Bragg equation (*Equation 2.7*):

Equation 2.7 $$\sin\theta = \left(\frac{\lambda}{2}\right) \cdot \left(\frac{1}{d_{hkl}}\right)$$

where θ is the diffraction angle. Thus the diffraction pattern is built up from a set of reflections, where each one is derived from the diffraction vector, and the end of the diffraction vectors defines a lattice with spacings inversely proportional to the crystal lattice. This is the reciprocal lattice, formally defined as follows: for every set of lattice planes in real space a reciprocal lattice point can generated in reciprocal space. The direction of the reciprocal lattice point *hkl* is given by the perpendicular dropped from the (*hkl*) lattice plane to the unit cell origin and the distance between the lattice origin and the reciprocal lattice point is $1/d_{hkl}$. As the crystal lattice is defined by the *a, b, c, α, β, γ* unit cell parameters, the reciprocal lattice is defined by related parameters a^*, b^*, c^*, α^*, β^*, γ^* and the relationship between them is described by the vector relationships in *Equation 2.8*:

Equation 2.8

$$\underline{a}^* = (1/V)\underline{b} \times \underline{c}$$
$$\underline{b}^* = (1/V)\underline{a} \times \underline{c}$$
$$\underline{c}^* = (1/V)\underline{a} \times \underline{b}$$

where V is the volume of the unit cell.

The most convenient way to describe the reciprocal lattice and its relation to diffraction geometry is the Ewald construction (*Figure 2-5*). A sphere is drawn around the crystal with a radius of 1/λ, the reciprocal lattice vector lies normal to the *hkl* plane of the crystal and has a length of $1/d_{hkl}$. The reciprocal lattice is drawn with origin at point *O*. To satisfy Bragg's law the vector connecting the points where the incident beam and diffracted beam exit the Ewald sphere (the scattering vector) must be equal to the lattice vector. From the following geometrical considerations:

Equation 2.9 $$|OP| = (2/\lambda)\sin\theta$$

Equation 2.10 $$\lambda = (2/|OP|)\sin\theta$$

Equation 2.11 $$\lambda = 2d_{hkl}\sin\theta$$

Equation 2.12 $$|OP| = 1/d_{hkl}$$

when Bragg's law is satisfied, diffraction is observed when the reciprocal lattice point touches the surface of the Ewald sphere with the rotation of the crystal.

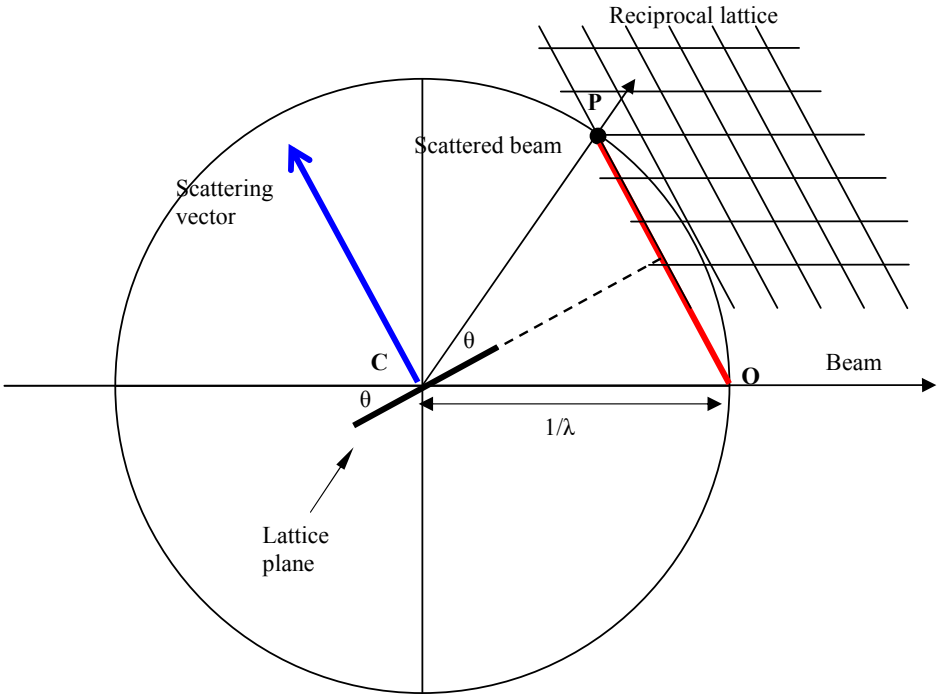

Figure 2-5. Ewald construction of the reciprocal lattice and diffraction geometry [124].

The most common method for X-ray diffraction data collection involves the rotation of the centred crystal in the incident beam and thus the orientation of the reciprocal lattice rotates with the respect to the reflecting sphere. In this case the wavelength of the radiation is fixed (monochromatic beam). The other possible method is Laue diffraction. In this case the incident radiation is a white beam (polychromatic beam) and there is a corresponding set of multiple Ewald spheres, one for each wavelength in the λ_{min} to the λ_{max} range. Many of the reciprocal lattice points will intersect this extended shell of Ewald sphere for every orientation of the crystal, therefore there are many reflections collected simultaneously and the interpretation of the data can be rather difficult.

2.5 Structure solution

After the data has been collected, integrated and corrected using various software packages, which will be discussed in more detail in the Techniques and Instrumentation Chapter (Chapter 3), the next step in an X-ray diffraction experiment is the structure solution. From the data collection, the necessary information has been gained for the structure solution: the intensities (I_{hkl}) of the reflections contain the information about the unit cell contents, amongst other factors. The relation of the intensities to the unit cell contents is quantified by the structure factor:

Equation 2.13

$$F_{hkl} = \sum_{j=1}^{N} f_j \exp\left[2\pi i\left(hx_j + ky_j + lz_j\right)\right]$$

where, j is an individual atom, f_j is the scattering factor (modified as appropriate by the displacement parameters) for the jth atom with coordinates (x_j, y_j, z_j) within the unit cell and h, k, and l are the Miller indices of the particular reflection. This is the mathematical expression relating each reflection to the crystal structure itself. The observed diffraction intensities I_{hkl} are proportional to $\left|F_{hkl}\right|^2$.

The mathematical function relating the diffraction pattern and the crystal structure is the Fourier transform. As X-rays are diffracted by the electron density, to identify individual atoms in the structure the scattering density $\rho(xyz)$ is required. This can be calculated through the Fourier transform of the structure factor.

Equation 2.14

$$\rho(xyz) = \frac{1}{V}\sum_{hkl} F_{hkl} \exp\left[-2\pi i(hx + ky + lz)\right]$$

To simplify the equations there are numerous factors which have not been included in this outline, but which affect the model, such as angular variation of

scattering factors, thermal motion, anisotropic displacement parameters, static disorder.

2.5.1 Phase problem

The aim of structure determination is to end up with an accurate set of atomic positions which represent the scattering density in the crystal structure. This is based around the quantity determined from the data measured in a diffraction experiment, the measured intensities, which are proportional to the square of the structure factor. The structure factor is a complex quantity,

Equation 2.15 $$F_{hkl} = |F_{hkl}| \exp(i\alpha_{hkl})$$

where

Equation 2.16 $$|F_{hkl}| \propto \sqrt{I_{hkl}}$$

In the experiment we can measure the intensity of the reflection but not the phase. If we have a model of the structure from which we can calculate structure factors, the calculated structure factor F^c_{hkl} contains both the magnitude and phase information, while the observed structure factor F^o_{hkl} (observed structure factors) contains only the magnitude information (without the phases α_{hkl} in the above expression). This difference is also known as the phase problem. There are several ways used to solve the phase problem, such as isostructural substitution (isomorphous replacement), Patterson methods (heavy atom methods) and Direct Methods. The latter two are the most frequently used for small molecule structures and will be discussed here.

2.5.2 Patterson methods

Patterson methods work best on structures where a small number of the atoms are significantly heavier than the other atoms in the structure, therefore they have significantly larger electron density. To solve the structure from the Fourier transform of the structure factor would require the phase of the reflections, but the Patterson method deals in a different way with the data. It

eliminates the phase problem by setting all phases to 0 by using the squared of the structure factors and thus generating a Patterson map:

Equation 2.17 $$P(xyz) = \frac{1}{V}\sum_{h,k,l}\left|F_{hkl}^{o}\right|^{2} \cdot \exp\left[-2\pi i(hx + ky + lz)\right]$$

The peaks on this map are vectors between pairs of atoms in the structure with coordinates relative to each other but not to the unit cell origin. The size of the peaks is proportional to the product of the sizes of the concerned pair of atoms. Vectors are produced from every pair of atoms including self-pairs. The self vectors have a length of 0 and all are located at the origin. If there are a small number of atoms that are heavier than the others then the vectors between symmetry-related pair of these heavy atoms will be clearly the highest peaks in the Patterson map. Once the heaviest atom has been found the rest of the atoms can be located by Fourier methods (see below).

2.5.3 Direct methods

Direct Methods are the most automated and most widely used method of structure solution. This method creates mathematical relation between the observed amplitudes and the structure factor phases through knowledge of the electron density. To understand how these can be related two significant properties of the electron density function have to be considered: the fact that the electron density everywhere is positive $\rho(r) \geq 0$ (positivity); and the fact that it is composed of discrete atoms (atomicity)[128]. When the method was first developed in middle of the twentieth century it was not widely used because it is based on complicated mathematical calculations which need powerful computers. With the development of computers the technique began to be used and today it is one of the most widely used methods.

In order to be able to define a relationship between the observed intensities and the structure factor phases the structure factors are normalized to an "expectation value" E^2, to an average intensity value determined for different

ranges of scattering angles, as the intensities fall with the scattering angle and also dependent on the atomic vibration, etc. The following relationship was first defined by Sayre, that states that any *hkl* reflection can be calculated by the sum of the products of the structure factor of all pairs of reflections that sum to it.

Equation 2.18 $$E_{222} = E_{221} \cdot E_{001} + E_{112} \cdot E_{110} + E_{212} \cdot E_{010} + \ldots$$

Knowing that the pairs of reflections where one or both reflections are weak do not contribute too much in the calculation of a strong reflection they can be ignored at first and the "triplet relationship" has been developed for centrosymmetric space groups. Strong reflections are paired in group of threes, based on the Sayre equation:

Equation 2.19 $$E_{hkl} \approx E_{h'k'l'} \cdot E_{h-h',k-k',l-l'}$$

and give a probabilistic sign of the E_{hkl}. If both $E_{h'k'l'}$ and $E_{h-h',k-k',l-l'}$ have the same sign, then E_{hkl} will probably be positive, while if they have different signs then E_{hkl} will be negative.

The number of atoms lying in a set of lattice planes will all scatter in phase and if this plane is taken as the origin the phase angle of these reflections will be 0° or a positive sign, which means that a strong reflection with a 0° phase angle will have a large contribution of the electron density in a Fourier synthesis at the crest of its lattice planes. If the atom lies in a plane midway and parallel to this plane the reflection will have a phase angle of 180° or a negative sign. When there is a triplet relationship between three strong reflections then the electron density is concentrated at a d interval for all three lattice planes, and if the phases of two reflections are known then the phase of the third reflection is determined by them. To solve the structure this method is used to find the best available set of calculated phases. Once a set of estimated phases has been obtained, these can then be used along with the observed structure factors to calculate a Fourier (electron density) map using Equation 2.14 for ρ(xyz). If the estimated phases are sufficiently close, atom peaks will be present in the map

that can be assigned to atoms, giving an initial model of the structure. With the availability of the initial model, the phase problem can be said to be "solved" and the remainder of the structure developed from this initial solution.

2.6 Structure completion

After the structure solution, often the structure is incomplete and the missing atoms have to be found. The partial structure model is used for the generation of a diffraction pattern using forward Fourier transforms based on the observed structure factor magnitudes and the phases calculated from the initial model. In this way missing atoms can often appear as a peak in the Fourier map calculated using these quantities in the electron density calculation. The structure factors generated from the model contains information about the phase as well as the amplitudes ($|F_c|$ and α_c) whereas the observed structure factors contain no phase information. Using a Fourier calculation with $|F_o|$ and the phases from the calculated structure factor a new model of the electron density can be generated. If the errors in the calculated phases are not too large, then the missing electron density of any missing atoms should show up in the new model. Repeating this process should reveal all missing atoms from the model until no more improvement can be seen in the comparison between the calculated and observed structure factor.

Adding atoms to the structure in this way is called Fourier recycling and with this method the structure can be developed. This works because although the initial model is often very inaccurate it contains enough information (gives sufficiently good phases) to reveal the remainder of the structure. When only a small part remains unidentified, the method to locate the remaining atoms is to calculate the difference Fourier map using the difference structure factor $|F^o_{hkl}| - |F^c_{hkl}|$ as coefficients.

There is an important difference between neutron diffraction and X-ray diffraction in this process. In the case of neutron diffraction, from the difference Fourier synthesis the hydrogen will appear with approximately the same strength as other atomic species (but as a negative peak). Hence the

location of the missing hydrogen atoms in most cases is successful, while in the case of X-ray diffraction the hydrogen atoms can remain obscured.

As the structure model is improved, the generated structure factors F_c can then be compared to the observed structure factors F_o. The comparison of these two structure factors reveals how good the model is compared to the real structure. These two values can be compared in different ways – one of the most used comparisons is the residual factor (R –factor):

Equation 2.20

$$R = \frac{\sum \left| |F_o| - |F_c| \right|}{\sum |F_o|}$$

The R-factor has a usual value between 0.02-0.07 for a refined structure where structure is complete and well defined. Another agreement factor used is the weighted R-factor:

Equation 2.21

$$wR2 = \sqrt{\frac{\sum w\left(F_o^2 - F_c^2\right)^2}{\sum w\left(F_o^2\right)^2}}$$

In this expression, each reflection has its own weight, incorporating the relative reliability of different measurements. A good agreement between the structure and the model would typically lead to a value under 0.20 but there is no generally agreed value of wR2 required for a "good" structure as in the case of the R-factor.

2.7 Structure refinement

The raw structure from the Fourier calculations (all non-hydrogen atoms found) can be improved by refinement which means the alteration of determined parameters until the calculated diffraction pattern from the model gives the best agreement with the observed diffraction pattern. Many automated programs are available which allow many parameters to be varied like atomic

positions, thermal parameters, scale factors, and absorption corrections to get the best fit between the calculated and the observed structure factors. By far the most common method is the least-squares structural refinement (used for structures with up to about 2000 atoms). The method used defines the best fit between the data set of observed structure factor and the calculated structure factors to minimise the sum of the least-squares (*Equation2.22, Equation 2.23*).

Equation 2.22 $$M = \sum w\left(F_o^2 - F_c^2\right)^2$$

Equation 2.23 $$M = \sum w\left(|F_o| - |F_c|\right)^2$$

There are many advantages of using F^2 refinement against using F. For example, it reduces the problem of dealing with weak or negative measured intensities, and is not very sensitive to the weights applied to each reflection. All the reflections used in this refinement are weighted according to their standard uncertainties from the measurement.

The initial atomic positions are already given from the structure solution and completion process. The principle of the refinement is similar to that of structure completion but during the least-squares refinement the fine structural parameters are optimised. Before this stage the non-hydrogen atoms have usually been defined with the three coordinates (x, y, z) and a single displacement parameter U. After this, an anisotropic refinement is carried out, in which the non-hydrogen atoms are refined with anisotropic displacement parameters (ADPs; typically 6 per atom), and the hydrogen atoms are located and refined. The improvement of the data continues until the best fit is found for the structural model with respect to the measured data.

There are other residual factors apart from the mentioned R-factor and *w*R2 that are used to check the quality of the data, such as the Goodness-of-Fit (Goof or GoF or S):

Equation 2.24 $$S = \left[\frac{\sum w\left(F_o^2 - F_c^2\right)^2}{\left(N_R - N_p\right)}\right]^{1/2}$$

where N_R is the number of independent reflections and N_P is the number of refined parameters. Collecting more independent reflections for each parameters results in a better structure refinement as it reflects on the Goodness-of-Fit, which should ideally have a value close to 1. A widely accepted ratio of independent reflections to parameter for a reliable good refinement is 10 to 1.

2.8 Neutron diffraction

Neutron diffraction in this investigation will be used to get information about the structure that is not available from other methods. With this method it is possible to determine accurately the positions and atomic thermal displacement parameters of the light atoms, such as hydrogen, when other heavier atoms are also present in the structure. Neutron diffraction is the method of choice for accurate location of hydrogen and also for determining the anisotropic displacement parameters of the hydrogen atoms in the crystal structure. The method has difficulties associated with required crystal sizes (approx. $1mm^3$) and the need to access central facilities at which neutron diffractometers must be located, but in the end the effort is justified by the results. In contrast to other techniques such as X-ray or electron diffraction, neutrons are scattered by the nucleus, rather than the electrons in an atom. The nature of this interaction means that the method offers a description of all atoms in a structure at approximately the same level of precision, with a variation in scattering length as shown in *Figure 2-6*.

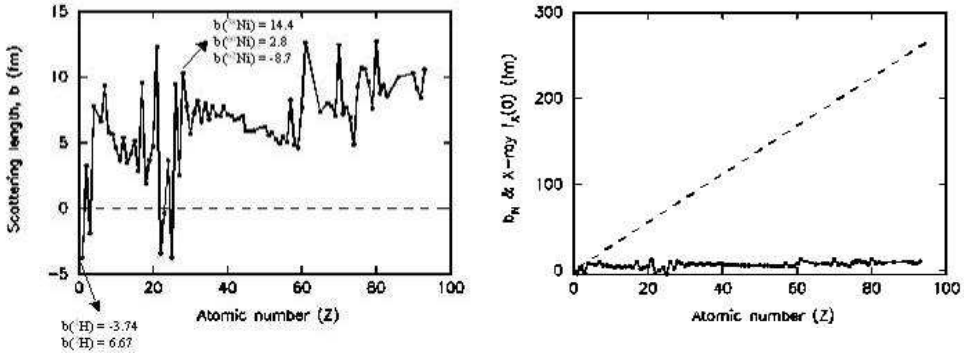

Figure 2-6. Scattering factors of atoms from neutron diffraction (left) and in comparison with those from X-ray diffraction (right), dotted line[124].

Although modern high resolution, low temperature X-ray crystallography can, in favourable cases, reveal the location of the hydrogen atoms, these positions are still determined both less accurately and less precisely than the remainder of the structure and the centre of the electron density is located rather than the nuclear position, so an X-ray experiment is not measuring the same thing as a neutron experiment. It is only neutron diffraction that offers the possibility of accurately refining anisotropic atomic displacement parameters for hydrogen atoms. Thus, while X-ray diffraction is adequate for most structural problems, neutron diffraction is required when hydrogen atom positions and/or displacement parameters are important and needed to high accuracy. The recent improvements in instrumentation have allowed neutron single crystal diffraction, intrinsically a flux-limited technique, to move towards allowing structure determination from small molecule samples in just a few hours per data set. This new improvement also allows the study of the samples at variable temperature and pressure[129,130], which again will be used in this work.

The most important improvement in single crystal neutron diffraction is the availability of very large area detector diffractometers. One of the new large-detector instruments that has been used for this work is the time-of-flight Laue diffractometer SXD at the ISIS spallation neutron source in the UK[131]. This type of source is able to optimize signal-to-noise and use the full white neutron beam via the time-of-flight approach, an advantage offered by the pulsed spallation method. For neutrons produced in a pulsed manner, the production time of the neutrons can be precisely defined as the moment when the proton beam hits the

target. It is thus possible, by recording the subsequent arrival time of each neutron at the detector, to determine its wavelength providing the flight path is known. The use of white beams, sorted using the time-of-flight technique, allows multiple order reflections to be extracted and signal-to-noise optimized via background discrimination. The typical velocities of thermal neutrons are convenient for this method – a neutron of wavelength 1 Å travels 10 m in approximately 2 ms. The time-of-flight technique is used on a pulsed neutron source such as the ISIS source at Rutherford Appleton Laboratory, where the SXD instrument is based. It is also beneficial in allowing fixed scattering geometries to be adopted which greatly simplifies the use of sample environments such as high pressure cells.

Variable temperature and pressure neutron diffraction determinations of the average proton scattering density in both terminal hydrogen atoms and those involved in hydrogen bonds allow a more complete direct view of the details of the hydrogen atom potential to be built up than if data were only available from one or two temperatures. The recent instrument advances mean that data collection times have been reduced to a typical 6–12 h for a full single crystal neutron data set from a material of moderate complexity. The refinement of the structure from each data set in the variable temperature data allows the positions of the atoms, their thermal parameters and any partial site occupancies to be obtained.

Neutron diffraction will be discussed in more detail, including a description of the techniques used and the instruments employed, in the Techniques and Instrumentation Chapter (Chapter 3).

Chapter 3

3. Techniques and instrumentation

This chapter is intended to present the techniques and instrumentation used throughout the work. The main technique utilised is single crystal X-ray diffraction and therefore more details will be given on this topic, presenting step by step from the sample preparation through the data collection to the solved structure. The instrumentation used will also be described, focusing more on the single crystal diffractometers including the two Laue diffractometers used at neutron diffraction facilities, giving more insight into the techniques used. An introduction to the other techniques used will also be given.

3.1 Single crystal X-ray diffractometers

Through the work mainly single crystal diffractometers have been used for structure determinations. The advantage of using single crystal diffraction techniques have been detailed before, concerning their ability to provide routine full 3-D structure determination, but the practical aspects of the technique has not yet been addressed, and will be done here.

There are three in-house diffractometers have been used through this work. There are two diffractometers equipped with charge coupled device (CCD) detectors, a Nonius/Bruker Kappa CCD[132-136] and a Bruker APEX II[137-138], and one diffractometer equipped with an image plate (IP) detector, a Rigaku R-AXIS/RAPID[139] (*Figure 3-1*). All three diffractometers are normally equipped with Mo X-ray tubes, ideal for the high resolution data collection presented through this work. The diffractometers are also equipped with cooling equipment based on the flow of cold nitrogen gas, able to collect temperature as low ~77K. In the case of the APEX II there is also the potential to use a cold helium gas flow, offering temperature as low as ~30K. This temperature control capability creates the possibility of variable temperature studies, extensively used in this work.

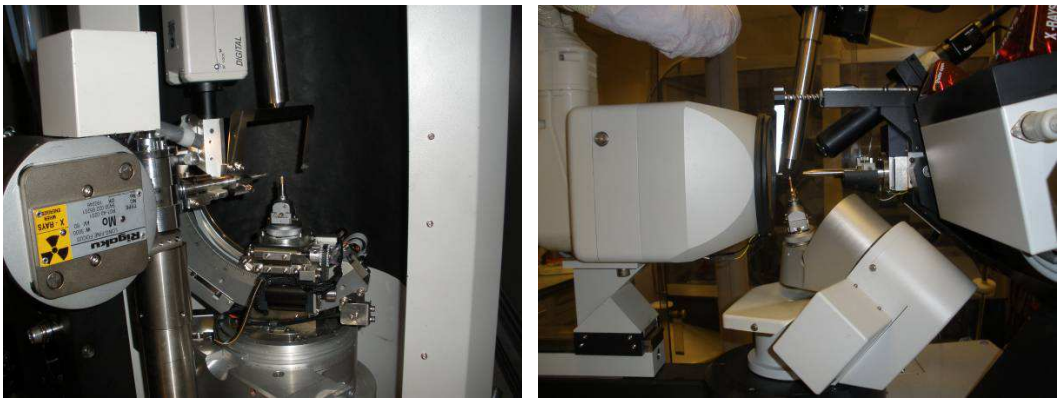

Figure 3-1. The two types of the single crystal X-ray diffractometers used in this work, showing the detector, goniometer, cold head and the collimator of the X-ray tubes and their arrangement on the instruments; the R-AXIS RAPID Rigaku (left) and Nonius/Bruker Kappa CCD (right).

3.1.1 Sample selection

In planning a single crystal X-ray diffraction measurement, the first thing to do is to obtain a good sample for the experiment. The size and the quality of the sample will determine the method which will be used for the characterisation. Smaller (0.01-0.5mm^3) single crystals can be used for X-ray diffraction while bigger crystals (approx. 1mm^3 or larger) can be used for neutron diffraction. Sometimes the crystal does not grow to a size large enough to perform single crystal X-ray diffraction, in which case other methods as powder diffraction can be used to gain insight into the structure, but the powder diffraction method has been used only for sample screening during this work.

The type of data to be used is very often decided by the particular interest in the structure of the molecular system. If in the structure the hydrogen bonds are playing important roles, in order to understand the complete system the choice of structure determination method might be neutron diffraction because of the accurate determination of the hydrogen atom positions and thermal parameters offered by that technique, although it is often difficult to gain access to neutron facilities.

Choosing a good quality crystal is essential for data collection. The crystal chosen has to be clear of any dust, oils from the crystallisation process or small crystal particles (including crystalline powder) on the surface and has to have no sign of cracks or signs of physical defects. Use of a low crystal quality would compromise the quality of data collected, and thus could cause problems from the structure solution through to the refinement, which in turn would affect the clarity of the final structure.

3.1.2 Crystal growth

While (re-)crystallisation is frequently used in synthetic chemistry as a method for purification of the sample, often resulting in very small crystals, in crystallography and structural chemistry it is often used as a method to create crystals of molecules or complexes that are relatively large sized, suitable for diffraction. There are many methods of crystallisation and many variations of these. The solution evaporation method is the most widely used crystallisation technique since this method is the simplest to apply, while still offering flexibility and variety in its application. The type of solvent used in the crystallisation is one of the important variables in this method. Most often this will involve use of a single solvent, for example water, methanol, ethanol, acetone, acetonitrile, diethyl ether, etc, but mixtures of different solvents can also be used, allowing further options for controlling the solubility of the compound and also the evaporation rate. Temperature can also often be used as a control parameter in the crystallisation. For example, by keeping the solution of dissolved sample in the solvent in a cool place such as a fridge or freezer this slows down the rate of evaporation of the solvent and could lead to successful crystallisation or an increased size crystal compared to crystallisations carried out at ambient temperature. Heating up the solvents on hot plates can also be used as a technique and the solution can then be kept at a constant temperature or slowly cooled to induce crystallisation. Slowing down the evaporation process during the crystallisation by covering the vial or beaker and leaving just a small hole for solvent evaporation is also commonly used as a technique in crystallisation. Changing of the concentration of the dissolved samples by heating up and thus oversaturating the solvent can also be successful in

obtaining crystals. Using more sophisticated equipment such as the ReactArray Microvate (*Figure 3-2*), a programmable temperature controlled rack offers more flexibility. The Microvate offers the opportunity to have up to 12 different temperature or temperature ramping regimes, with up to four samples at each condition, and is often used for a gradient cooling or heating of the sample. This method has successfully been used to grow larger size crystals for neutron diffraction experiments. There are many more variations of these techniques, here are listed just a few examples of these variations as an insight into the methods used during this work.

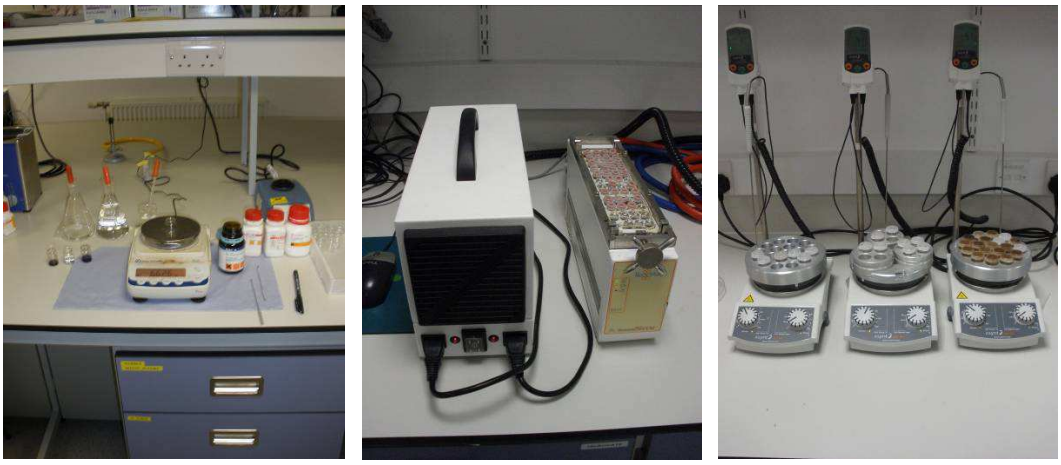

Figure 3-2. Typical crystallisation setup and equipment used in evaporation crystallisation (left); elevated temperature crystallisations can use the ReactArray Microvate (centre) or hot plates (right).

In this work, mainly 7mm^3 vials have been used as crystallisation vessels and mostly with a slow evaporation crystallisation process using lids with small holes in them (*Figure 3-2*). The quantity of the chemicals has been measured in equimolar or different molar ratios, often involving two or in some rare cases three different compounds in the co-crystallisation. In the case of the DMAN complexes 0.04 grams of DMAN with the molar ratio given in the experimental section of each complex with ~5 mL solvent or solvent mixture has been used, unless otherwise stated. The compounds were then dissolved in solvents or solvent mixtures and left in place to evaporate free of any external disturbance (e.g. agitation) with temperature chosen according to the method used in crystallisation, until the solvents completely evaporated or suitable crystal sizes

were achieved. The vials have been examined visually and where crystalline samples have been obtained the sample could be further examined by diffraction methods. In cases where the outcome of the crystallisation has not been successful the process of the crystallisation was re-started from the beginning using different methods since with the combination of crystallisation methods there are many possible distinct trials that can be attempted – only the imagination and time of the researcher limits this. However, where multiple crystallisation attempts were made, the outcomes of these could indicate any required changes in the setup of further crystallisations to be attempted. In many of the cases presented here, a range of parallel crystallisations were set up under different conditions, and these repeated as necessary to produce the required good quality crystals of the desired material.

3.1.3 Unit cell screening and data collection

After a successful crystallisation the crystals are extracted from the crystallisation vials and a good quality crystal is chosen for initial screening. It should be noted that one crystal picked out from the vial does not represent the whole content of the product, this is especially true in the case of co-crystallisation, where more than one compound is crystallised together, often resulting in crystal structures with different molecular ratios than those from the initial setup or resulting in different polymorphs. For an entire screening of the vial contents a better approach is to use powder diffraction, since the entire content can be grinded and screened for indication of the presence of multiple products, including new complexes, multiple forms of a product material (polymorphs) or starting materials left from the crystallisation.

The selected crystal is mounted on the glass fibre of the goniometer which is mounted on the diffractometer and the first step to a data collection is the unit cell determination. This step also allows the screening of samples to ensure that the crystal produced is of a previously unknown structure – i.e. it does not match a structure previously deposited in the CSD. All three diffractometers use different software for sample screening and data collection but they work in a very similar way. Initially a few (4-10) images of the diffraction pattern are

collected at different diffractometer angle settings, then the orientation and the primitive cell parameters are calculated from the observed reflections. After the initial scan, the Bravais lattice is chosen and the required parameters for the data collection are determined. A typical data collection setup for the structures in the work presented here is a d-spacing resolution of ~0.8Å with a minimum redundancy (over-determination of equivalent reflections) of typically four for each reflection observed and with a completeness of 100%. The required data collection time is dependent on many factors such as how well the sample diffracts, sample size, symmetry, intensity of the X-ray tube, but a typical data collection for one temperature takes between 4 and 24 hours with the resolution setting mentioned above.

After the data has been collected the next step is the integration. The integration process is done by the diffractometer software, in order to determine the intensity of the diffraction peaks and to reduce these to structure factors. During the integration several correction factors are applied including multiplicity correction, extinction and absorption, until the final reflection file (*hkl*) is produced. Once the data is integrated the next step is the structure solution and refinement, carried out in this work using the WinGX[140] program suite with implemented codes such as SHELX[141-142] and SIR92[143]. The non-hydrogen atoms have been freely refined including isotropic and anisotropic parameters, while the hydrogen atoms have been refined with isotropic thermal parameters only in the case of X-ray diffraction data collection and with anisotropic thermal parameters in the case of the neutron diffraction experiments, unless otherwise stated. Once the refinement is complete the results can be visualised in MERCURY[144] or ORTEP[145], the most widely used programs for molecular viewing. The structures in this work where the presentation includes the anisotropic thermal parameters of the atoms have been presented with a 50% probability of the thermal ellipsoids. Difference Fourier maps can be visualised in MAPVIEW within WinGX[140] as a two dimension map or MCE[146] as a three dimensional alternative created by stacking two dimensional maps of the density. Finally a *cif* file has to be produced, containing all data collection parameters, information about the crystal physical parameters and the parameters of the final refined structure as a requirement for publishing the results[147].

3.2 X-ray powder diffraction (XRPD)

Powder diffraction is a method very often used for sample screening, thanks to its speed when the main interest is in the rapid detection of any possible new materials resulting from crystallisations. This is especially true when there is a high volume of samples to be screened. The technique has limitations compared to single crystal diffraction, particularly if the final goal is a fully solved and refined three-dimensional high quality structure, but there are some types of information about the sample that cannot be gathered in other ways. In some cases it is possible to obtain the full structure solution using powder diffraction but that is still not common. XRPD is thus a very powerful tool providing complementary information on the samples, especially in the field of crystallisation-based materials research where often more than one product or polymorph can arise from the same crystallisation setup in a single vial. XRPD is also a very good method if information is needed about the purity of the whole sample or the yield of the crystallisation from a particular process. It is therefore very often used in the pharmaceutical industry for reliable and quick matching (fingerprinting) of the samples with patterns from known crystalline materials to ensure that the final product is in the right mixture and it has no impurities. XRPD is also used for gaining structural information from the sample, when it is not possible to obtain a crystal large enough for single crystal diffraction from solution methods or if the sample is produced by grinding in the first place.

Fingerprinting is the method used through this work to identify any possible phase in the bulk, where the generated powder pattern from a structure determined by single crystal diffraction is used for comparison to the data collected on the XRPD instrument. If the patterns match, then the product represents the crystalline material whose structure is already known. If the pattern does not match that resulting from any known structure or structures, then there may be a new crystalline phase present. As has been mentioned before, one crystal picked from the sample vial used for crystallisation and

solved through single crystal diffraction, does not necessarily represent the structure of samples from the whole content of that vial.

The powder diffractometer used in this project is a PANalytical X'Pert Pro diffractometer equipped with Cu X-ray source. A typical data collection takes around 45 minutes from 2θ = 5 - 50° at a scan rate of 1 minute/degree. In a powder sample, the orientation of the many small crystallites that make up the sample are randomly oriented in every direction, in the ideal case, therefore the three dimensional diffraction patterns of a single crystal experiment are reduced to a one dimensional pattern with intensities normally plotted against 2θ angle (*Figure 3-3*). The positions of the peaks are determined by the geometry of the unit cell, the intensities of the peaks are determined by the arrangement of the atoms within the unit cell and their shapes are determined by the microstructure of the sample as well as instrumental parameters such as resolution.

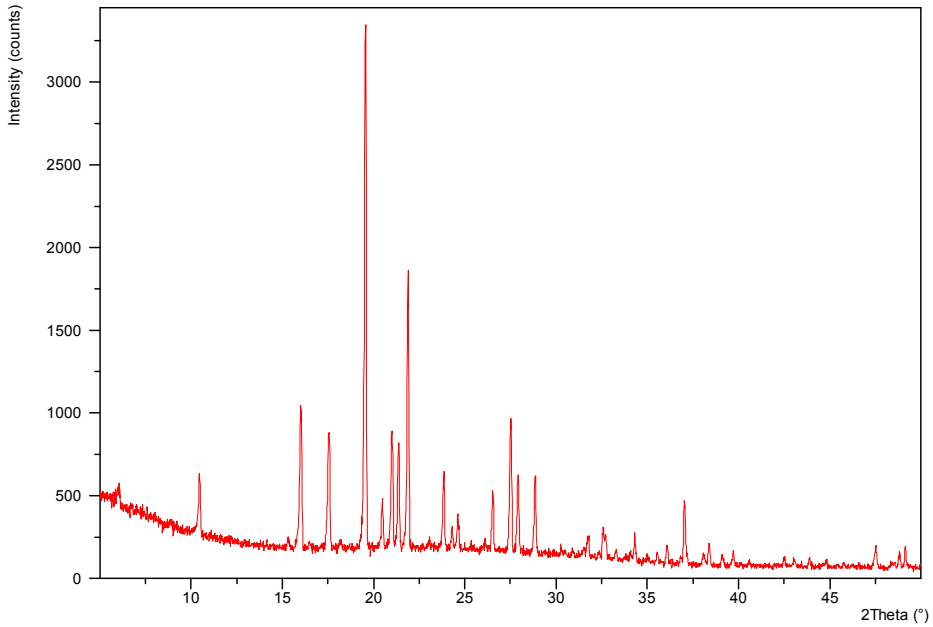

Figure 3-3. Powder diffraction pattern of 4-phenoxyphenol (see Chapter 8), measured from 2θ = 5 to 50° with 1 minute/degree continuous scanning.

3.3 Thermal analysis methods - DSC and TGA

While diffraction techniques can give a complete three-dimensional structure solution, in some cases there are other techniques have to be used to complement our understanding of the structural behaviour. These include the thermal methods of DSC and TGA, to be discussed here.

Differential Scanning Calorimetry (DSC) has been developed for the direct measurement of the heat capacity of a material[148], widely used in drug analyses, polymer analysis, etc. The technique is based on measurement of the difference between the amount of heat required to heat up a sample and that for a reference sample, as a function of the temperature. Every material to be heated up by certain temperature requires a certain amount of heat; the amount of heat taken to reach that certain temperature is called heat capacity. To calculate the heat capacity, the amount of heat used is divided by the resulting temperature increase. In a DSC measurement the two samples (reference and the sample under investigation) are heated with an initially set temperature rate and the heat flow required to achieve the set temperature rate is measured as a function of temperature. When the sample undergoes a phase transition, the heat flow required to maintain the rising of the temperature will be different than the heat flow required by the reference sample, therefore the technique is a strong indicator of thermal transitions, including phase transitions.

Three types of transitions can occur in a DSC plot, two first-order phase transitions (involving a latent heat), melting and crystallisation, and a second-order phase transition (not involving a latent heat), the glass transition. The glass transition occurs when amorphous solid materials (e.g. polymers) become molten upon heating and their heat capacity will change. This change in the heat capacity will appear as a change in slope in a DSC measurement. The two first-order transitions, melting and crystallisation can be seen in the example of the DSC plot of 4-phenoxyphenol, shown in *Figure 3-4*. Melting is an endothermic transition and therefore requires additional heat to go through the phase transition compared to the reference sample while maintaining the same rate of increase in temperature. It will thus appear as a minimum peak in the DSC plot. Crystallisation is an exothermic transition and therefore the sample

requires less heat flow when it goes through the crystallisation phase transition in order to keep the set cooling rate than the reference sample, hence it appears as a maximum peak in the DSC plot. It should be noted that, as in the example (showing the melting and the crystallisation and no glass transition) not every DSC plot will show every type of thermal transition, since they are dependent on the properties of materials.

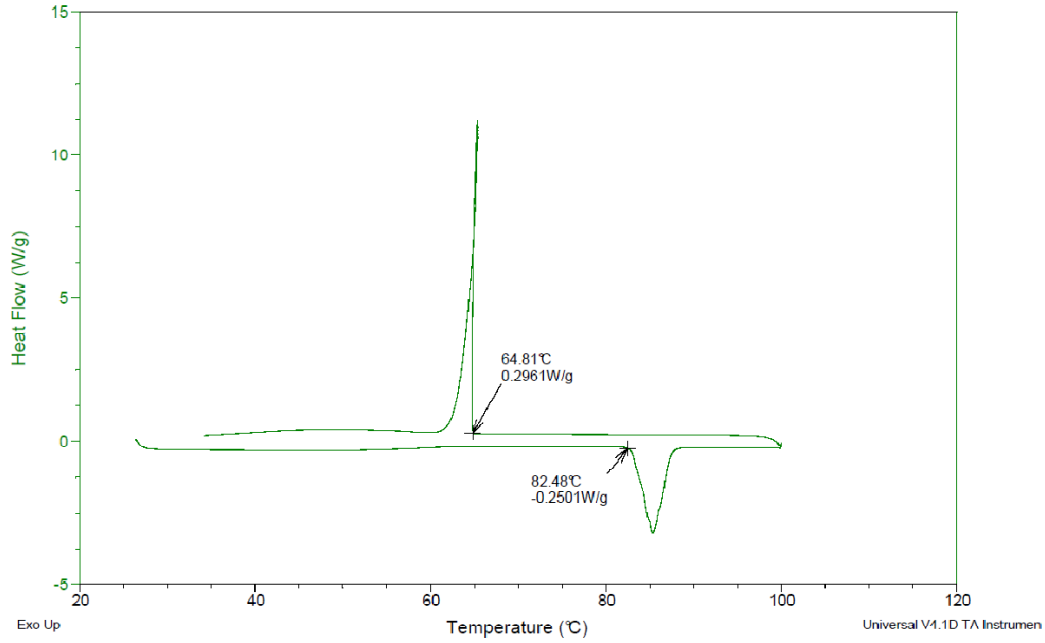

Figure 3-4. DSC plot of 4-phenoxyphenol, showing the melting (82.5°C) and crystallisation (65°C) phase transitions in the sample.

Thermogravimetric analysis (TGA) provides quantitative information on the mass change of materials, associated with physical or chemical changes in their structure such as dehydration, oxidation, physical degradation, etc as a function of temperature. It is widely used in the pharmaceutical, biological, food, polymer, chemical sectors. In this work it has been used for the detection of physical degradation and in quantifying solvent evaporation from the sample.

The DSC and TGA plots have been collected on a DSC Q100 and TGA Q500 respectively, from TA Instruments[132], situated in the Department of Chemistry, and analysed with *TA Instruments Universal Analysis 2000* software package, provided as a tool by the instrument suppliers[149].

3.4 Neutron diffraction

Neutron diffraction has been used extensively through this work for its advantage of allowing the accurate determination of hydrogen atom parameters. While it would be excellent to use it every required time when hydrogen positions play an important role in the materials being studied, the use of these methods requires large, central facilities with high cost of operation and limited availability; to gain access to such facilities can be difficult. However, during this research access has been gained several times to two of these facilities carrying out single crystal neutron diffraction. This section is intended to present the apparatus and the techniques used in these experiments.

3.4.1 SXD at ISIS

SXD is the single crystal neutron diffractometer at the ISIS neutron spallation facility[150] at the Rutherford Appleton Laboratory. At this facility (*Figure 3-5*) the neutron beam is produced in a pulsed manner, thus creating the possibility to use the time-sorted (time-of-flight) Laue technique.

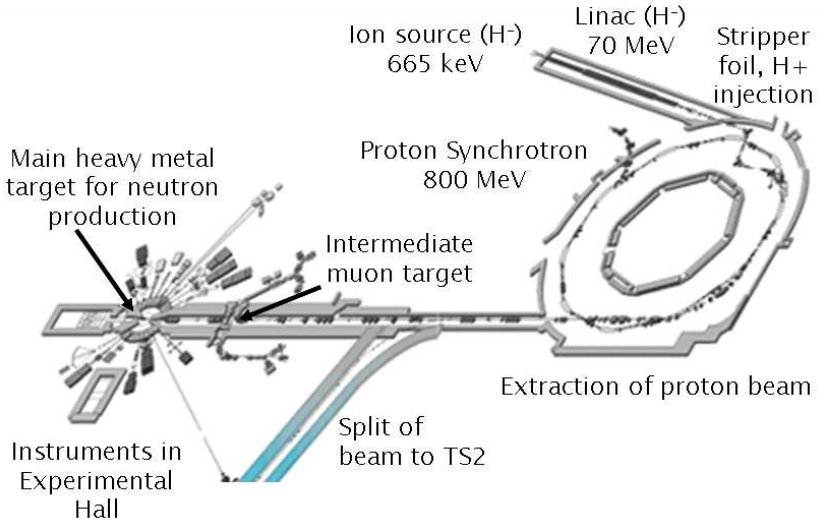

Figure 3-5. Schematic view of the ISIS spallation neutron source at the Rutherford Appleton Laboratory, representing the accelerator and Target Station 1[150].

The production of the neutron beam starts at the injector, where negatively charged hydrogen ions (H^-) are produced using electric discharge. The stream of hydrogen ions is accelerated to 34% of the speed of light. At the end of the linear accelerator the hydrogen ions are stripped of their electrons and introduced into the synchrotron accelerator as a beam of protons. At the synchrotron accelerator the protons are further accelerated and separated into two bunches. When the two streams of protons reach the required energy and speed the protons are released to the target station line and collided into the target. The first target is a thin carbon block for the production of muons and the main target station is a tungsten block where the neutrons are produced. There are two target stations at ISIS. *Target Station 1* is the main target, where the SXD instrument is situated; *Target Station 2* has recently been developed for slow neutron experiments and has not been used in this work.

The use of polychromatic beams for single crystal diffraction experiments can normally cause difficulties with the integration of the data due to the overlay of diffraction from the patterns resulting from different wavelengths. At ISIS, however, the neutron beams are produced in a pulsed manner and as a result there is a linear relationship between the time taken for the neutron to travel along its flight path (from target to sample to detector) and the wavelength of neutrons (and hence to the *d*-spacing for a given scattering angle)[131]. Since the time is recorded between the spallation process and the detection of the neutron beam, orders of a reflection resulting from neutrons of different wavelengths are collected in the same detector pixel but each order is collected at a different time-of-flight. This separation makes the integration of the data much more straightforward.

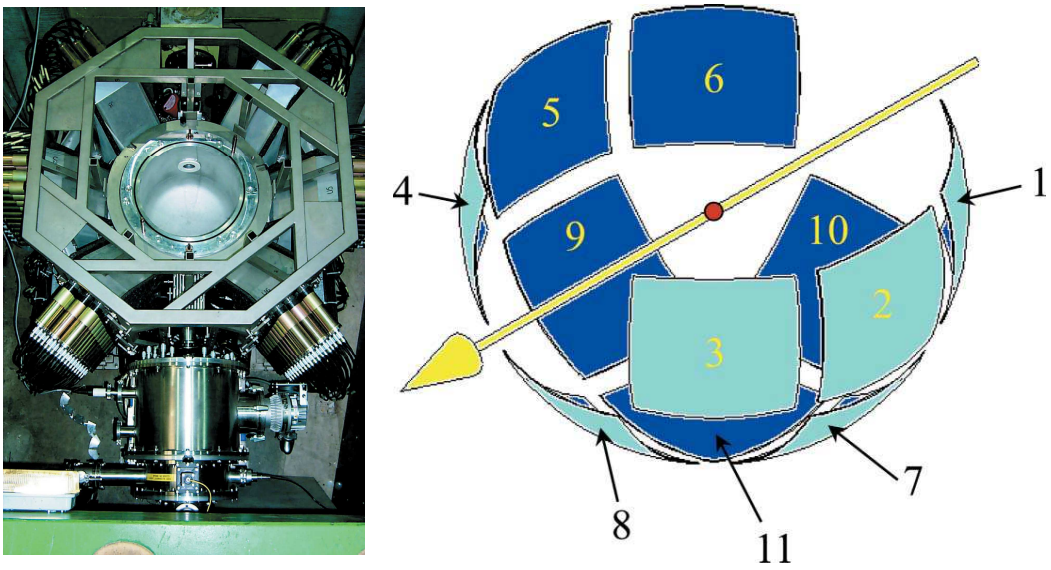

Figure 3-6. View of the SXD instrument from the top showing the sample tank with the surrounding detectors (left) and a diagram of the detector layout of the 11 detectors around the sample on the instrument (right)[131].

The SXD instrument is equipped with a number of position sensitive detectors (*Figure 3-6*). There are 11 detectors around the sample tank covering a large area of reciprocal space in a wide scattering angle range, which makes collecting data very efficient. It also has an advantage by using time-of-flight method, as outlined above, which makes it possible to collect scattering data in reciprocal space between two Ewald spheres of radius from $2\pi/\lambda_{min}$ to $2\pi/\lambda_{max}$ (*Figure 3-7*). The maximum wavelength range accessible is between ~0.2 and ~8.5 Å. This enables collection of a large number of Bragg reflections with a single crystal orientation.

In an SXD experiment, due to the relatively low flux of the neutron source, a multiple crystal sample approach is normally used to speed up the data collection[151]. A small number of crystals of the same compound are mounted on the diffractometer in different orientations (typically three, with a maximum number of six individual crystals in the stack) and the Bragg reflections are recorded simultaneously for all crystals. Using the time-sorted Laue method means that after the data collection the software SXD 2001[131] can be used to extract the reflections for each individual crystal and omit any overlapped reflections (where two reflections from different crystals occur too close to each

other on the detector – in position and time-of-flight). With this enhancement of the diffractometer data collection method, a faster data collection time is achieved, in some cases taking just five hours per data set[130]. The sample size for single crystal neutron diffraction on SXD has a minimum requirement of ~1 mm^3 for efficient data collection, with the maximum unit cell size up to ~6000 $Å^3$.

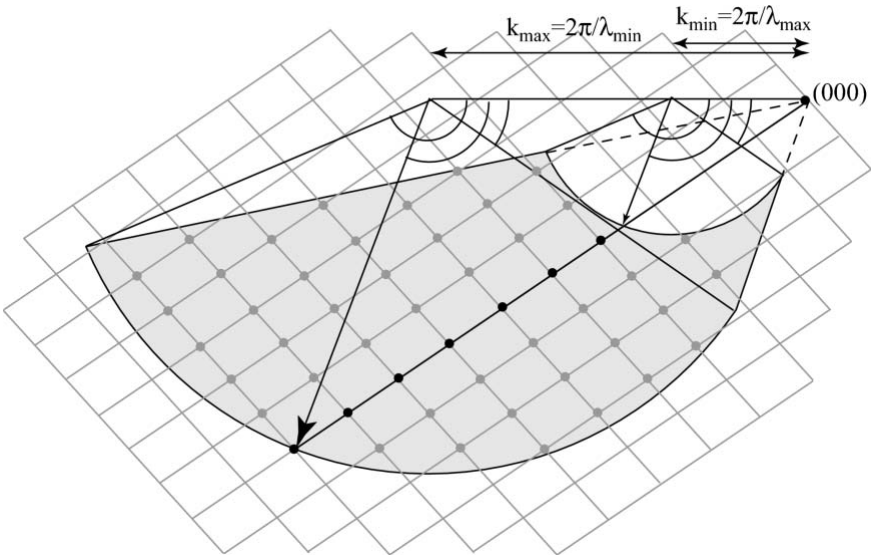

Figure 3-7. The Laue construction for data collection using an area detector, showing the Ewald spheres of different radii corresponding to different wavelengths of the incident beam. Using time-of-flight, the diffraction corresponding to different wavelengths is separated; all of the reflections inside the shaded area of the diagram are measured in a single shot[131].

The collection of a large number of reflections with a single crystal orientation also makes it possible to create a simple sample environment geometry, and hence it allows the routine use of sample environment equipment such as pressure cells. SXD is equipped with a closed-cycle helium refrigerator and a helium cryostat making it possible to make measurements in a temperature range between 1.6K and 300K and use of a pressure cell with pressures up to 0.5GPa routinely available.

3.4.2 VIVALDI at ILL

The VIVALDI (Very Intense Vertical Axis Laue Diffractometer) is situated at the ILL (Institut Laue-Langevin) international research centre based in Grenoble, France[152]. At ILL, the neutron production is realised through nuclear fission and the reactor is one of the most powerful neutron sources in the world for scattering experiments, and is equipped with more than 40 instruments. The reactor produces 1.5×10^{15} neutrons/second/cm^2 and it operates in reactor cycles of 50 days continuous operation before refuelling; four reactor cycles a year are operated, leading to 200 days of operation in a year. The produced neutrons are in a large range of (initially high) energies, but these can be tuned by moderators to the lower (close to thermal) energies required by the instruments. Once the neutrons have been slowed in the moderators, they are usually passed through a monochromator to produce the desired wavelength for the particular experiment. However, in some cases a wavelength range is selected instead, by use of filters placed in the white beam.

The instrument used in the work presented here, VIVALDI, has been running since late 2001 (*Figure 3-8*). The diffractometer operates with thermal neutrons using a wide spectrum of the white beam. The instrument can operate with wavelengths between 0.8–5.2 Å, with the wavelength range 0.8-3.0 Å usually chosen for small molecule experiments such as those presented here. Using this white beam for data collection gives the advantage of very fast data collection compared to monochromatic beam, but has a big disadvantage, by adding extra complication with data processing. The diffractometer is equipped with a cylindrical image plate detector around the sample, covering 2π Sr solid angle with an area of 800 x 400 mm^2. The image plate has to be read and erased after every image collected but this is all controlled by the software of the instrument.

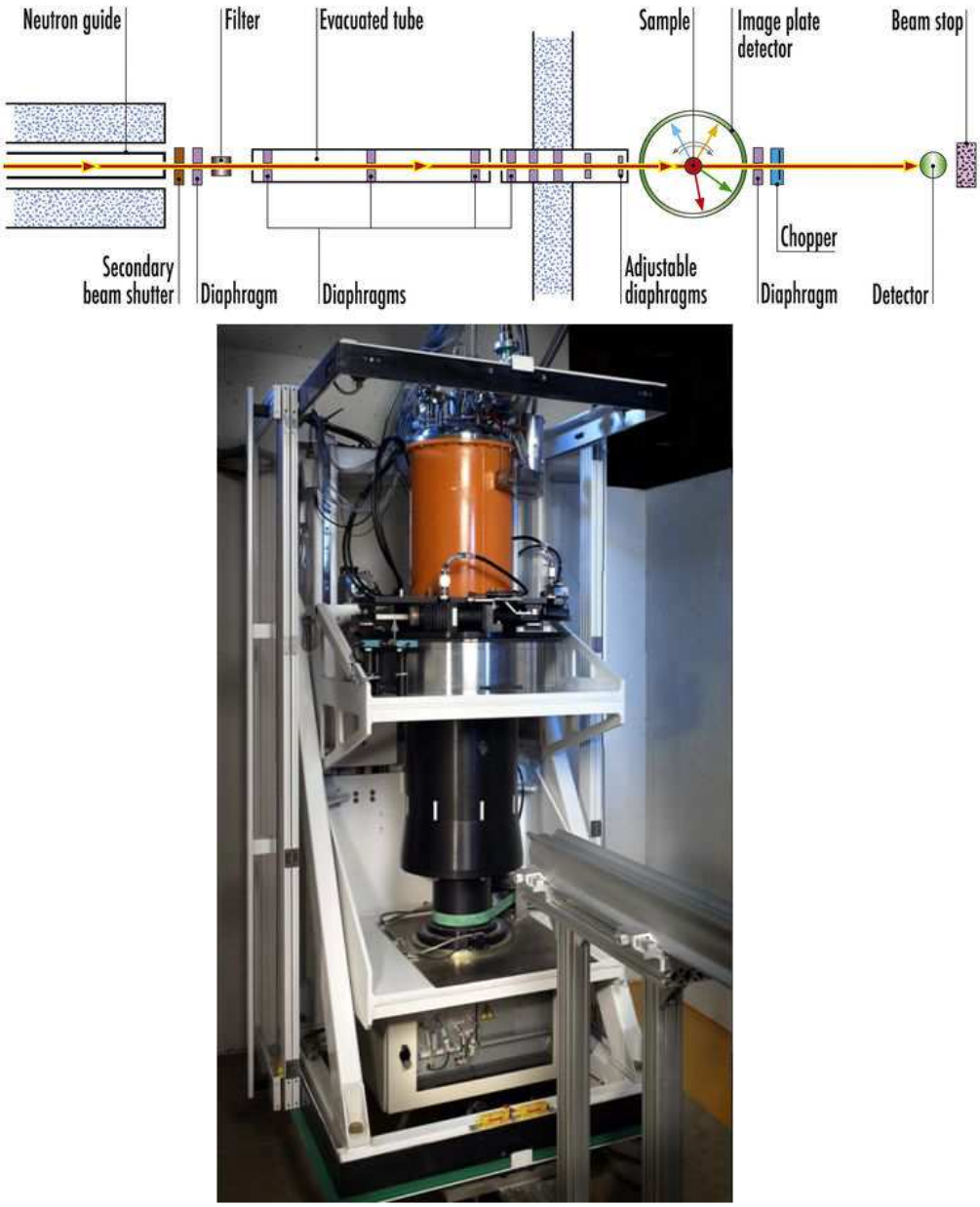

Figure 3-8. The instrument layout (top) and a picture of the VIVALDI instrument at the ILL, Grenoble (bottom).

The instrument arrangement means that the flux of the neutron beam is high and with the use of a white beam not just faster data collection, but also smaller sample sizes can be used. The maximum unit cell parameters are limited to ~25 Å per cell axis to prevent overlap of reflections, which would further complicate the data processing. The instrument is equipped with a helium cryostat making possible data collections at a range of temperatures between

1.5 and 300 K and it is also equipped with a furnace increasing the possibility of data collection up to 1500 K. VIVALDI can also be used to carry out high pressure experiments, allowing use of a pressure cell of up to 49 mm in diameter.

Chapter 4

4. Molecular complexes of DMAN and benzoic acids – inducing charge-assisted short hydrogen bonds via proton transfer

As described before (Chapter 1) hydrogen bonding between the benzoic acids has attracted a large amount of research. There are many reported structures of benzoic acids and their complexes with different molecules have been studied and compared. However, these structures are very different from each other, with many parameters, hydrogen bonds, short contacts, etc, involved in the creation of the molecular complex and it packing in their crystal structure. The number of parameters involved can make it difficult to analyse trends in these structures and understanding the influence of the underlying effects, that are often competing with each other. This the reason for identifying and using trends in the motifs adopted by the hydrogen-bonded components often seen and recognised as a powerful technique in crystal engineering.

While the recognition of molecular motifs in crystal structures is a good starting point, in trying to utilise these in controlling molecular self-assembly, there is a rather inconvenient fact that crystallisation usually happens in a single experimental step. When compared to synthetic chemistry, crystallisation has this disadvantage. In the former, there are usually several steps from the starting material to the final product and during these steps there are many variables that can be changed in the process. Because of this, if one step did not work in the initially planned way it can be changed, while this is not true for normal crystallisation processes. As a result, to gain a better understanding of the different ways in which intermolecular interactions affects the packing in the crystal structure of molecular complexes, it is essential to have an extensive and systematic study of complexes. In this way, it is possible to create a large number of molecular complexes with just a small number of variables in the starting materials and follow the changes occurring in their molecular complexes. In order to achieve this it is important to find a motif which can be used as an engineering tool in the co-crystallisation of these series of complexes, as gaining information of such series can lead to a better understanding of their

behaviour in the molecular complexes and can open opportunities in fine tuning of crystal structures.

This chapter is intended to present the extensive research carried out in this project on the co-crystallisation of the DMAN proton sponge material with a series of co-components in creating molecular complexes. This will include the investigation of a full series of halogen substituted benzoic acids, presenting a full detailed comparison of their structures, including proton transfer, supramolecular motifs and packing patterns.

Values of the relevant bond lengths and angles which will be discussed through this chapter are listed in *Table 4-1* with the legend of particular distances/angles marked on *Figure 4-1*.

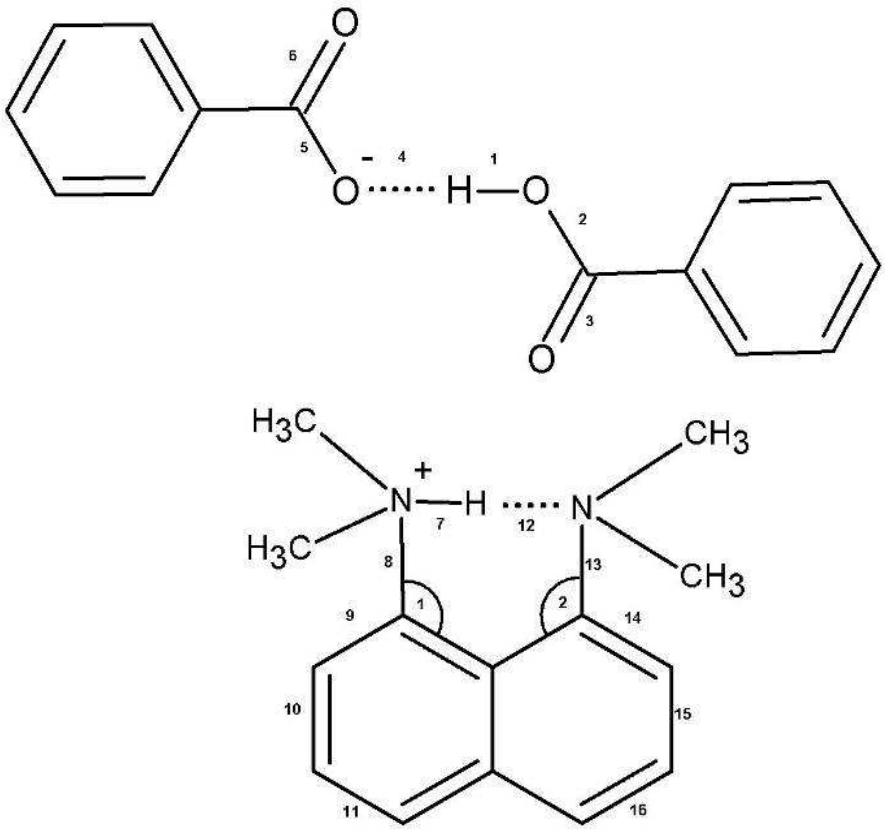

Figure 4-1. Diagram of the DIMER$^-$ (top) and the DMANH$^+$ (bottom) marking the bonds listed in Table 4-1 .

Table 4-1. Bond lengths and angles measured at 100/110K from X-ray data (and the 100K neutron values for DMAN:2IBA) in the molecular complexes of DMAN and halogen substituted benzoic acid marked in Figure 4-1.

bond (Å) /angle (˚)	DMAN : BA	DMAN : 2FBA	DMAN : 2CBA	DMAN : 2BBA	DMAN : 2IBA x-ray	DMAN : 2IBA neutron	DMAN : 3FBA	DMAN : 3FBA hydrate	DMAN : 3CBA	DMAN : 3BBA	DMAN : 3BBA_2	DMAN : 3IBA	DMAN : 4FBA hydrate	DMAN : 4CBA	DMAN : 4BBA	DMAN : 4IBA
1. O-H	1.13(2)	1.18(3)	1.21(3)	1.10(4)	1.09(4)	1.207(4)	1.16(4)	-	1.03(3)	0.821(5)	0.819(5)	1.14(4)	1.16(3)	1.13(3)	1.11(5)	1.57(7)
2. C-O	1.302(1)	1.297(2)	1.285(2)	1.282(2)	1.294(3)	1.291(2)	1.292(2)	-	1.309(2)	1.294(8)	1.295(8)	1.298(3)	1.271(3)	1.310(2)	1.305(3)	1.309(5)
3. C=O	1.223(2)	1.221(3)	1.212(2)	1.212(3)	1.227(3)	1.225(2)	1.221(2)	-	1.220(2)	1.211(8)	1.205(8)	1.223(3)	1.212(3)	1.221(2)	1.214(4)	1.217(5)
4. O···H	1.35(3)	1.28(3)	1.23(3)	1.35(4)	1.38(4)	1.249(4)	1.29(4)	-	1.45(3)	1.750(5)	1.714(4)	1.33(4)	1.25(3)	1.34(3)	1.38(5)	0.90(7)
5. C-O	1.275(2)	1.279(2)	1.292(2)	1.288(2)	1.279(3)	1.280(3)	1.288(3)	-	1.277(2)	1.284(8)	1.296(8)	1.281(3)	1.278(3)	1.289(2)	1.283(3)	1.290(4)
6. C=O	1.234(2)	1.227(2)	1.224(2)	1.225(2)	1.230(3)	1.231(3)	1.227(2)	-	1.237(2)	1.221(9)	1.236(9)	1.232(3)	1.207(3)	1.234(2)	1.242(3)	1.225(5)
7. N-H	1.25(2)	1.30(3)	1.08(2)	1.21(3)	1.08(4)	1.198(5)	1.02(3)	1.08(2)	1.09(2)	-	-	1.05(4)	1.09(2)	0.99(2)	0.96(3)	1.08(3)
8. C-N	1.466(2)	1.463(2)	1.466(2)	1.468(2)	1.470(3)	1.460(2)	1.475(2)	1.474(2)	1.476(2)	1.493(9)	1.496(9)	1.467(3)	1.448(3)	1.475(2)	1.478(3)	1.478(4)
9. C-C	1.362(2)	1.368(3)	1.371(2)	1.374(2)	1.370(4)	1.373(3)	1.368(2)	1.368(2)	1.369(2)	1.35(1)	1.38(1)	1.367(4)	1.353(3)	1.369(2)	1.367(3)	1.365(5)
10. C-C	1.411(2)	1.403(2)	1.410(2)	1.412(3)	1.410(4)	1.412(2)	1.407(2)	1.413(2)	1.407(2)	1.44(1)	1.41(1)	1.401(3)	1.381(3)	1.407(3)	1.412(4)	1.402(5)
11. C-C	1.362(2)	1.366(3)	1.365(2)	1.359(3)	1.367(3)	1.370(2)	1.366(3)	1.362(2)	1.370(3)	1.37(1)	1.37(1)	1.367(3)	1.345(3)	1.362(2)	1.361(4)	1.364(5)
12. N···H	1.38(2)	1.33(3)	1.53(3)	1.41(3)	1.51(4)	1.414(5)	1.63(3)	1.56(2)	1.55(2)	-	-	1.57(4)	1.51(2)	1.65(1)	1.67(3)	1.57(3)
13. C-N	1.462(2)	1.468(2)	1.460(2)	1.463(2)	1.461(3)	1.451(2)	1.460(2)	1.458(2)	1.459(2)	1.455(9)	1.461(8)	1.461(3)	1.432(3)	1.454(2)	1.456(3)	1.450(4)
14. C-C	1.363(2)	1.365(3)	1.370(2)	1.372(3)	1.364(3)	1.369(2)	1.373(3)	1.372(2)	1.373(2)	1.35(1)	1.38(1)	1.372(3)	1.354(3)	1.370(2)	1.369(3)	1.378(5)
15. C-C	1.407(2)	1.406(2)	1.414(2)	1.415(3)	1.406(4)	1.412(2)	1.413(2)	1.410(2)	1.408(2)	1.42(1)	1.42(1)	1.403(3)	1.378(3)	1.408(3)	1.417(3)	1.392(5)
16. C-C	1.359(2)	1.363(3)	1.364(2)	1.365(2)	1.365(5)	1.373(3)	1.367(3)	1.366(2)	1.364(3)	1.36(1)	1.36(1)	1.365(4)	1.339(3)	1.360(3)	1.366(4)	1.377(5)
1. N-C-C	118.2(1)	118.2(2)	118.1(1)	118.1(1)	117.9(2)	1.207(4)	118.3(1)	118.3(1)	118.2(1)	116.8(6)	117.7(6)	118.0(2)	118.1(2)	118.5(1)	118.2(2)	118.1(3)
2. N-C-C	118.4(1)	117.9(2)	118.0(1)	118.5(1)	117.9(2)	1.291(2)	118.5(2)	118.3(1)	118.3(1)	118.0(6)	119.0(6)	118.0(2)	118.5(2)	118.6(1)	118.2(2)	118.7(3)

4.1 1:2 DMAN : benzoic acid molecular complex

The molecular complex of DMAN : benzoic acid offers a good representation of the typical trends found in these molecular complexes and it will be presented with full descriptive details. The other molecular complexes of DMAN in the series with benzoic acid derivatives can then compared to this complex as the only change is in the nature of the substituent on the benzoic acids. The structures of the DMAN: benzoic acid complexes are also investigated by variable temperature techniques to unveil any potential interesting hydrogen bond (HB) behaviour. The study is therefore focused not only on the structural behaviour occurring as a change of the substituent but also the possibility of tuning the HB behaviour with temperature within the short hydrogen bonds present in these structures.

1:2 Molecular complex of DMAN : benzoic acid (BA) - 2:1 molar ratio of BA (0.1 g) and DMAN (0.114 g) were dissolved in methanol and evaporated at a constant temperature of 36˚C, slowing the evaporation by closing the vial with a pierced small clipped lid. After the evaporation of the solvent, colourless prisms were formed. Single crystal X-ray diffraction data were collected at 110, 200 and 300K on a Bruker Nonius Kappa CCD. The data were solved with SHELXS97 and refined with SHELXL97, within the WinGX package, with the details of the crystal data listed in *Table 4-2*.

Table 4-2. X-ray data collection and refinement information for the 1:2 DMAN : BA complex.

Compound	1:2 DMAN : BA		
Diffractometer	Nonius Kappa CCD	Nonius Kappa CCD	Rigaku R-AXIS Rapid
Formula	$C_{28}H_{30}N_2O_4$	$C_{28}H_{30}N_2O_4$	$C_{28}H_{30}N_2O_4$
Molecular weight / gmol^{-1}	458.54	458.54	458.54
Temperature (K)	110	200	300
Space Group	$P\bar{1}$	$P\bar{1}$	$P\bar{1}$
a (Å)	10.3129(3)	10.3771(3)	10.4803(15)
b (Å)	11.6275(4)	11.7119(5)	11.8302(15)
c (Å)	12.0263(5)	12.0553(5)	12.1478(17)
α (°)	76.899(2)	77.045(2)	77.133(4)
β (°)	67.781(2)	67.617(2)	67.453(5)
γ (°)	65.502(2)	65.429(2)	65.315(4)
Volume (Å^3)	1210.66(7)	1228.30(8)	1260.4(3)
Z	2	2	2
θ range/°	1.84-30.15	1.83-30.1	3.34-27.48
Completeness (%)	99.3	98.9	99.4
Reflections Collected	22991	23098	29011
Independent	7107	7147	5764
Refln (obs.I>2theta(I))	4601	3543	3361
R_{int}	0.0451	0.0524	0.0328
Data/Rest./Param.	7107/0/427	7147/0/427	5764/0/427
GooF on F^2	1.014	0.997	1.03
R_1 (Observed)	0.0485	0.0539	0.0564
R_1 (all)	0.0919	0.1368	0.1007
wR_2 (all)	0.1211	0.1457	0.1665
ρ (max / min) / e-Å^{-3}	0.251 / -0.221	0.154 / -0.182	0.167 / -0.164
RMS / eÅ^{-3}	0.043	0.035	0.04

The co-crystallisation of DMAN and benzoic acid resulted in a molecular complex of 1:2 DMAN:BA ratio. The DMAN molecule is protonated ($DMANH^+$) by transfer of a carboxylic acid proton from one of the BA molecules. The deprotonated BA molecule, in order stabilise the charge loss, bonds to the other BA molecule, creating a very short very strong charge-assisted $COOH\cdots COO^-$ hydrogen bond (SSHB) between the BA molecules. To allow for easier description an abbreviation will be used for these pairs of benzoic acid molecules connected through a single HB, $DIMER^-$, thus differentiating them from the dimer motif of the double hydrogen bonded carboxylic acids discussed in more detail in Chapter 1. The unit cell contains two $DIMER^-$s of BA and two $DMANH^+$ molecules, the $DIMER^-$ of BA and the $DMANH^+$ molecule are presented in *Figure 4-2*.

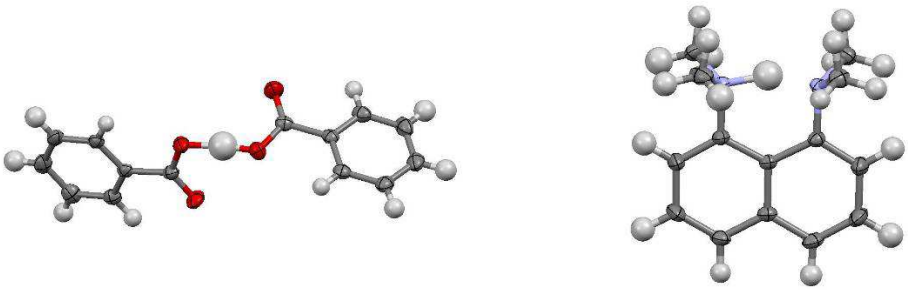

Figure 4-2. The single hydrogen bonded benzoic acid DIMER$^-$ (left) and the protonated DMANH$^+$ molecule (right).

The intramolecular HB between the two nitrogen atoms of the DMANH$^+$ molecule has, as expected, a shorter D····A distance, with an N····N distance of 2.574(1) Å at 110K, which is ~0.1 Å shorter than the distance found between the nitrogen atoms of unprotonated DMAN molecules[153]. This is in good agreement with the structures of the protonated DMANH$^+$ published in the literature[154]. The methyl groups on the nitrogen atoms are positioned perpendicular to the plane of the naphthalene group. The two BA molecules are connected through a single, charge-assisted, SSHB with an O····O separation of 2.477(1) Å. Since the BA molecules are connected through just a single SSHB the BA molecules have a rotational freedom around the intermolecular SSHB and the carboxylic groups are not in the planar arrangement found in the double hydrogen bonded dimers, instead showing a dihedral angle of 70.26° between the mean planes of their rings. In turn the individual BA molecules are not in a planar arrangement with the carboxylic acid / carboxylate groups showing dihedral angles of 10.45° and 7.24° to the respective parent benzene rings (*Figure 4-3*).

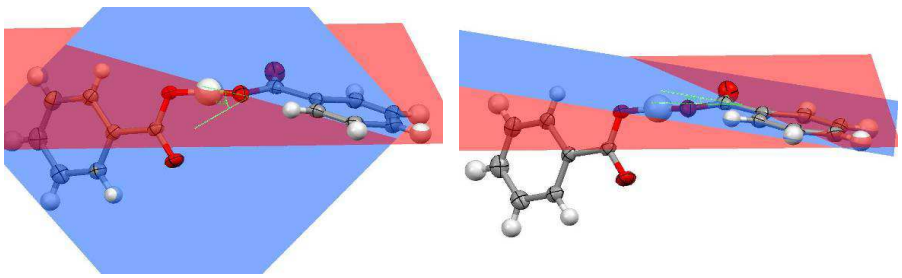

Figure 4-3. The benzoic acid DIMER$^-$ showing the dihedral angles between the planes of the carboxylic acid groups (left) and the planes between the benzene ring and the carboxyl group (right) of one of the BA molecules.

Pairs of $DMANH^+$ molecules are connected to each other through π····π displaced stacking interactions with a distance of ~2.99 Å between the planes (*Figure 4-4*).

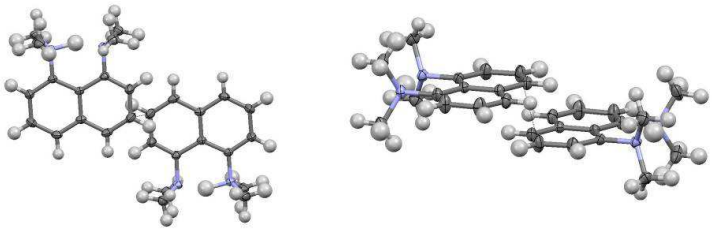

Figure 4-4. Pairs of $DMANH^+$ molecules showing through displaced π···π stacking, viewed from above (left) and along (right) the planes of $DMANH^+$ molecules.

The pairs of displaced π···π stacked DMAN molecules also stack in the overall packing (with a distance of 4.04 Å between the two planes of half-overlapped naphthalene groups of the $DMANH^+$) forming a chain of $DMANH^+$ molecules (*Figure 4-5*).

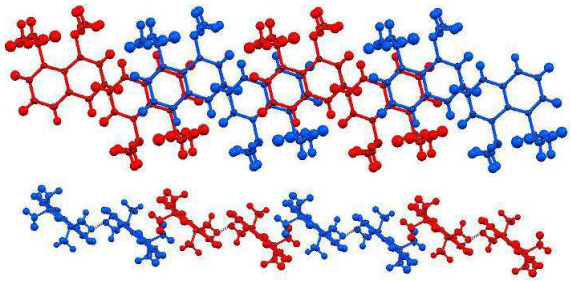

Figure 4-5. Chain formed from the $DMANH^+$ molecules; from a view in the plane (top) and along the plane of the naphthalene rings (bottom). Pairs of π···π stacked DMAN are coloured differently for clarity.

In recent work on four different molecular complexes of $DMANH^+$ with four organic acids containing N–H and O–H donor sides[155], it has been concluded that C–H···O and N–H···O weak hydrogen bonds work together with the π···π and C–H···π interactions (weak HBs, see Chapter 1.2.3) to form the overall packing. In three out of four structures a π···π tape stacking of $DMANH^+$ molecules has been recognised. However, no conclusiuon has been made regarding a distance limit of these interactions; i.e. there is no well-defined distance at which a

π···π interaction becomes simply a stacking in the overall packing. In the present work, to reveal these interactions and their significance and how they can be related to the weak hydrogen bonds, the stacking of $DMANH^+$ molecules will be followed and to omit any misunderstanding it will called π···π stacking in cases where the parallel stacking of the $DMANH^+$ molecules occurs at a distance shorter or equal with ~3.6 Å[156].

There are a number of intermolecular interactions between the $DIMER^-$ and the $DMANH^+$. The largest number of weak hydrogen bonds within the sums of van der Waals radii appears between the $DMANH^+$ molecule and the non hydrogen bonded oxygen atom of the benzoic acid (*Figure 4-6*). The oxygen atom of the carboxyl group is positioned above the four methyl groups in a close to symmetrical position between the two nitrogen atoms. Within the sum of van der Waals radii there are C–H···O weak hydrogen bonds with distances between 3.141(2) Å and 3.310(2) Å, one N···O with distance of 3.044(2) Å between the oxygen atom and the donor nitrogen atom of the N–H···N intramolecular hydrogen bond, and one O···H contact with a distance of 2.53(2) Å between the oxygen atom and the hydrogen atom from the N–H···N intramolecular HB.

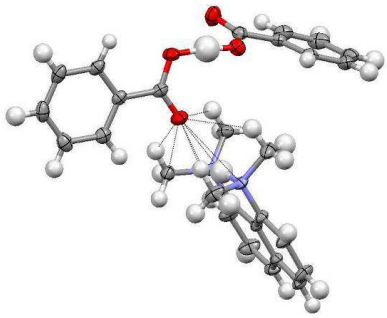

Figure 4-6. The short contacts between the non hydrogen bonded oxygen atom of the carboxylic acid and the $DMANH^+$ molecule.

Each individual $DMANH^+$ molecule is also connected to four other other $DIMER^-$s through a number of intermolecular short contacts. There are C–H···π weak hydrogen bonds between the benzene rings of three different $DIMER^-$s with lengths between ~3.01 Å and ~3.59 Å, between the methyl group of the naphthalene and the benzene ring of the $DIMER^-$ with a length of ~3.76 Å, in

front and behind the planes of the $DMANH^+$ molecule. There is also a C–H···π weak HB between the naphthalene and the benzene ring of the $DIMER^-$, positioned below the $DMANH^+$ molecule with a distance of ~3.88 Å (*Figure 4-7, left*). The $DMANH^+$ molecule is also connected to two $DIMER^-$ on the side of the molecule with C–H···π weak HBs between the $DMANH^+$ methyl and naphthalene groups and the two benzene rings of two $DIMER^-$s, with distances between ~3.59 Å and ~3.99 Å (*Figure 4-7, right*).

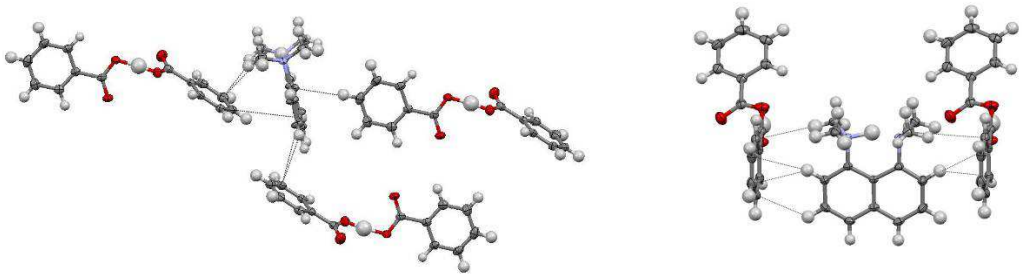

Figure 4-7. C–H···π weak hydrogen bonds between the $DMANH^+$ and the surrounding $DIMER^-$s; with the three $DIMER^-$s in front and behind the planes of the naphthalene and below the $DMANH^+$ molecule (left), and two on the $DIMER^-$s on the side of $DMANH^+$ molecule (right).

The structure as a whole can be described as chains of $DMANH^+$ molecules caged and held together by intermolecular interaction between the $DMANH^+$ and the $DIMER^-$ building blocks of the structure (*Figure 4-8*).

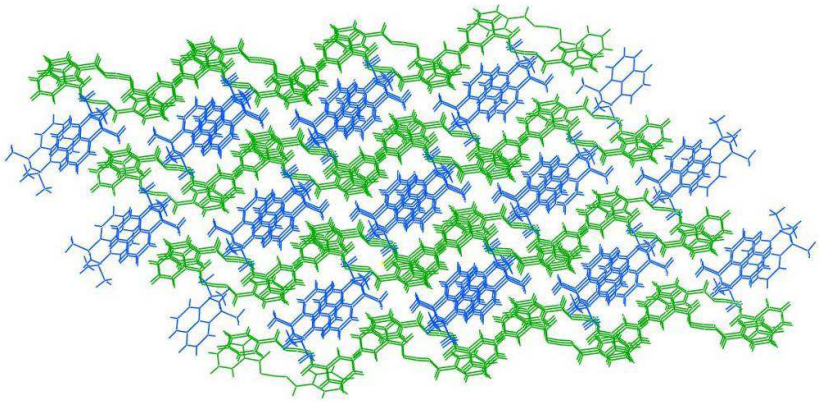

Figure 4-8. The build up of the structure along the chain of the $DMANH^+$ molecules (blue), surrounded by the BA $DIMER^-$s (green).

The intramolecular HB within the $DMANH^+$ molecule is asymmetrical with distances of N–H = 1.25(2) Å and H···N = 1.38(2) Å, with a large thermal parameter of the hydrogen atom. The asymmetric bonding is often reflected in the C–N (carbon of the naphthalene ring) bond lengths, with a slightly longer bond length at the donor site than the acceptor site. However, this difference is not significant in this case, and the symmetrically positioned C–C bond lengths in the naphthalene ring and the C-N-N bond angles between the donor acceptor side also agree within the magnitude of the standard uncertainties (*Table 4-1*). The hydrogen atom in the intermolecular charge-assisted SSHB in the $DIMER^-$ is positioned asymmetrically between the two oxygen atoms with O–H = 1.13(2) Å and H···O = 1.35(2) Å with similarly large isotropic thermal parameters compared to the rest of the hydrogen atoms in the structure to the intramolecular HB. While there is a difference between the length of the C=O and that of the C–O as is clear from the nature of the bonding, the carboxyl group from the donor side shows a greater deviation between the double and the single carbon oxygen bond than in the acceptor carboxylate group. The C–O bond length on the carboxyl group of the donor side is longer than that of the C–O in the carboxyl of the acceptor side. In addition, the C=O bond is shorter on the donor and longer on the acceptor side (*Table 4-1*). These bond length differences between the C–N bonds as well as the difference between C–O and C=O on the donor and acceptor side will be followed throughout the analysis of the series of complexes presented here, as they represent complementary information of these charge assisted hydrogen bonds and might be correlated to the position of the hydrogen atom within these hydrogen bonds.

Since there is no significant difference either between the two C–N bonds of the $DMANH^+$ or in the symmetrically positioned C–C bonds of the naphthalene ring, the position of the H atom in the $DMANH^+$ intramolecular hydrogen bond may result from fairly subtle forces in the structure. The complex has therefore been further investigated by varying the temperature to see if there is any variation in this hydrogen atom behaviour as a resulting of changing external conditions. Additional X-ray diffraction data sets were collected at temperatures of 200 and 300 K to investigate the positions and large thermal parameters of the hydrogen atoms in the HBs. With the increase of the temperature from 100K to 300K, both

the isotropic parameters of the hydrogen atoms and the anisotropic parameters of the rest of the atoms are increasing as expected (*Figure 4-9*), but as described before (Chapter 1), X-ray measurements can usually only give qualitatively better insight in the case of the hydrogen behaviour and any anomalous trends used to justify neutron data collection.

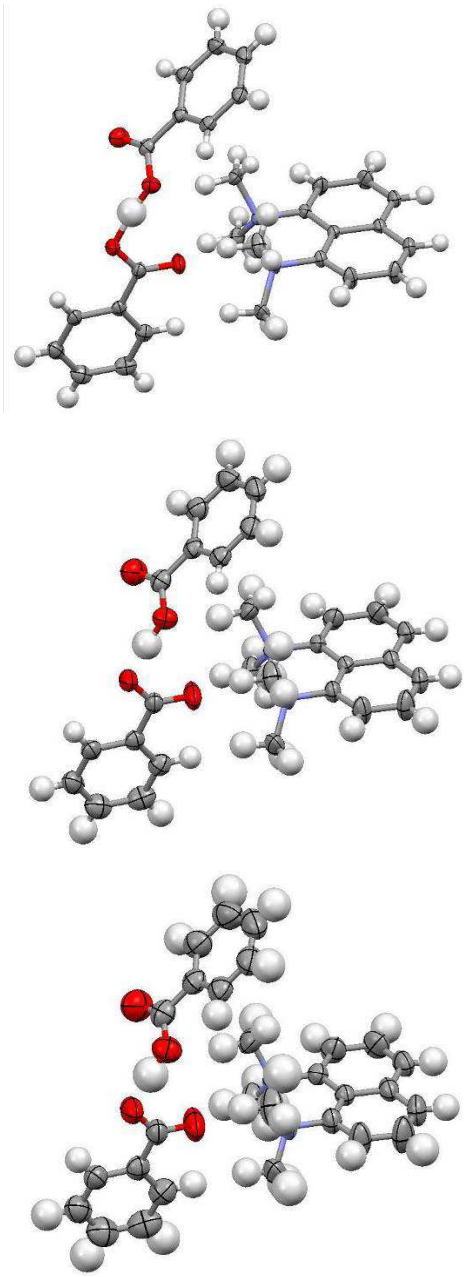

Figure 4-9. The evolution of structure of the 1:2 DMAN : BA complex as a function of temperature from top to bottom at 110, 200 and 300K, respectively.

The hydrogen bridges, both inter- and intramolecular, show a slight increase in their lengths as a result of the thermal expansion of the whole structure as expected with the increase of the temperature (*Table 4-3*). However there are differences in trends between the inter- and intramolecular donor-acceptor bond lengths. While the asymmetry in donor-acceptor distance remains approximately the same for the intermolecular hydrogen bond, in the case of the intramolecular HB between the two nitrogen atoms of the $DMANH^+$ molecules this appears not to be the case. At 110 K this is slightly asymmetrical, becoming more symmetrical at 200 K and at 300K becomes asymmetrical again, with a slight increase in the standard uncertainties caused by increased thermal parameters. It should be noted, though, that these trends are determined with low precision and reliability with the available X-ray data.

Table 4-3. The hydrogen bond distances as a function of temperature in the 1:2 molecular complex of DMAN : BA.

Type	Temp (K)	D····A (Å)	D–H (Å)	H···A (Å)
O–H···O	110	2.477(1)	1.13(2)	1.35(3)
	200	2.476(2)	1.11(3)	1.37(3)
	300	2.479(3)	1.13(4)	1.35(4)
N–H···N	110	2.574(1)	1.25(2)	1.38(2)
	200	2.580(2)	1.31(2)	1.31(2)
	300	2.586(2)	1.24(3)	1.39(3)

To investigate this possible effect further, difference Fourier maps were generated in the planes of each of the hydrogen bonds by omitting the hydrogen from the calculated electron density from the refinement, hence revealing the electron density of the hydrogen measured from the experiment (*Figure 4-10*).

In the 110K difference Fourier map, the shape of the electron density shows a slight deviation from the spherical shape with the electron density concentrated closer to the donor atom, explaining the slightly asymmetrical hydrogen bridge measure from the structure solution. Since the isotropic refinement of the hydrogen atom can not take into account the orientation or shape of the hydrogen atom electron density, the large isotropic parameter determined in the refinement and shown in the image taken from the Mercury[144] can be explained with the elongation shown on the difference Fourier map at 110K.

However, it has to be noted the maximum of the electron density peak does not represent the refined hydrogen position. The correct assignment of the hydrogen atoms donor side will be followed through this work and it will be attempted to identify any relationship between the donor side of the hydrogen atom and the C–N bond lengths or the C–O bond lengths in the case of the intramolecular N–H···N and intermolecular O–H···O hydrogen bonds, respectively. At 200K the hydrogen bond apparently becomes symmetrical from the measurement with an even larger isotropic displacement parameter. While recognising that X-ray determinations are inaccurate in this respect, this can also be explained through the electron density of the hydrogen, which appears with a split nature concentrated in two different positions across the hydrogen bond. The 300K difference Fourier map shows a similar electron density of the hydrogen to that in the 110K measurement.

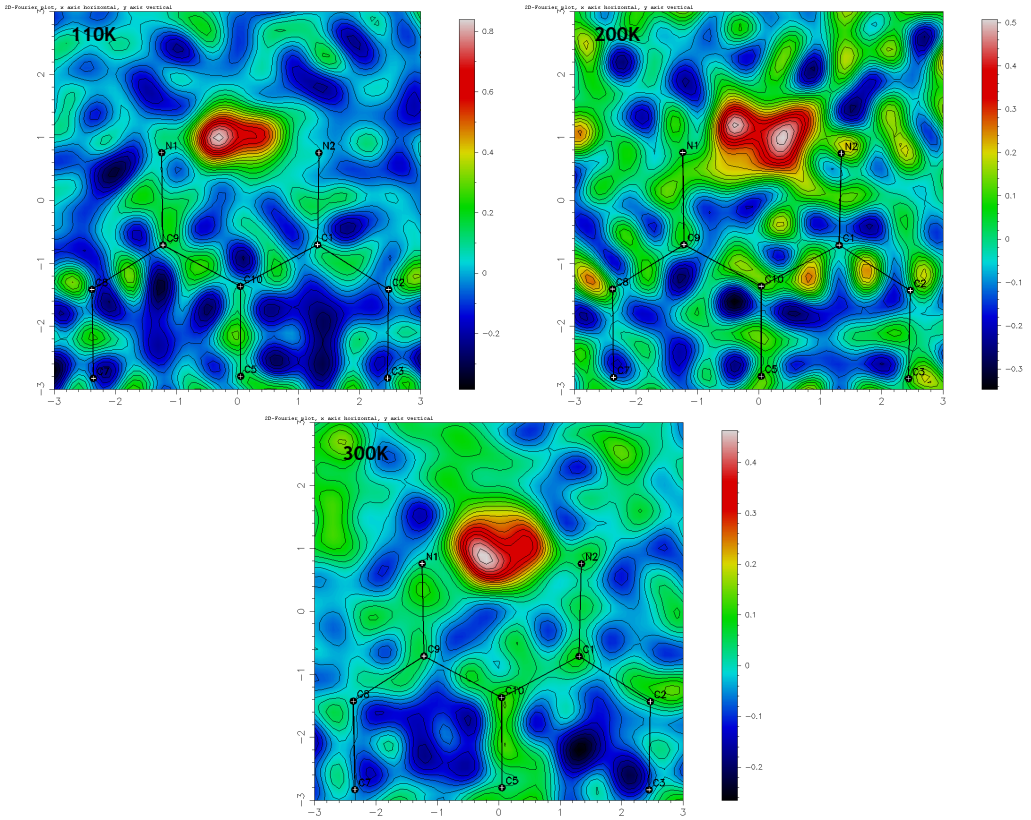

Figure 4-10. Difference Fourier maps generated in the plane of the naphthalene ring of the DMANH$^+$ at the three collected temperatures (110, 200 and 300K) with hydrogen omitted from the calculated structure of the 1:2 DMAN : BA molecular complex.

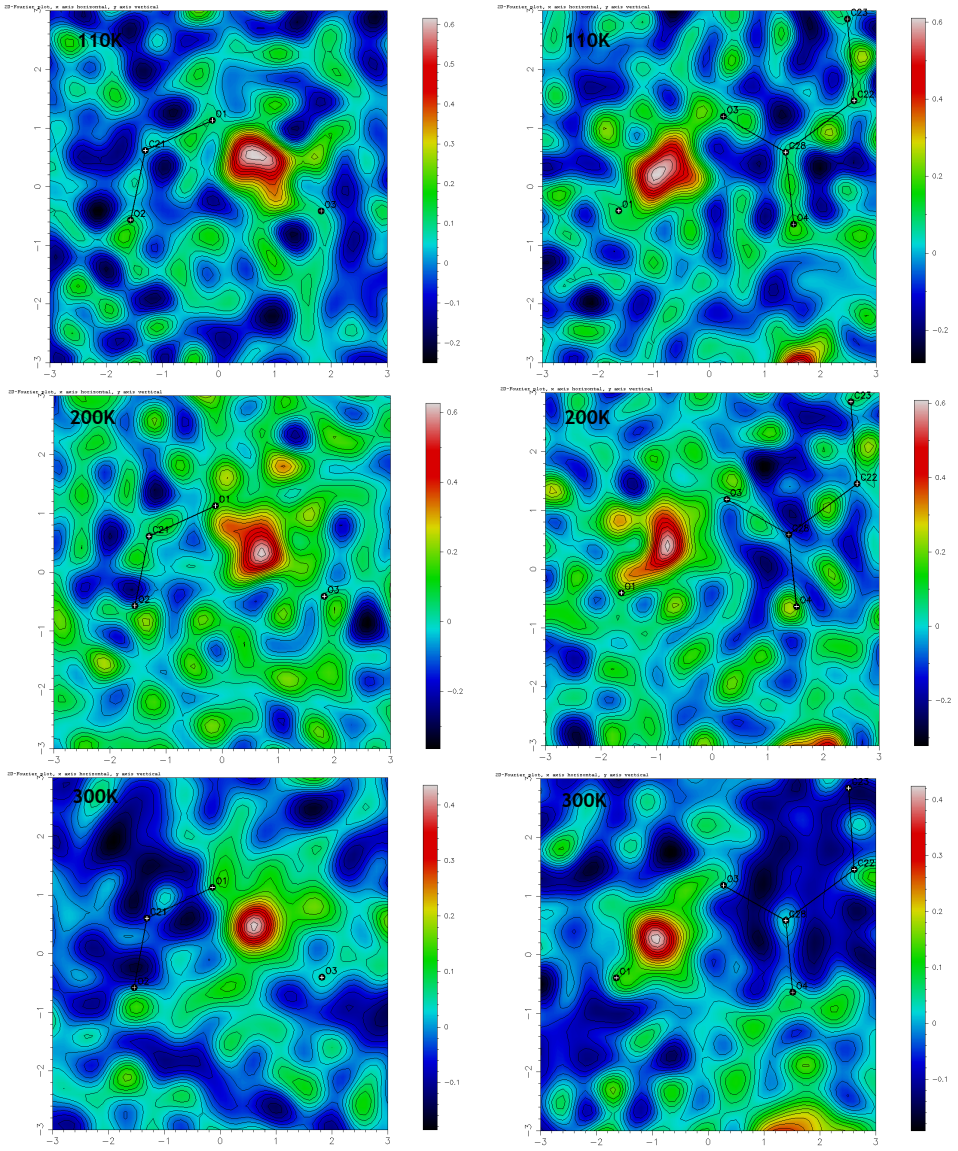

Figure 4-11. Difference Fourier maps showing the electron density of the hydrogen atom within the SSHB between the BA DIMER⁻s. Maps calculated in the two planes of the carboxyl groups at the temperatures marked on the maps.

In the hydrogen bond between the BA DIMER⁻s, the hydrogen position does not show significant difference at the temperatures studied but the large isotropic thermal parameters of the hydrogen even at low temperature suggest some elongation in the electron density of the hydrogen. Difference Fourier maps were generated in plane of the carboxylic acids from both benzoic acids (*Figure 4-11*). At low temperature the electron density shows a slight elongation in the hydrogen atom from the donor side to the acceptor, with most of the electron

density concentrated closer to the donor atom. With the increase of temperature this minor deviation of the electron density disappears at 300K with a regular spherical electron density in good agreement with the position and refined isotropic thermal parameter of the hydrogen atom in the HB from the measurements. Supplementary neutron diffraction would be required for accurate determination of the hydrogen atom parameters, but for reasons mentioned above (requirement of access to a large neutron facility), there is no neutron data available in the case of this structure, although there will be structures presented later in this work that have been determined with both neutron and X-ray diffraction methods.

4.2 Molecular complexes of DMAN and *ortho*-substituted benzoic acids

In this section a comparison of a series of four ortho-halogen substituted benzoic acids molecular complexes with DMAN studied by X-ray diffraction will be presented. In the case of the 2-iodobenzoic acid : DMAN complex neutron diffraction data will also be presented.

Experimental data

1:2 Molecular complex of DMAN : 2-fluorobenzoic acid (2FBA) - 1:1 molar ratio of 2FBA (0.1 g) and DMAN (0.065 g) were dissolved in dichloromethane and evaporated at room temperature, slowing the evaporation by closing the vial with a pierced small clipped lid. After the evaporation of the solvent, colourless blocks were formed. Single crystal X-ray diffraction data were collected on a Bruker Nonius Kappa CCD diffractometer at 100, 200 and 290K. The data were solved with SHELXS97 and refined with SHELXL97, within the WinGX package.

1:2 Molecular complex of DMAN : 2-chlorobenzoic acid (2CBA) - 1:2 molar ratio of DMAN and 2CBA were dissolved in isopropanol and evaporated at room temperature, slowing the evaporation by closing the vial with a small clipped lid. After the evaporation of the solvent, colourless blocks were formed. Single crystal X-ray diffraction data were collected on a Bruker APEX II diffractometer

at 100, 200 and 300K. The data were solved within the WinGX structure solution program suite.

1:2 Molecular complex of DMAN : 2-bromobenzoic acid (2BBA) - 1:2 molar ratio of DMAN and 2BBA were dissolved in diethyl ether and evaporated at room temperature, slowing the evaporation by closing the vial with a small clipped lid. After the evaporation of the solvent colourless blocks were formed. Single crystal X-ray diffraction data were collected on a Bruker Nonius Kappa CCD diffractometer at 110, 200 and 300K. The data were solved within the WinGX structure solution program suite. The hydrogen atoms are generated on the carbon atoms in the refinement of the 300K data set.

1:2 Molecular complex of DMAN : 2-iodobenzoic acid (2IBA) - 1:2 molar ratio of DMAN (0.1 g) and 2IBA (0.232 g) were dissolved in acetone and evaporated at room temperature, slowing the evaporation by closing the vial with a small clipped lid. After the evaporation of the solvent, colourless blocks were formed. Single crystal X-ray diffraction data were collected on a Bruker Nonius Kappa CCD diffractometer at 100, 200 and 300K. The data were solved within the WinGX structure solution program suite. Large single crystals suitable for neutron diffraction were grown at a constant temperature of 4˚C in a 100 mL beaker using 20 mL solvent and 0.5 g DMAN with 1.15 g 2IBA, slowing down the evaporation by covering the beaker with pierced parafilm. Variable temperature neutron diffraction data was collected at the ILL research centre on the VIVALDI diffractometer at temperatures of 30, 100, 200 and 300K. The neutron structure was refined within the WinGX program suite, using the X-ray determined structure as a starting point.

The crystallographic data for the structures are summarised in *Table 4-4* and *Table 4-5*.

Table 4-4. Crystallographic data of molecular complexes of DMAN with 2FBA, 2CBA, 2BBA from the X-ray refinements.

Compound	1:2 DMAN : 2FBA			1:2 DMAN : 2CBA			1:2 DMAN : 2BBA		
Diffractometer	Nonius Kappa CCD	Nonius Kappa CCD	Nonius Kappa CCD	Bruker Apex II	Bruker Apex II	Bruker Apex II	Nonius Kappa CCD	Nonius Kappa CCD	Nonius Kappa CCD
Formula	$C_{28}H_{30}N_2F_2O_4$	$C_{28}H_{30}N_2F_2O_4$	$C_{28}H_{30}N_2F_2O_4$	$C_{28}H_{28}Cl_2N_2O_4$	$C_{28}H_{28}Cl_2N_2O_4$	$C_{28}H_{28}Cl_2N_2O_4$	$C_{28}H_{28}N_2Br_2O_4$	$C_{28}H_{28}N_2Br_2O_4$	$C_{28}H_{28}N_2Br_2O_4$
Molecular weight / gmol^{-1}	494.52	494.52	494.52	527.42	527.42	527.42	616.34	616.34	616.34
Temperature (K)	100	200	290	100	200	300	110	200	300
Space Group	$P\bar{1}$	$P\bar{1}$	$P\bar{1}$	$P2_1/n$	$P2_1/n$	$P2_1/n$	$P2_1/n$	$P2_1/n$	$P\,2_1/n$
a (Å)	10.1927(4)	10.2380(3)	10.2661(3)	12.0499(4)	12.1108(4)	12.1593(9)	12.1469(2)	12.1849(2)	12.2376(2)
b (Å)	10.7936(5)	10.8940(3)	11.0212(4)	9.8672(3)	9.9552(3)	10.0811(7)	9.9425(2)	10.0223(2)	10.1407(3)
c (Å)	12.6360(4)	12.6815(3)	12.7509(4)	21.7068(6)	21.7811(6)	21.8520(14)	21.7278(4)	21.7919(4)	21.8559(5)
α (°)	72.193(2)	72.204(2)	72.277(2)	90	90	90	90	90	90
β (°)	68.765(2)	68.798(2)	68.838(2)	98.123(2)	98.085(2)	97.960(4)	97.5620(10)	97.6250(10)	97.620(2)
γ (°)	88.857(2)	89.442(2)	90.261(2)	90	90	90	90	90	90
Volume (Å^3)	1227.22(8)	1247.45(6)	1270.87(7)	2555.02(13)	2599.95(14)	2652.8(3)	2601.26	2637.71(8)	2688.32(11)
Z	2	2	2	4	4	4	4	4	4
θ range/°	0.83 – 27.5	1.82 – 27.48	1.81 – 27.57	1.83 - 29.13	1.82 -29.99	1.82 - 26.9	1.82- 30.01	1.82- 30.05	1.82- 30.034
Completeness (%)	99.4	99.6	99	100	99.5	98.4	99.9	99.8	98.8
Reflections Collected	19159	20822	20818	42381	42528	36948	41206	42248	40359
Independent	5597	5703	5819	6881	6889	5639	7573	7704	7867
Refln (obs.I>2theta(I))	3876	3774	3093	5435	4623	3534	6279	5552	4138
R_{int}	0.0515	0.0492	0.0503	0.0423	0.0472	0.0434	0.0729	0.0809	0.0905
Data/Rest./Param.	5597/0/433	5703/0/433	5819/0/433	6881/0/455	6889/0/455	5639/0/455	7573/16/475	7573/16/475	7876/16/375
GooF on F^2	1.033	1.025	1.023	1.016	1.022	1.022	1.054	1.042	1.026
R_1 (Observed)	0.0463	0.0492	0.0597	0.0411	0.0475	0.0592	0.0319	0.0433	0.0608
R_1 (all)	0.083	0.0877	0.1275	0.0564	0.0781	0.0974	0.0448	0.0715	0.1303
wR_2 (all)	0.1171	0.132	0.1777	0.1088	0.1322	0.1857	0.0754	0.1062	0.1684
ρ (max / min) / e-Å^{-3}	0.561 / -0.269	0.413 / -0.215	0.374 / -0.23	0.392 / -0.248	0.485 / -0.376	0.595 / -0.436	0.631 / -0.629	0.662 / -0.837	0.994 / -0.865
RMS / eÅ^{-3}	0.052	0.041	0.036	0.055	0.047	0.042	0.071	0.069	0.066

Table 4-5. Crystallographic data table of molecular complexes of DMAN with 2IBA from X-ray and neutron refinements.

Compound	1:2 DMAN : 2IBA			Compound	1:2 DMAN : 2IBA			
Diffractometer	Nonius Kappa CCD	Nonius Kappa CCD	Nonius Kappa CCD	Diffractometer	VIVALDI	VIVALDI	VIVALDI	VIVALDI
Formula	$C_{28}H_{30}N_2I_2O_4$	$C_{28}H_{30}N_2I_2O_4$	$C_{28}H_{30}N_2I_2O_4$	Formula	$C_{28}H_{30}N_2I_2O_4$	$C_{28}H_{30}N_2I_2O_4$	$C_{28}H_{30}N_2I_2O_4$	$C_{28}H_{30}N_2I_2O_4$
Molecular weight / $gmol^{-1}$	710.32	710.32	710.32	Molecular weight / $gmol^{-1}$	710.32	710.32	710.32	710.32
Temperature (K)	100	200	300	Temperature (K)	30	100	200	300
Space Group	$P\bar{1}$	$P\bar{1}$	$P\bar{1}$	Space Group	$P\bar{1}$	$P\bar{1}$	$P\bar{1}$	$P\bar{1}$
a (Å)	10.4436(2)	10.4880(2)	10.5311(3)	a (Å)	10.410(5)	10.440(5)	10.480(5)	10.530(5)
b (Å)	11.0780(3)	11.1489(3)	11.2477(5)	b (Å)	11.040(5)	11.070(5)	11.140(5)	11.240(5)
c (Å)	12.7047(4)	12.7920(4)	12.8868(5)	c (Å)	12.640(5)	12.690(5)	12.780(5)	12.880(5)
α (°)	68.4740(10)	68.4328(11)	68.4190(10)	α (°)	68.490(10)	68.460(10)	68.420(10)	68.370(10)
β (°)	88.308(2)	88.6947 (16)	89.195(2)	β (°)	88.000(10)	88.200(10)	88.680(10)	89.070(10)
γ (°)	79.665(2)	79.5821(16)	79.496(2)	γ (°)	79.610(10)	79.580(10)	79.520(10)	79.440(10)
Volume ($Å^3$)	1344.10(6)	1366.55 (6)	1393.31(9)	Volume ($Å^3$)	1328.6(10)	1340.7(10)	1362.7(10)	1390.9(11)
Z	2	2	2	Z	2	2	2	2
θ range/°	1.72- 27.48	1.72 - 27.75	1.7 -27.41	$sin\theta/\lambda_{min}$ - $sin\theta/\lambda_{max}$	0.03 – 0.81	0.03 – 0.69	0.03 – 0.61	0.03 – 0.55
Completeness (%)	99.4	98.7	99.2	Completeness (%)	-	-	-	-
Reflections Collected	19110	20191	19462	Reflections Collected	17197	13248	9885	10151
Independent	6076	6259	6249	Independent	5346	4018	2984	2619
Refln (obs.I>2theta(I))	5363	5023	4151	Refln (obs.I>2theta(I))	4171	3062	2158	1826
R_{int}	0.0573	0.0499	0.0492	R_{int}	0.1026	0.1118	0.1261	0.1473
Data/Rest./Param.	6076/0/433	6259/0/433	6249/0/433	Data/Rest./Param.	5346/0/578	4018/0/578	2984/0/578	2619/0/578
GooF on F^2	1.043	1.037	1.011	GooF on F^2	1.147	1.112	1.095	1.129
R_1 (Observed)	0.0273	0.0339	0.0477	R_1 (Observed)	0.0402	0.0436	0.0447	0.0449
R_1 (all)	0.0332	0.0484	0.0792	R_1 (all)	0.0676	0.0699	0.0786	0.0822
wR_2 (all)	0.0698	0.0864	0.1168	wR_2 (all)	0.0805	0.1038	0.1045	0.0968
ρ (max / min) / e-$Å^{-3}$	0.824 / -1.111	1.139 / -1.457	1.304 / -1.243	ρ (max / min) / fm-$Å^{-3}$	0.061 / -0.061	0.061/ -0.056	0.043/ -0.048	0.033/ -0.028
RMS / e$Å^{-3}$	0.105	0.097	0.087	RMS / fm$Å^{-3}$	0.014	0.012	0.009	0.007

4.2.1 DMAN : 2-fluorobenzoic acid (1:2)

The molecular complex of DMAN : 2FBA shows a very similar structure to that of the DMAN : BA structure. The unit cell contains two protonated $DMANH^+$ molecules and 2FBA $DIMER^-$s with the 2FBA molecules connected, as before, through a single charge-assisted SSHB representing the building blocks of the structure. While in the structure of the DMAN : BA the $DIMER^-$s do not have short contacts between them, in this complex there are a number of short contacts between the BA $DIMER^-$s within the sums of van der Waals radii (*Figure 4-12*). The contacts include C–H···π weak hydrogen bonds with a legth of ~3.65 Å and a C–H···O weak hydrogen bond with a distance of 3.611(2) Å.

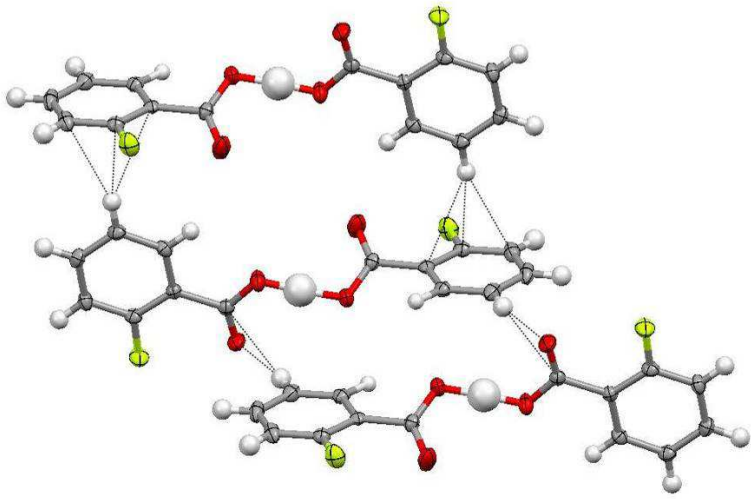

Figure 4-12. Intermolecular short contacts between the $DIMER^-$s of the 2FBA in the molecular complex of DMAN : 2FBA.

The 2FBA $DIMER^-$s are connected side-by-side through intermolecular short contacts to form a band and between these bands are packed the $DMANH^+$ molecules are packed holding together the structure (*Figure 4-13*).

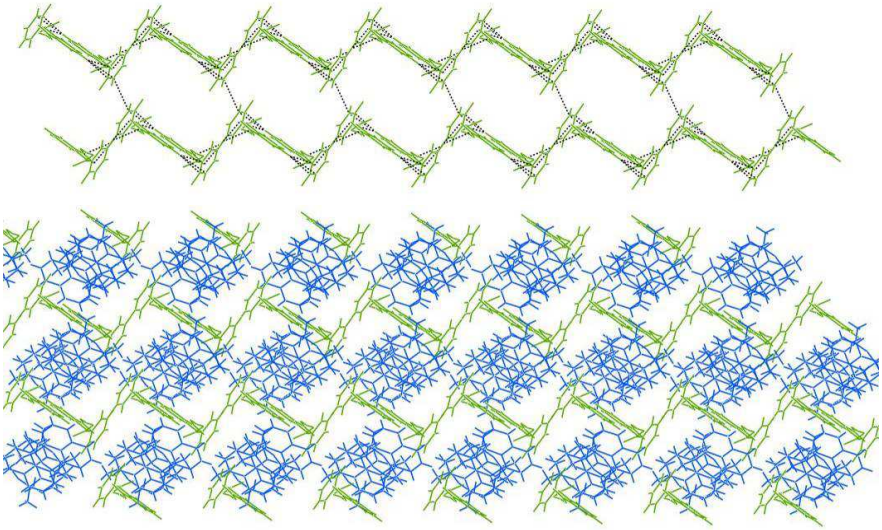

Figure 4-13. The layers of 2FBA DIMER$^-$s (green) without (top) and with the DMANH$^+$ (blue) molecules shown (bottom) in the molecular complex of DMAN : 2FBA.

The intermolecular interactions between the DMANH$^+$ and the 2FBA DIMER$^-$ are very similar to the interaction present in the complex of DMAN : BA, however the presence of the fluorine atom introduces a C–F···H weak hydrogen bond with a H···F distance of 2.61(2) Å. Pairs of DMANH$^+$ molecules are connected through parallel displaced π···π stacking with a distance of ~3.64 Å between the planes of the naphthalene rings but the pairs are stacked at a larger distance separated by the benzene rings of the DIMER$^-$s (*Figure 4-14*).

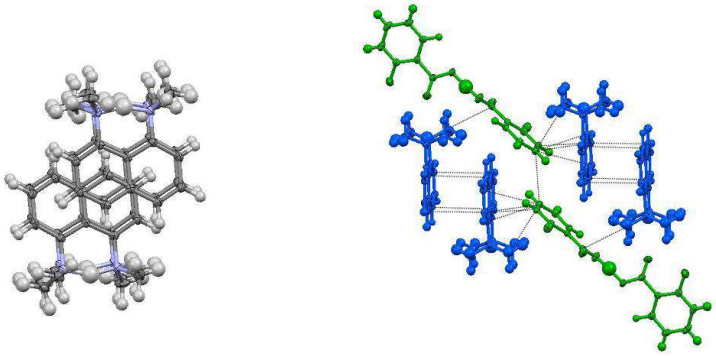

Figure 4-14. The alignment of the stacked DMANH$^+$ in the overall packing in the plane of the naphthalene rings (left) and the pairs of π···π stacked molecules separated by the benzene rings of the DIMER$^-$s (right). DMANH$^+$ molecules are coloured blue and the DIMER$^-$s in green for clarity.

There are no halogen-halogen interactions present in the structure but as described in the literature (Chapter 1.7), the strong dipolar character of the F···H interaction can have a stabilising role in close packing. By overlaying the $DMANH^+$ molecules from the DMAN : 2FBA and DMAN : BA complexes, it becomes more clear that the F···H interaction modifies the structure by twisting the relative positions of the $DIMER^-$s to the $DMANH^+$ molecule and making possible the formation of intermolecular interaction between the $DIMER^-$s themselves (*Figure 4-15*). Thus the presence of the fluorinated substituent plays a significant role in modifying the intermolecular interactions present and hence the packing of the structure of this complex.

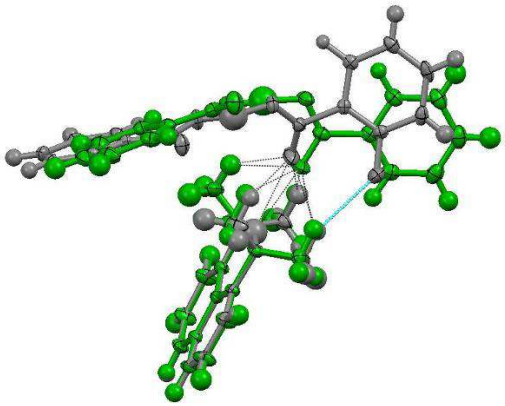

Figure 4-15. Overlay of the $DMANH^+$ molecules from the DMAN : BA (green) and DMAN : 2FBA (grey) molecular complexes(F··H marked in cyan).

The angle between the planes of the carboxyl group and the benzene ring shows a very large deviation in the case of the 2FBA molecule that makes short contacts to the DMAN, with a dihedral angle of 33.9°. The second 2FBA molecule, with no F···H interaction within the sum of van der Waals radii from the $DIMER^-$ has a very small deviation between the planes of its carboxyl group and benzene ring with a dihedral angle of just 5.9° angle (*Figure 4-16*).

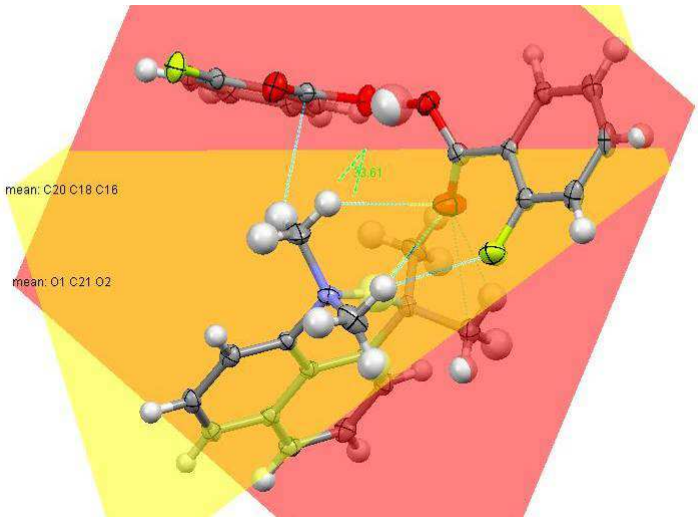

Figure 4-16. The angle measured between the plane of the carboxyl group and the benzene ring on the 2FBA molecules of the DIMER⁻ involved in the F···H interaction.

The intermolecular contacts between the $DMANH^+$ and the oxygen atom of the carboxyl group of the $DIMER^-$ also shows a slightly different behaviour compared to the DMAN : BA complex. The O···H distance is slightly longer with a length of 2.61(2) Å, still within the sum of van der Waals radii, whereas the C–H···O contacts with distances between 3.211(3) Å and 3.400(3) Å and the contact between the oxygen atom of the $DIMER^-$ and the nitrogen atoms of the $DMANH^+$ are not within this sum of radii.

Variable temperature X-ray diffraction data were collected at 100, 200 and 290K in order to reveal the hydrogen atoms potential anomalous behaviour since as in the complex of DMAN : BA both inter- and intramolecular hydrogen atoms show large thermal parameters at every studied temperature. The hydrogen atoms position within the intramolecular HB becomes slightly asymmetrical but the asymmetry of the hydrogen atoms position is not significant as the standard uncertainty on their length is very large compared to the change in the position within the HB. The intermolecular HB between the 2FBA molecules at 100 and 200K is asymmetric and this asymmetry becomes more pronounced at 300K. The lengths of the hydrogen bonds are listed in the *Table 4-6*. The C–N bond length in this case is longer at the acceptor side of the N–H···N bond, however the difference between the donor and acceptor bond lengths are very similar and

there is no difference appearing in the case of the C–C bonds and nor in the N-C-C bonding angles (*Table 4-1*). The differences between the two C–O and C=O bonds show similar behaviour as in the DMAN : BA molecular complex, the C–O being longer at the donor side and the C=O shorter in the donor side than at the acceptor side of the O–H···O intermolecular HB (see Table 4-1).

Table 4-6. The O-H···O and N-H···N hydrogen bond distances in the molecular complex of DMAN : 2FBA measured from the X-ray diffraction experiments.

Type	Temp (K)	D····A (Å)	D–H (Å)	H···A (Å)
O-H···O	100	2.447(1)	1.18(2)	1.28(3)
	200	2.445(2)	1.18(3)	1.27(3)
	290	2.447(3)	1.09(4)	1.36(4)
N-H···N	100	2.577(3)	1.30(3)	1.33(3)
	200	2.584(3)	1.30(3)	1.35(3)
	290	2.587(3)	1.25(4)	1.38(4)

The difference Fourier maps of the electron density in the region of the intramolecular hydrogen bond confirm the large uncertainty and the large thermal parameter determined in the refinements, as the electron density shows a split tendency, concentrating in two peaks across the hydrogen bridge (*Figure 4-17*).

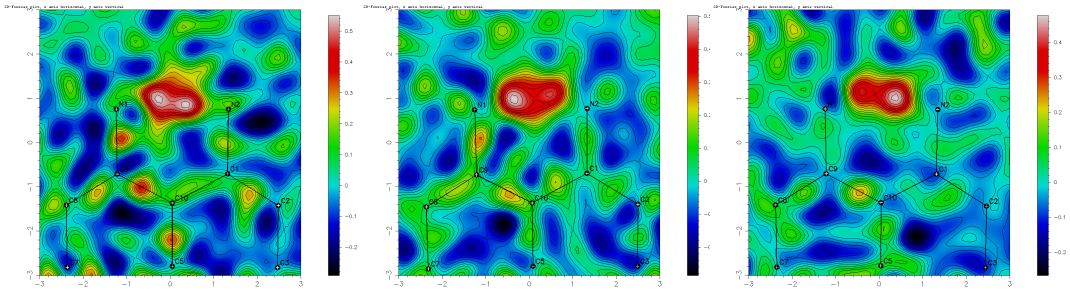

Figure 4-17. Difference Fourier maps of the electron density of the hydrogen atoms of the $DMANH^+$ molecule, of the DMAN : 2FBA complex from left to right at 100, 200 and 290K.

The difference maps of the intermolecular HB between the 2FBA molecules show a similar behaviour of the electron density to that of the intramolecular HB, with an electron density clearly showing two separated concentration points within

the hydrogen bridge at 100K. With the increase of the temperature to 200K the two separate positions are not clearly visible and the electron density is spread across the hydrogen bridge. With further increase of the temperature to 290K, most of the electron density is concentrated to the donor side with a small elongation along the HB. All of these images of the electron density from the X-ray experiments are in good agreement with the HB lengths (*Figure 4-18*).

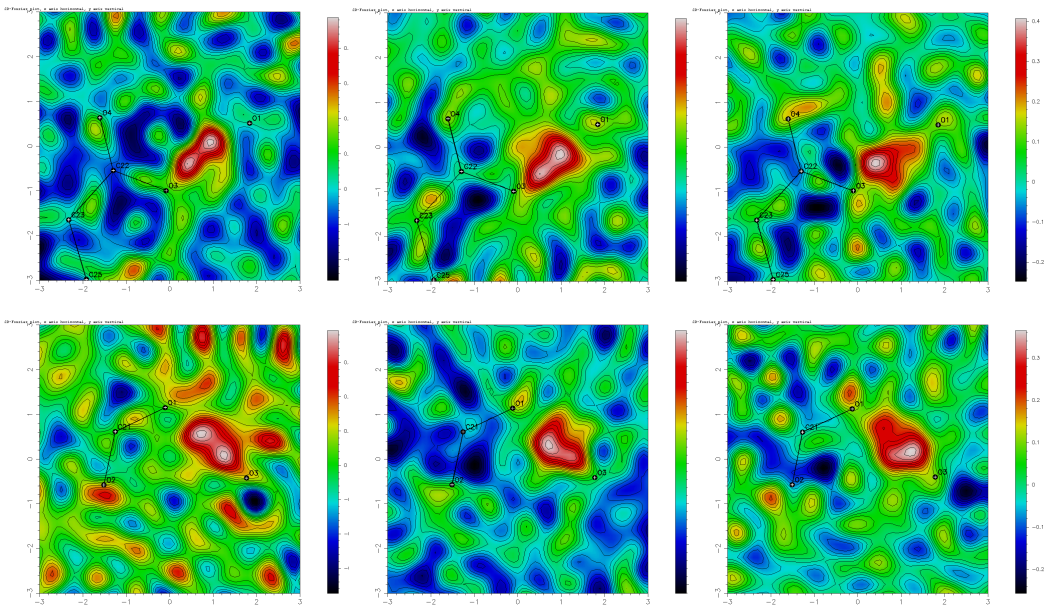

Figure 4-18. Difference Fourier maps of the hydrogen atom electron density within the intermolecular hydrogen bond in the molecular complex of DMAN : 2FBA; top and bottom are the planes of the two carboxyl groups of the DIMER⁻, from left to right at 100, 200, 290K.

4.2.2 DMAN : 2-chlorobenzoic acid (1:2)

As in the molecular complexes discussed before, DMAN and 2CBA form a 1:2 ratio molecular complex in their crystal structure. The DMAN molecule is protonated and the single hydrogen bonded 2CBA DIMER⁻ is formed as a result of the deprotonation of 2CBA. While from this point of view the structure is similar to the others reported above, the differences first of all appear in the symmetry. The complex crystallises in a higher symmetry space group ($P2_1/n$ compared to $P\bar{1}$), but the asymmetric unit similarly has one DIMER⁻ and one $DMANH^+$ molecule, so that the unit cell contains four $DMANH^+$ molecules and four DIMER⁻s. The

hydrogen bond distance between the two 2CBA molecules is in the expected range for the charge-assisted SSHB with bond distances listed in *Table 4-7* at all three measured temperatures from the X-ray diffraction experiments. Similarly, the intramolecular hydrogen bond between the nitrogen atoms of the $DMANH^+$ molecule is also in the expected range. The difference between the C–O and C=O bond lengths is apparent in this case as well; even though there is no significant difference in the donor-acceptor bond lengths or the C–N bond length, the bond is still slightly longer on the donor side of the N-H···N hydrogen bridge. There is no significant difference appearing in the C–C bonds nor in the N-C-C angles (Table 4-1).

Table 4-7. O–H···O and N–H···N hydrogen bond distances in the molecular complex of DMAN : 2CBA measured from X-ray diffraction experiments.

Type	Temp (K)	D····A (Å)	D–H (Å)	H···A (Å)
O-H···O	100	2.442(2)	1.21(3)	1.23(3)
	200	2.443(2)	1.17(4)	1.27(3)
	300	2.446(5)	1.12(5)	1.34(5)
N-H···N	100	2.573(2)	1.08(2)	1.53(3)
	200	2.579(2)	1.13(3)	1.49(3)
	300	2.580(3)	1.23(4)	1.40(4)

In the $DIMER^-$ of the 2CBA one of the benzene rings is disordered – it was possible to resolve two positions for this using Fourier difference maps. In the model for the disorder of the benzene ring (85%:15% population of the two configurations; *Figure 4-19*), the atoms in the case of the molecule with the major occupancy and the chlorine atom from the molecule with minor occupancy are refined anisotropically while the carbon atoms with minor occupancy are only refined isotropically. The H atoms on the major and the minor configuration are included at calculated positions. The angle between the planes of the two disordered benzene rings is found to be 9.62°, while in both configurations the carbon atoms and the oxygen atoms of the carboxyl group are in the same position and can be refined anisotropically.

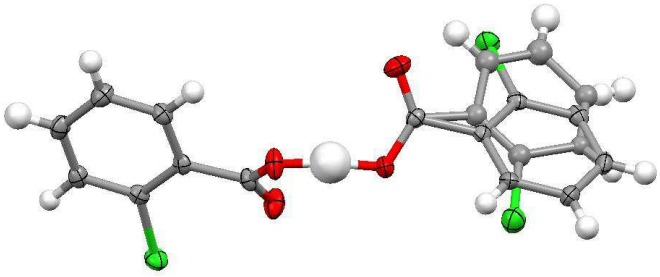

Figure 4-19. The DIMER⁻ of the 2:1 2CBA : DMAN molecular complex, showing the disorder of one of the 2CBA molecules.

In the case of the benzene ring which shows 85% occupancy, the angle between the plane of the carboxyl group and the plane of the benzene ring is 40.1°, while this angle for the benzene ring with the 15% occupancy is 30.4° which is similar to the angle between the planes of the benzene ring and carboxyl group on the non-disordered 2CBA molecules. There is a halogen-halogen type II interaction between the 2CBA molecule of the minor disordered configuration and the fully ordered benzoic acid molecule with a Cl····Cl distance of 3.382(3) Å, well under the 3.5 Å sum of the van der Waals radii for Cl····Cl (*Figure 4-20*).

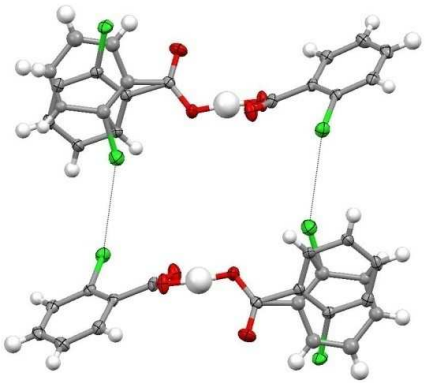

Figure 4-20. The Cl···Cl interaction between the 2CBA DIMER⁻s in the molecular complex of DMAN : 2CBA.

Two $DMANH^+$ molecules in the structure are connected through a parallel displaced π···π stacking with a distance of ~3.37 Å between the planes of the naphthalene rings. The pair of DMAN molecules is surrounded by the 2CBA $DIMER^-$s and as in the case of the DMAN : 2FBA complex, are separated by the benzene rings of the $DIMER^-$ from the next pair of π···π stacked $DMANH^+$ molecules (*Figure 4-21*).

The intermolecular interaction between the oxygen of the carboxyl group of the 2CBA and the $DMANH^+$ is similar to that found in the structure of the 2FBA : DMAN complex with C–H···O weak hydrogen bonds with C···O distances between 3.205(2) Å and 3.357(2) Å and an O···H contact with a distance of 2.67(3) Å. The $DIMER^-$s of 2CBA make short contacts to each other through C–H···π weak HBs between the disordered benzene rings and through further C–H···π weak HBs between the disordered and non-disordered benzene rings forming a layer of $DIMER^-$s with inclusion of $DMANH^+$ molecules (*Figure 4-22*)

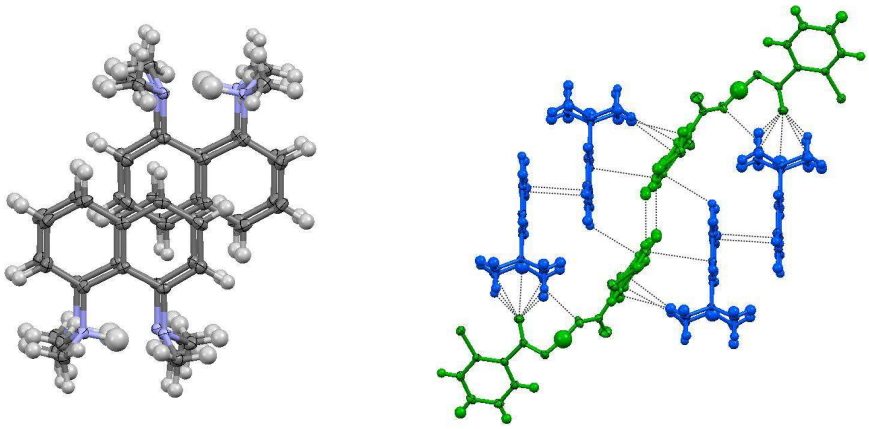

Figure 4-21. The stacked $DMANH^+$ molecules in the plane of the naphthalene ring (left), and the pairs of π···π stacked $DMANH^+$ molecules separated by the benzene ring of the $DIMER^-$s (right) in the overall packing. $DMANH^+$ molecules are coloured blue and $DIMER^-$s green for clarity.

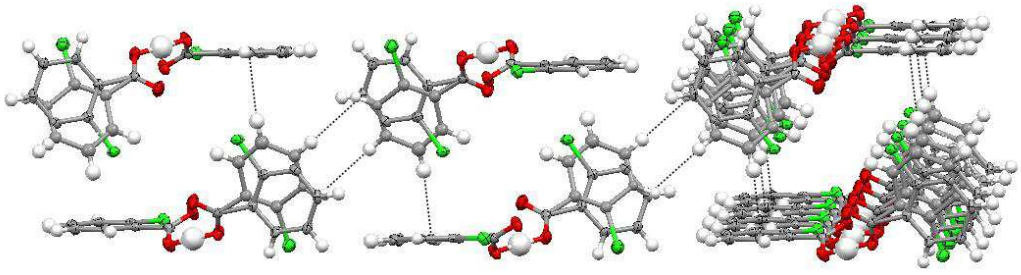

Figure 4-22. The C–H···π intermolecular interactions between the 2CBA $DIMER^-$s, on the left showing single $DIMER^-$s for clarification of the intermolecular contacts and on the right the inclusion space formed from side by side connected $DIMER^-$s.

These layers then are held together by C–H···π intermolecular interactions between the $DMANH^+$ and the benzene rings of the 2CBA molecules with distances between ~3.67 Å and ~3.73(2) Å, forming the packing of the structure as a whole (*Figure 4-23*).

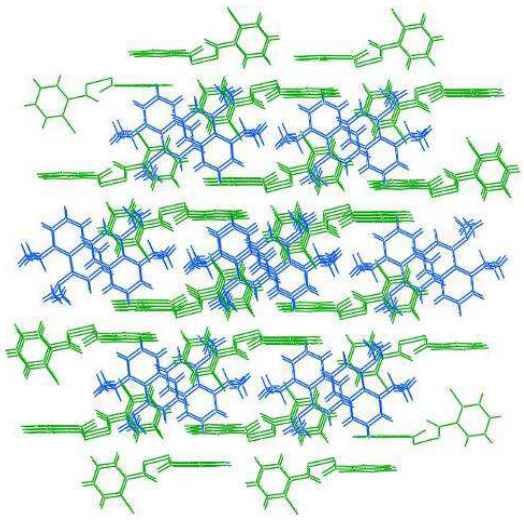

Figure 4-23. The structure as a whole presented with the intermolecular interactions between the molecules; stacked $DMANH^+$ molecules (blue), 2CBA $DIMER^-$s (green).

While this is similar to the 2FBA : DMAN complex with respect to the short contacts within the sums of van der Waals radii, the isotropic thermal parameter of the hydrogen atom in the intramolecular HB is very large and its position significantly asymmetric, unlike the case of the 2FBA : DMAN complex. The difference Fourier map shows variable electron distribution across the intramolecular HB as in the two other complexes presented above.

4.2.3 DMAN : 2-bromobenzoic acid (1:2)

The DMAN-2CBA and DMAN-2BBA complexes are isostructural with very similar unit cell parameters and the overlay of the structures shows a very good agreement between the two complexes (*Figure 4-24*). One of the 2BBA molecules shows disorder of the benzene ring (85%:15% population of the two configurations) as in the case of the DMAN : 2CBA molecular complex, and as

before the atom refinements are treated in the same way: the major component of disordered benzene ring and the bromine atom from the minor are refined anisotropically while the carbon atoms of the minor component of the disorder are only refined isotropically.

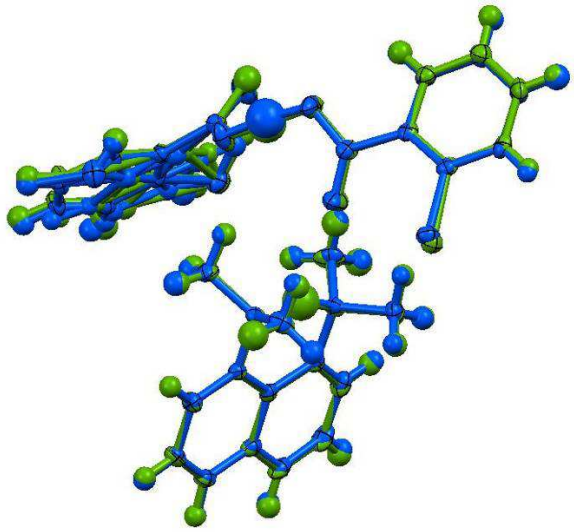

Figure 4-24. The overlay of the asymmetric units of the isostructural DMAN : 2CBA (blue) and DMAN : 2BBA (green) molecular complexes.

The H atoms on the disordered benzene ring are included at calculated positions. In addition there is a secondary position of the non-hydrogen bonded oxygen atom in the minor (15%) position in the case of 2BBA $DIMER^{-}$, which was introduced as the originally refined single oxygen atom had a large elongated anisotropic displacement parameter. The angle between the planes of the two disordered benzene rings is found to be ~10˚.

There are Br···Br interactions between the bromine atom of the minor (15%) disordered ring and the bromine atom of the fully ordered benzoic acid, with Br····Br = 3.357(2) Å, similar to that found in the DMAN : 2CBA complex with Cl····Cl = 3.375(4) Å distance, while the sum of the van der Waals radii are 3.7 Å and 3.5 Å, respectively. It is interesting to note that the halogen-halogen distance is not significantly affected by the change in atom type. The structure overlay presented in *Figure 4-24* shows the same alignments of the disordered rings where the differences appear just in the length of the halogen bonds.

As the two molecular complexes are isostructural the intermolecular interactions between the molecules are also similar. The intermolecular interaction between the oxygen atom from the carboxyl group and the methyl groups of the $DMANH^+$ consist of C–H···O contacts between 3.210(3) Å and 3.383(3) Å and an O···H contact with a distance of 2.68(4) Å, while the C–H···π weak HBs distances between the $DMANH^+$ and the benzene ring of the 2BBA $DIMER^-$ are between ~3.72 Å and ~3.77 Å, holding together the layers formed from the 3BBA $DIMER^-$s enclosing the $DMANH^+$ molecules (these layers connected through C–H···π interactions are presented in Figure 4-23 for the DMAN : 2CBA complex).

The variable temperature measurement shows minor differences in the lengths of both the intermolecular and intramolecular hydrogen bond distances, but taking in account the nature of the measurement (X-ray data collection), the large isotropic thermal parameters on the hydrogen atoms, the presence of a heavy atom (bromine) and the greater standard uncertainties that increase with the temperature, the list of the measured distances is presented (*Table 4-8*), but not considered sufficiently reliable for further discussion. The C–N and C=O bond lengths correlation (*Table 4-1*) between the donor side and the acceptor side are found to be as in the case its isostructural DMAN : 2CBA complex. The C–O, however, in this case shows a slightly longer distance in the case of the acceptor, but since the oxygen atom of the carboxyl group is disordered these measurements are less reliable.

Table 4-8. O–H···O and N–H···N hydrogen bond distances in the molecular complex of DMAN : 2BBA measured from X-ray diffraction experiments.

Type	Temp (K)	D····A (Å)	D–H (Å)	H···A (Å)
O–H···O	100	2.444(2)	1.10(4)	1.35(4)
	200	2.442(3)	1.11(5)	1.34(5)
	300	2.444(6)	0.97(7)	1.47(7)
N–H···N	100	2.578(2)	1.21(3)	1.41(3)
	200	2.583(3)	1.30(4)	1.34(4)
	300	2.586(4)	1.31(6)	1.32(6)

4.2.4 DMAN : 2-iodobenzoic acid (1:2)

The molecular complex of DMAN : 2IBA crystallises in the same ratio and symmetry as the DMAN : BA and DMAN : 2FBA complexes. The DMAN molecule is protonated by transfer of the proton from the carboxylic acid group of one of the 2IBA molecules and the 2IBA molecules form a $DIMER^{-}$ connected through a charge-assisted SSHB. The carboxyl groups of the 2IBA molecules in this case have an even larger dihedral angle to their parent benzene ring planes than in the molecular complexes presented before, with angles of 52.30° and 41.69° (*Figure 4-25*).

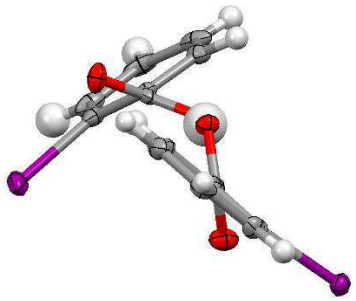

Figure 4-25. The 2IBA $DIMER^{-}$ showing the large dihedral angles between the carboxyl group and the benzene ring planes of the 2IBA molecules.

This large dihedral angle could be caused by the number of intermolecular short contacts involving the carboxyl group, and the strong intermolecular interactions, since they are larger than those found in the pure *ortho*-substituted benzoic acid crystal structures taken from the CSD[157-160]. The increasing deviation between the plane of the carboxyl group and its parent benzene ring with the size of the substituent on the benzoic acid molecules lead to the conclusion that is mainly caused by the nature of the substituent leading to different intermolecular interactions and influencing the relatively free rotation around the C–C bond. The change in the relative positions of the $DIMER^{-}$ and the $DMANH^{+}$ is significant as well compared with the other ortho-substituted benzoic acid and $DMANH^{+}$ complexes as shown in *Figure 4-26*.

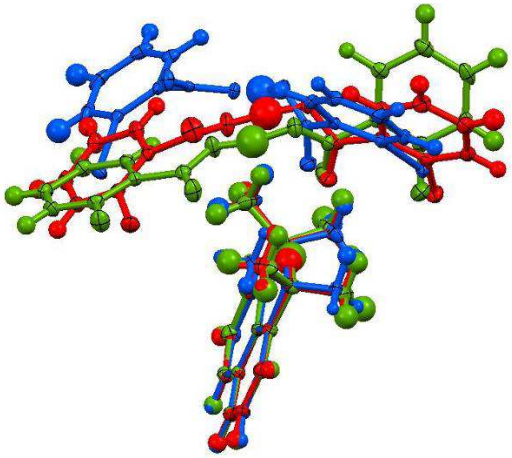

Figure 4-26. The overlay of DMAN : 2FBA (green), DMAN : 2CBA (red) (minor disorder part has been removed for clarity) and the DMAN : 2IBA molecular complexes, showing the changes of the relative position of the DIMER$^-$s in each complex.

The number of interactions between the oxygen atom of the carboxyl group and the methyl group of the DMANH$^+$ is smaller in this case, having just C–H···O interactions within the sum of van der Waals radii, with lengths between 3.230(4) Å and 3.558(4) Å.

There are a number of interactions between the 2IBA DIMER$^-$s. A π···π interaction with a distance of ~3.36 Å and an I···π interaction with a distance of ~3.65 Å form a layer of the DIMER$^-$s (*Figure 4-27*) and through a further I···π interaction the layer of DIMER$^-$s are connected to each other, encaging the π···π stacked pairs of DMANH$^+$ molecules (*Figure 4-28*). The DMANH$^+$ molecules are connected through parallel displaced π···π interactions in pairs, however, in this case the pair of DMANH$^+$ molecules show an inclined arrangement (*Figure 4-29*) encaged between the DIMER$^-$s.

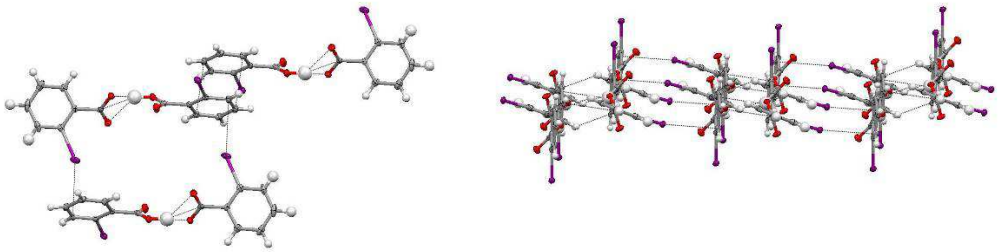

Figure 4-27. Intermolecular interactions between the DIMER⁻s of the 2IBA molecules (left) and the layer formed by the DIMER⁻s(right).

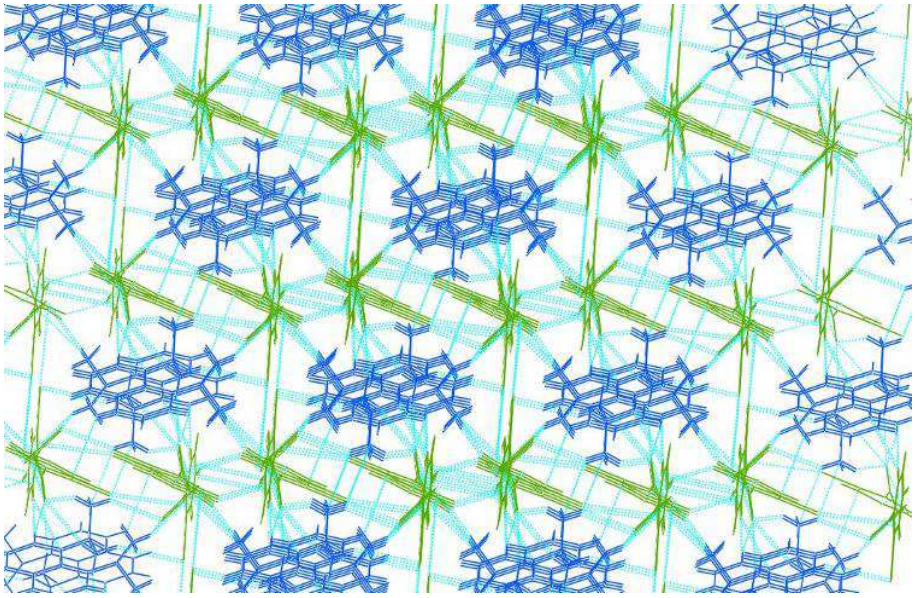

Figure 4-28. The build up of the structural packing as a whole; the layers of DIMER⁻s (green) encage the DMANH⁺ molecules (blue).

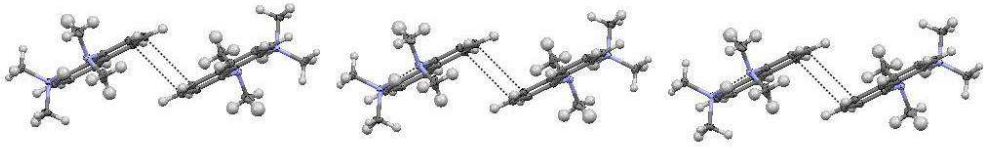

Figure 4-29. The π···π stacked pairs of DMANH⁺ molecules relative inclined arrangement.

Variable temperature X-ray and neutron diffraction data have been collected on the molecular complex in order to reveal further information on the nature of

the intermolecular SSHB between the 2IBA molecules and the intramolecular HB between the nitrogen atoms of the $DMANH^+$ molecules (*Table 4-9*). This is particularly important since as found in the other substituted benzoic acid : DMAN molecular complex, in this structure a large isotropic thermal parameter is again associated with the hydrogen atom in these hydrogen bonds.

Table 4-9. Hydrogen bond distances in the molecular complex of DMAN : 2IBA, for the intermolecular O–H···O and the intramolecular N–H···N from the X-ray and neutron data collections.

Type	Temp (K)	D····A (Å)	D–H (Å)	H···A (Å)
O–H···O X-ray data	100	2.466(2)	1.09(4)	1.38(4)
	200	2.459(3)	1.13(5)	1.33(5)
	300	2.468(4)	0.92(5)	1.55(5)
N–H···N X-ray data	100	2.566(3)	1.08(4)	1.51(4)
	200	2.552(4)	1.13(4)	1.48(3)
	300	2.570(5)	1.10(6)	1.51(6)
O–H···O Neutron data	30	2.460(2)	1.208(2)	1.254(2)
	100	2.455(2)	1.207(4)	1.249(4)
	200	2.459(3)	1.200(5)	1.259(5)
	300	2.462(4)	1.207(7)	1.257(7)
N–H···N Neutron data	30	2.568(2)	1.196(3)	1.418(3)
	100	2.567(2)	1.198(5)	1.414(5)
	200	2.566(3)	1.199(6)	1.414(6)
	300	2.573(3)	1.242(7)	1.387(6)

This pair of experiments (X-ray and neutron) show the importance and value of the latter. While the SSHB between the 2IBA molecules from the X-ray data shows apparent different trends in the lengths of the HB but in this case the X-ray data are even less reliable than in the other 3 substituted benzoic acids, since the iodine is a heavy atom in the structure and the residual density deviation is large (*Table 4-5*) compared to the other structures. However, from the neutron diffraction measurements the hydrogen positions are determined accurately. These measurements offer a more accurate picture of both SSHBs in the complex, confirming that both are slightly asymmetric at all temperatures and they do not show any systematic deviation in the distances (*Table 4-9*). The intramolecular N-H···N hydrogen bond shows no significant changes in distances at any temperature from X-ray diffraction data and shows only a small change in the donor-acceptor distance at 300K from the neutron diffraction data, which shows evidence for a decreased asymmetry of this HB at this higher

temperature. However, at 300K the anisotropic displacement parameters are very large for every atom compared to the data collected at lower temperatures and the libration of the methyl groups on the acceptor side of the $DMANH^+$ are particularly pronounced (*Figure 4-30*).

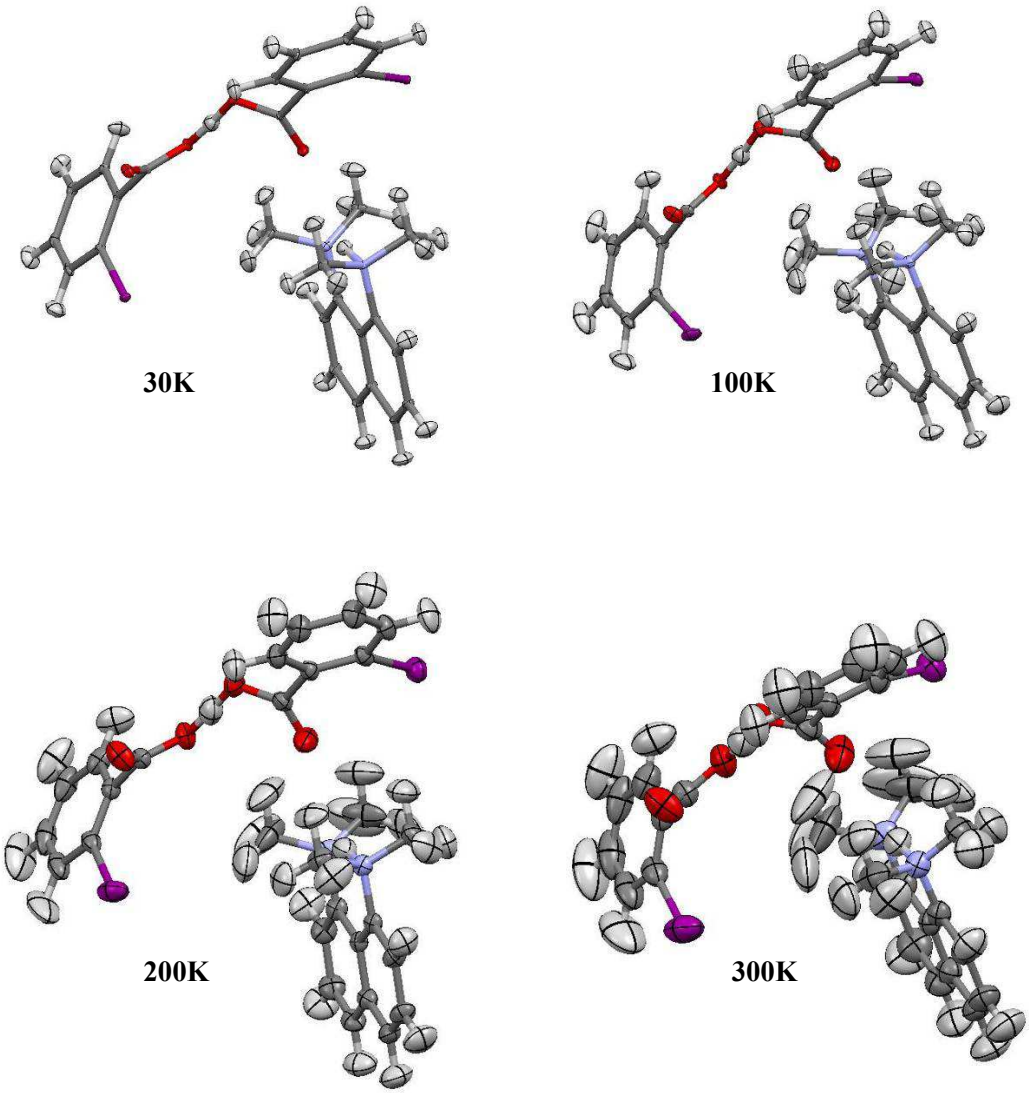

Figure 4-30. The evolution of the structure as a function of temperature from the neutron diffraction data.

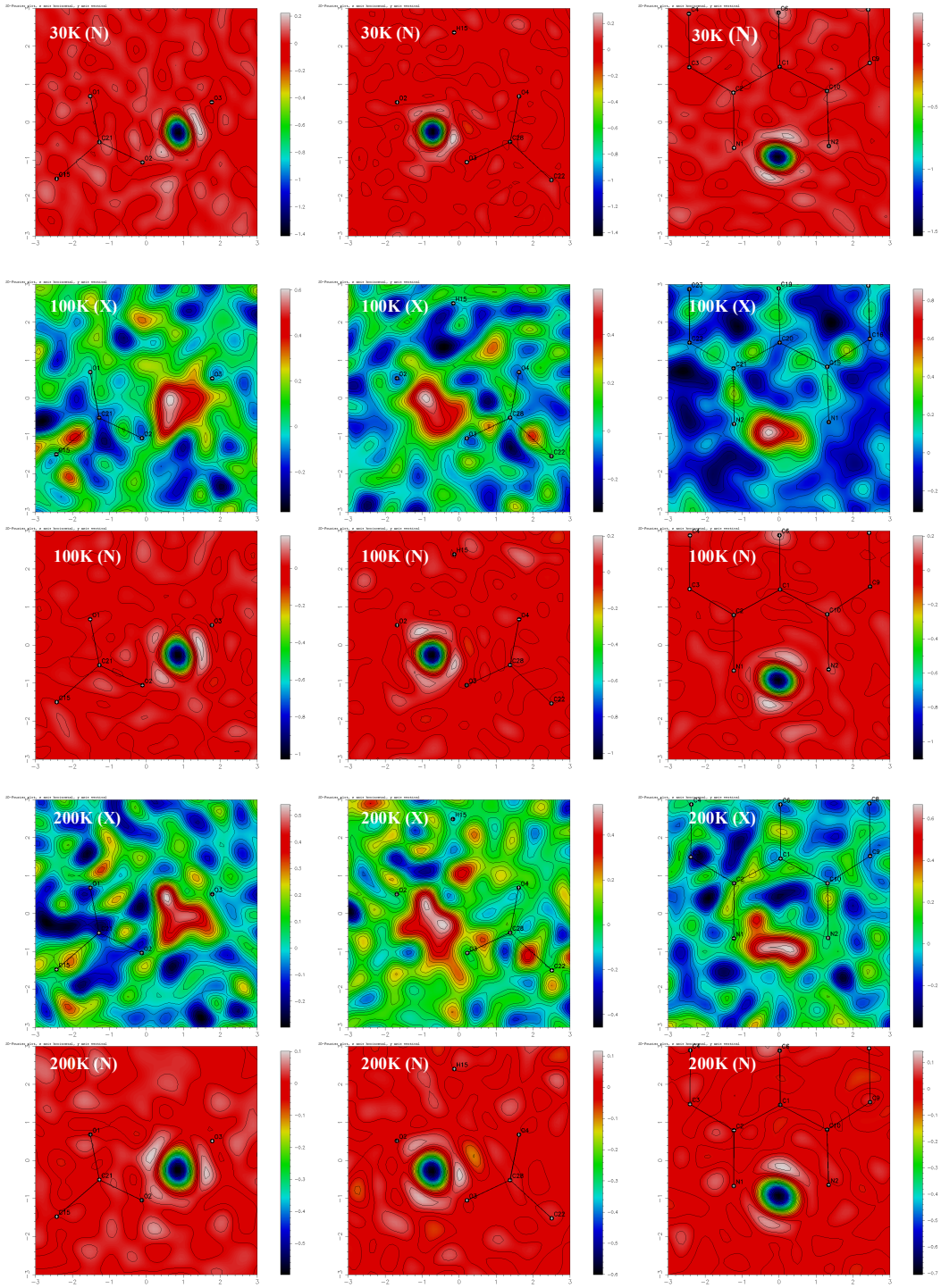

Figure 4-31. The Difference Fourier maps of the inter- and intramolecular HB with removed hydrogen in the planes of the carboxylic acid DIMER^{-} (left and middle) and plane of the naphthalene ring (right), showing the nuclear density (N) and the electron density (X) of the hydrogen atom at the marked temperatures.

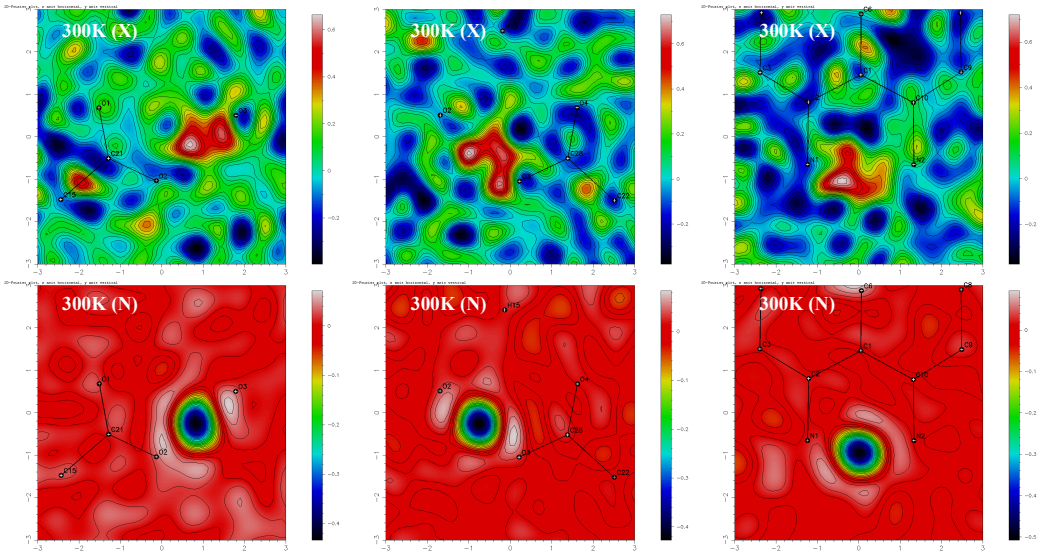

Figure 4-32. The Difference Fourier maps of the inter- and intramolecular HB with removed hydrogen in the planes of the carboxylic acid DIMER^{-} (left and middle) and plane of the naphthalene ring (right), showing the nuclear density (N) and the electron density (X) of the hydrogen atom at 300K.

The difference Fourier maps of the hydrogen atom electron density is very noisy, which can explained by the presence of a heavy atom in the structure (iodine) which results in less reliable electron density determination for the hydrogen atoms (*Figure 4-31, Figure 4-32*). The nuclear densities of the hydrogen atom measured from the neutron diffraction, on the other hand, are as accurate and consistent as the other atoms and as far as can be seen are consistent with the X-ray maps. In one sense it is unfortunate that this is the complex which has been measured by both determination methods, the presence of the heavy atom meaning it is difficult to compare the electron density to the nuclear position of the atom. However, the presence of this heavy atom can also be said to give the ideal rationale for using neutrons, to determine the HB parameters that would otherwise be difficult to obtain reliably from just X-ray data. The neutron difference Fourier map shows that, in this case, the hydrogen atoms nuclear position is consistent across the measured temperatures and does not show any anomalous behaviour seen in some SSHB (see Chapter 1). The C–N, C–O and C=O bond length correlations to the donor positions presented in Table 4-1 are relevant since the neutron diffraction data shows these correlation with reliable bond lengths in the case of the intra- and intermolecular hydrogen bonds. From

both neutron and X-ray measurements the difference between the C–N is longer in the donor side of the N–H···N bond and the C–O bond longer and the C=O shorter in the case of the donor side of the O–H···O bond.

4.3 Molecular complexes of DMAN and *meta*-substituted benzoic acids

In this section a description and comparison of five of the meta-halogen substituted benzoic acids molecular complexes with DMAN as studied by X-ray diffraction will be presented. In addition to the four different meta-substituted halo-benzoic acid complexes, a hydrated structure of the DMAN : 3FBA molecular complex will also be presented.

Experimental data

1:2 Molecular complex of DMAN : 3-fluorobenzoic acid (3FBA) - 1:1 molar ratio of 3FBA and DMAN were dissolved in diethyl ether and evaporated at room temperature, slowing the evaporation by closing the vial with a pierced small clipped lid. After the evaporation of the solvent, colourless blocks were formed. Single crystal X-ray diffraction data were collected on a Bruker APEX II diffractometer at 100K. The data were solved with SHELXS97 and refined with SHELXL97, within the WinGX package.

2:1 Molecular complex of DMAN : 3-fluorobenzoic acid (3FBA) hydrate – 1:1.4 molar ratio of 3FBA (0.037 g) and DMAN (0.08 g) were dissolved in ethanol and evaporated at room temperature, slowing the evaporation by closing the vial with a pierced small clipped lid. After the evaporation of the solvent, colourless prisms were formed. Single crystal X-ray diffraction data were collected on a Bruker Nonius Kappa CCD diffractometer at 110K. The data were solved with SHELXS97 and refined with SHELXL97, within the WinGX package.

3:4 Molecular complex of DMAN : 3-chlorobenzoic acid (3CBA) - 2:1 molar ratio of 3CBA and DMAN were dissolved in diethyl ether and evaporated at room temperature, slowing the evaporation by closing the vial with a pierced small

clipped lid (very slow evaporation with one small perforation). After the evaporation of the solvent, colourless blocks were formed. Single crystal X-ray diffraction data were collected on a Bruker Nonius Kappa CCD diffractometer at 100K. The data were solved with SHELXS97 and refined with SHELXL97, within the WinGX package.

1:2 Molecular complex of DMAN : 3-bromobenzoic acid (3BBA) - 1:1 molar ratio of 3BBA and DMAN were dissolved in methanol and water mixture (~10:1) and evaporated at room temperature, slowing the evaporation by closing the vial with a pierced small clipped lid. After the evaporation of the solvent, colourless prisms were formed. Single crystal X-ray diffraction data were collected on a Rigaku R-AXIS RAPID diffractometer at 100K. T The data were solved with SHELXS97 and refined with SHELXL97, within the WinGX package.

1:2 Molecular complex of DMAN : 3-iodobenzoic acid (3IBA) - 1:2 molar ratio of DMAN and 3IBA were dissolved in dichloromethane and evaporated at room temperature, slowing the evaporation by closing the vial with a pierced small clipped lid. After the evaporation of the solvent, colourless prisms were formed. Single crystal X-ray diffraction data were collected on a Bruker Nonius Kappa CCD diffractometer at 110, 200 and 300K,. The data were solved with SHELXS97 and refined with SHELXL97, within the WinGX package. In the refinement of 200 and 300K data set the hydrogen atoms are generated on the carbon atoms.

The crystallographic data for the structures are summarised in *Table 4-10*.

Table 4-10. Crystallographic data of molecular complexes of DMAN with 3FBA, 3CBA, 3BB, 3IBA from the X-ray refinements.

Compound	1:2 DMAN : 3FBA	2:1:1 DMAN : 3FBA hydrate	3:4 DMAN : 3CBA	1:1 DMAN : 3BBA	1:2 DMAN : 3IBA	1:2 DMAN : 3IBA	1:2 DMAN : 3IBA
Diffractometer	Bruker APEX II	Nonius Kappa CCD	Nonius Kappa CCD	Rigaku R-AXIS Rapid	Nonius Kappa CCD	Nonius Kappa CCD	Nonius Kappa CCD
Formula	C_{28} H_{30} N_2 F_2 O_4	C_{35} H_{43} F N_4 O_3	C_{70} H_{74} Cl_4 N_6 O_8	C_{42} H_{45} Br_2 N_4 O_4	C_{28} H_{30} N_2 I_2 O_4	C_{28} H_{30} N_2 I_2 O_4	C_{28} H_{30} N_2 I_2 O_4
Molecular weight ($gmol^{-1}$)	494.52	586.73	1269.15	829.62	710.35	710.35	710.35
Temperature (K)	100	110	100	100	110	200	300
Space Group	C 2/c	Pbca	C2/c	P b c 2_1	$P\bar{1}$	$P\bar{1}$	$P\bar{1}$
a (Å)	31.6074(9)	35.1663(6)	25.7026(4)	9.9057(3)	10.3719(2)	10.4438(2)	10.5845(7)
b (Å)	9.7387(3)	14.3501(2)	20.6846(7)	23.1670(6)	11.5082(3)	11.5492 (3)	11.6230(7)
c (Å)	21.6684(7)	12.6551(2)	12.1660(5)	34.1525(12)	12.2917(3)	12.3375(3)	12.4373(9)
α (°)	90	90	90	90	110.4750(10)	110.6287(11)	110.913(2)
β (°)	131.3230(10)	90	96.896(2)	90	90.5440(10)	90.6079(12)	90.786(2)
γ (°)	90	90	90	90	93.3110(10)	93.4789(1)	93.912(2)
Volume ($Å^3$)	5009.1(3)	6386.27(17)	6421.2(4)	7837.5(4)	1371.49(6)	1389.32(6)	1424.76(16)
Z	8	8	4	8	2	2	2
θ range/°	1.72 – 27.88	1.83 – 30.02	1.27 - 29.14	1.87 – 27.48	1.77 – 29.99	1.77 – 30.2	3.00 – 27.48
Completeness (%)	100	95.5	99.8	96.7	99.8	99.4	99.3
Reflections Collected	45531	33070	73623	42211	33080	33658	6481
Independent	5975	8904	8657	9127	7985	8091	6967
Refln (obs.I>2theta(I))	4619	6266	6143	10944	6473	5420	3671
R_{int}	0.0507	0.043	0.0525	0.0714	0.0483	0.0431	0.0452
Data/Rest./Param.	5975/2/443	8904/2/566	8657/0/572	9127/1/937	7985/0/437	8091/0/337	6481/0/337
GooF on F^2	1.02	0.92	1.017	1.081	1.025	1.023	1.024
R_1 (Observed)	0.0458	0.0508	0.0443	0.0516	0.0272	0.0374	0.0509
R_1 (all)	0.0634	0.0827	0.075	0.1005	0.0404	0.0715	0.099
wR_2 (all)	0.1239	0.149	0.1194	0.1591	0.0626	0.0883	0.1196
ρ (max / min) / e-$Å^{-3}$	0.377 / -0.595	0.297/ -0.234	0.534 / -0.574	0.759 /-1.075	0.764 / -09.49	1.08 / -1.377	1.382 / -0-957
RMS / e$Å^{-3}$	0.047	0.042	0.047	0.115	0.093	0.092	0.075

4.3.1 DMAN : 3-fluorobenzoic acid (1:2)

The molecular complex of DMAN : 3FBA is similar to the other DMAN and ortho-substituted halogen benzoic acid complexes, crystallising in 1:2 ratio with a protonated $DMANH^+$ and a 3FBA $DIMER^-$ connected through the charge assisted SSHB. The $DMANH^+$ molecules are connected through displaced π···π stacking between themselves, with a length of ~3.50 Å between the two closest π bonds, forming pairs of DMAN through the structure in two different orientations. Each 3FBA $DIMER^-$ is connected to five other $DIMER^-$s through intermolecular interactions. A zig-zag ribbon of $DIMER^-$s is formed through C–H···π and C–F···H weak HBs with lengths of C···π ~3.65 Å and F···H 2.532(2) Å respectively, and this ribbon is extended into a layer through further π···π and F···π contacts with lengths of ~3.37 Å and ~3.11 Å, respectively (*Figure 4-33*).

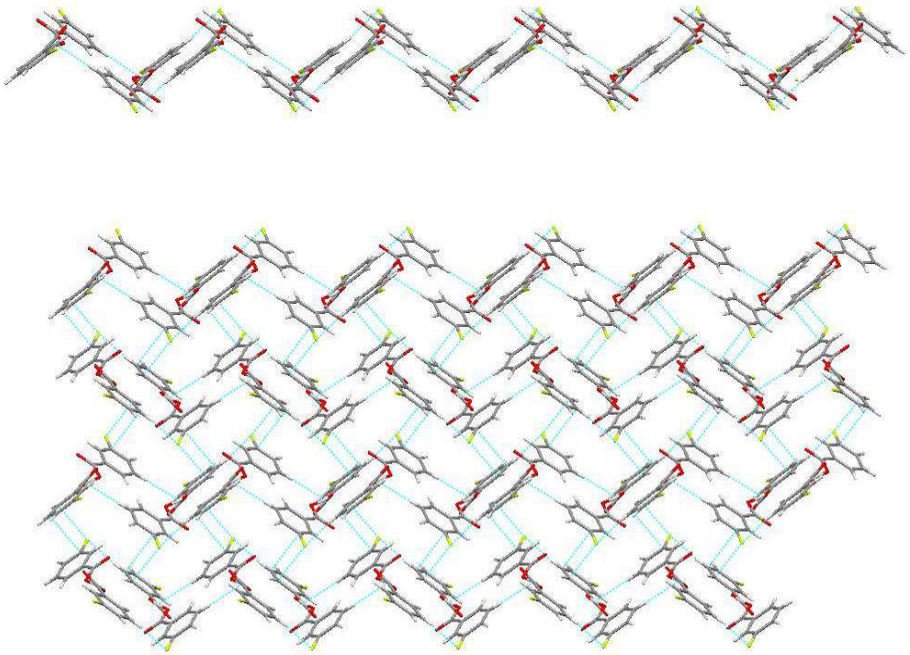

Figure 4-33. The ribbon (top) and the layer (bottom) formed by the intermolecular interaction between the 3FBA $DIMER^-$s.

The layers of $DIMER^-$s make are connected to each other through further C–F···H weak hydrogen bond with a F···H distance of 2.54(2) Å and encaging the $DMANH^+$ molecules. There are a number of intermolecular interactions between the

$DMANH^+$ and the $DIMER^-$s holding the layers together and form the structure as a whole (*Figure 4-34*).

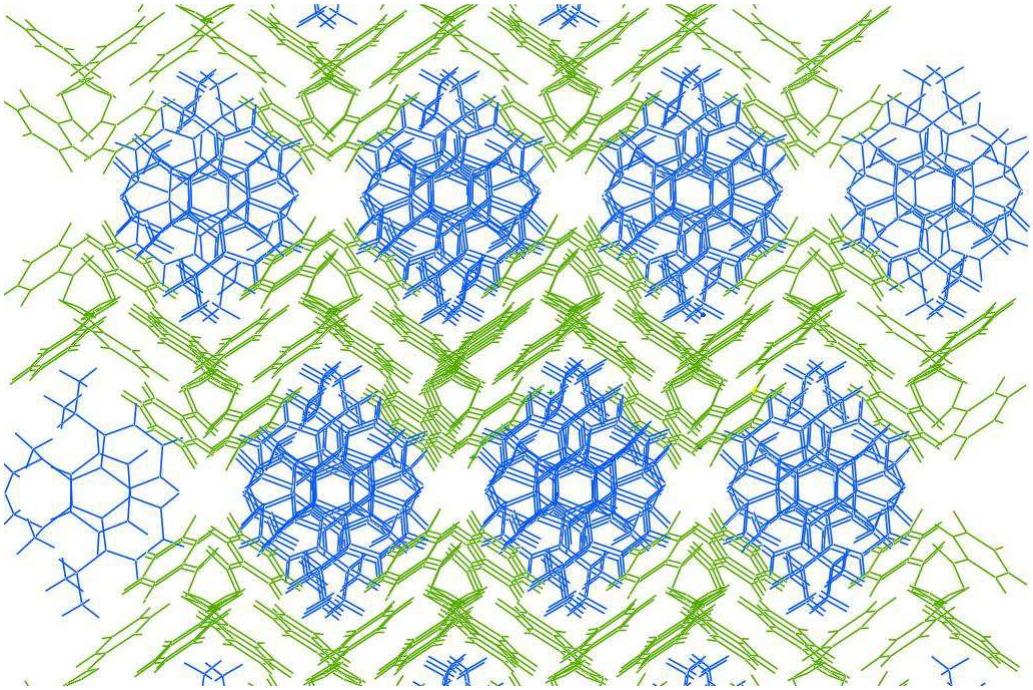

Figure 4-34. The structure of 1:2 DMAN : 3FBA as a whole, with the layers of $DIMER^-$s (green) encaging the $DMANH^+$ (blue) molecules.

The 3FBA molecules form similar $DIMER^-$s as in the complexes of DMAN and 2-halo-substituted benzoic acids but the angles between the plane of the carboxyl group and the benzene ring are more similar to those found in the DMAN : BA complex, measuring between 2˚ and 11.8˚. The fluorine atom in one of the 3FBA molecules from the $DIMER^-$ shows disorder with an 25% : 75% occupancy across the two sites. This disorder of the fluorine is present in just one of the 3FBA molecules in the $DIMER^-$ while the other, which has the non-hydrogen bonded oxygen atom short contacted to the methyl groups, shows a single, well-defined position (Figure 4-35). There are three C–H···O weak hydrogen bonds between the non-hydrogen bonded oxygen atom and the methyl group within the sum of van der Waals radii, with lengths between 3.285(2) Å and 3.335(3) Å.

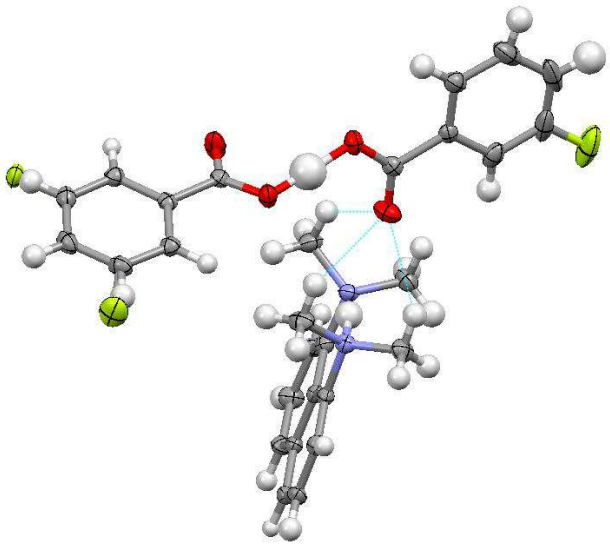

Figure 4-35. The asymmetric unit of the DMAN : 3FBA complex showing the short contacts between the oxygen atom of the 3FBA and the methyl group of the $DMANH^+$ as well as the disordered fluorine atom on one of the 3FBA molecules.

The intramolecular N–H···N hydrogen bridge shows an asymmetric hydrogen position with N–H distance of 1.02(3) Å and H···N of 1.63(3) Å. The intermolecular SSHB has a bond length of 2.446(2) Å with O–H = 1.16(4) Å and H···O = 1.29(4) Å, and as usual shows a large isotropic displacement parameter. The difference Fourier map shows a split feature in the electron density of the hydrogen within the intermolecular SSHB and a slightly elongated single position electron density in the case of the intermolecular hydrogen-bonded hydrogen atom (*Figure 4-36*). As the intramolecular hydrogen bridge becomes significantly asymmetric, the difference between C–N bond length on the donor and acceptor side becomes more significant as well, while the correlation between the C–O and C=O bond lengths showing more significant differences between these bonds on the donor side remains. Neither the C–C bond lengths nor the N-C-C bonding angles show significant differences between the donor side and acceptor side of the molecule (*Table 4-1*).

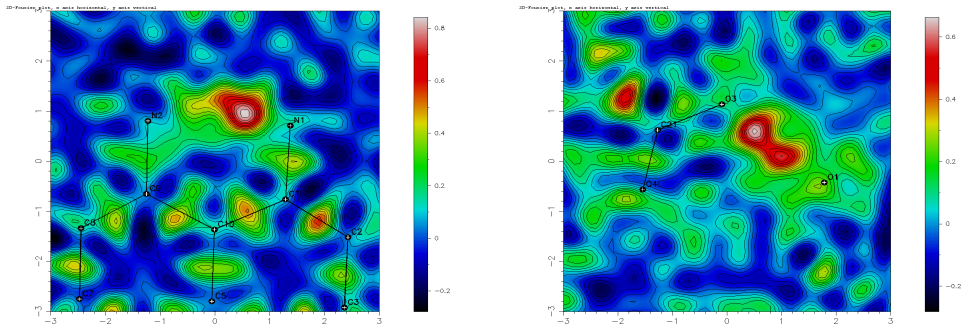

Figure 4-36. Difference Fourier maps of the electron density within the intramolecular N–H···N (left) and the intramolecular O–H···O(right) hydrogen bonds in the molecular complex of DMAN : 3FBA.

4.3.2 DMAN : 3-fluorobenzoic acid hydrate (2:1:1)

The DMAN : 3FBA hydrate complex is very different from any of the DMAN complexes presented before. The molecular complex has one protonated $DMANH^+$ molecule but, unusually, a second DMAN is present in the structure, and this remains unprotonated. The altered stoichiometry in this complex (DMAN : 3FBA ratio of 2:1 as opposed to 1:2 in the others presented to date) means that the $3FBA^-$ molecule is no longer stabilised through the single SSHB described in the other complexes. The main intermolecular interaction between the $3FBA^-$ molecules and the $DMANH^+$ molecules in this complex involves interaction of one of the oxygen atoms of the carboxyl group through C–H···O intermolecular interactions within the sum of van der Waals radii to the methyl group of the $DMANH^+$, with distances between 3.219(2) Å and 3.359(2) Å. This shows a similarity to other complexes of DMAN and halogen substituted benzoic acid complexes as does the further O···H contact between the carboxylate oxygen and the hydrogen from the intramolecular hydrogen bond on the $DMANH^+$, with distance of 2.66(2) Å (*Figure 4-37*).

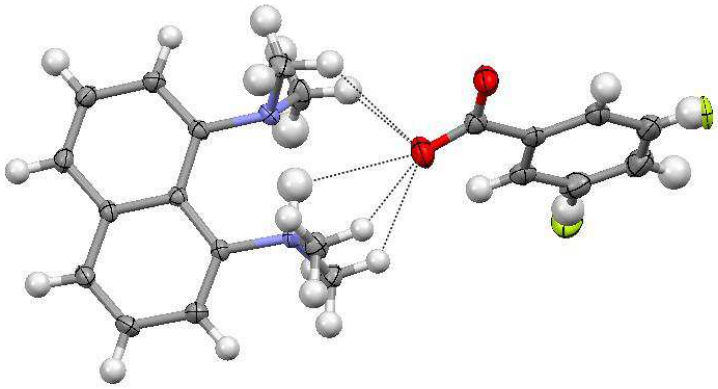

Figure 4-37. The intermolecular interactions between the $DMANH^+$ (methyl hydrogens and the N–H···N intramolecular HB) and one of the oxygen atoms of the $3FBA^-$ molecule.

The asymmetric unit contains two DMAN molecules. One of these is protonated as usual, with an N–H····N distance of 2.588(2) Å and a very asymmetric intramolecular hydrogen bond, N–H = 1.08(2) Å and H····N = 1.56(2) Å, with an electron density showing a rather well-defined single position from the difference Fourier map (*Figure 4-38*). The differences appearing in the C–N bond lengths between the donor and acceptor side of the N–H···N bond are increased as well (> 0.02 Å) (*Table 4-1*).

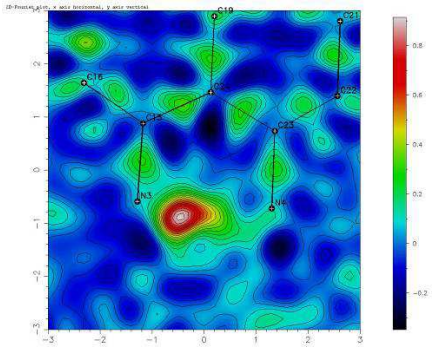

Figure 4-38. Difference Fourier map of the hydrogen atom electron density within the N–H···H intramolecular hydrogen bond.

The other DMAN molecule is unprotonated with the methyl group twisted from the perpendicular position compared to the plane of the naphthalene group. This is the first example of a DMAN complex where the DMAN is present in the same structure in both protonated and unprotonated form[161]. The N····N distance is

longer, at 2.802(2) Å, between the nitrogen atoms of the unprotonated DMAN as would be expected and the methyl groups twisted position is similar to that found in the unprotonated form of DMAN found in the parent DMAN crystal structure (*Figure 4-39*).

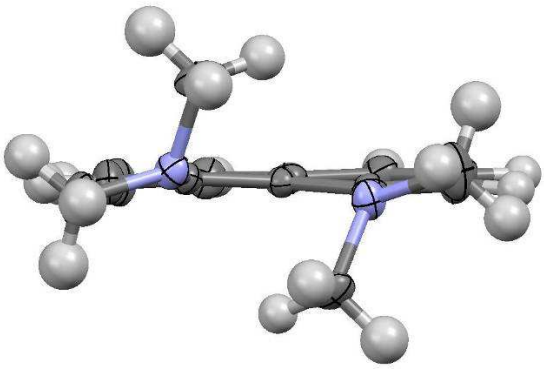

Figure 4-39. The unprotonated DMAN molecule viewed along the naphthalene ring plane in the molecular complex of the 2:1:1 DMAN : 3FBA hydrate.

Two of the protonated $DMANH^+$ molecules are located side by side in an inverted orientation through a centre of symmetry, and are connected through four C–H···π weak HBs between the naphthalene group and the methyl groups with lengths of ~3.43 Å and ~3.57 Å (*Figure 4-40*). Between the pair of $DMANH^+$ molecules and the unprotonated DMAN molecules the closest contacts are between C–H groups, however these are not significant interactions.

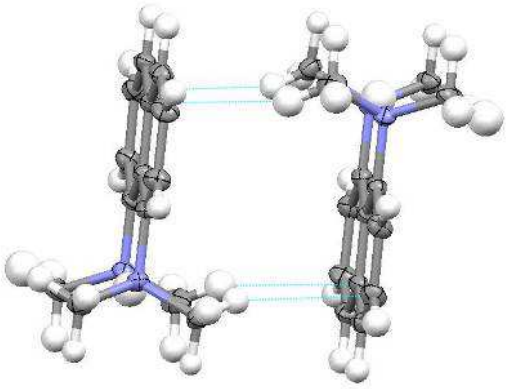

Figure 4-40. The pair of $DMANH^+$ molecules connected through C–H···π weak HBs.

This pattern is very different from that found in the other halo-benzoic acid : DMAN complexes because it lacks the benzoic acid DIMER$^-$ which is present in all the other halo-benzoic acid –DMAN complexes presented previously.

The protonated DMANH$^+$ (blue) and the unprotonated (yellow) DMAN molecules form separate ribbons within the packing and in the overall structure, these ribbons by the overall packing (*Figure 4-41*).

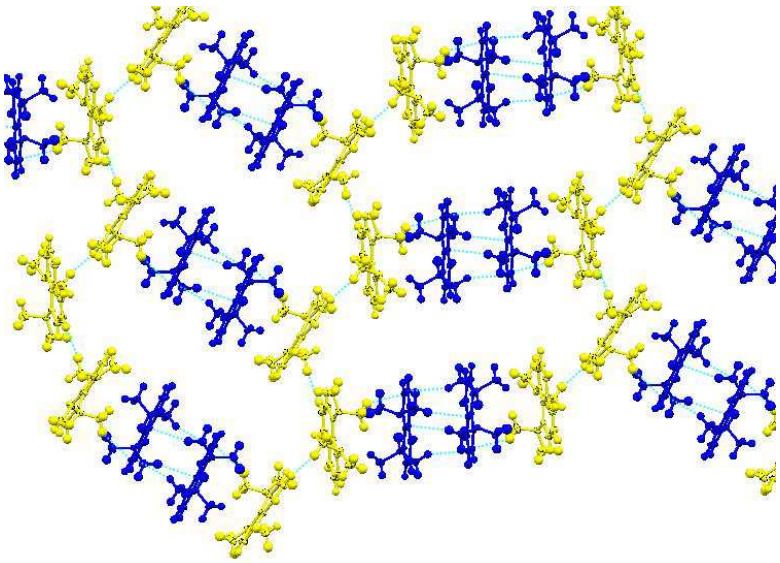

Figure 4-41. Ribbons of DMANH$^+$ (blue) and DMAN (yellow), forming layers within the molecular complex of DMAN : 3FBA hydrate.

As mentioned above, the fully deprotonated 3FBA$^-$ molecules are no longer stabilised by the charge assisted SSHB present in the previously described DMAN complexes. Instead, in this complex the 3FBA$^-$ molecules are connected through two water molecules which take over the role of that single hydrogen bond (*Figure 4-42*). The fluorine atom is disordered between two sites with a 75% : 25% occupancy, in both cases there is a C–F···H weak HB with the hydrogen of the methyl group from the unprotonated DMAN molecule with F···H lengths of 2.48(2) Å and 2.26(2) Å, respectively.

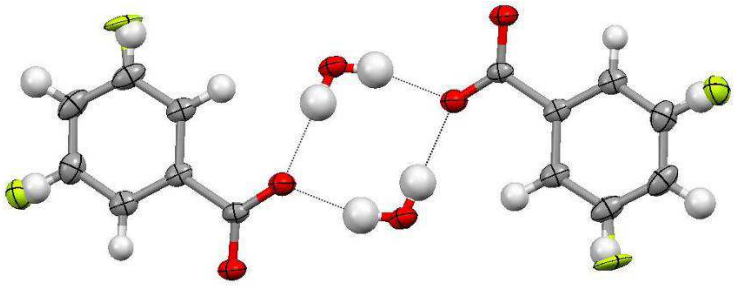

Figure 4-42. Symmetry-related deprotonated 3FBA$^-$ molecules connected through two water molecules in the molecular complex of DMAN : 3FBA hydrate.

The hydrogen bonding between the oxygen atom of the carboxyl group and the two water molecules is moderate in both cases, with O····O distances of 2.746(2) Å and 2.835(2) Å, while the other oxygen atom in the carboxylate group as described above is connected through short contacts to the methyl group of the DMANH$^+$.

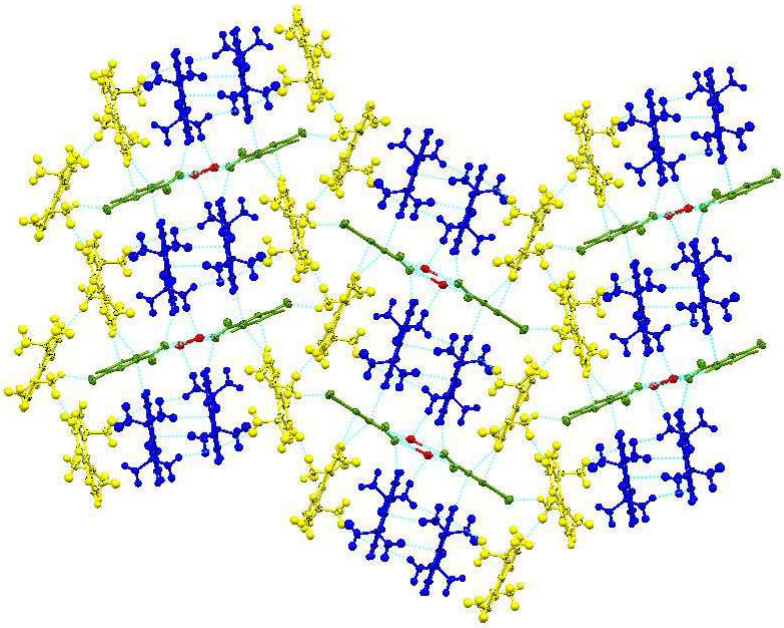

Figure 4-43. The overall packing showing the layer of DMAN (yellow) and DMANH$^+$ (blue) with the pairs of 3FBA$^-$ (green) bridged through the water molecules (red) in the molecular complex of DMAN : 3FBA hydrate.

The structure as a whole builds from the layers of connected DMAN and $DMANH^+$ molecules where the pairs of $3FBA^-$ molecules bridged through the water molecules are interlocked between the $DMANH^+$ molecules (*Figure 4-43*). The interactions between the carboxyl group of the $3FBA^-$ and the methyl group of the $DMANH^+$, connecting them to the next layer of DMAN and $DMANH^+$ molecules, are specified above (*Figure 4-37*).

4.3.3 DMAN : 3-chlorobenzoic acid (3:4)

The DMAN – 3CBA molecular complex crystallises in a 3:4 DMAN : 3CBA ratio. The asymmetric unit contains one protonated $DMANH^+$, half of a disordered unprotonated DMAN, and two 3CBA molecules. To stabilise the proton loss, the 3CBA molecules are connected through a single charge-assisted SSHB, forming a $DIMER^-$ as described previously in most of the DMAN complexes presented, with an intermolecular O···O bond length of 2.472(2) Å and separations of O-H = 1.03(2) Å and O···H = 1.45 (3) Å. A single well defined electron density peak for the hydrogen atom is indicated in the difference Fourier map and differences apparent in the C–O and C=O bond lengths between the donor and acceptor side of the asymmetric HB as well (*Table 4-1*). The oxygen atoms of the carboxyl groups of the $DIMER^-$ are connected to the methyl group of the $DMANH^+$ through C–H···O weak hydrogen bonds with lengths between 3.156(2) Å and 3.246(2) Å in the case of the carboxyl group of the donor 3CBA molecule and 3.291(2) Å and 3.477(2) Å in the case of the carboxylate group from the other 3CBA molecule (Figure 4-45).

The unprotonated DMAN in this molecular complex is disordered having the naphthalene rings in the same plane in a slightly shifted position. The twisted position of the methyl groups relative to the naphthalene group are in the same direction in both disordered parts with respect to each other. The disordered sites show a 50:50% occupancy and these positions have been refined anisotropically except in the case of one carbon atom where the two symmetry related positions are too close and have been left with an isotropic thermal parameter in the final refinement (*Figure 4-45*).

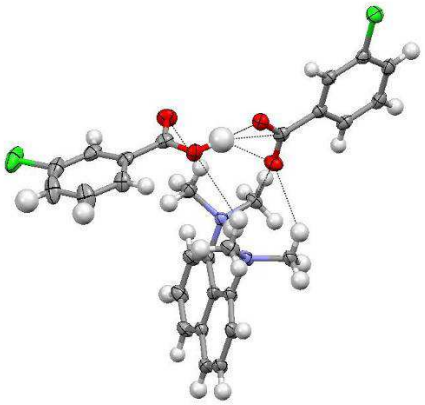

Figure 4-44. The intermolecular interactions between the $DMANH^+$ and the oxygen atoms of the $DIMER^-$ in the molecular complex of DMAN : 3CBA.

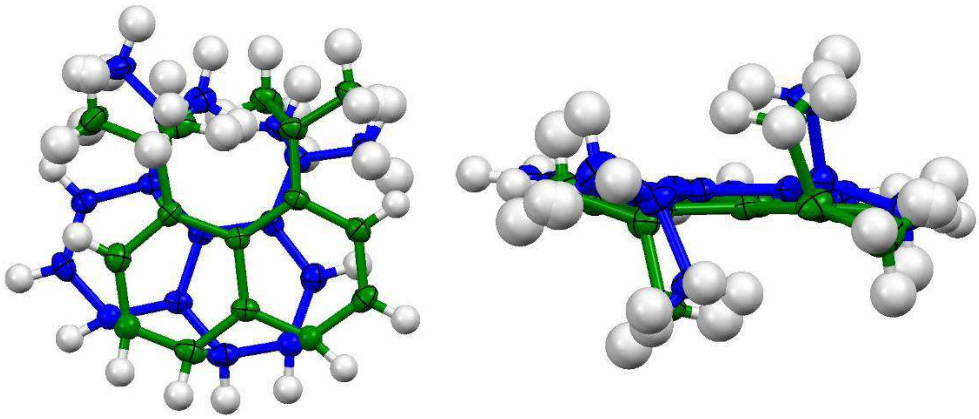

Figure 4-45. The disordered DMAN viewed perpendicular to the plane (left) and along the plane (right) of the naphthalene ring in the complex of DMAN : 3CBA. The blue and green colours mark the two sets of occupied atomic sites.

The hydrogen atoms are refined independently in the non disordered molecules and are generated in calculated positions in the case of the disordered DMAN molecule. In the protonated $DMANH^+$ molecules the intramolecular N–H···N hydrogen bond has length 2.583(2) Å with N–H = 1.09(2) Å and H···N = 1.55(2) Å and a slightly elongated electron density showing in the difference Fourier map, while the disordered unprotonated DMAN has a N···N separation of 2.788(5) Å. The correlation between the C–N bond length and the donor acceptor side is

again present, with differences between the two bond lengths longer than 0.02 Å (*Table 4-1*).

The benzoic acids are connected through intermolecular C–O···H weak hydrogen bonds between the non-hydrogen bonded oxygen of the carboxyl group and a hydrogen from the benzene ring within the sum of the van der Waals radii, with a C···O distance of 3.374(2) Å, in a saw tooth like arrangement describing a chain of $DIMER^{-}$s (Figure 4-46).

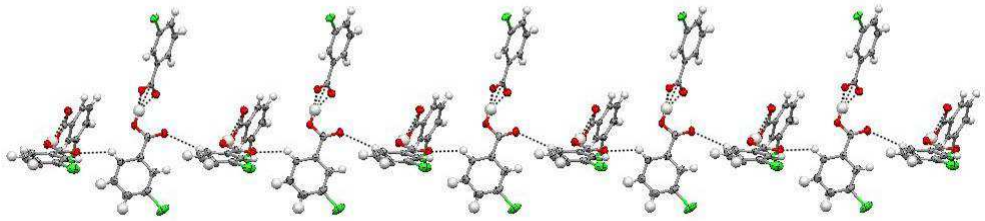

Figure 4-46. C–H···O intermolecular interactions between the 3CBA $DIMER^{-}$s in the molecular complex of DMAN : 3CBA.

The protonated $DMANH^{+}$ and the unprotonated DMAN molecules are connected through C–H···π weak HBs with lengths between ~3.54 Å and ~4 Å and interlocked between chains of the $DIMER^{-}$s through further C–H···π weak HBs with lengths between ~3.73 Å and ~3.81 Å, as well as C–H···O weak hydrogen bonds between the methyl group of the $DMANH^{+}$ and the carboxyl group of the $DIMER^{-}$, with distances of 3.354(2) Å and 3.391(2) Å. The two protonated $DMANH^{+}$ molecules are in a parallel stacked arrangement in the overall packing chain of stacked DMAN and $DMANH^{+}$ molecules between benzoic acids in the overall structural packing (*Figure 4-47*).

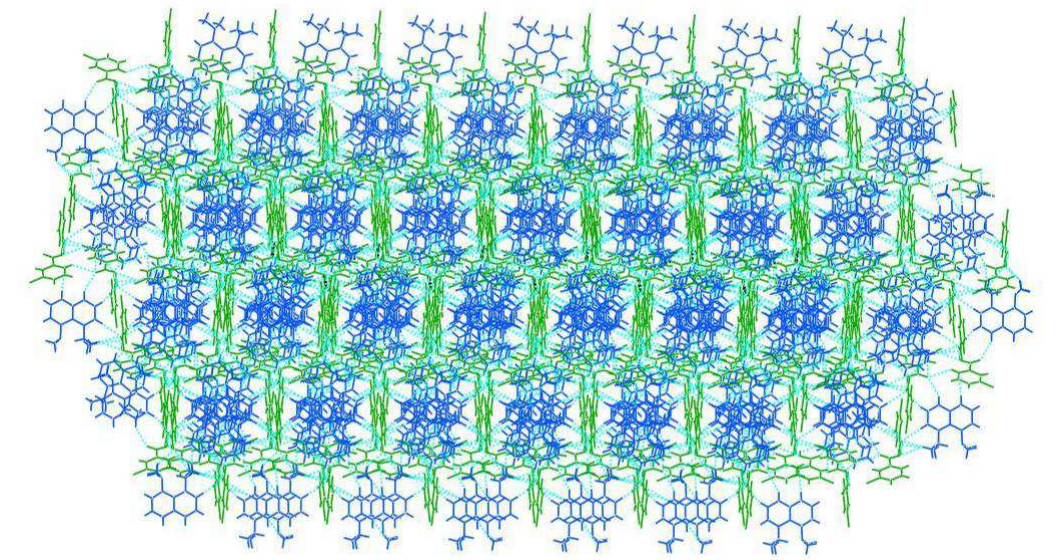

Figure 4-47. The structure of DMAN :3CBA as a whole, with the $DMANH^+$ and DMAN molecules (blue) held between the chains of 3CBA $DIMER^-$s (green).

4.3.4 DMAN : 3-bromobenzoic acid (1:1)

The DMAN : 3BBA complex crystallises in a 1:1 ratio with four DMAN molecules, two protonated and two unprotonated, and four 3BBA molecules in the asymmetric unit. The SSHB is present in the structure as in most of the halogen substituted benzoic acid – DMAN complexes. One proton is transferred from each of two of the 3BBAs to two DMANs and the usual $DIMER^-$ unit is formed through single SSHBs between neutral and deprotonated 3BBA molecules, leaving two DMAN molecules unprotonated.

In this case the collected data is not as high resolution as in the other complexes presented, creating difficulty in determining H atom parameters. In the structure, the protonation state of the DMAN molecules is thus established by the comparison of the torsion angle between the methyl and naphthalene group (given previous findings for these in the different cases of $DMANH^+$ and DMAN) and the N····N distances, combined with the difference Fourier map of the hydrogen atom electron density in the region of the possible intramolecular hydrogen bond created on protonation. While in one $DMANH^+$ the difference Fourier map shows a rather clear electron density peak corresponding to the

hydrogen in the intramolecular HB, in the other case the map is very noisy and the electron density is smeared between the two nitrogen atoms and is far less convincing (*Figure 4-48*).

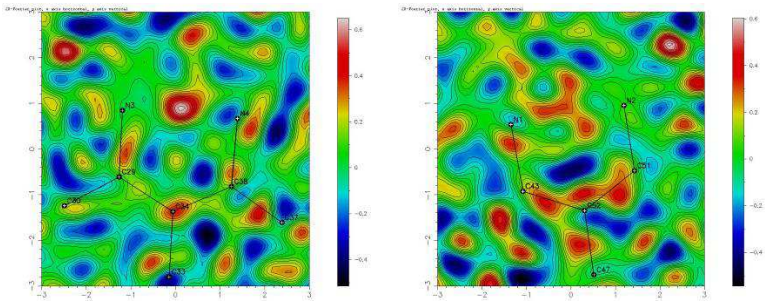

Figure 4-48. Difference Fourier maps of the two protonated DMANH$^+$ molecules in the plane of the two nitrogen atoms and the carbon atom from the naphthalene ring in molecular complex of DMAN and 3BBA.

Comparing the two unprotonated DMAN molecules, these are found to differ slightly in the torsion angles of the methyl groups to the naphthalene ring (*Figure 4-49; Table 4-11*), and in the N····N separations, of 2.805(7) Å (red) and 2.772(7) Å (green), respectively.

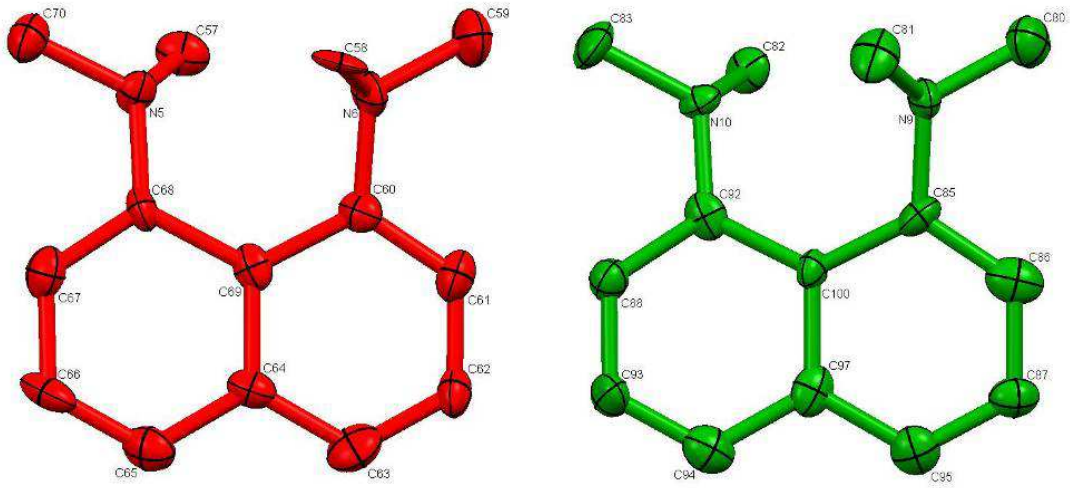

Figure 4-49. The two unprotonated DMAN molecules in the molecular complex of DMAN : 3BBA, viewed perpendicular to the plane of the naphthalene ring.

Table 4-11. The torsion angles of the methyl group within the two unprotonated DMAN molecules in the molecular complex of DMAN : 3BBA.

DMAN molecule	Methyl carbon	Nitrogen	Naphthalene carbon	Naphthalene carbon	Torsion (°)
Green	C83	N10	C92	C100	-164.3(6)
	C82	N10	C92	C100	63.6(8)
	C80	N9	C85	C100	-159.1(6)
	C81	N9	C85	C100	64.1(8)
Red	C70	N5	C68	C69	-166.8(6)
	C57	N5	C68	C69	62.4(8)
	C59	N6	C60	C69	-158.8(6)
	C58	N6	C60	C69	70.6(8)

The protonated DMAN molecules have similar small deviations between the torsion angles, but the plane of the methyl groups (defined by the N and two methyl carbons) on each side is in this case perpendicular to the plane of the naphthalene ring. The intramolecular hydrogen bond in the two $DMANH^+$ molecules have N····N distances of 2.576(7) Å and 2.580(7) Å (*Figure 4-50*). The relatively large difference appearing in the C–N bond lengths (>0.02 Å) could be a sign of an asymmetrically positioned hydrogen atom within the N–H···N intramolecular hydrogen bridge (*Table 4-1*).

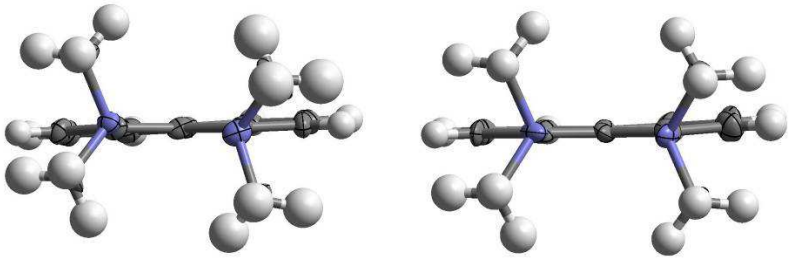

Figure 4-50. The protonated $DMANH^+$ molecules, with N····N distances of 2.576(7) Å (left) and 2.580(7) Å (right), in the molecular complex of DMAN : 3BBA, showing the perpendicular orientations of the methyl groups in both molecules.

The hydrogen bonds between the 3BBAs in the $DIMER^-$ units are in the range of charge-assisted SSHBs as in the case of the other halogen substituted benzoic acids. The hydrogen bonds in the two $DIMER^-$ units have a small (~0.02 Å) difference between their lengths, with bond lengths of 2.461(7) Å and 2.443(6) Å. The differences between the C–O and C=O bond lengths suggest an assignment of the donor side of the generated hydrogen atom as shown in the

DMAN complexes above (*Table 4-1*). The difference Fourier map is very noisy, precluding further comment on the bonding (Figure 4-51).

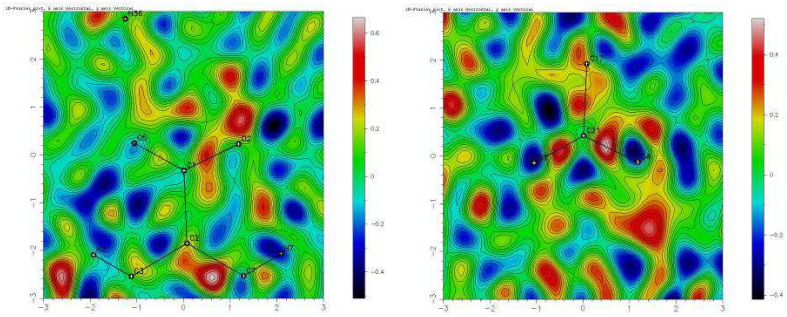

Figure 4-51. The difference Fourier maps of the hydrogen atom electron density in the two intermolecular SSHBs within the DIMER⁻ units in the molecular complex of DMAN : 3BBA.

The four DMAN molecules (two protonated and two unprotonated) are connected together through intermolecular C–H···π weak HBs with distances from ~3.57 Å to ~3.59 Å and displaced π····π stacking with a distance of ~3.58 Å between the closest π bonds (*Figure 4-52*) into a single four-molecule building block unit in the structure, as are the 3BBA DIMER⁻s.

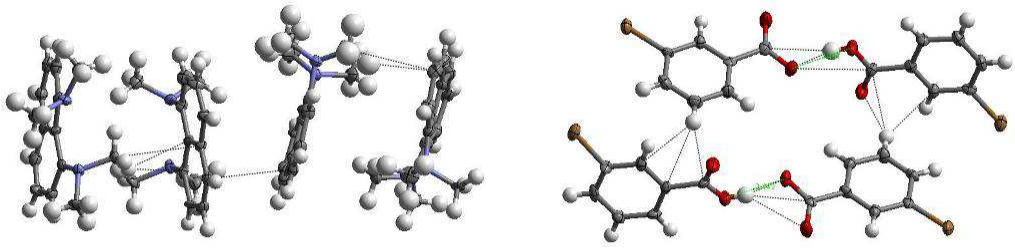

Figure 4-52. The building blocks of two protonated and two unprotonated DMAN molecules (left) and the 3BBA DIMER⁻s in the molecular complex of DMAN : 3BBA, both connected through C–H····π weak HBs.

The asymmetric unit of the DMAN : 3BBA molecular complex contains four 3BBA molecules and as consequence of the deprotonation they form two 3BBA single hydrogen bonded DIMER⁻s. The DIMER⁻s of the 3BBA are connected side-by-side forming a long ribbon of dimers which are connected through halogen-halogen interactions between the bromine atoms, creating a zig-zag layer of dimers

(*Figure 4-53*). The layer of 3BBA DIMER$^-$s are held together by blocks of DMAN molecules (*Figure 4-54*).

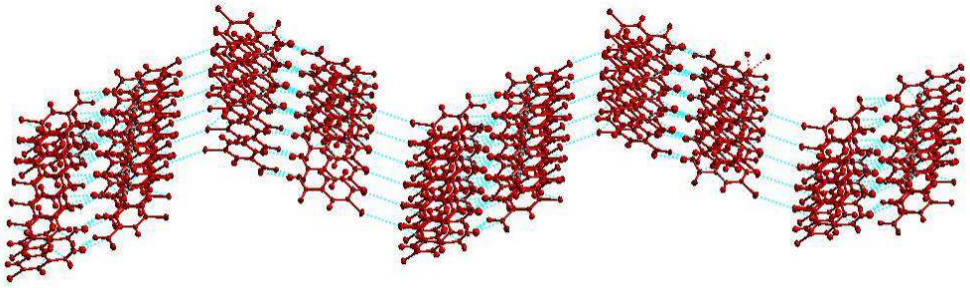

Figure 4-53. The layer of 3BBA DIMER$^-$s connected through halogen-halogen interactions, in the molecular complex of DMAN : 3BBA.

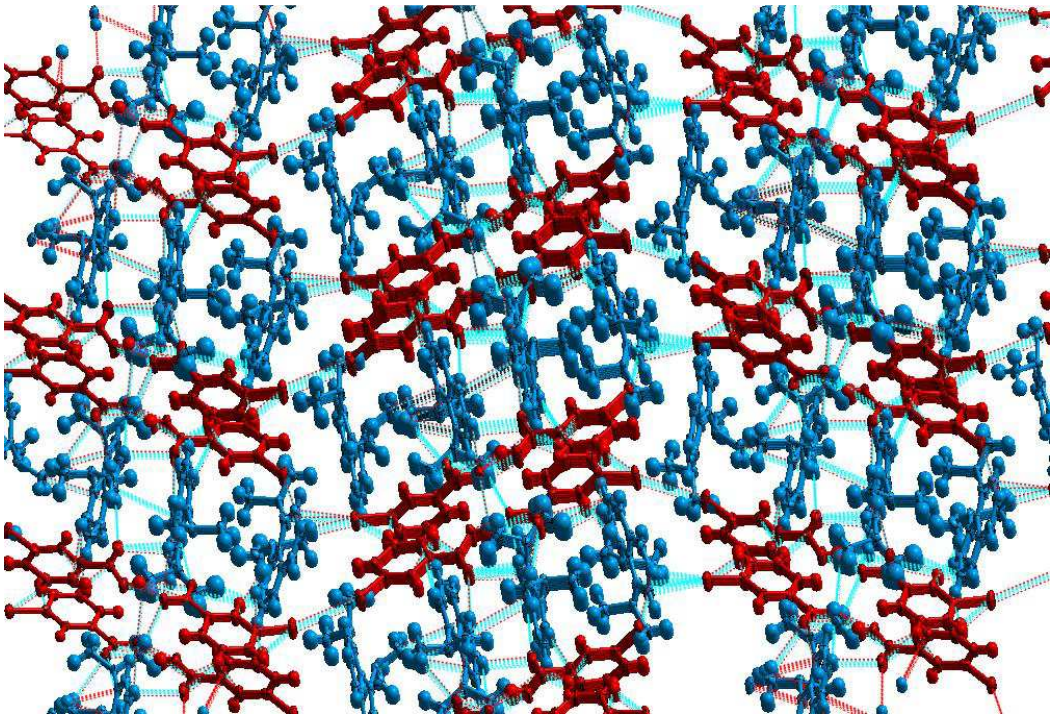

Figure 4-54. The structure layout of the DMAN – 3BBA complex showing the zig-zag layer of 3BBA DIMER$^-$s (red) held together by the DMAN and DMANH$^+$ building blocks (blue), in the molecular complex of DMAN : 3BBA.

While the two DIMER$^-$s have the same components and are connected through a very similar SSHB, there are significant differences in the role they play in the overall structure. The layers formed by the benzoic acid DIMER$^-$s are connected

through type I halogen-halogen interactions but in only one of the two DIMER⁻ units are these interactions within the sum of the van der Waals radii, with a Br····Br distance of 3.608(1) Å and thus considered as a force with possible significant effect[81] on the crystal packing as a whole. These halogen bonded DIMER⁻s create a long chain which holds together the formed ribbon. The 3BBA molecules in the two different DIMER⁻s show a difference between the torsion of the carboxyl group and the benzene ring. This arrangement is more planar in the case of the dimer not involved in the halogen interaction and more twisted in the case of the dimer involved in the halogen-halogen interaction (*Figure 4-55*), with relevant torsion angles listed in *Table 4-12*.

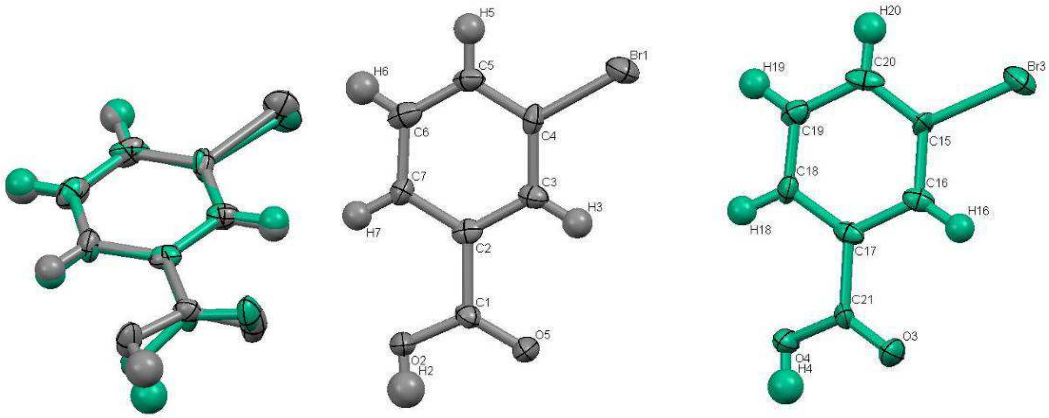

Figure 4-55. Structure overlay of the 3BBA from the dimer involved (green) and not involved (grey) in the halogen-halogen interaction in the molecular complex of DMAN : 3BBA. For clarity the labelled molecules are separated.

Table 4-12. Torsion angle of carboxyl group to the benzene ring in the two different DIMER⁻s, within the molecular complex of DMAN : 3BBA

Dimer	Atoms of the measurement points				Torsion (°)
Halogen bonded	O3	C21	C17	C16	18(1)
	O4	C21	C17	C18	17.6(9)
	O6	C8	C9	C10	-9.0(9)
	O1	C8	C9	C14	-11(1)
Non-Halogen bonded	O5	C1	C2	C3	-7(1)
	O2	C1	C2	C7	-3.4(9)
	O7	C28	C26	C27	3(1)
	O8	C28	C26	C25	4(1)

A similar difference in the torsional arrangements is seen in the $DIMER^-$ units, with the two $DIMER^-$s having a difference in the relative orientation of the two 3BBA molecules to each other (*Figure 4-56*). This is measured by the torsion angle of the three atoms along one of the 3BBA molecules and the carbon atom of the carboxyl group on the other benzoic acid in the $DIMER^-$s, as shown in *Table 4-13*.

Table 4-13. The torsion angles of the two different $DIMER^-$s along the overlaid molecule and the carbon atom of the carboxyl group from the other 3BBA molecule, in the molecular complex of DMAN : 3BBA.

Green	C20	C17	C21	C8	-127(9)
Grey	C5	C2	C1	C28	108(10)

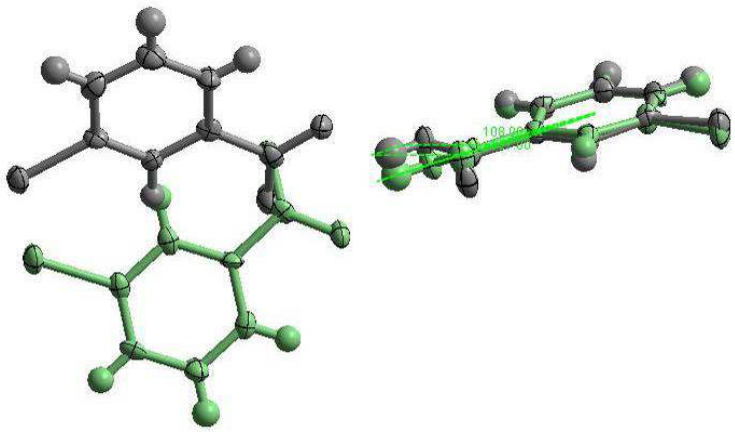

Figure 4-56. Overlay of the two different $DIMER^-$s in the DMAN-3BBA complex where the overlay is of the 3BBA molecules in one side of the $DIMER^-$; the colours indicate the dimer involved (green) and not involved (grey) in the halogen-halogen interaction.

There are differences in the two $DIMER^-$s in the length of the intermolecular interactions between the oxygen atoms of the carboxyl groups and the methyl groups of the $DMANH^+$ molecules. In the case of the $DIMER^-$ involved in the Br···Br interactions, these short contacts consist of C–H···O weak hydrogen bonds with C···O distances between 3.17(1) Å and 3.30(1) Å, while in the case of the other $DIMER^-$ these contacts have distances from 3.08(1) Å to 3.284(8) Å. All of these interactions are within the sum of the van der Waals radii and in both

instances the carboxyl groups in the $DIMER^-$s make these short contacts to the protonated $DMANH^+$ molecules.

This is the first structure studied here that contains two different $DIMER^-$ units and allows a comparison between the $DIMER^-$s having the same unit and maintaining the very short single hydrogen bond and yet having distinct $DIMER^-$ characteristics as a result of being involved in different local interactions.

4.3.5 DMAN : 3-idobenzoic acid (1:2)

The molecular complex of DMAN : 3IBA structure is more similar to those of the the *ortho*-halogen substituted benzoic acid complexes with DMAN. The asymmetric unit contains a protonated $DMANH^+$ and a single hydrogen bonded $DIMER^-$. The other similarities of the structure to those of the *ortho*-substituted complexes are the relative position of the $DIMER^-$s to the $DMANH^+$ and the intermolecular interaction between the non-hydrogen bonded oxygen atoms from the carboxyl group and the methyl groups of the $DMANH^+$. These intermolecular contacts comprise C–H···O interactions with C···O lengths between 3.183(3) Å and 3.351(5) Å, and O···H contacts with a length of 2.68(3) Å. The intramolecular hydrogen bond is asymmetric with a length 2.580(3) Å with N–H = 1.05(4) Å and H···N = 1.57(4) Å. Although the hydrogen bond appears very asymmetric this does not appear in the differences between the C–N bond on the donor-acceptor side, but as a heavy atom is present in the structure the position of the hydrogen atom within the hydrogen bond is not well defined in this case (*Table 4-1*).

Compared to the DMAN : 2IBA where are no halogen-halogen interactions present within the sum of van der Waals radii, in this complex the $DIMER^-$s are connected through such interactions (*Figure 4-57*). The length of the I···I type II halogen-halogen interaction is significantly shorter than the sum of van der Waals radii (4.00 Å), with a length of 3.7370(3) Å.

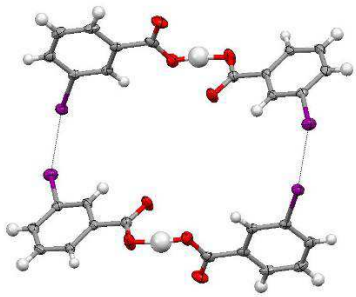

Figure 4-57. The I···I interaction between the 3IBA DIMER⁻s in the molecular complex of DMAN : 3IBA.

The pair of halogen bonded DIMER⁻s are connected through further C–H···π weak HBs with length of ~3.56 Å to another pair of DIMER⁻s forming a layer of DIMER⁻s and these layers are held together by C–H···O and O···H intermolecular interactions listed above (between the carboxyl group of the DIMER⁻ over the methyl groups of the $DMANH^+$) with additional C–H···O weak hydrogen bonds with distances between 3.086(4) Å and 3.193(5) Å and C–H···π weak HBs with distances between ~3.622 Å and ~3.69 Å (*Figure 4-58*). Pairs of $DMANH^+$ molecules are π···π stacked through a parallel displaced stacking with a distance of ~3.65 Å between the two planes.

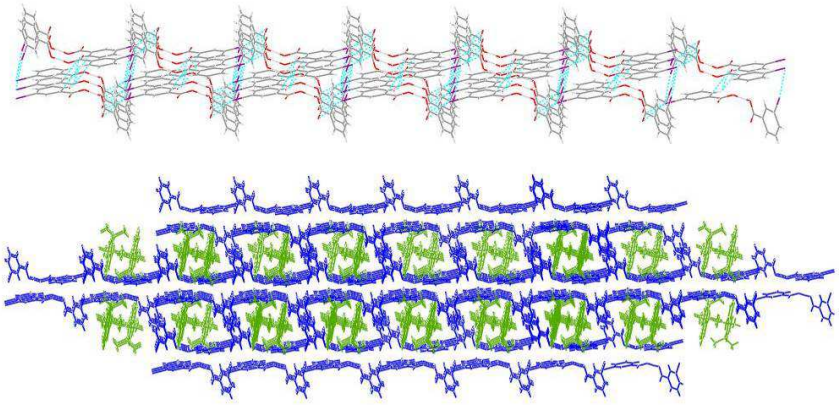

Figure 4-58. The layers of 3IBA DIMER⁻s (top) and the $DMANH^+$ molecules (green) encaged between these layers of DIMER⁻s in the molecular complex of DMAN : 3IBA.

Variable temperature X-ray data were collected for this complex (Table 4-5), but since the iodine is a heavy atom in the structure the difference Fourier maps generated are very noisy and do not provide evidence for further reliable

conclusions to be drawn regarding the detail of the hydrogen bonded hydrogen atom parameters, apart from the fact that in this case as well the donor side C–O and C=O bonding suggest the right donor side assignment of the hydrogen atom (*Table 4-1*).

4.4 Molecular complexes of DMAN and *para*-substituted benzoic acids

Experimental data

1:2 Molecular complex of DMAN : 4-fluorobenzoic acid (4FBA) -hydrate - 1:2 molar ratio of 4FBA and DMAN were dissolved in acetonitrile and evaporated at room temperature, slowing the evaporation by closing the vial with a small clipped lid. After the evaporation of the solvent, colourless blocks were formed. Single crystal X-ray diffraction data were collected on a Rigaku R-AXIS RAPID diffractometer at 100K. The data has were solved within the WinGX structure solution program suite.

1:1 Molecular complex of DMAN : 4-chlorobenzoic acid (4CBA) - 1:1 molar ratio of 4CBA and DMAN were dissolved in methanol and evaporated at room temperature, slowing the evaporation by closing the vial with a small clipped lid. After the evaporation of the solvent, colourless blocks were formed. Single crystal X-ray diffraction data were collected on a Bruker APEX II diffractometer at 100K. The data were solved within the WinGX structure solution program suite.

1:2 Molecular complex of DMAN : 4-bromobenzoic acid (4BBA) - 1:2 molar ratio of 4BBA and DMAN were dissolved in methanol and acetone 1:1 solvent mixture evaporated at constant temperature of 4°C, slowing the evaporation by closing the vial with a small clipped lid. After the evaporation of the solvent, pale brown blocks were formed. Single crystal X-ray diffraction data were collected on a Bruker Nonius Kappa CCD diffractometer at 100, 200, 300K. The data were solved within the WinGX structure solution program suite. The hydrogen atoms are generated on carbon atoms in the refinement 300K data set.

1:2 Molecular complex of DMAN : 4-iodobenzoic acid (4IBA) - 1:2 molar ratio of DMAN and 4IBA were dissolved in acetone and evaporated at room temperature, slowing the evaporation by closing the vial with a small clipped lid. After the evaporation of the solvent, purple blocks were formed. Single crystal X-ray diffraction data were collected on a Bruker Nonius Kappa CCD diffractometer at 110, 200 and 300K. The data were solved within the WinGX structure solution program suite.

The crystallographic data for the structures are summarised in *Table 4-14*.

4.4.1 DMAN : 4-fluorobenzoic acid hydrate (1:2:1)

The DMAN : 4FBA hydrated complex is a second molecular complex found with water in its structure. The complex however, is very different from the DMAN : 3FBA hydrated complex. The crystallisation ratio of 4FBA and DMAN is 2:1 with an additional water molecule in the complex. The structure shares many of the structural features shown in the complexes with the "normal" 2:1 co-crystallisation ratio in the case of the benzoic acid and DMAN complexes. The crystal structure of the complex contains one protonated $DMANH^+$ molecule with an asymmetric N-H···N hydrogen bond as shown in the other DMAN complexes presented here, with an N···N distance of 2.562(3) Å and N–H = 1.09(2) Å, H···N = 1.51(2) Å donor and acceptor distances, respectively. The 4FBA molecules form a single hydrogen bonded $DIMER^-$ with a charge-assisted SSHB the shortest found in the DMAN and halogen substituted benzoic acids complexes with an O···O bond length of 2.411(2) Å. The hydrogen bond is asymmetric with O–H = 1.16(3) Å and H···O = 1.25(3) Å. The C–O and C=O bond distance correlation between the carboxyl group in the donor side and the acceptor side does not match in those found in the above described DMAN and halogen substituted benzoic acids, but since this HB is significantly shorter than the next shortest in the above discussed complexes and the carboxyl group is also bonded to the water molecule, this could have a significant effect in this correlation found in the other complexes (Table 4-1).

Table 4-14. Crystallographic data of molecular complexes of DMAN with 4FBA, 4CBA, 4BB, 4IBA from the X-ray refinement.

Compound	1:2 :1 DMAN : 4FBA hydrate	1:1 DMAN : 4CBA	1:2 DMAN : 4BBA			1:2 DMAN : 4IBA		
Diffractometer	Rigaku R-AXIS RAPID	Bruker APEX II	Nonius Kappa CCD	Nonius Kappa CCD	Nonius Kappa CCD	Nonius Kappa CCD	Nonius Kappa CCD	Nonius Kappa CCD
Formula	C_{28} H_{30} F_2 N_2 O_5	C_{42} H_{46} Cl_2 N_4 O_4	C_{28} H_{30} N_2 Br_2 O_4	C_{28} H_{30} N_2 Br_2 O_4	C_{28} H_{30} N_2 Br_2 O_4	C_{28} H_{30} N_2 I_2 O_4	C_{28} H_{30} N_2 I_2 O_4	C_{28} H_{30} N_2 I_2 O_4
Molecular weight / gmol^{-1}	512.544	741.73	616.34	616.34	616.34	710.35	710.35	710.35
Temperature (K)	100	100	100	200	300	110	200	300
Space Group	$P2_1/n$	$P\bar{1}$	$P2_1/n$	$P2_1/n$	$P2_1/n$	$P2_1/n$	$P2_1/n$	$P2_1/n$
a (Å)	13.530(5)	9.7429(5)	11.3276(1)	11.35880 (10)	11.4098(2)	11.4230(2)	11.4836(2)	11.5585(2)
b (Å)	11.220(5)	11.7142(5)	7.6916(1)	7.73860(1)	7.79690(10)	7.75020(10)	7.7761(1)	7.8151(1)
c (Å)	16.137(5)	18.8782(9)	29.9623(4)	30.1256(4)	30.3204(4)	30.7590(6)	30.8558(5)	30.9328(5)
α (°)	90.000(5)	95.910(2)	90	90	90	90	90	90
ß (°)	94.043(5)	101.181(3)	96.0070(10)	96.1268(7)	96.1838(8)	96.8230(10)	96.9309(7)	96.9770(8)
γ (°)	90.000(5)	112.787(2)	90	90	90	90	90	90
Volume (Å^3)	2443.6(16)	1910.57(16)	2596.20(5)	2632.95(7)	2681.64(7)	2703.83(8)	2734.92(7)	2773.49(7)
Z	4	2	4	4	4	4	4	4
θ range/°	3.11 – 27.48	1.12 – 26.37	1.37 – 30.03	1.37 – 30.15	1.35 – 30.45	1.33 – 30.02	1.33 – 30.07	1.33 – 26.63
Completeness (%)	99.8	99.5	99	99.1	97.6	100	100	99.4
Reflections Collected	29859	36804	38997	43605	40129	41636	42245	52167
Independent	5589	7761	7522	7599	7687	7891	7923	5659
Refln (obs.I>2theta(I))	3695	5924	5938	4852	3503	5152	4073	3322
R_{int}	0.0611	0.0351	0.0585	0.0883	0.0935	0.0757	0.0932	0.0757
Data/Rest./Param.	5589/0/454	7761/0/674	7522/0/437	7599/0/437	7686/0/337	7891/0/437	7923/0/437	5659/0/437
GooF on F^2	1.016	1.026	1.044	1.052	1.016	1.054	1.008	1.167
R_1 (Observed) / R_1 (all)	0.0503 / 0.083	0.0382 / 0.0572	0.0438 / 0.0632	0.0539 / 0.0993	0.0653 / 0.164	0.0436 / 0.0944	0.0471 / 0.1363	0.0427 / 0.1014
wR_2 (all)	0.1729	0.1028	0.1181	0.1441	0.1876	0.0749	0.0834	0.0789
ρ(max / min) / e-Å^{-3}	0.286 / -0.361	0.292 / -0.429	1.52 / -0.961	0.0903 / -0.781	0.586 / -0.0635	0.636 / -0.733	0.461 / -0.608	0.535 / -0.913
RMS / eÅ^{-3}	0.084	0.04	0.126	0.105	0.109	0.168	0.105	0.166

The DIMER$^-$s relative position to the DMANH$^+$ molecules shows similarities as well between this and the other DMAN complexes described here with intermolecular interactions between the carboxyl group of the DIMER$^-$ and the DMANH$^+$ (*Figure 4-59*).

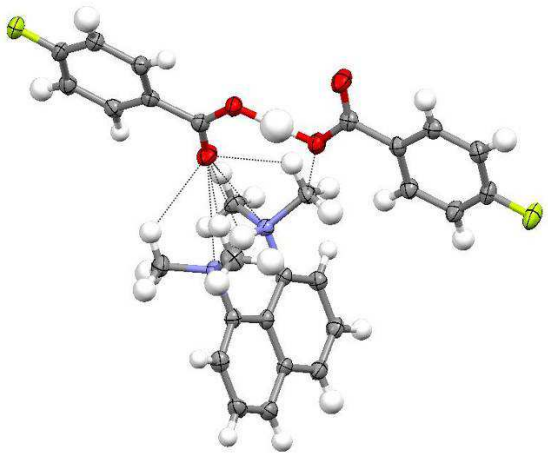

Figure 4-59. Intermolecular interactions between the methyl groups of DMANH$^+$ and carboxyl group of the DIMER$^-$.

These interactions consist of C–H···O weak hydrogen bonds with C···O distances between 3.112(3) Å and 3.214(3) Å, N···O contacts with distances of 2.991(2) Å and 3.042(2) Å and an O···H contact with a distance of 2.50(3) Å. All of these interactions, the crystallisation ratio and the DMAN and 4FBA DIMER$^-$s relative positions make them similar to the 1:2 DMAN and halogen substituted benzoic acids complexes. However the complex is hydrated and this changes the overall packing of the complex. The water molecule is hydrogen bonded to the carboxyl groups of the DIMER$^-$ through moderate hydrogen bonds with O···O distances of 2.765(2) Å and 2.767(2) Å (*Figure 4-60*).

The DIMER$^-$s of 4FBA form a layer within the structure in a herring bone like arrangement (*Figure 4-61*). The water molecules links together these layers through an intermolecular C–H···O hydrogen bond with a C···O length of 3.318(3) Å and also connects the DIMER$^-$ to the DMANH$^+$ through an additional C–H···O hydrogen bond with a C···O distance of 3.369(3) Å.

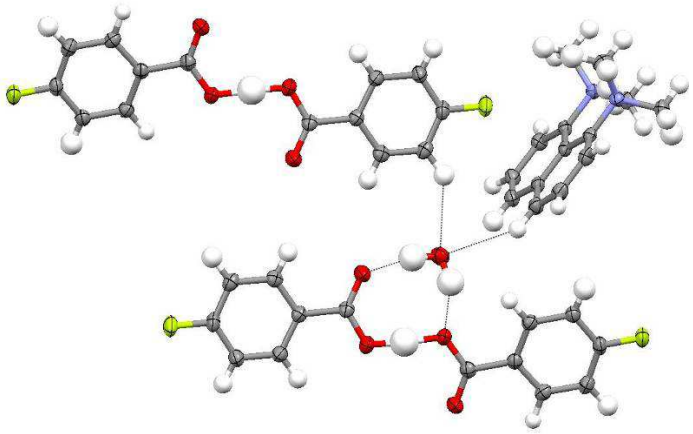

Figure 4-60. The water molecules intermolecular interactions with the DIMER⁻s and the DMANH⁺ molecule within the molecular complex of DMAN : 4FBA hydrate..

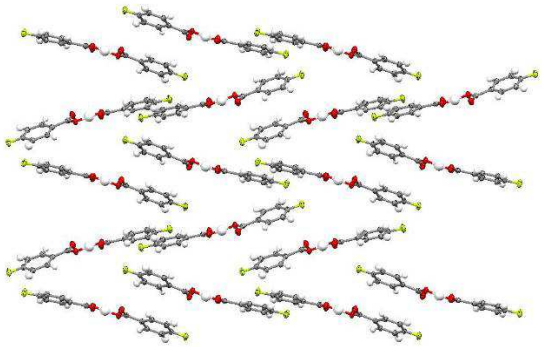

Figure 4-61. Layer formed from DIMER⁻s in a herring bone like arrangement.

The $DMANH^+$ molecules are connected in pairs through intermolecular C–H···π weak HBs with lengths between ~3.54 Å and ~3.85 Å. These pairs of $DMANH^+$ molecules are between the layers holding together these layers through the intermolecular interactions between the $DMANH^+$ molecules and the carboxyl groups of the $DIMER^-$s discussed above (*Figure 4-62*). The pairs of $DMANH^+$ molecules shows similar orientation relative to each other as in the 1:2 DMAN : substituted benzoic acids complexes, but between the $DMANH^+$ are π···π interactions with a larger overlapped surface and separation between the pairs of $DMANH^+$ molecules is larger.

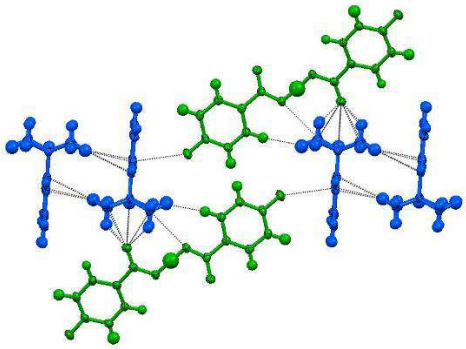

Figure 4-62. Pairs of DMANH$^+$ molecules connected through C–H···π weak HBs and the pairs relative position to each other.

The halogens form an additional C–H···F weak hydrogen bond in one side with an F···H length of 2.34(3) Å and F···π interactions with a length of ~3.16 Å in the other side between DMANH$^+$ and DIMER$^-$s, connecting two DMANH$^+$ molecules on the two sides of the 4FBA DIMER$^-$s layer (Figure 4–63).

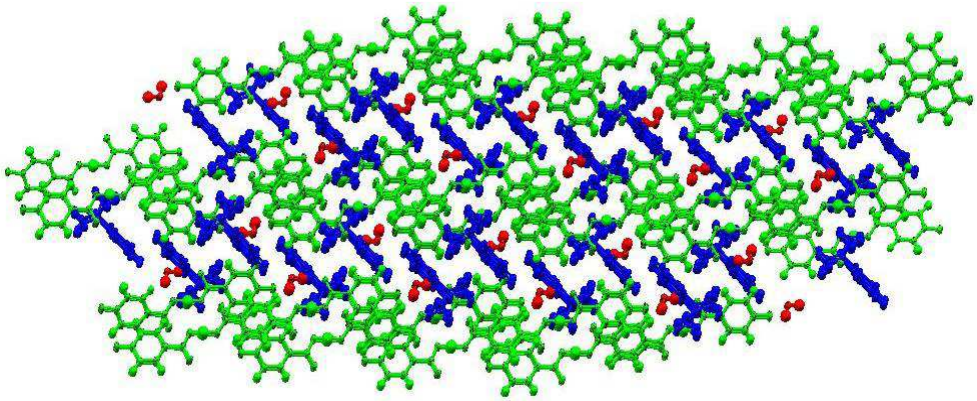

Figure 4-63. Overall packing of the 4FBA : DMAN hydrate complex, showing the DMANH$^+$ molecules (blue) holding together the layers of DIMER$^-$s (green) with additional intermolecular interaction from the water molecules (red).

The electron density within the intermolecular O–H···O and the intramolecular N–H···N hydrogen bonds is slightly elongated but there is no sign of splitting behaviour (Figure 4-64).

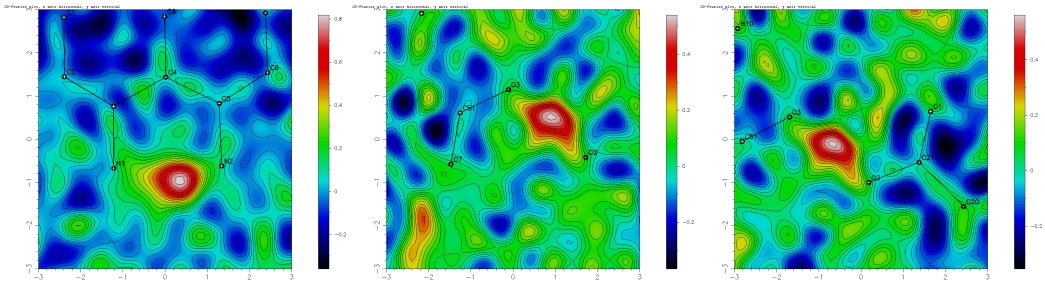

Figure 4-64. Difference Fourier maps of the hydrogen atom electron density within the intramolecular N–H···N hydrogen (left) and the intermolecular O–H···O (centre, right) hydrogen bonds.

4.4.2 DMAN : 4-chlorobenzoic acid (1:1)

The DMAN : 4CBA molecular complex crystallises in 1:1 ratio with an asymmetric unit containing one protonated $DMANH^+$ molecule, a 4CBA $DIMER^-$ connected through the familiar single charge-assisted SSHB and an unprotonated DMAN molecule. The protonated $DMANH^+$ with the $DIMER^-$ of the benzoic acid have been well described in all previously presented structures except the DMAN : 3FBA hydrate. This is the fourth complex presented with an unprotonated DMAN, and shows different features from the other three complexes containing unprotonated DMAN molecules.

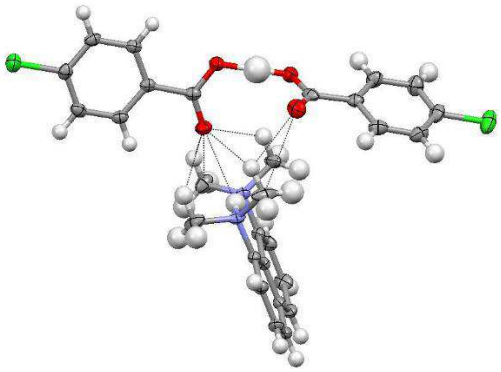

Figure 4-65. The relative position and the short contacts within the sum of van der Waals radii between the protonated $DMANH^+$ and the single hydrogen bonded $DIMER^-$s in the molecular complex of DMAN : 4CBA.

The intramolecular N–H···N hydrogen bond is asymmetric, with N···N distance of 2.602(1) Å and the asymmetric hydrogen position indicated by N–H = 0.99(2) Å and H···N = 1.65(1) Å bond lengths. The trend found in the in the C–N bond lengths with respect to the hydrogen donor side within the N–H···N hydrogen bond, and that of the C–O and C=O bond lengths showing a larger deviation in the case of the carboxyl group found on the donor side is followed (*Table 4-1*). The relative positions of the $DIMER^-$ and the $DMANH^+$ are similar to the other DMAN : halogen-substituted benzoic acid complexes, with the short contacts between the non-hydrogen bonded oxygen atom of the $DIMER^-$ carboxyl group and the methyl group of the $DMANH^+$ molecule, consisting of C–H···O weak hydrogen bonds with C···O distances between 3.085(3) Å and 3.298(3) Å and the O···H with a distance of 2.69(2) Å, all within the sum of van der Waals radii (*Figure 4-65*).

The single hydrogen bond between the 4CBA $DIMER^-$, as in the other complexes, is within the range expected for the charge-assisted SSHB with a bond length of 2.478(2) Å with an asymmetric hydrogen position within the hydrogen bridge, with distances of O–H = 1.13(3) Å and 1.34(3) Å. The hydrogen atom has a large isotropic thermal parameter confirmed by the slightly elongated electron density from the difference Fourier map (*Figure 4-66*).

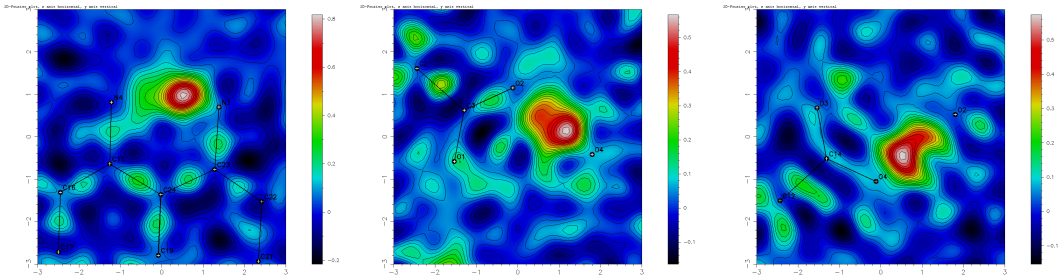

Figure 4-66. Difference Fourier maps of the hydrogen atoms electron density within the intramolecular N-H···N hydrogen (left) and the intermolecular O-H···O (centre, right) hydrogen bonds.

All three previously presented complexes containing both unprotonated DMAN and protonated $DMANH^+$ in their structures have shown differences in either the ratio of components (3:4 in the case of the DMAN : 3CBA complex, which also

contained a disordered DMAN molecule), inclusion of water in the case of DMAN : 3FBA hydrate or in having a very large asymmetric unit consisting of two different DMAN, $DMANH^+$ and $DIMER^-$ components. The molecular complex of DMAN : 4CBA is no exception to this observation. While the ratio of the DMAN and benzoic acid is 1:1 and the asymmetric unit contains just one protonated $DMANH^+$ and one unprotonated DMAN, but the methyl groups of the unprotonated DMAN molecules are occupationally disordered across their two twisted positions. The occupancy ratio of the two orientations of the methyl group is 75%:25% and the torsion angles describing both orientations are consistent with those for the unprotonated DMAN molecules described in the literature[161] (*Figure 4-67*).

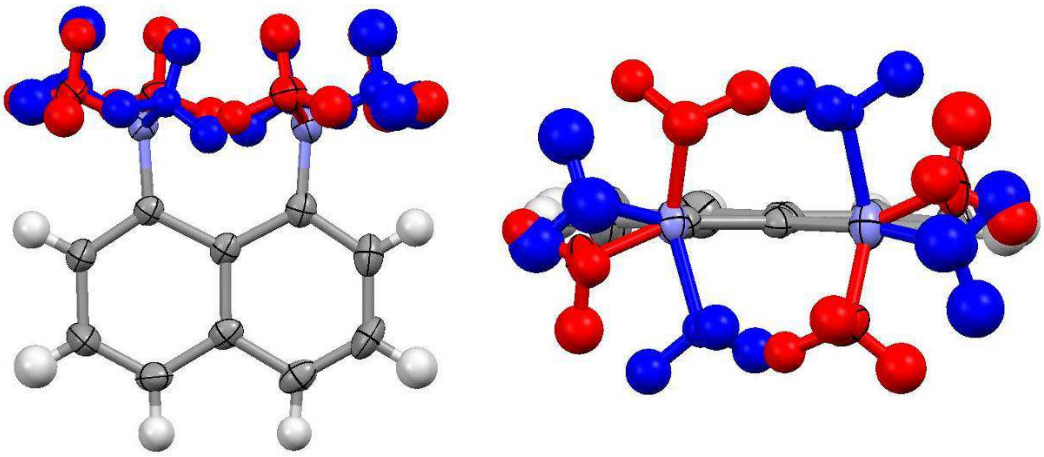

Figure 4-67. The unprotonated DMAN in the molecular complex of DMAN : 4CBA viewed perpendicular to (left) and along (right) the plane of the naphthalene ring, showing the methyl group with the 75% (red) and 25% occupancy(blue).

The carbon atoms of the methyl groups with the lower occupancy have not been refined anisotropically and the hydrogen atoms on these carbons are generated.

The 4CBA $DIMER^-$s are connected to each other through four C–H···O intermolecular short contacts with lengths between 3.346(3) Å and 3.391(2) Å on one side and through two C–H···π interactions with a length of 3.644(2) Å on the other, forming a zig-zag band of $DIMER^-$s. The bands of $DIMER^-$s are connected through Cl···Cl interactions with a distance of 3.4823(7) Å forming a layer in the structure (*Figure 4-68*).

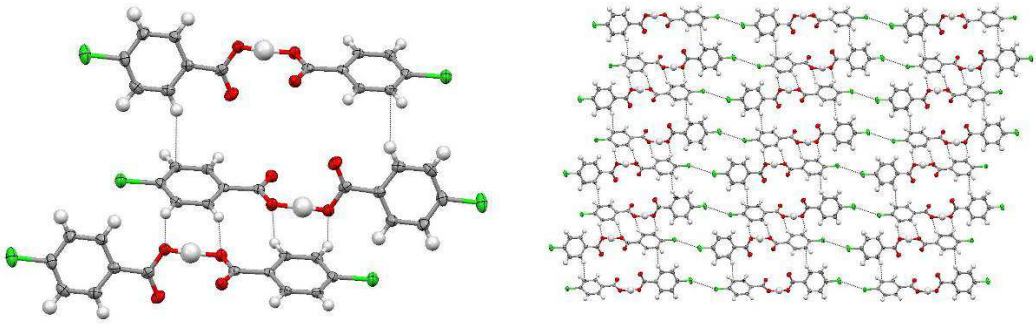

Figure 4-68. Intermolecular interactions forming the band of DIMER⁻s (left) and the layer formed through the halogen-halogen interactions between the DIMER⁻s (right) in the molecular complex of DMAN : 4CBA.

The DMAN and $DMANH^+$ molecules are connected in pairs. Two $DMANH^+$ molecules are connected to each other through C–H···π weak HBs with distances between ~3.67 Å and ~3.74 Å in a head-to-tail arrangement. The unprotonated pair of DMAN molecules is connected in similar manner with distances between ~3.27 Å and ~3.65 Å. The pairs of DMAN and $DMANH^+$ molecules are then linked through further π···π interactions with a distance of ~3.31 Å, and C–H···π weak HBs with distance between ~3.50 Å and ~3.53 Å, forming a chain of protonated and unprotonated molecules (*Figure 4-69*) holding together the layer of $DIMER^-$s (*Figure 4-70*).

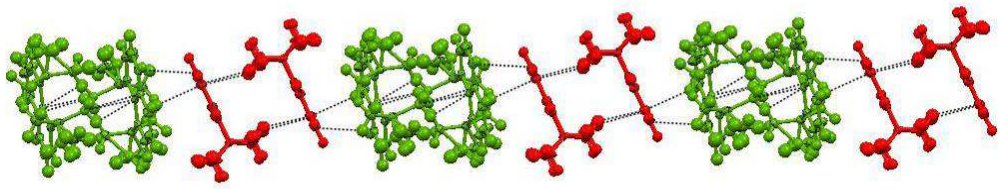

Figure 4-69. The chain of $DMANH^+$ molecules formed by the pairs of unprotonated DMAN (green) and protonated $DMANH^+$ molecules (red) in the molecular complex of DMAN : 4CBA.

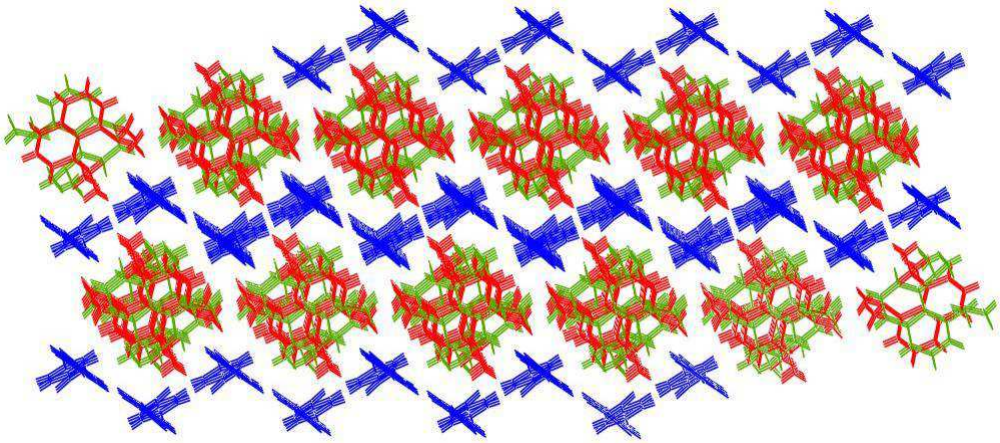

Figure 4-70. The structure as a whole in the molecular complex of DMAN : 4CBA, with the DMAN (green) and DMANH$^+$ (red) chains holding together the zig-zag layer formed by the 4CBA DIMER$^-$s (blue).

4.4.3 DMAN : 4-bromobenzoic acid (1:2)

The structure of the molecular complex of DMAN : 4BBA is more similar to that of the *ortho*-halo-substituted benzoic acid complexes with DMAN. The complex crystallises in a 1:2 DMAN : 4BBA ratio with a protonated DMANH$^+$ and the 4BBA DIMER$^-$ connected through a single, charge-assisted SSHB. The intramolecular HB within the DMANH$^+$ has a length of 2.602(3) Å and is asymmetric, with distances of N–H = 0.96(3) Å and H···N = 1.67(3) Å. The intermolecular interactions between the non-hydrogen bonded oxygen atom of the carboxyl group and the methyl group of the DMANH$^+$ consist of C–H···O weak hydrogen bonds of C···O distances 3.280(3) Å and 3.444(4) Å, similarly to those found in the *ortho* complexes. The relative positions of the DIMER$^-$ and DMAN units are also similar. However, the position of the substituent halogen atom and the presence of the halogen interactions has a different effect than that seen in the 4CBA : DMAN molecular complex or the hydrated 4FBA : DMAN complex, as in this complex the 4BBA DIMER$^-$s linearity is affected. The DIMER$^-$s present in the molecular complexes of DMAN and halo-substituted benzoic acids normally have an approximately linear arrangement in the relative position of the benzoic acids to each other while in the complex of DMAN : 4BBA this linearity is no longer present and the DIMER$^-$ is bent along the SSHB (*Figure 4-71*). Concerning the

hydrogen bond between the 4BBA molecules in the DIMER$^-$, this is in the normal range of charge-assisted SSHB with a length of 2.476(3) Å and distances of O–H = 1.11(5) Å and H···O = 1.38(5) Å. Variable temperature data has been collected at 100, 200 and 300K, but the presence of the heavy atom causes the difference Fourier maps to be noisy and makes it difficult to draw any significant conclusion regarding the H atom electron densities in the short hydrogen bonds. As in the other complexes presented the C–N bond length is longer on the donor side of the hydrogen bridge and the difference between the C–O and C=O bond lengths are more significant in the case of the carboxyl group on the donor side, following the trend of the above described complexes (*Table 4-1*).

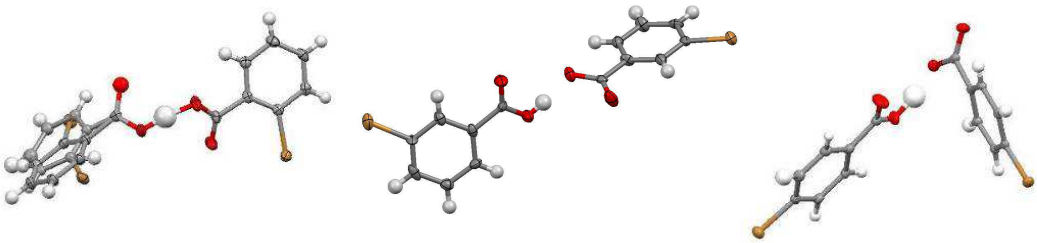

Figure 4-71. Halogen substituted benzoic acid DIMER$^-$s of 2BBA (left), 3BBA (centre) and 4BBA (right) from the individual DMAN complexes showing the comparison of the DIMER$^-$s relative arrangement, close to linear in the first two but significantly bent in the latter.

The DIMER$^-$s are connected to each other by Br···Br type II halogen interactions with a length of 3.5888(4) Å forming a zig-zag chain of DIMER$^-$s which are connected through intermolecular C–H···O weak hydrogen bonds within the sum of van der Waals radii, with distances between 3.397(3) Å and 3.444(3) Å, building up a layer (*Figure 4-72*).

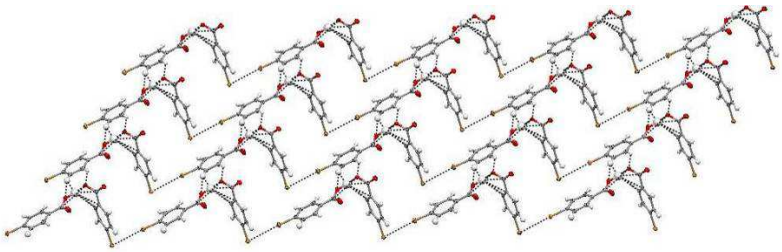

Figure 4-72. The layer of DIMER$^-$s in the molecular complex of DMAN : 4BBA.

The $DMANH^+$ molecules are connected to each other through C–H···π weak HBs with distances between ~3.48 Å and ~3.71 Å forming a chain in a herring bone arrangement (*Figure 4-73*) packed between the layers of the $DIMER^-$s (*Figure 4-74*).

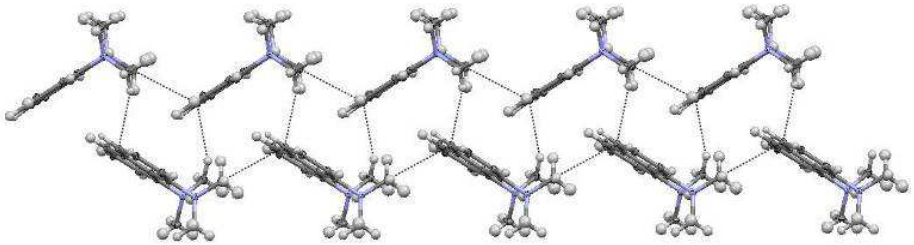

Figure 4-73. $DMANH^+$ molecules connected through C-H···π weak HBs, packed in a herring bone like pattern.

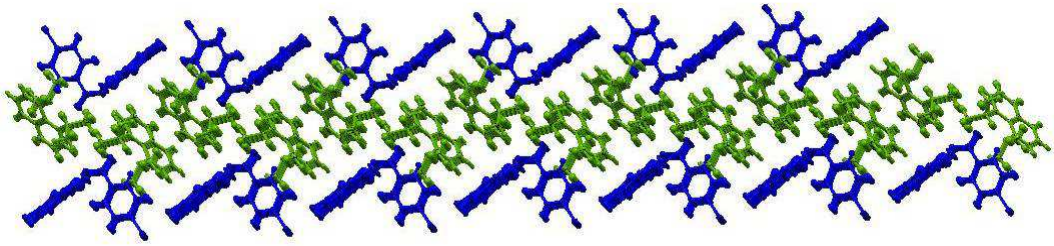

Figure 4-74. The structure of DMAN : 4BBA complex as a whole, showing the $DMANH^+$ (green) molecules packed between the layers of 4BBA $DIMER^-$s (blue).

4.4.4 DMAN : 4-idobenzoic acid (1:2)

The molecular complex of DMAN : 4IBA is isostructural with the DMAN : 4BBA complex. Overlaying the $DMANH^+$ molecules in the structures of the two complexes shows that the difference between the relative positions of the molecules to each other is very small (*Figure 4-75*).

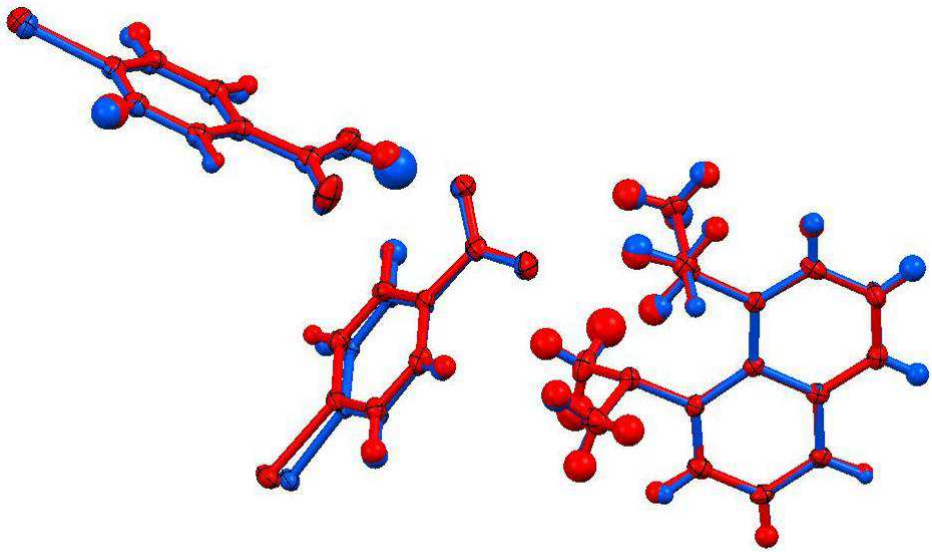

Figure 4-75. The structure overlay of the $DMANH^+$ molecules and the $DIMER^-$s in the molecular complexes of DMAN : 4IBA(red) and DMAN : 4BBA.

The intermolecular SSHB shows similar length of 2.463(3) Å with a slightly more asymmetrical position of the hydrogen with O–H = 0.90(7) Å and H···O = 1.57(7) Å in the case of the DMAN : 4IBA complex. This complex also has a similar intramolecular HB length to that in the 4BBA complex, of 2.582(4) Å, this time with a slightly less asymmetrical hydrogen position defined by the distances N–H = 1.08(3) Å and H···N = 1.57(3) Å. Variable temperature X-ray data has also been collected for this complex, but as in the case of the DMAN : 4BBA, neutron diffraction data would be required for reliable further discussion on the hydrogen bond lengths and behaviour. The C–N, C–O and C=O bond length correlations to the hydrogen bonds donor-side are present in this case as well (*Table 4-1*).

The intermolecular interactions between the carboxyl group of the $DIMER^-$ and the methyl group of the $DMANH^+$ are also very similar to those in the isostructural complex, with intermolecular C-H···O weak hydrogen bonds of distances between 3.243(5) Å and 3.415(5) Å forming the layer of $DIMER^-$s, with I···I interactions of 3.8781(3) Å and the layers of $DMANH^+$ building up the structure as a whole.

While in case of the DMAN : 2CBA and DMAN : 2BBA isostructural complexes presented before, the length of the halogen-halogen interactions do not change as significantly as their van der Waals radii, in the case of the DMAN : 4BBA and DMAN : 4IBA complexes the length of the halogen-halogen contacts does increase accordingly to their van der Waals radii. However in the first instance the halogen-halogen interactions are between the disordered and the non-disordered components, which is not the case in the 4BBA and 4IBA complexes.

4.5 Conclusion

A broad series of single halogen substituted benzoic acid : DMAN complexes have been presented, including *ortho*-, *meta*- and *para*- position substitution with four different halogen atoms as well as the parent benzoic acid itself. Proton transfer has been observed in every molecular complex presented in this chapter from the benzoic acid to the DMAN molecule. The DMAN : BA forms a molecular complex in a 1:2 stoichiometric ratio, which is followed by the majority of the complexes. By using DMAN as a crystal engineering tool, instead of the creation of the well known dimer motif connected through a medium strength HB between the benzoic acids (see Chapter 1), consistently a different type of $DIMER^{+-}$ have been created connected through a single charge-assisted SSHB. The influence of the position and the kind of halogen has presented, from twisting the carboxyl group out of the plane of the benzene ring, through causing disorder in the benzene ring of the $DIMER^{-}$ to breaking the stoichiometric ratio of the crystal structure from 1:2 to 1:1 to 3:4.

For the first time a molecular complex of DMAN where both the protonated and unprotonated form is present in the same structure has been presented.

It also been presented how this bonding motif breaks up with the inclusion of water molecules. In the case of the DMAN : 3FBA hydrate, the deprotonated benzoic acid which has been present in every other DMAN complex presented here, forming the single hydrogen bonded $DIMER^{-}$, is no longer present. Instead,

the stabilising role of the charge-assisted SSHB is taken over by two water molecules.

A trend also been found between the C–N bond length of the $DMANH^+$ and the donor side of the N–H···N hydrogen bond as well as in the C-O and C=O bond lengths with respect to their relation to the donor carboxyl group. The lengths of the inter- and intramolecular hydrogen bonds have been discussed, however, as has been shown from the available neutron diffraction data, for reliable conclusions and more detailed discussions neutron diffraction data are still required.

Chapter 5

5. Molecular complexes of DMAN with hydroxyl-, nitro- and methyl-substituted benzoic acids

This chapter is intended to present the extensive research carried out on the co-crystallisation of DMAN with a series of non-halogen substituted benzoic acids, complementing the work on the DMAN and halogen-substituted benzoic acids presented in the previous chapter. This will include hydroxyl- and dihydroxyl-substituted benzoic acid, methyl-substituted benzoic acids, nitro-substituted benzoic acid, all co-crystallised with DMAN. The structure descriptions will include a comparison of the bonding motifs found in the structures with motifs already discussed in the previous chapter.

A comparison between the bond lengths of the $DMANH^+$ will be also included in the *Table 5-1*, however, since the bonding motifs of the benzoic acids are different their parameters will be included separately in the structure discussions.

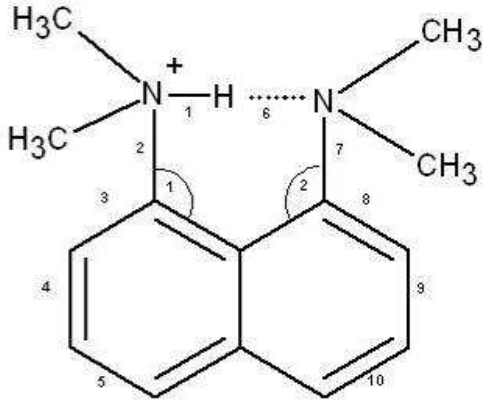

Figure 5-1. Diagram of the $DMANH^+$ the bonds are marked with numbers and their lengths are listed in the Table 5-1.

Table 5-1. Bond lengths and angles measured at 100K from X-ray data (except DMAN:26DOHBA, where the parameters from 100K neutron data are also shown) in the molecular complexes of DMAN and hydroxyl-, methyl- and nitro-substituted benzoic acid marked in.

bond (Å) /angle (˚)	DMAN : 3OHBA	DMAN : 4OHBA "symm"	DMAN : 4OHBA "asymm"	DMAN : 23OHBA	DMAN : 24OHBA	DMAN : 26OHBA X-ray	DMAN : 26OHBA neutron	DMAN : 3TOLA	DMAN : 4TOLA	DMAN : 3NBA
1. N-H	1.19(3)	1.29(2)	1.03(2)	1.08(2)	1.16(2)	1.26(2)	1.293(6)	1.12(2)	1.11(3)	1.22(3)
2. C-N	1.467(2)	1.466(2)	1.471(2)	1.471(2)	1.467(3)	1.465(2)	1.465(3)	1.472(1)	1.480(3)	1.464(3)
3. C-C	1.369(2)	1.360(2)	1.368(2)	1.369(1)	1.367(3)	1.369(2)	1.373(3)	1.370(2)	1.367(3)	1.362(3)
4. C-C	1.410(3)	1.405(2)	1.401(2)	1.410(2)	1.406(3)	1.406(2)	1.417(4)	1.411(2)	1.413(3)	1.409(3)
5. C-C	1.366(3)	1.360(3)	1.354(2)	1.366(2)	1.364(3)	1.366(2)	1.367(4)	1.366(2)	1.371(3)	1.358(3)
6. N···H	1.42(3)	1.34(2)	1.63(2)	1.55(2)	1.46(2)	1.36(2)	1.339(6)	1.50(2)	1.56(3)	1.37(3)
7. C-N	1.464(2)	1.465(2)	1.457(2)	1.461(2)	1.463(3)	1.469(2)	1.464(3)	1.461(1)	1.462(3)	1.462(3)
8. C-C	1.373(2)	1.368(2)	1.363(2)	1.371(2)	1.370(3)	1.368(2)	1.380(3)	1.371(2)	1.374(3)	1.368(4)
9. C-C	1.409(3)	1.403(2)	1.407(2)	1.413(2)	1.401(3)	1.410(2)	1.414(3)	1.411(2)	1.417(3)	1.401(4)
10. C-C	1.362(3)	1.359(2)	1.362(3)	1.368(2)	1.369(3)	1.362(2)	1.374(3)	1.367(2)	1.363(3)	1.361(4)
1. N-C-C	117.8(1)	118.0(1)	118.7(1)	118.3(1)	117.7(2)	118.0(1)	118.1(2)	118.6(2)	118.4(1)	117.7(2)
2. N-C-C	118.3(1)	118.3(1)	118.1(1)	118.5(1)	118.0(2)	118.0(1)	118.6(2)	118.6(2)	117.9(1)	117.8(2)

5.1 DMAN : hydroxyl-substituted benzoic acids

Two molecular complexes of DMAN and hydroxy-substituted benzoic acids have been successfully co-crystallised. By introducing a potential hydrogen donor on the form of the hydroxyl group, these molecular complexes have developed a very different structure from the DMAN : halogen-substituted benzoic acid complexes presented in Chapter 4. Both complexes are hydrates and their structures as determined from the X-ray diffraction measurements will be presented with full structural descriptions, highlighting the hydrogen bonding motifs determined.

(2:2:1) DMAN : 3-hydroxybenzoic acid hydrate (3OHBA): 1:1 molar ratio of DMAN and 3OHBA were dissolved in diethyl ether and evaporated at room temperature, slowing the evaporation by closing the vial with a small clipped lid with holes pierced in the lid. After the evaporation of the solvent, colourless blocks were formed. Single crystal X-ray diffraction data were collected on a Bruker Nonius Kappa CCD diffractometer at 110, 200 and 300K (*Table 5-2*). The

data were solved with SHELXS97 and refined with SHELXL97, within the WinGX package.

(2:2:1) DMAN : 4-hydroxybenzoic acid hydrate (4OHBA): 1:1 molar ratio of DMAN and 4OHBA were dissolved in ethanol and evaporated at room temperature, slowing the evaporation by closing the vial with a small clipped lid. After the evaporation of the solvent colourless prisms were formed. Single crystal X-ray diffraction data were collected on a Bruker Nonius Kappa CCD diffractometer at 100, 200 and 300K (*Table 5-2*). The data were solved with SHELXS97 and refined with SHELXL97, within the WinGX package. The hydrogen atoms are generated on the carbon atoms in the refinement of the 300K data set.

5.1.1 DMAN : 3-hydroxybenzoic acid hydrate (2:2:1)

The molecular complex of DMAN :3OHBA crystallises with a very different motif to that seen in the halogen-substituted benzoic acids and DMAN molecular complexes. The co-crystallisation ratio is also different, the asymmetric unit containing one protonated $DMANH^{+}$ molecule, a deprotonated $3OHBA^{-}$ molecule and a half water molecule. The $3OHBA^{-}$ molecules are deprotonated through loss of the hydrogen of the carboxyl group, and pairs of $3OHBA^{-}$ molecules are stabilised through a hydrogen bond between the deprotonated carboxyl group and the hydroxyl group of the next $3OHBA^{-}$ molecules, forming a long zig-zag chain (*Figure 5-2*). This motif replaces the carboxyl-carboxylate dimerization found between pairs of protonated and deprotonated carboxylic acid molecules in the complexes discussed in Chapter 4.

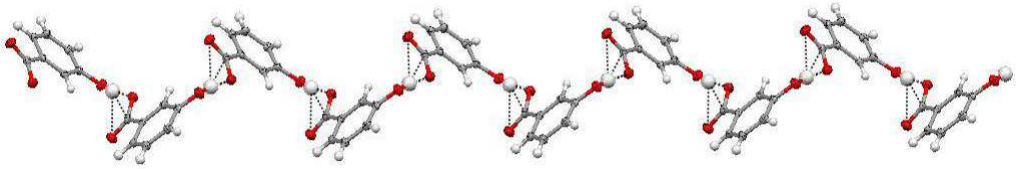

Figure 5-2. Chain formed through HB between the deprotonated $3OHBA^{-}$ molecules in the molecular complex of DMAN : 3OHBA hydrate.

Table 5-2 X-ray data refinement details of DMAN : 3OHBA, DMAN : 4OHBA.

Compound	2:2:1 DMAN : 3OHBA			2:2:1 DMAN : 4OHBA		
Diffractometer	Nonius Kappa CCD	Nonius Kappa CCD	Nonius Kappa CCD	Bruker Apex II	Bruker Apex II	Bruker Apex II
Formula	C_{42} H_{50} N_4 O_7	C_{42} H_{50} N_4 O_7	C_{42} H_{50} N_4 O_7	C_{42} H_{50} N_4 O_7	C_{42} H_{50} N_4 O_7	C_{42} H_{50} N_4 O_7
Molecular weight / $gmol^{-1}$	722.88	722.88	722.88	722.88	722.88	722.88
Temperature (K)	110	200	300	100	200	300
Space Group	Pbcn	Pbcn	Pbcn	$P\bar{1}$	$P\bar{1}$	$P\bar{1}$
a (Å)	9.6592(2)	9.7335(3)	9.8438(4)	11.8998(3)	11.9004(3)	11.9911(3)
b (Å)	20.4667(6)	20.4594(6)	20.3952(9)	12.0777(3)	12.0779(3)	12.1072(4)
c (Å)	18.9378(4)	18.9998(5)	19.0736(6)	14.1438(4)	14.1434(4)	14.1823(4)
α (°)	90	90	90	93.6730(10)	93.6780(10)	93.706(2)
β (°)	90	90	90	95.7740(10)	95.7730(10)	95.430(2)
γ (°)	90	90	90	111.4720(10)	111.4710(10)	111.584(2)
Volume ($Å^3$)	3743.85(16)	3783.65(19)	3829.3(3)	1870.89(8)	1870.96(8)	1894.97(9)
Z	4	4	4	2	2	2
θ range/°	1.99 – 30.05	1.99 – 30	2 – 30	1.46 – 30.1	1.46 – 29.98	1.45 – 29.18
Completeness (%)	99.8	99.9	95.1	99.1	99.6	95.5
Reflections Collected	38073	37893	33970	52236	51927	48033
Independent	5482	5528	5312	10909	10833	9824
Refln (obs.I>2theta(I))	3496	2768	1946	6562	6578	5061
R_{int}	0.0955	0.1049	0.1271	0.0476	0.0473	0.0526
Data/Rest./Param.	5482/0/340	5528 /0/340	5312/0/340	109090/0/678	10833/0/678	9824/0/510
GooF on F^2	0.96	0.874	1.014	1.016	1.081	1.059
R_1 (Observed) / R_1 (all)	0.053 / 0.1003	0.0685 / 0.1543	0.0829 / 0.2365	0.0446 / 0.0918	0.0449 / 0.092	0.0485 / 0.117
wR_2 (all)	0.1617	0.1994	0.2405	0.1163	0.1187	0.1392
ρ (max / min) / $e\text{-}Å^{-3}$	0.319 / -0.267	0.67 / -0.262	0.0529 / -0.252	0.221 / -0.181	0.231 / -0.171	0.282 / -0.17
RMS / $eÅ^{-3}$	0.052	0.049	0.044	0.038	0.038	0.032

The hydrogen bond between the carboxylate group and the hydroxyl group is slightly longer than the charge-assisted SSHB formed in the case of the $DIMER^{-}$; this has an O···O bond length of 2.522(2) Å with O–H = 1.02(3) Å on the donor side of the carboxylate group and H····O = 1.51(3) Å on the acceptor side of the carboxylate group. The C-O bond lengths found within the carboxylate group shows a similar differentiation between the oxygen involved in the O–H···O hydrogen bond having a bond length of 1.272(2) Å, while the other is 1.247(2) Å. However, the difference between the "single" and "double" bond is smaller than between the carboxyl groups shown in the DMAN and halogen substituted benzoic acid complexes connected through a SSHB. The water molecules hold together these chains of $3OHBA^{-}$ molecules through O(w)–H···O(hydroxyl) contacts bridging the hydroxyl groups of $3OHBA^{-}$ molecules with an O···O distance of 2.797(2) Å (Figure 5-3).

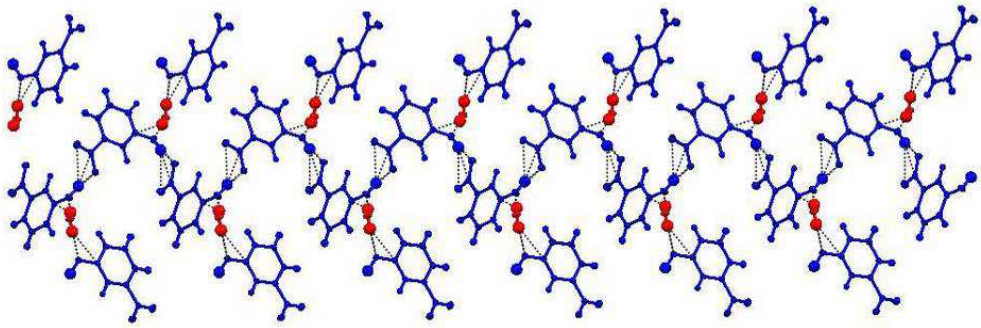

Figure 5-3. Layer formed from the chain of $3OHBA^{-}$ molecules (blue), held together by the water molecules (red) in the molecular complex of DMAN : 3OHBA hydrate.

Water molecules are also connected to $DMANH^{+}$ molecules through C–H···O weak hydrogen bonds, from the methyl group with a length of 3.240(2) Å and with the naphthalene ring with a length of 3.351(2) Å (*Figure 5-4*). These play a role not just in holding together the $3OHBA^{-}$ chains but also in connecting the layer formed to the $DMANH^{+}$ molecules.

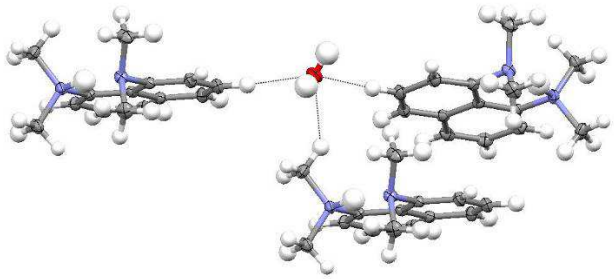

Figure 5-4. C–H···O weak hydrogen bonds between the water molecule and the DMANH^{+}.

There are C–H···π weak hydrogen bonds between pairs of DMANH^{+} with lengths between ~3.53 Å and ~3.57 Å in a "head to tail" arrangement, and these pairs are stacked in a displaced arrangement in the packing as a whole (the distance between the centroids of the two overlapped ring is ~3.82 Å) (*Figure 5-5*) and are being held in pockets formed by the zig-zag layers of 3OHBA molecules.

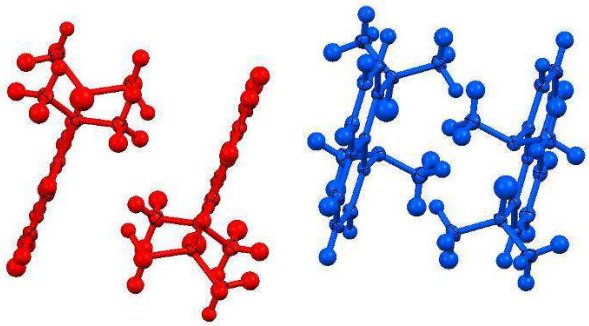

Figure 5-5. Stacked arrangement of the pairs of DMANH^{+} *molecules in the overall packing.*

This arrangement is formed through a number of short contacts between the DMANH^{+} and the 3OHBA^{-} molecules. Whereas in the case of the complexes formed by DMAN and halogen-substituted benzoic acids, the non-hydrogen bonded oxygen has a number of short contacts with the methyl group of the DMANH^{+}, in this case both oxygen atoms make such contacts. These comprise C–H···O weak hydrogen bond distances of 3.427(2) Å and 3.407(2) Å from the carboxylate group at the top of the DMANH^{+} molecule, and 3.543(2) and 3.553(2) Å from the side of the DMANH^{+} molecule (*Figure 5-6*).

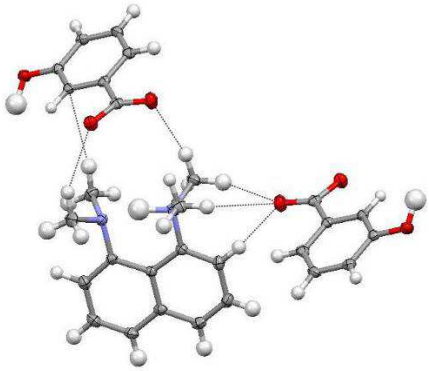

Figure 5-6. Short contacts between the methyl groups of $DMANH^+$ and the carboxylate group of the $3OHBA^-$ in the molecular complex of DMAN : 3OHBA hydrate.

There are additional C–H···π weak hydrogen bonds between the methyl groups and the benzene ring of the $3OHBA^-$ molecule with a length of ~3.82 Å and between the hydrogen atom of the naphthalene group and the benzene ring of the $3OHBA^-$ with lengths between ~3.41 Å and 3.71 Å , building up the structure as a whole (*Figure 5-7*).

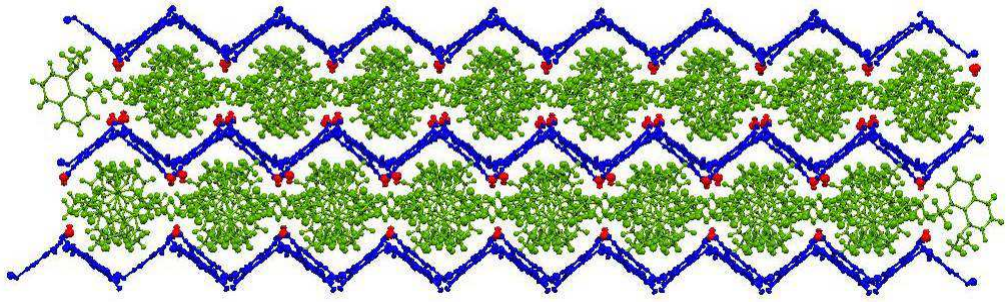

Figure 5-7. Build up of the structure in the molecular complex of DMAN 3OHBA hydrate with $DMANH^+$ molecules (green) held in pockets between the layer of $3OHBA^-$ (blue) and water molecules (red).

The usual intramolecular N–H···N hydrogen bond is present between the nitrogen atoms of the $DMANH^+$. This has an N···N separation of 2.580(2) and shows an asymmetric position of the hydrogen atom with N–H = 1.19(3) Å and H···N = 1.42(3) Å. The C–N bonds lengths do not exhibit large deviations between the donor and acceptor site, but as has been shown in the case of the

halogen substituted benzoic acid and $DMANH^+$, larger differences appear in the case where the N–H···N bond is very asymmetric (*Table 5-1*).

Variable temperature data have been collected at 110, 200 and 300 K, as the intermolecular HB between the hydroxyl and carboxylate group has a large isotropic thermal parameter and was considered worthy of further investigation. The difference Fourier map at 110K shows a large but well defined single peak in the region of the hydrogen atom electron density in the case of the intermolecular HB and an electron density peak that is slightly elongated along the bond of the intramolecular hydrogen atom (*Figure 5-8*). Unfortunately, the difference Fourier maps at 200 and 300 K become very noisy due to the lower quality of the data set, and are not of sufficient quality to allow for further interpretation.

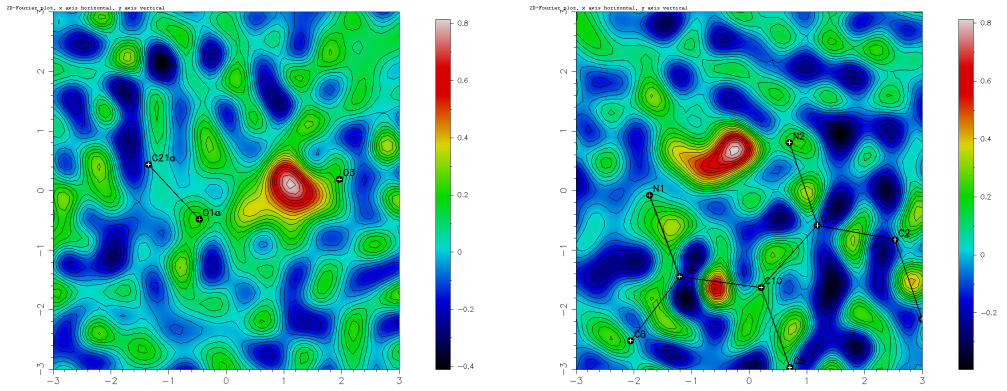

Figure 5-8. Difference Fourier map of the electron density in the region of the hydrogen bonded H atom in the intermolecular O–H···O (left) and intramolecular N–H···N (right) hydrogen bonds at 100 K in the molecular complex of DMAN : 3OHBA hydrate.

5.1.2 DMAN : 4-hydroxybenzoic acid hydrate (2:2:1)

The DMAN 4OHBA hydrate complex is in many respects similar to the DMAN : 3OHBA hydrate complex, with the same co-crystallisation ratio and similar bonding motif. However, the asymmetric unit contains two protonated $DMANH^+$ molecules, two deprotonated $4OHBA^-$ and a water molecule. As in the case of the DMAN : 3OHBA hydrate, the carboxylate group of the $4OHBA^-$ is

deprotonated and hydrogen bonded to the hydroxyl group of the other 4OHBA$^-$ molecule in the asymmetric unit. This produces two HBs with different lengths, one of 2.559(1) Å with O–H = 0.93(2) Å and H···O = 1.64(2) Å, where the oxygen atom of the hydroxyl group is also involved in a C–H···O interaction with a length of 3.618(2) Å and the other O–H···O bond with a length of 2.526(1) Å and, O–H = 0.95(2) Å and H···O = 1.59(2) Å (*Figure 5-9*). The C–O bond lengths of the carboxylate group in the case of the shorter O–H···O bond are 1.239(2) Å and 1.261(1) Å while in the case of the longer these are 1.250(2) Å and 1.261(2) Å. These differences between the two C–O bonds of the deprotonated carboxyl group become less apparent in cases where the O–H···O hydrogen bond length is longer.

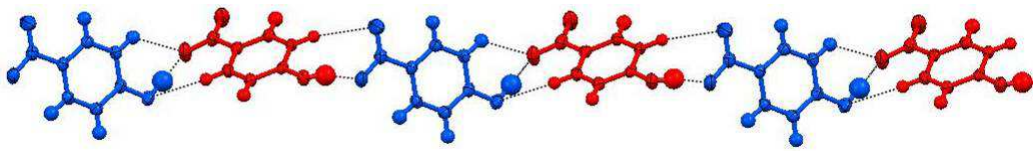

Figure 5-9. The two different O–H···O hydrogen bonds, between the 4OHBA$^-$ molecules the longer hydrogen bond is involved in a C–H···O interaction as well.

The asymmetric unit contains two DMANH$^+$ molecules with two different lengths for the intramolecular N–H···N hydrogen bonds. One of these is more asymmetric, with a length of 2.603(2) Å, N–H = 1.03(2) Å, H···N = 1.63 Å, while the more symmetric hydrogen bond has an N···N length of 2.579(2) Å with N–H = 1.29(2) Å and H···N = 1.34(2) Å.

As in the molecular complex of DMAN : 3OHBA hydrate, a zig-zag chain is formed through the intermolecular O–H···O hydrogen bonds between the 4OHBA$^-$ molecules. These chains are connected through C–H···O intermolecular interactions with a length of 3.511(1) Å to the next chain on one side and through O–H···O interactions through the water molecules on the other side with lengths between 2.736(2) Å and 2.834(2) Å. This forms a layer of 4OHBA$^-$ and water molecules (*Figure 5-10*).

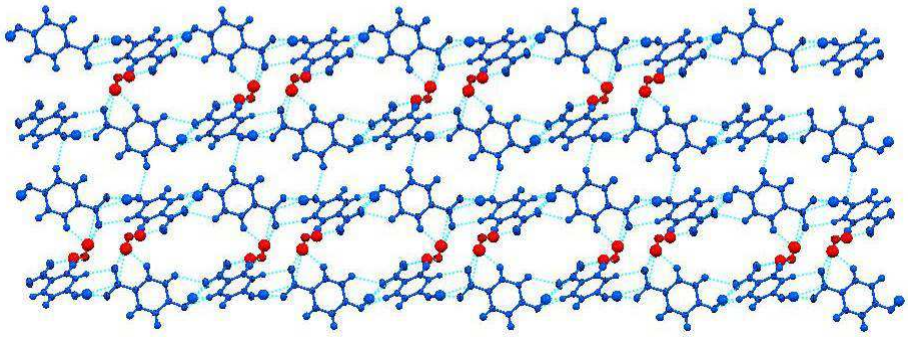

Figure 5-10. The layer formed from water (red) and 4OHBA⁻ molecules (blue) in the molecular complex of DMAN : 4OHBA hydrate.

The layers of 4OHBA⁻ and water molecules are held together by the $DMANH^+$ molecules. The $DMANH^+$ molecules in this case have weak C–H···π weak hydrogen bonds between themselves, with lengths between ~3.51 Å and ~3.91 Å. These weak interactions link pairs of $DMANH^+$ with asymmetric hydrogen bridges, and pairs of symmetrically bridged $DMANH^+$. These pairs in turn pack in a stacked arrangement, similarly to the DMAN : 3OHBA hydrated complex, with a slightly displaced arrangement of the naphthalene rings (with a shortest distance between the naphthalene rings centroids of ~4.17 Å), with further C–H···π weak hydrogen bonds with length of ~3.78 Å (*Figure 5-11*) which is sandwiched between the layers of 4OHBA⁻ and water molecules (*Figure 5-12*).

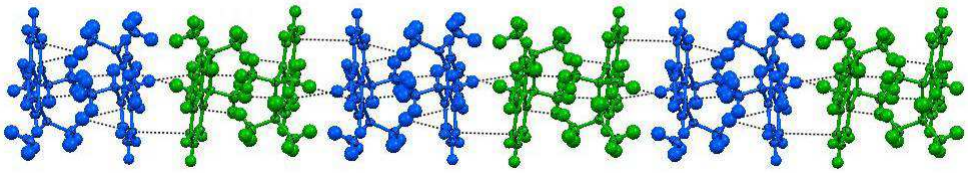

Figure 5-11. Chains of $DMANH^+$ molecules formed by the linking of pairs with symmetrical intramolecular HB (green) and pairs with asymmetrical intramolecular HB (blue), in the molecular complex of DMAN : 4OHBA hydrate.

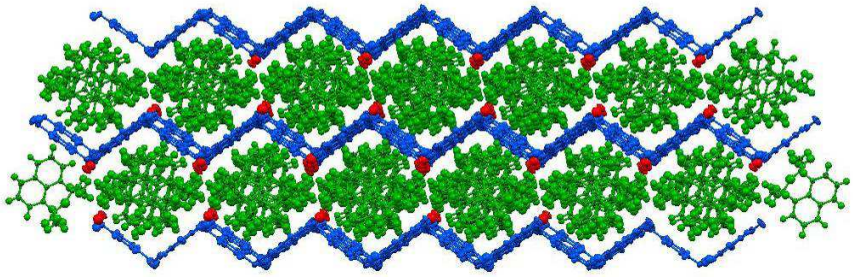

Figure 5-12. The structure of the molecular complex of DMAN : 4OHBA hydrate as a whole with the $DMANH^+$ molecules (green) held in pockets between the layers of $4OHBA^-$ (blue) and water molecules (red).

Variable temperature X-ray data have also been collected on the molecular complex of DMAN : 4OHBA hydrate at 100, 200 and 300 K. Neither the inter- nor the intramolecular hydrogen bond lengths or donor- acceptor distances change significantly at the three measured temperatures. As mentioned above, the intermolecular hydrogen bonds are both asymmetric, which is retained consistently at the various temperatures. However, the N–H···N intramolecular hydrogen bond shows very different hydrogen behaviour in the two different bonds, with one hydrogen bridge having a symmetrically positioned hydrogen atom while the other is asymmetric. Once again, these show no significant changes as a function of temperature (*Table 5-3*).

Table 5-3. Donor acceptor distances from the X-ray diffraction measurement of the inter- and intramolecular hydrogen bonds at 100, 200 and 300 K in the molecular complex of DMAN : 4OHBA hydrate

Type	Temp	D····A (Å)	D-H (Å)	H···A (Å)
N-H···N	100	2.579(2)	1.29(2)	1.34(2)
	200	2.578(2)	1.27(2)	1.35(3)
	300	2.579(2)	1.31(2)	1.31(3)
N-H···N	100	2.603(2)	1.03(2)	1.63(2)
	200	2.606(2)	1.05(2)	1.61(2)
	300	2.606(2)	1.10(3)	1.55(2)
O-H···O	100	2.559(1)	0.93(2)	1.64(2)
	200	2.561(1)	0.95(2)	1.62(2)
	300	2.564(2)	0.90(2)	1.66(2)
O-H···O	100	2.526(1)	0.95(2)	1.59(2)
	200	2.528(1)	0.96(2)	1.58(2)
	300	2.529(2)	1.00(3)	1.54(3)

In order to gain a better understanding of these differences appearing between these hydrogen bonds, difference Fourier maps were generated in the region of the hydrogen bonds at every measured temperature (*Figure 5-13*). The difference Fourier maps shows no diversity of the observed electron density in the intermolecular hydrogen bonds between the 4OHBA$^-$ molecules, at every measured temperature, showing single well-defined electron density in the region of the hydrogen atom.

There are, however, significant differences in the behaviour of the hydrogen atom electron density in the two different intramolecular hydrogen bonds within the N-H···N hydrogen bridge. The asymmetric bonding shows a single well-defined density, while the in the symmetrical bridge, an elongated electron density is observed along the bonding direction. These slight, qualitatively indicated, differences appearing in the behaviour of the electron density in the intramolecular hydrogen bond bridges must reflect local interactions with the environment, which are discussed below.

Symmetric N–H···N (*Figure 5-14*): Both C–N bonds have a similar length within the standard uncertainty with lengths of C–N3 = 1.465(2) Å and C–N4 = 1.466(2) Å. Intermolecular short contacts are formed between the oxygen atom of the hydroxyl group from the 4OHBA$^-$ to the nitrogen on one side of the bridging hydrogen bond (N3) with a length of 3.558(2) Å, and a C–H···O weak hydrogen bond with a length of 3.279(2) Å to the other nitrogen (N4). There are three intermolecular short contacts connected to the methyl groups of nitrogen atom N4, consisting of two C–H···O interactions with length of 3.152(2) Å and 3.518(2) Å and a C–H···π contact with a length of 3.809(3) Å. The C–H···π intermolecular interactions between the DMANH$^+$ molecules have been described above, however they are not located in the direction along the hydrogen bridge, and thus must not be considered among the potential interactions causing different behaviour of the hydrogen atoms electron density within the intramolecular N–H···N hydrogen bond.

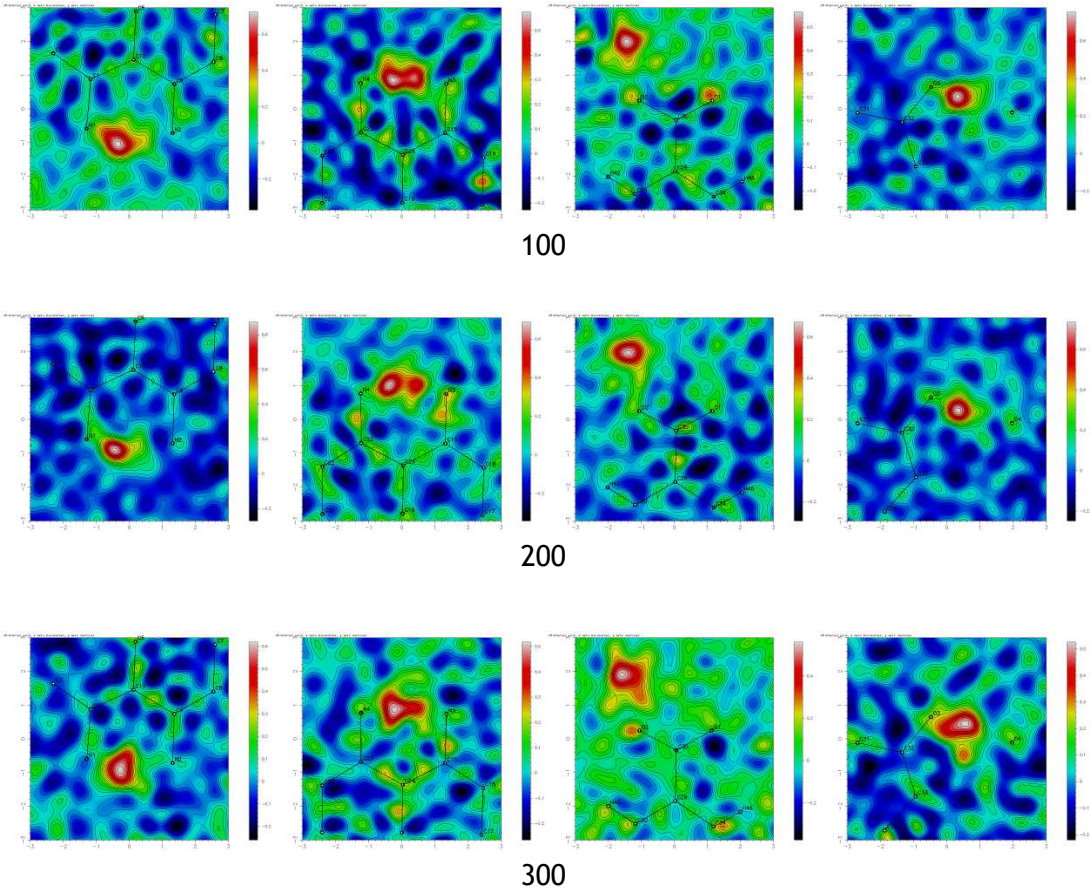

Figure 5-13. Difference Fourier maps of the hydrogen atom electron density in the molecular complex of DMAN : 4OHBA hydrate within the inter- and intramolecular hydrogen bond from left to right: asymmetric N–H···N, symmetric N–H···N, shorter O–H···O and the longer O–H···O. The temperatures of measurement are marked below the maps.

Asymmetric N–H···N (*Figure 5-15*): Significant differences are evident in the C–N bond lengths in this case with lengths of C–N1 = 1.471(2) Å on the donor side and C–N2 = 1.457(2) Å on the acceptor side. On the acceptor side of the N–H···N hydrogen bond there are no intermolecular short contacts to the methyl groups along the direction of the hydrogen bridge. For the methyl groups connected to the nitrogen atom on the donor side (N1) of the hydrogen bond, there are two C–H···O weak hydrogen bonds between the methyl group and the oxygen atom of the water molecule with lengths of 3.138(3) Å and 3.342(2) Å. In addition, there is one C–H···O weak hydrogen bond between the oxygen atom of the carboxylate group and the methyl group with a length of 3.583(2) Å.

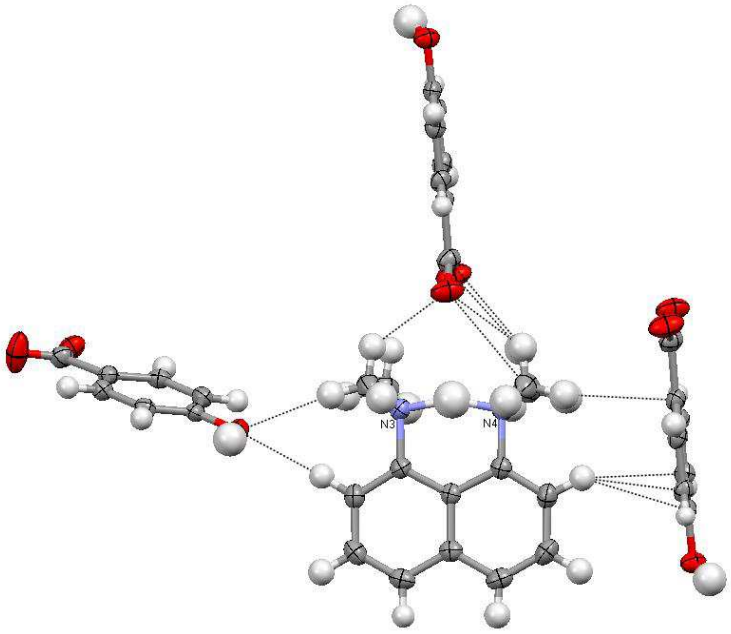

Figure 5-14. View of the $DMANH^+$ molecule with the symmetrical N–H···N hydrogen bond, showing the short contacts between the methyl groups and the environment in the direction along the hydrogen bond in the molecular complex of DMAN : 4OHBA hydrate.

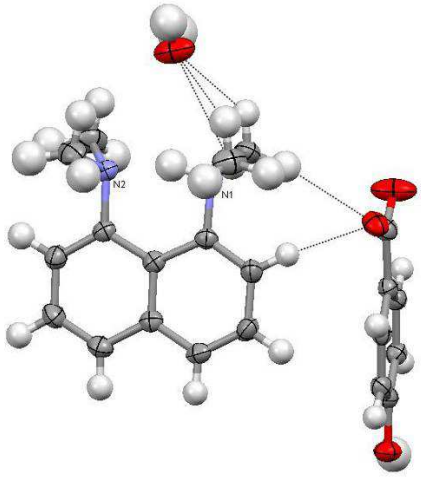

Figure 5-15. The $DMANH^+$ with the asymmetrical N–H···N hydrogen bond, showing the short contacts between the methyl groups and environment in the direction along the hydrogen bond in the molecular complex of DMAN : 4OHBA hydrate.

The variation of intermolecular contacts around the symmetric and asymmetric N–H··N intramolecular hydrogen bonds suggest that the number and position of these might influence the discrepancy between the electron density distributions in the region of the hydrogen atoms. While the hydrogen atom with the elongated electron density refining to a centred position in the bond has a more symmetrical environment, the asymmetrically positioned electron density has an asymmetrical environment. Further discussion of the nature of the hydrogen bonds would require detailed description of the hydrogen atom nuclear position to accompany the revealed electron density distributions, which could be obtained from neutron diffraction experiments.

5.2 DMAN : dihydroxy-substituted benzoic acids

(1:1) DMAN : 2,3-dihydroxybenzoic acid (23DOHBA): 1:1 molar ratio of DMAN and 23DOHBA were dissolved in methanol and evaporated at room temperature, slowing the evaporation by closing the vial with a small pierced clipped lid. After the evaporation of the solvent, colourless blocks were formed. Single crystal X-ray diffraction data were collected on a Bruker Nonius Kappa CCD diffractometer at 100, 200 and 300K (*Table 5-4*). The data were solved with SHELXS97 and refined with SHELXL97, within the WinGX package.

(1:1) DMAN : 2,4-dihydroxybenzoic acid (24DOHBA): 1:1 molar ratio of DMAN and 2,4DOHAB were dissolved in diethyl ether and evaporated at room temperature, slowing the evaporation by closing the vial with a small pierced clipped lid. After the evaporation of the solvent, colourless prisms were formed. Single crystal X-ray diffraction data were collected on a Bruker Nonius Kappa CCD diffractometer at 100 K (*Table 5-4*). The data were solved with SHELXS97 and refined with SHELXL97, within the WinGX package.

(1:1) DMAN : 2,6-dihydroxybenzoic acid (26DOHBA): 1:1 molar ratio of DMAN and 2,6DOHAB were dissolved in ethanol and evaporated at room temperature, slowing the evaporation by closing the vial with a small pierced clipped lid. After

the evaporation of the solvent, colourless prisms were formed. Single crystal X-ray diffraction data were collected on a Bruker Nonius Kappa CCD diffractometer at 100, 200, 300 K (*Table 5-4*) and neutron diffraction data on the SXD instrument at ISIS at 30, 100, 200, 300 K (*Table 5-5*). The data were solved with SHELXS97 and refined with SHELXL97, within the WinGX package.

5.2.1 DMAN and 2,3-dihydroxybenzoic acid (1:1)

In the case of the molecular complex of DMAN 23DOHBA, the carboxyl group is deprotonated once again but unlike in 3OHBA and 4OHBA there are two competing hydrogen bond donors. The DMAN molecule deprotonates the $23DOHBA^-$ molecule and the hydrogen atom from the hydroxyl group in the *ortho*- position forms a hydrogen bond to the oxygen atom of the deprotonated carboxylate group forming an intramolecular O–H···O SSHB. The SSHB has a length of 2.425(2) Å with O–H = 1.12(3) Å and H···O = 1.33(3) Å with the hydrogen atom located closer to the carboxylate group (Figure 5-16). In this case the there is a larger difference between the two C–O bond lengths (1.227(2) Å and 1.317(1) Å) than in the case of single hydroxyl substituted benzoic acids and DMAN complexes. However this is not surprising since there is an intramolecular SSHB to the carbonyl oxygen atom, which is much shorter (~0.22 Å) than the intramolecular O–H···O bond in the pure 23DOHBA structure[162] and the double bond character (length) shifts to the deprotonated C–O bond as the deprotonated oxygen is not involved in other strong or moderate hydrogen bonding. Two $23DOHBA^-$ molecules are held together by two moderate strength hydrogen bonds created between the hydroxyl group in the *meta*- position from one molecule and the oxygen from the *ortho*- position from the other (*Figure 5-16*). The pairing of $23DOHBA^-$ molecules in this way is made possible by the unique positions of the substituent hydroxyl groups together with the deprotonation (breaking up the dimer motif seen in the pure structure[162]), causing the hydrogen atoms bonding to the carboxylate group and such creating an intramolecular O–H···O SSHB.

Table 5-4. X-ray data refinement details of DMAN : 23DOHBA, DMAN : 24DOHBA, DMAN : 26DOHBA.

Compound	1:2 DMAN : 23DOHBA			1:2 DMAN : 24DOHBA	1:2 DMAN : 26DOHBA		
Diffractometer	Nonius Kappa CCD	Nonius Kappa CCD	Nonius Kappa CCD	Nonius Kappa CCD	Nonius Kappa CCD	Nonius Kappa CCD	Nonius Kappa CCD
Formula	$C_{21}H_{24}N_2O_4$	$C_{21}H_{24}N_2O_4$	$C_{21}H_{24}N_2O_4$	$C_{21}H_{24}N_2O_4$	$C_{21}H_{24}N_2O_4$	$C_{21}H_{24}N_2O_4$	$C_{21}H_{24}N_2O_4$
Molecular weight / $gmol^{-1}$	368.42	368.42	368.42	368.42	368.42	368.42	368.42
Temperature (K)	100	200	300	100	100	200	300
Space Group	$P\bar{1}$	$P\bar{1}$	$P\bar{1}$	$P2_1/n$	$P2_1/c$	$P2_1/c$	$P2_1/c$
a (Å)	9.8417(4)	9.8900(4)	9.9309(4)	9.5542(5)	9.2556(3)	9.2994(3)	9.3488(4)
b (Å)	9.9626(3)	9.9654(3)	9.9806(4)	19.7472(13)	10.6424(4)	10.6926(4)	10.7635(5)
c (Å)	10.7489(4)	10.8054(4)	10.8699(4)	10.0316(6)	18.8926(6)	18.9674(7)	19.0469(8)
α (°)	67.496(2)	67.533(2)	67.642(2)	90	90	90	90
β (°)	81.947(2)	81.823(2)	81.866(2)	91.931(4)	91.126(2)	91.342(2)	91.618(2)
γ (°)	71.922(2)	72.095(2)	72.323(2)	90	90	90	90
Volume ($Å^3$)	925.33(6)	936.09(6)	948.93(6)	1891.6(2)	1860.60(11)	1885.50(12)	1915.85(15)
Z	2	2	2	4	4	4	4
θ range/°	2.05 – 30	2.04 – 30	2.03 – 29.4	2.06 – 25.62	2.16 – 29.99	2.15 – 27.88	2.14 – 26.73
Completeness (%)	99.7	99.9	96.5	99.9	99.8	100	1
Reflections Collected	24913	26192	24454	21218	36444	32770	31380
Independent	5368	5447	5046	3572	5399	4497	4066
Refln (obs.I>2theta(I))	4116	3624	2716	2097	3397	2540	1952
R_{int}	0.048	0.0438	0.044	0.0949	0.0711	0.0715	0.0781
Data/Rest./Param.	5368/0/340	5447/0/340	5046/0/340	3572/0/340	5399/0/340	4497/0/340	4066/0/340
GooF on F^2	0.809	0.987	0.975	1.009	0.97	0.989	0.962
R_1 (Observed) / R_1 (all)	0.042 / 0.0614	0.0461 / 0.0801	0.0437 / 0.0978	0.0453 / 0.102	0.0483 / 0.0953	0.048 / 0.1072	0.0503 / 0.1328
wR_2 (all)	0.1193	0.1098	0.123	0.1141	0.1057	0.1107	0.1264
P (max / min) / e-$Å^{-3}$	0.382 / -0.222	0.226 / -0.217	0.149 / -0.156	0.235 / -0.207	0.416 / -0.199	0.242 / -0.168	0.166 / -0.144
RMS / e$Å^{-3}$	0.045	0.038	0.035	0.042	0.046	0.037	0.031

Table 5-5. Neutron diffraction data refinement details of DMAN : 26DOHBA.

Compound	1:2 DMAN : 26DOHBA			
Diffractometer	SXD	SXD	SXD	SXD
Formula	$C_{21}\ H_{24}\ N_2\ O_4$	$C_{21}\ H_{24}\ N_2\ O_4$	$C_{21}\ H_{24}\ N_2\ O_4$	$C_{21}\ H_{24}\ N_2\ O_4$
Molecular weight / gmol^{-1}	368.42	368.42	368.42	368.42
Temperature (K)	30	100	200	300
Space Group	$P2_1/c$	$P2_1/c$	$P2_1/c$	$P2_1/c$
a (Å)	9.2609(18)	9.288(2)	9.331(2)	9.371(2)
b (Å)	10.6575(19)	10.684(2)	10.738(2)	10.793(2)
c (Å)	18.843(4)	18.892(4)	18.960(4)	19.025(4)
α (°)	90	90	90	90
β (°)	91.219(14)	91.275(15)	91.437(16)	91.666(16)
γ (°)	90	90	90	90
Volume (Å^3)	1859.4(6)	1874.1(7)	1899.0(7)	1923.4(7)
Z	4	4	4	4
λ range (Å)	0.7 – 6.9	0.7 – 6.9	0.7 – 6.9	0.7 – 6.9
Completeness (%)	-	-	-	-
Reflections Collected	15098	10557	9135	7243
Independent	15098	10557	9135	7243
Refln (obs.I>2theta(I))	12380	8618	8077	6461
R_{int}	-	-	-	-
Data/Rest./Param.	15098/0/466	10577/0/466	9135/0/466	7243/0/466
GooF on F^2	1.123	1.281	1.533	1.683
R_1 (Observed)	0.0737	0.0736	0.0684	0.0725
R_1 (all)	0.0905	0.0926	0.0839	0.0912
wR_2 (all)	0.1402	0.1558	0.1466	0.1524
***P* (max / min) / fm-Å^{-3}**	2.392 / -1.642	1.717 / -1.505	1.019 / -0.947	0.697 / -0.602
RMS / fmÅ^{-3}	0.376	0.463	0.233	0.147

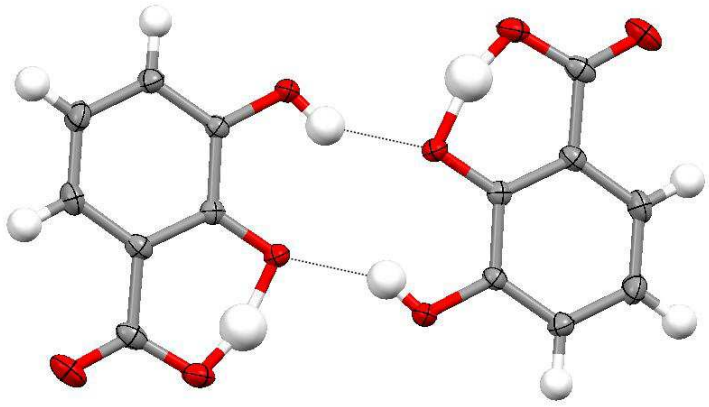

Figure 5-16. The asymmetric intramolecular HBs in the 23DOHBA$^-$ molecules (with the H atom located closer to the carboxylate group), and the connection of these molecules through O–H···O moderate HBs in the molecular complex of DMAN :23DOHBA.

The structure of the molecular complex is not similar to any pattern seen in those presented prior in this work. Pairs of $DMANH^+$ molecules are stacked through a head to tail arrangement with C–H···π interaction between the methyl groups and the naphthalene rings with distances between ~3.50 Å and ~3.63 Å (between the methyl group and the centroid of the naphthalene rings). The structure is built up from the stacked pairs of $23DOHBA^-$ molecules and $DMANH^+$ molecules. These are held together by C–H···O weak hydrogen bonds between the methyl group of the $DMANH^+$ and the oxygen atom of the carboxylate group as well as between the naphthalene group and the hydroxyl group oxygen atoms in the *meta*- position of the 23DOHBA molecule with lengths between 3.215(2) Å and 3.582(2) Å. There are also C–H···π weak hydrogen bonds from the $23DOHBA^-$ to the naphthalene group of the $DMANH^+$ with a length of ~3.81 Å forming a layer in which there are linear regions of each type of molecule (*Figure 5-17*).

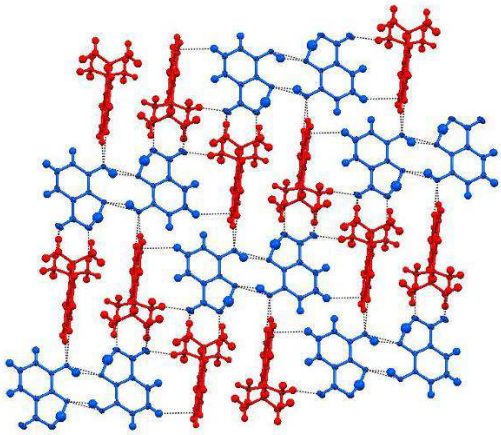

Figure 5-17. Interspersed pairs of $DMANH^+$ (red) and pairs of $23DOHBA^-$ (blue) connected through intermolecular C–H···O and C–H···π weak hydrogen bonds in the molecular complex of DMAN : 23DOHBA.

These layers of stacked pairs of $DMANH^+$ and $23DOHBA^-$ molecules are connected to the next layer through further C–H···π weak hydrogen bonds with lengths between ~3.57 Å and ~3.74 Å and C–H···O weak hydrogen bonds between 3.350(1) Å and 3.531(1) Å. The interactions between the methyl groups of the $DMANH^+$ and the oxygen atoms of the carboxylate groups shows similarities with those found in the molecular complex of DMAN : 4OHBA hydrate in the case of

the $DMANH^+$ molecule with the symmetrical intramolecular HB. However, in this case the intramolecular N–H···N HB is asymmetric with N–H = 1.08(2) Å and H···N = 1.55(2) Å. As the N–H···N bond is very asymmetric it is not unexpected that the N–C bond length is longer on the donor side of the N–H···N bond (*Table 5-1*).

Variable temperature X-ray data have been collected on the molecular complex to determine any possible anomalous behaviour of the hydrogen atoms within the hydrogen bonds. There are no significant changes in the donor-acceptor lengths measured from the X-ray data collection; the measured hydrogen bond lengths are listed in *Table 5-6*, showing that the D–H and H···A distances also do not vary significantly with temperature. In keeping with this, the difference Fourier maps in the case of the intramolecular N–H···N and O–H···O HBs show only a slight elongation of the electron density with increasing temperature, while the intermolecular O–H···O hydrogen bond has a single, well-defined position of the hydrogen atom electron density at all three measured temperatures(*Figure 5-18*).

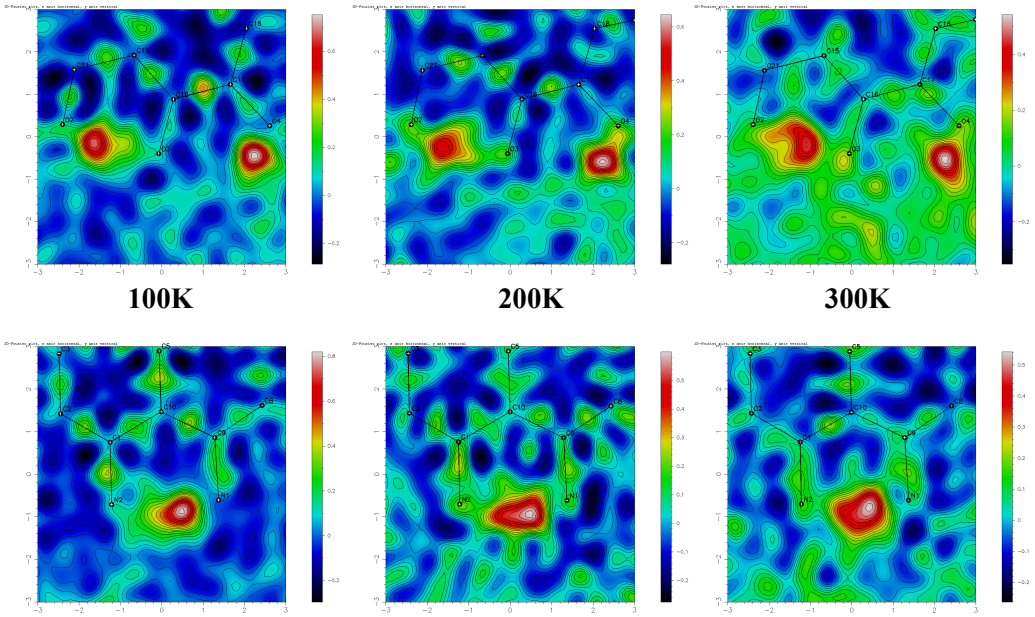

Figure 5-18. The difference Fourier maps of the hydrogen atoms electron density within intermolecular(top) and intramolecular hydrogen bonds at the three measured temperature.

Table 5-6. N–H···N and O–H···O hydrogen bond lengths in the molecular complex of DMAN : 23DOHBA at variable temperature from X-ray diffraction data.

Type	Temp	D····A (Å)	D-H (Å)	H···A (Å)
N-H···N	100	2.587(1)	1.08(2)	1.55(2)
	200	2.590(1)	1.11(2)	1.53(2)
	300	2.593(1)	1.13(2)	1.50(2)
Intramolecular O-H···O	100	2.425(2)	1.12(3)	1.33(3)
	200	2.422(2)	1.14(3)	1.30(2)
	300	2.425(2)	1.18(3)	1.27(2)
Intermolecular O-H···O	100	2.677(1)	0.86(2)	1.90(2)
	200	2.687(1)	0.88(2)	1.88(2)
	300	2.702(1)	0.90(2)	1.87(2)

5.2.2 DMAN and 2,4-dihydroxybenzoic acid (1:1)

The molecular complex of DMAN : 24DOHBA crystallises in 1:1 ratio with a protonated $DMANH^+$ and a deprotonated $24DOHBA^-$ molecule. The pattern of the bonding between the $24DOHBA^-$ molecules is similar to that found in the complex of DMAN : 4OHBA hydrate, with the hydroxyl group in the *para*- position hydrogen bonding to the oxygen atoms of the carboxylate group through a medium strength O–H···O intermolecular hydrogen bond with O···O separation of 2.589(2) Å, O–H = 1.06(4) Å and H···O = 1.54(4) Å. The hydrogen atom from the *ortho*- hydroxyl group forms an intramolecular hydrogen bond with the other oxygen atom from the carboxylate group; this is a SSHB with a length of 2.492(2) Å with O–H = 1.20(3) Å and H···O = 1.37(3) Å. The C–O bond length of the carboxylate group is 1.251(2) Å on the side of the SSHB and 1.276(3) Å on the side of the moderate intermolecular HB; the C–O on the side of the SSHB is not as short as in the case of the $23DOHBA^-$ molecule C–O, but the intramolecular SSHB in this case is longer as well. The $24DOHBA^-$ molecules create a zig-zag chain through the intermolecular hydrogen bonds, as in the case of the $4OHBA^-$ molecules in the DMAN : 4OHBA complex. These chains are connected through C–H···O weak hydrogen bonds between the hydroxyl group in the *meta*- position and the benzene ring of the other $24DOHBA^-$ with a length of 3.550(3) Å; in this case these interactions are present on both sides as there are no water

molecules in the structure. This forms a layer of 24DOHBA$^-$ molecules (*Figure 5-19*).

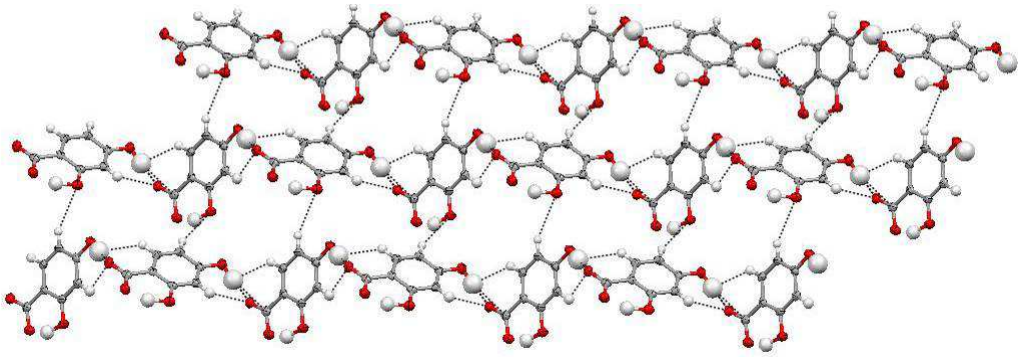

Figure 5-19. Layer of 24DOHBA$^-$ formed through the O–H··O and C–H···O hydrogen bonds between the 24DOHBA$^-$ molecules in the molecular complex of DMAN : 24DOHBA.

There are C–H···π weak hydrogen bonds between the methyl groups of one DMANH$^+$ molecule and the naphthalene group of the other with lengths between ~3.73 Å and ~3.92 Å showing a head to tail stacking arrangement of the DMANH$^+$ molecules forming a chain (*Figure 5-20*) and as in other complexes described in this chapter, they are sandwiched between the layers of 24DOHBA$^-$ molecules, holding these layers together (*Figure 5-21*).

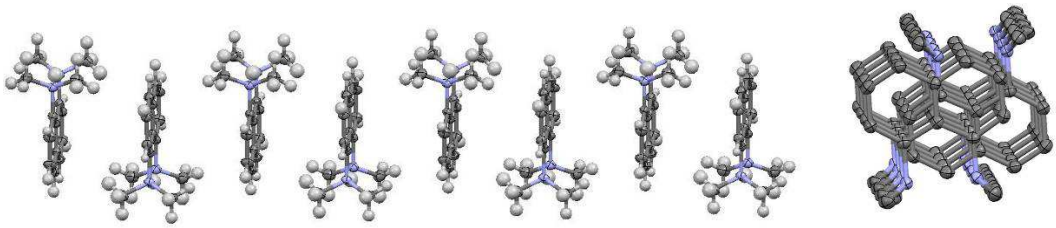

Figure 5-20. Chain of DMAN molecules from side (left) and along the chain (right) view. The hydrogen atoms have been omitted from the view along the chain for clarity.

The intermolecular interactions are comprised of C–H···π weak hydrogen bonds between the naphthalene of the DMANH$^+$ molecule and the benzene ring of the 24DOHBA$^-$ with lengths between ~3.39 Å and ~3.45 Å and two C–H···O weak hydrogen bonds. One of these is between the carbon of the naphthalene ring and

the hydroxyl group in the para- position, while the other is between the methyl group and the carboxylate group with lengths of 3.460(3) Å and 3.352(3) Å respectively.

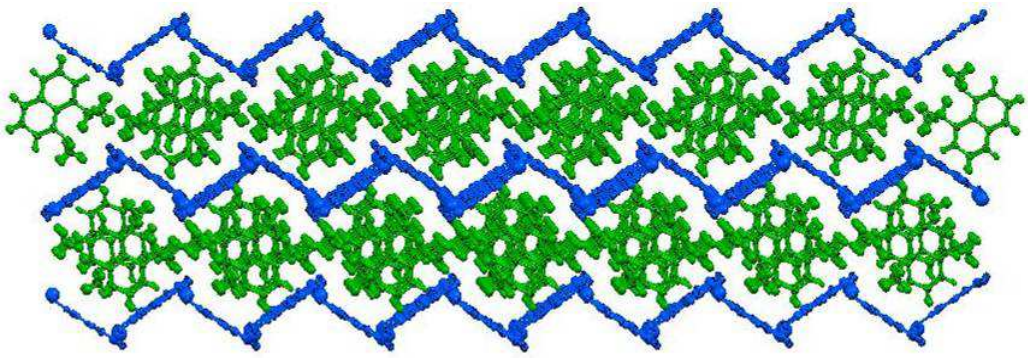

Figure 5-21. The structure of the molecular complex of DMAN : 24DOHBA as a whole, showing the zig-zag layers of 24DOHBA$^-$ (blue) with DMANH$^+$ molecules sandwiched between them.

The relative position of the 24DOHBA$^-$ to the DMANH$^+$ molecules is similar to that found in the DMAN : 23DOHBA complex, where both oxygen atoms are connected to the methyl groups through C–H···O intermolecular interactions with lengths between 3.235(3) Å and 3.521(3) Å.

The DMANH$^+$ has the usual N–H···N intramolecular hydrogen bonded bridge with an N···N separation of 2.567(2) Å; in this case the bridge is asymmetrical with N–H = 1.16(2) Å and H···N = 1.46(2) Å. However, there is no significant difference between the C–N bond lengths on the donor and acceptor side (*Table 5-1*).

The isotropic thermal parameter of the hydrogen atom within the intermolecular hydrogen bond is very large compared to those of the rest of the hydrogen atoms, but the resolution of the data set is rather low and the generated difference Fourier map is too noisy to allow for any further interpretation.

5.2.3 DMAN and 2,6-dihydroxybenzoic acid (1:1)

The molecular complex of DMAN : 26DOHBA, similarly to the other two dihydroxy-substituted benzoic acid complexes with DMAN presented previously, crystallises in 1:1 ratio, with a protonated $DMNAH^+$ and a deprotonated dihydroxybenzoic acid. The position of the substitution in this case generates two intramolecular SSHBs involving the deprotonated carboxylate instead of one since both hydroxyl groups are in the *ortho*- position. As both potential hydrogen bond donors are involved in intramolecular interactions there are no O–H···O intermolecular hydrogen bonds present in the structure and the $26DOHBA^-$ molecules are connected through C–H···O weak hydrogen bonds between the benzene ring of one and the oxygen atoms of the carboxylate group of the other $26DOHBA^-$ molecule with lengths between 3.490(2) Å and 3.593(2) Å. In this way, each $26DOHBA^-$ molecule is connected to another four $26DOHBA^-$ molecules forming a zig-zag layer (*Figure 5-22*).

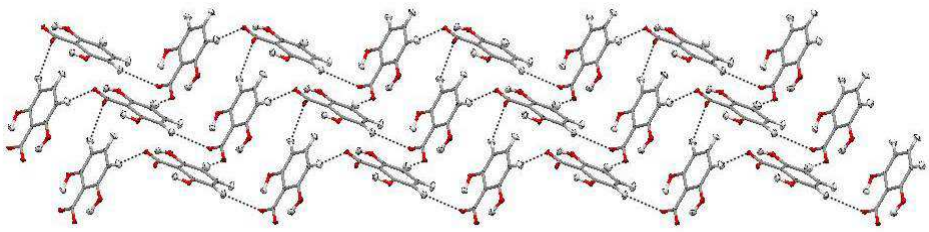

Figure 5-22. Zig-zag layers of $26DOHBA^-$ connected together through C–H···O weak hydrogen bonds in the molecular complex of DMAN : 26DOHBA.

The $DMANH^+$ molecules are stacked in pairs and connected through C–H···π weak hydrogen bonds between the methyl groups of one molecule to the naphthalene group of the other with lengths between the ~3.33 Å and ~3.84 Å (between the methyl carbon atom and the centroid of the napthalene). The pairs of $DMANH^+$ molecules shows a displaced stacked arrangement of their naphthalene ring with the next pair of $DMANH^+$ molecules, forming a chain (*Figure 5-23*).

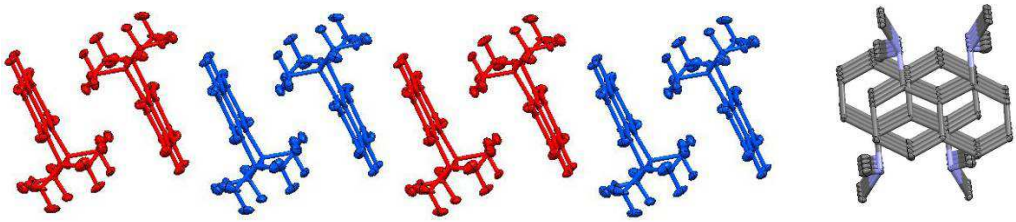

Figure 5-23. Chain formed from the stacked DMAN molecules from side (left, pairs are coloured for clarifications of the pairs of C–H···π hydrogen bonded $DMANH^+$) and viewed along the chain (right, hydrogen atoms are omitted for clarity).

The layers formed from the 26DOHBA molecules are similar to those formed in the molecular complex of DMAN : 24DOHBA, sandwiching the $DMANH^+$ between these layers, but in this case the relative orientations of the $DMANH^+$ molecules are inclined (*Figure 5-23*), and the chain orientation between the layers are different (*Figure 5-24*).

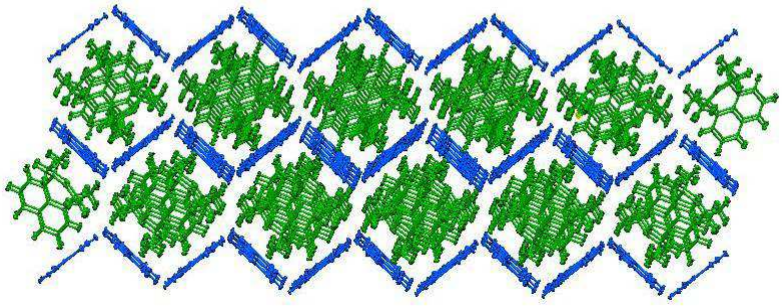

Figure 5-24. The structure as a whole with the $DMANH^+$ molecules (green) holding together the layers of $26DOHBA^-$ molecules (blue) in the molecular complex of DMAN : 26DOHBA.

There are C–H···O weak hydrogen bonds between the methyl groups of the $DMANH^+$ and the $26DOHBA^-$ molecules positioned above the $DMANH^+$ molecule, but in this case, the interactions involve one oxygen atom from the carboxylate group and one of the hydroxyl oxygen atoms (*Figure 5-25*). In addition to the three C–H···O weak hydrogen bonds with lengths between 3.357(3) Å and 3.468(3) Å, there are two C–H···π interactions between the methyl group and the benzene ring of $26DOHBA^-$ molecules with lengths of ~3.79 Å and ~3.83 Å.

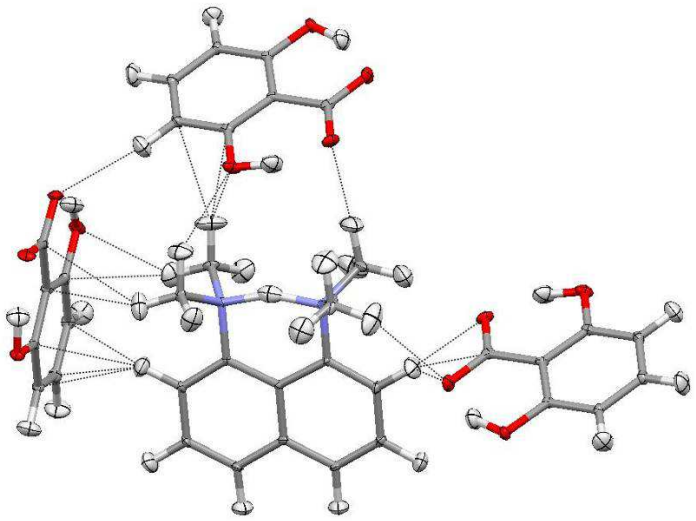

Figure 5-25. Intermolecular interactions between the DMANH$^+$ molecule methyl groups and neighbouring 26DOHBA$^-$ molecules, in the molecular complex of DMAN : 26DOHBA.

In the direction along the N–H···N hydrogen bond, the methyl group is connected to further two 26DOHBA$^-$ molecules through intermolecular interactions within the sum of the van der Waals radii (*Figure 5-25*). There is one C–H···O weak hydrogen bond with length of 3.607(3) Å, as well as two C–H···π weak hydrogen bonds with lengths between ~3.78 Å and ~3.83 Å on one side and one C–H···O weak hydrogen bond with a length of 3.557(3) Å on the other side.

The intramolecular N–H···N hydrogen bond has been more fully characterised by the neutron diffraction data. This shows that the HB bridge is nearly symmetric at 30 K, and becomes slightly more symmetrical with increasing temperature. While the less accurate measurements from the X-ray data do not show changes outside the range of standard uncertainties, the small changes in hydrogen bonding distances appearing from the neutron diffraction data are within the much higher standard uncertainties in the parameters determined from the X-ray diffraction experiment (*Table 5-7*).

Table 5-7. N–H···N and O–H···O distances measured from X-ray and neutron diffraction experiments at variable temperature in the molecular complex of DMAN : 26DOHBA

Measurement temp. °K	N···N	N-H	H···N	O···O	O-H	H···O	O···O	O-H	H···O
30 n	2.586(2)	1.291(4)	1.341(4)	2.497(3)	1.032(4)	1.520(4)	2.520(3)	1.030(4)	1.546(4)
100 n	2.585(2)	1.293(6)	1.339(6)	2.499(4)	1.029(6)	1.524(6)	2.518(5)	1.033(7)	1.545(7)
200 n	2.591(2)	1.314(5)	1.326(5)	2.499(5)	1.032(6)	1.524(6)	2.513(5)	1.013(8)	1.560(7)
300 n	2.598(3)	1.320(7)	1.328(8)	2.480(7)	1.01(1)	1.53(1)	2.511(8)	1.04(1)	1.53(1)
100 X	2.577(2)	1.26(2)	1.36(2)	2.492(1)	1.02(2)	1.52(2)	2.515(2)	1.03(2)	1.54(2)
200 X	2.579(2)	1.27(2)	1.36(2)	2.485(2)	1.04(2)	1.48(2)	2.506(2)	1.17(3)	1.39(3)
300 X	2.579(2)	1.27(2)	1.35(2)	2.476(3)	1.13(3)	1.38(3)	2.509(3)	1.20(3)	1.35(3)

In both intramolecular O–H···O HBs there is a small contraction of the lengths, though one of these does show a larger (in the longer O–H···O HB) apparent contraction with temperature from both sets of data (by 0.017 Å from the neutron and 0.016 Å from the X-ray data sets), though these are at the limits of significance. Since both neutron and X-ray diffraction data have been collected at variable temperatures to get a better insight in the hydrogen bonding, Fourier maps were generated for the electron and nuclear densities in the region of the hydrogen bonded hydrogen atoms (*Figure 5-26, Figure 5-27*). The hydrogen atoms of the shorter O-H···O are on the left and the longer on the right on the difference maps of the $26DOHBA^-$ molecule (*Figure 5-27*).

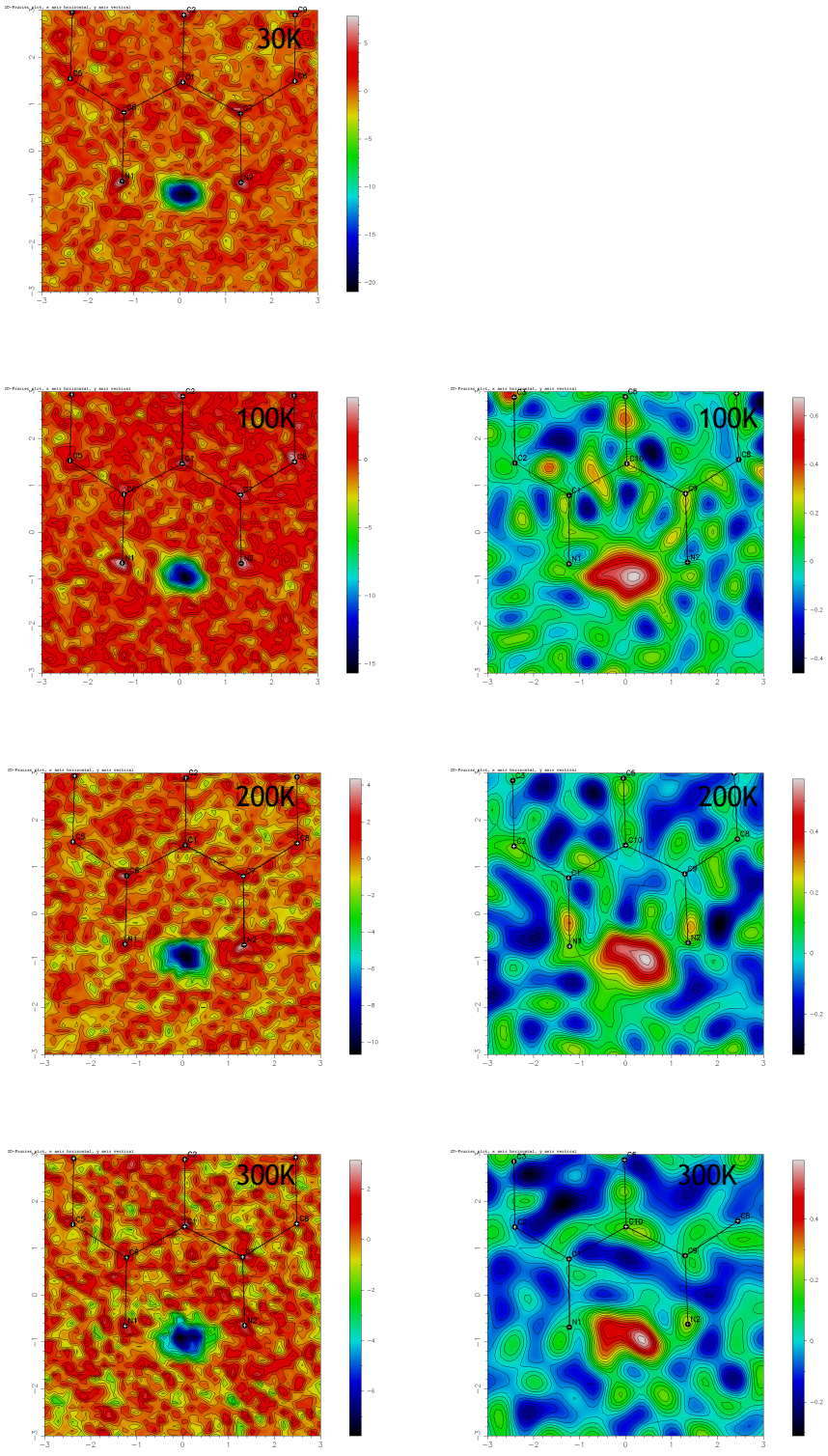

Figure 5-26. Difference Fourier maps in the region of the hydrogen atom within the N–H···N intramolecular hydrogen bond generated from neutron (left) and X-ray (right) diffraction data at variable temperature of 30 (neutron only), 100, 200, 300 K in the molecular complex of DMAN : 26DOHBA.

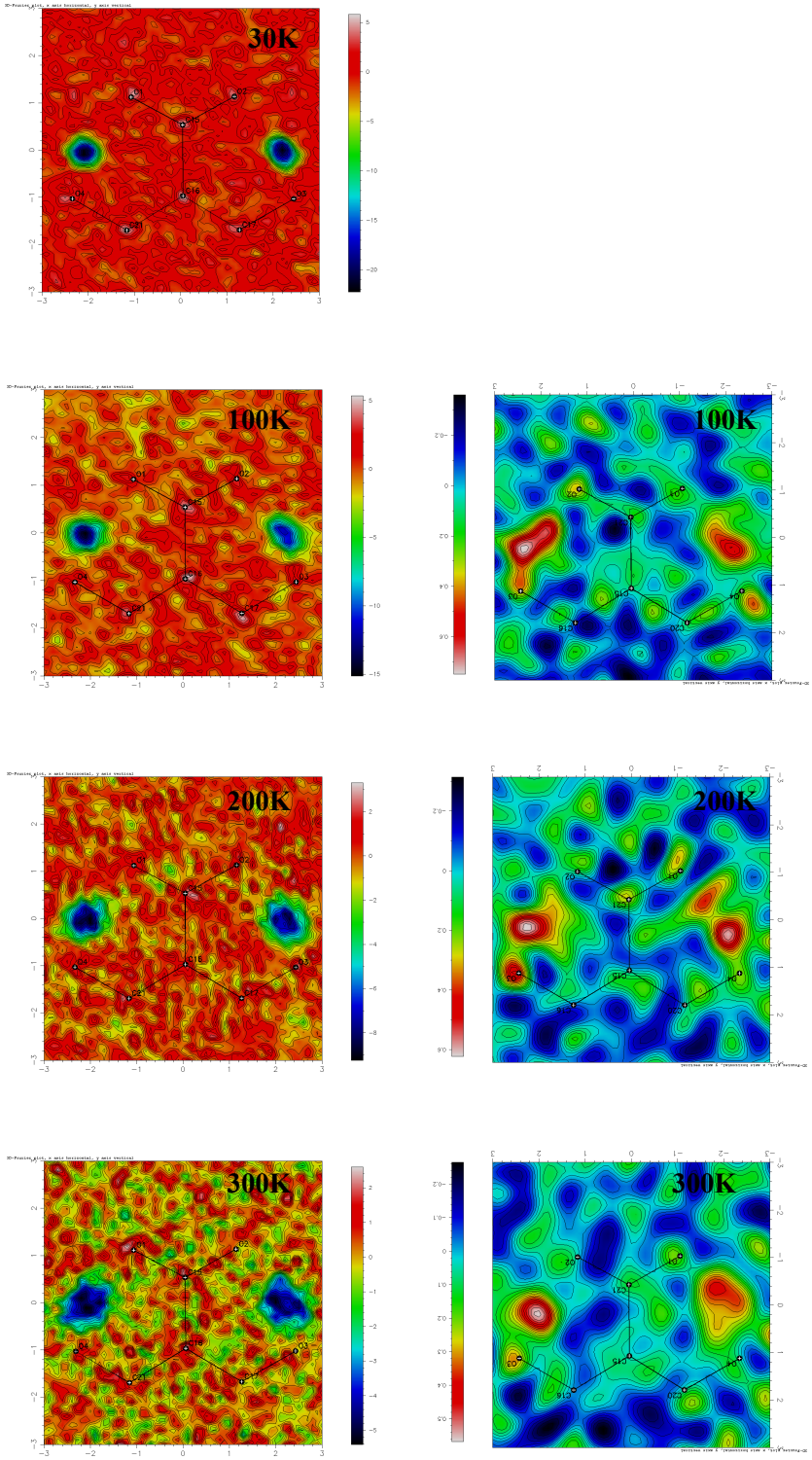

Figure 5-27. Difference Fourier maps in the region of the hydrogen atom within the O–H···O intramolecular hydrogen bond generated from neutron (left) and X-ray (right) diffraction data at variable temperature of 30 (neutron only), 100, 200, 300 K in the molecular complex of DMAN : 26DOHBA.

The donor-acceptor distance does not change in the case of the intramolecular N–H···N, and from the difference Fourier maps appear that the electron density of the hydrogen atom shows only very limited if any elongation at all three measured temperatures. These views of the electron density are placed in the context of the nuclear density from the neutron diffraction, which shows that at all four temperatures the hydrogen atom is located in a single, well-defined position. The N–C bond shows no significant differences between the lengths of the donor and acceptor sides measured either from X-ray or from neutron diffraction experiments as the hydrogen position within the bond is just slightly asymmetric (*Table 5-1*).

There is more variation in the imaged electron density in the O–H···O intramolecular hydrogen bonds, but although there is evidence of elongation of this density and in some cases slight splitting, there is no change in the position or elongation of the hydrogen from the difference Fourier map of the nuclear density beyond that expected from an increased thermal parameter at higher temperature. As both oxygen atoms from the carboxylate group are hydrogen bonded to the hydroxyl group through intramolecular hydrogen bonds, the small differences in their lengths is not unexpected, with a slightly longer bond length (1.271(2) Å) for the oxygen atom involved in the longer O–H···O and slightly shorter (1.262(2) Å) for the case of the oxygen atom involved in the shorter O–H···O HB.

5.3 DMAN : methyl- and nitro-substituted benzoic acids

(1:2) DMAN : 3-toluic acid (3TOLA; 3-methylbenzoic acid): 1:2 molar ratio of DMAN and 3TOLA were dissolved in diethyl ether and evaporated at room temperature, slowing the evaporation by closing the vial with a small pierced clipped lid. After the evaporation of the solvent, colourless prisms were formed. Single crystal X-ray diffraction data were collected on a Rigaku R-AXIS/RAPID diffractometer at 100K (*Table 5-8*). The data were solved with SHELXS97 and refined with SHELXL97, within the WinGX package.

(1:2) DMAN : 4-toluic acid (4TOLA; 4-methylbenzoic acid): 1:2 molar ratio of DMAN and 4TOLA were dissolved in acetone and evaporated at room temperature, slowing the evaporation by closing the vial with a small pierced clipped lid. After the evaporation of the solvent, colourless prisms were formed. Single crystal X-ray diffraction data were collected on a Rigaku R-AXIS/RAPID diffractometer at 100K (*Table 5-8*). The data were solved with SHELXS97 and refined with SHELXL97, within the WinGX package.

(1:2) DMAN : 3-nitrobenzoic acid (3NBA): 1:2 molar ratio of DMAN and 3NBA were dissolved in dichloromethane and evaporated at room temperature, slowing the evaporation by closing the vial with a small pierced clipped lid. After the evaporation of the solvent colourless prisms were formed. Single crystal X-ray diffraction data were collected on a Bruker Nonius Kappa CCD diffractometer at 100K (*Table 5-8*). The data were solved with SHELXS97 and refined with SHELXL97, within the WinGX package.

Table 5-8. X-ray data refinement details of DMAN : 3TOLA, DMAN : 4TOLA, DMAN : 3NBA

Compound	1:2 DMAN : 3TOLA	1:2 DMAN : 4TOLA	1:2 DMAN : 3NBA
Diffractometer	Rigaku R-AXIS/Rapid	Rigaku R-AXIS/Rapid	Nonius Kappa CCD
Formula	C_{30} H_{34} N_2 O_4	C_{30} H_{34} N_2 O_4	C_{28} H_{28} N_4 O_8
Molecular weight / gmol^{-1}	486.60	486.60	548.55
Temperature (K)	100	100	100
Space Group	$P\bar{1}$	$P2_1/n$	Pbna
a (Å)	9.9319(8)	11.3676(8)	8.4497(2)
b (Å)	11.7523(8)	7.6630(7)	13.1735(3)
c (Å)	11.9665(7)	29.8880(16)	48.2689(12)
α (°)	109.995(2)	90	90
β (°)	93.384(2)	97.012(2)	90
γ (°)	91.426(3)	90	90
Volume (Å^3)	1308.77(16)	2584.07	5372.9(2)
Z	2	4	8
θ range/°	3.00– 27.56	3.21– 27.48	3.09 – 27.5
Completeness (%)	99.3	99.1	99.1
Reflections Collected	30360	30825	45900
Independent	5960	5860	6109
Refln (obs.I>2theta(I))	4931	3727	3779
R_{int}	0.0225	0.0743	0.1093
Data/Rest./Param.	5960/0/461	5860/0/461	6109/0/473
GooF on F^2	1.069	0.995	1.087
R_1 (Observed)	0.0387	0.048	0.0543
R_1 (all)	0.0486	0.0945	0.1134
wR_2 (all)	0.1064	0.1488	0.1287
ρ (max / min) / e-Å^{-3}	0.256 / -0.172	0.315 / -0.226	0.21 / -0.272
RMS / eÅ^{-3}	0.04	0.061	0.056

The bond lengths of the C–O and C=O bonds of the carboxyl groups are given in *Table 5-9*. The labelling corresponds to that shown in *Figure 5-28*.

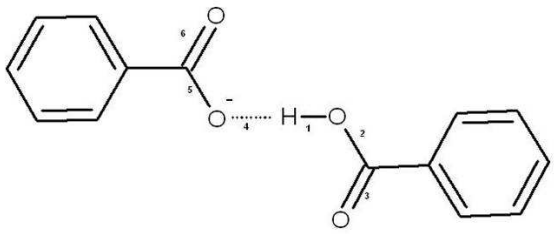

Figure 5-28. Diagram of the DIMER⁻. The bonds are marked with numbers and their lengths are listed in Table 5-9

Table 5-9. Bond lengths measured at 100K from X-ray data in the molecular complexes of DMAN and the methyl- and nitro- substituted benzoic acids with labelling as shown in Figure 5-28.

Bond (Å)	1. O-H	2. C-O	3. C=O	4. O···H	5. C-O	6. C=O
3TOLA	1.15(2)	1.301(2)	1.220(2)	1.32(2)	1.288(2)	1.234(1)
4TOLA	1.16(3)	1.317(3)	1.218(3)	1.36(3)	1.289(3)	1.243(3)
3NBA	1.16(3)	1.295(2)	1.227(2)	1.30(3)	1.290(2)	1.226(2)

5.3.1 DMAN : 3-toluic acid (3-methylbenzoic acid) (1:2)

The 3TOLA molecules, unlike the hydroxyl-substituted benzoic acids, have no hydrogen donor apart from the carboxyl group. In this respect they are similar to the halogen-substituted benzoic acids. The DMAN molecule deprotonates one of the 3TOLA molecules and in order to stabilise the lost charge, the deprotonated $3TOLA^-$ molecule hydrogen bonds to the neutral 3TOLA molecule forming a $DIMER^-$ connected through one charge-assisted SSHB as seen in the structures of the DMAN : halogen-substituted benzoic acid complexes. The asymmetric unit contains one $DMANH^+$ and one $DIMER^-$.

The intermolecular interactions between the $DMANH^+$ molecules methyl group and the non hydrogen-bonded oxygen atom of the $DIMER^-$ and their relative position to each other are also similar to those in the DMAN : halo-benzoic acid complexes (*Figure 5-29*). There are four C–H···O weak hydrogen bonds between

one of the non-hydrogen bonded oxygens and the methyl group, with lengths between 3.191(1) Å and 3.358(2) Å. There is a similar interaction with the other non-hydrogen bonded oxygen atom from the $DIMER^-$ with a length of 3.229(2) Å. There is also an O···H contact between the oxygen of the carboxyl group and the hydrogen atom within the N–H···N intramolecular hydrogen bond with a length of 2.69(2) Å.

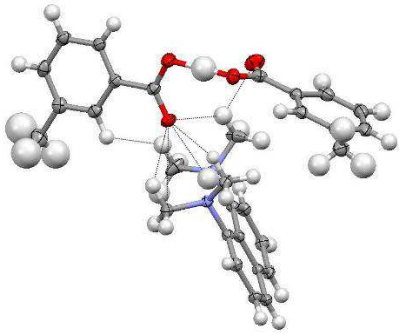

Figure 5-29. The asymmetric unit of the DMAN : 3TOLA complex showing the intermolecular interactions between the methyl group of the $DMANH^+$ and the $DIMER^-$.

The $DIMER^-$s are connected together through C–H···O weak hydrogen bonds with lengths of 3.543(2) Å and a C–H···π weak hydrogen bond with a length of ~3.69 Å forming ribbons of $DIMER^-$s connected in a "head to tail" arrangement (*Figure 5-30*).

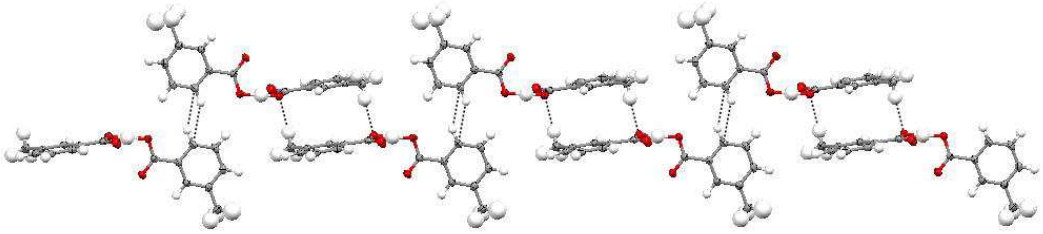

Figure 5-30. The ribbon formed by the $DIMER^-$s connected through intermolecular C–H··O and C–H···π interactions in the molecular complex of DMAN : 3TOLA.

$DMANH^+$ molecules are stacked in pairs in a "head to tail" pattern and connected through π···π interactions with length of ~3.47 Å between the planes of the two naphthalene ring, each connected through the weak hydrogen bonds between

the methyl group of $DMANH^+$ and the $DIMER^-$ to a ribbon above and below of the stacked $DMANH^+$ pairs and through additional C–H···π weak HB between the methyl groups and the benzene ring of the $DIMER^-$. The $DMANH^+$ molecules are also connected through C–H···π weak HBs with lengths between ~3.63 Å and ~3.86 Å and C–H···O weak HBs between the oxygen atoms of the carboxyl groups and the methyl groups of the $DMANH^+$ with length between 3.024(2) Å and 3.433(2) Å to another two ribbons on the side of the $DMANH^+$ molecules (*Figure 5-31*).

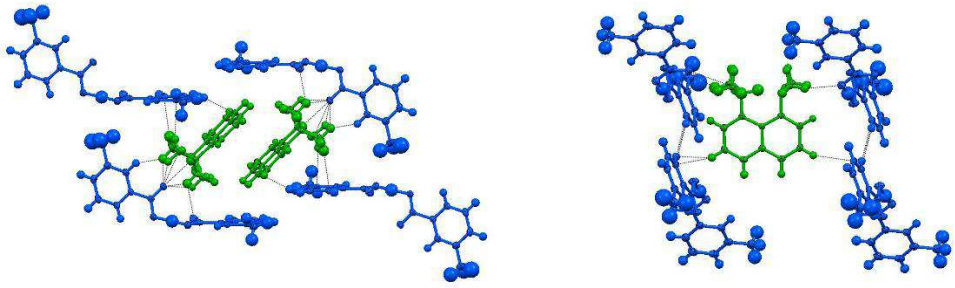

Figure 5-31. The pairs of stacked $DMANH^+$ molecules showing the ribbons connected above and below (left) and the other two ribbon connected on the side of the of the $DMANH^+$ molecule. 3TOLA $DIMER^-$s are coloured blue and $DMANH^+$ molecules are coloured green for a clarified view.

Through the above discussed interactions between ribbons of $DIMER^-$s and $DMANH^+$ molecules, the overall packing of the structure is formed (*Figure 5-32*).

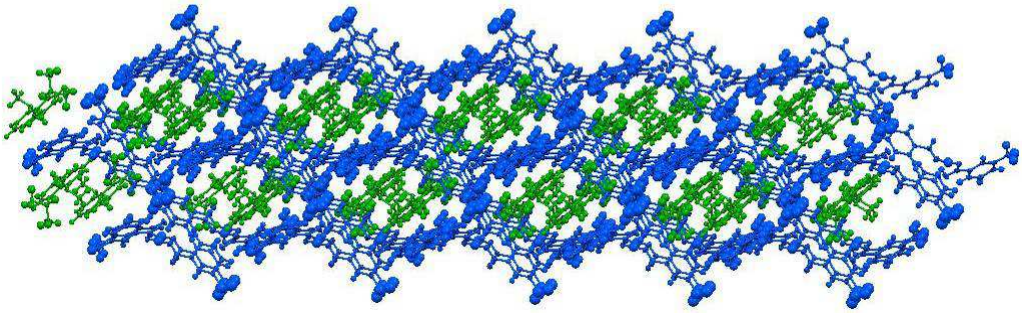

Figure 5-32. The structure of the DMAN : 3TOLA complex as a whole showing the ribbon of 3TOLA $DIMER^-$s (blue) held together by $DMANH^+$ molecules (green).

The use of methyl-substituted benzoic acid to co-crystallise with DMAN has been driven by the fact that the volume of the methyl group is comparable with that of the chlorine atom, allowing a comparison of the packing patterns of sterically-similar groups. Around 30% of the isostructural pairs found in the CSD are formed for pairs where a methyl group has been interchanged with chlorine, with a recent study showing that engineering of such pairs can often lead to isostructural complexes[163]. However, in this case there is no possible of isostructurality as the determined crystal structure of the related DMAN : 3CBA has a different co-crystallisation ratio (3:4) and contains both protonated and unprotonated DMAN in the structure, thus forming a very different molecular complex. Nonetheless, the DMAN :3TOLA complex fits very well with the trend seen often in the molecular complex of DMAN and halo-substituted benzoic acids. The common features include a co-crystallisation ratio of 1:2 DMAN : benzoic acid, the relative position of the carboxyl groups of the $DIMER^{-}$s to the $DMANH^{+}$ and the packing similarities between the structures, with the $DMANH^{+}$ molecules surrounded by the $DIMER^{-}$s and holding the structure together.

The intramolecular N–H···N hydrogen bond in the $DMANH^{+}$ shows an asymmetric bridge with N···N length of 2.575(2) Å, N–H = 1.12(2) Å and H···N = 1.50(2) Å. As the N–H···N bond is very asymmetric these differences appear in the C-N bond lengths as well, with a longer C–N bond length on the donor side of the hydrogen bridge (*Table 5-1*). The intermolecular O···O HB between the carboxyl and carboxylate groups is in the range of the charge-assisted SSHB found in the other DMAN complexes which have a $DIMER^{-}$s within the structure, with an O···O separation of 2.473(1) Å with distances O–H = 1.15(2) Å and H···O = 1.32(2) Å. The difference between the C–O bonds in the carboxyl group shows the same behaviour as in all the other DMAN complexes containing a benzoic acid $DIMER^{-}$ in the structure, showing a slightly larger difference between the length of the C–O and C=O bonds on the donor side of the intermolecular SSHB (*Table 5-1*).

5.3.2 DMAN : 4-toluic acid (4-methylbenzoic acid) (1:2)

The molecular complex of DMAN : 4TOLA crystallises in 1:2 ratio as for most of the halogen-substituted benzoic acids, with the familiar features of the protonated $DMNAH^+$ molecule and the single charge-assisted short, strong hydrogen bonded $DIMER^-$. Comparing the structure of the complex with that of the 4-chlorobenzoic acid equivalent is again hampered by the different crystallisation ratio in the two complexes. The DMAN : 4CBA complex has a 1:1 ratio, has a protonated $DMANH^+$, and an unprotonated DMAN molecule containing a disordered methyl group, while the complex of DMAN : 4TOLA has none of these. However, considering the other three *para*-halogen substituted benzoic acids, it is found that two of the three complexes are isostructural (DMAN : 4BBA and 4IBA:DMAN, see Chapter 4) and with their 1:2 molecular complex ratios do offer the opportunity for comparison with the DMAN : 4-TOLA structure. This point is emphasised by the present of a significantly bent $DIMER^-$ unit in all three structures. The structure overlay shows that the DMAN : 4TOLA and the two para-halogen substituted benzoic acid and DMAN complexes in fact are isomorphous with even more similar unit cell parameters between the DMAN : 4TOLA and DMAN : 4BBA than between the DMAN : 4BBA and DMAN : 4IBA complexes (*Figure 5-33*) (*Table 5-10*).

Table 5-10. Unit cell parameters of DMAN : 4TOLA, DMAN : 4BBA and DMAN : 4IBA at 100 K from X-ray diffraction data.

Molecular complex	Space group	Volume ($Å^3$)	a (Å)	b (Å)	c (Å)	α(°)	β (°)	γ (°)
DMAN : 4TOLA	$P2_1/n$	2584.1(3)	11.3676(8)	7.6630(7)	29.8880(16)	90	97.012(2)	90
DMAN :4BBA	$P2_1/n$	2596.20(5)	11.3276(1)	7.6916(1)	29.9623(4)	90	96.0070(10)	90
DMAN : 4IBA	$P2_1/n$	2703.83(8)	11.4230(2)	7.7761(1)	30.7590(6)	90	96.8230(10)	90

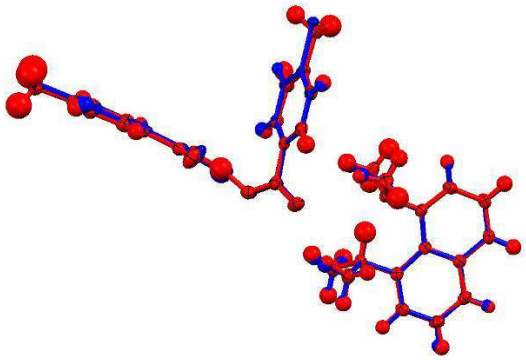

Figure 5-33. The structure overlay of the molecular complexes of DMAN : 4BBA (blue) and DMAN 4TOLA (red), showing the overlay of the asymmetric unit, based on the best fit overlay of the naphthalene rings.

In the DMAN : 4TOLA complex, the ribbon of $DIMER^{-}$s is again formed through C–H···O weak hydrogen bonds with lengths between 3.488(3) Å and 3.562(3) Å (*Figure 5-34*). The main differences appear in the nature of the connection between the ribbons formed; there are no intermolecular interactions since in both other cases halogen-halogen interactions play a role in the formation of layer from the ribbon of $DIMER^{-}$s, and these are not of course present here (Figure 5-34).

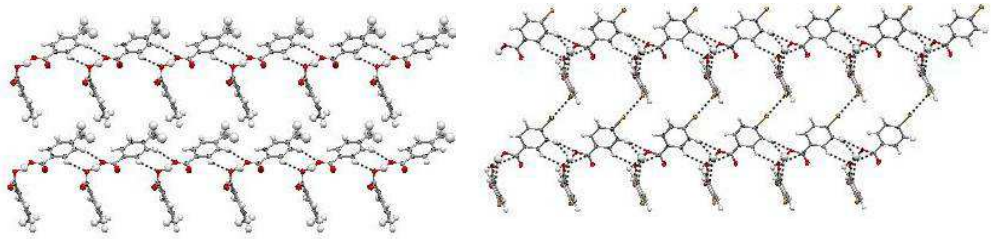

Figure 5-34. The ribbons of $DIMER^{-}$s showing no intermolecular interactions between the ribbons in the molecular complex of DMAN : 4TOLA within the van der Waals radii (left). For comparison the presence of Br···Br interaction between the ribbons is illustrated in the case of DMAN : 4BBA (right).

Despite the fact that there are no intermolecular interactions between the ribbons of $DIMER^{-}$s. the structure builds up in the same way, with the $DMANH^{+}$ molecules connected through C–H···π weak hydrogen bonds with lengths between ~ 3.47 Å and ~3.98 Å in a "herring bone" formation, interlocked

between the ribbons of 4TOLA DIMER$^-$s. The isostructural nature of the two halogen-substituted benzoic acid : DMAN complexes and the 4TOLA : DMAN molecular complexes suggests that the halogen-halogen interactions do not play the key role in the bent nature of the DIMER$^-$s. It may be that the size and the position of the substituent have more influence on the deviation from the more linear form of DIMER$^-$s and that the overall assembly of these three isostructural complexes is driven by other moderate interactions between the DIMER$^-$s and the DMANH$^+$ molecules.

The fact that the three molecular complexes are isostructural gives a good opportunity to compare the influence of the intermolecular interactions along the direction of the intramolecular N–H···N hydrogen bonds. In the molecular complex of DMAN : 4TOLA, the intramolecular hydrogen bridge is asymmetric with a length of 2.613(2) Å, with N–H = 1.11(3) Å and H···N = 1.56(3) Å. This is similar to the geometry found in the molecular complex of DMAN : 4BBA, with N···N = 2.602(3) Å, N–H = 0.96(3) Å and H···N = 1.67(3), and in DMAN : 4IBA, where N···N = 2.582(4) Å, N–H = 1.08(3) Å and H···N = 1.57(3) Å. In all three molecular complexes, the asymmetry in the hydrogen bond bridge is such that the donor side belongs to the same side of the intermolecular interactions between the DMANH$^+$ and its environment along the hydrogen bonding direction (*Figure 5-35*).

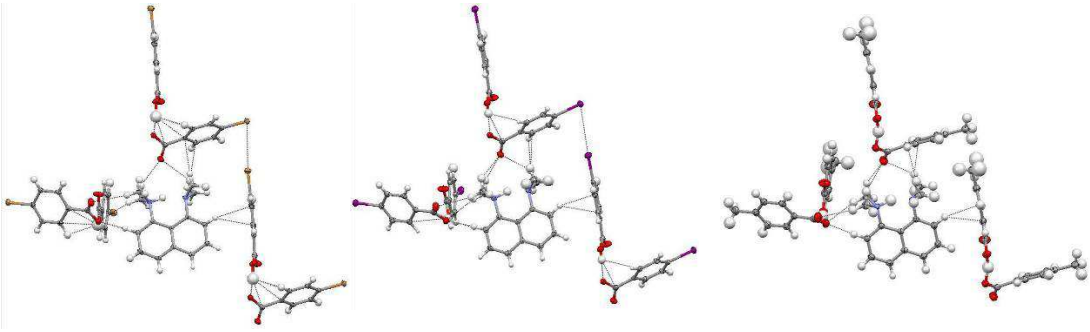

Figure 5-35. The intermolecular interactions along the N–H···N hydrogen bond direction in the three isomorphous complexes DMAN :4BBA (left), DMAN :4IBA (centre) and DMAN 4TOLA (right) complexes.

A similar effect appears in the C–N bond length as well, showing a longer bond length on the donor side of the very asymmetric N–H···N bond, as in the other two complexes (*Table 5-1*).

This result, together with the results from DMAN : 4OHBA, where two different N–H···N HBs have been compared within the same complex, could be an indication that the main reason for the asymmetry of the hydrogen atom electron density across the series of DMAN complexes is the local weaker interactions within the molecular complexes.

The hydrogen atom in the intermolecular hydrogen bond has a very large isotropic thermal parameter in all three isomorphs, with rather noisy difference Fourier maps; it will therefore not be discussed further.

5.3.3 DMAN : 3-nitrobenzoic acid (1:2)

The DMAN : 3NBA molecular complex co-crystallises in the same ratio as most of the halogen-substituted benzoic acid : DMAN complexes and shares the similarity of the molecular building blocks, showing the protonated $DMANH^+$ and the $DIMER^-$ unit of the benzoic acids connected through a single charge-assisted SSHB.

The unit cell (Z=8) contains 8 $DMANH^+$ and 8 3NBA $DIMER^-$s and the assembly of the structure from the building units is very different from those of the the halogen-substituted benzoic acid : DMAN complexes. By introducing into the complex a hydrogen bond acceptor with the nitro group, the 3NBA $DIMER^-$s are connected to each other in a side-by-side fashion by a single C–H···O weak hydrogen bond with a length of 3.305(3) Å between the oxygen atom of the nitro group and a hydrogen of the benzene ring along the crystallographic *b*-axis, and through displaced π···π stacking of the benzene ring along the crystallographic *a*-axis with a length of ~3.46 Å between the two closest π bonds (*Figure 5-36*).

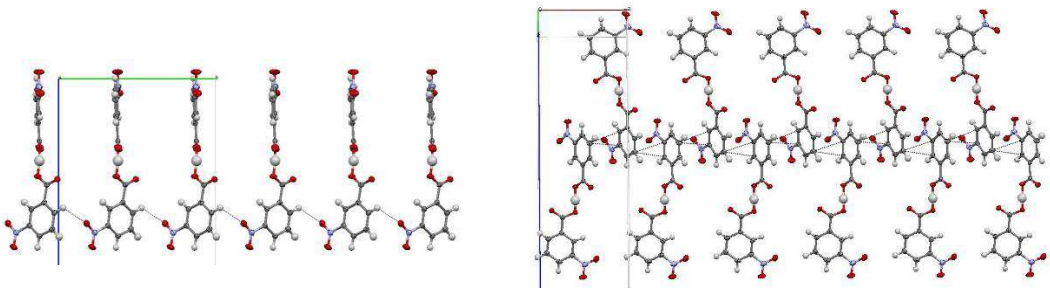

Figure 5-36. *The 3NBA DIMER–s connected through the single C–H···O weak hydrogen bond along the crystallographic b-axis (left) and through displaced π···π stacking along the a-axis (right), in the molecular complex of DMAN : 3NBA.*

Each $DMANH^+$ molecule is connected to six 3NBA $DIMER^-$s. The relative position of the methyl groups of the $DMANH^+$ molecules and the carboxyl groups of the $DIMER^-$s is very different from that found in the other 1:2 DMAN : substituted benzoic acid complexes. Four $DIMER^-$s are connected through intermolecular C–H···O weak hydrogen bonds between their carboxyl group and the $DMANH^+$ methyl groups, with distances between 3.097(3) Å and 3.422(3) Å and a C-H···π weak hydrogen bond with a length of ~3.92 Å, surrounding the $DMANH^+$ molecule (*Figure 5-37 right*). Two further $DIMER^-$s are above the methyl groups of the $DMANH^+$, one connected through C–H···O weak hydrogen bonds with length of 3.481(3) Å, contributing to the linking of the chain formed by the $DIMER^-$s, while the other is connected through a C–H···π weak HB (*Figure 5-37 left*).

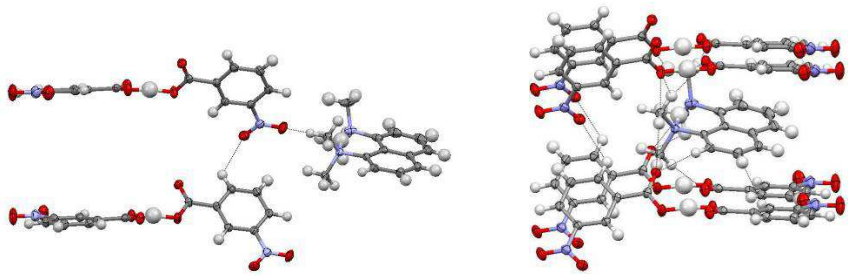

Figure 5-37. Short contacts between the methyl groups of the $DMANH^+$ and the 3NBA $DIMER^-$s; two above the $DMANH^+$ molecules methyl group (left) and four surrounding it (right).

The $DMANH^+$ molecules are connected to a further $DIMER^-$ through a C–H···O weak HB with a length of 3.334(3) Å (*Figure 5-38, left*). There are C–H···π weak HBs between the $DMANH^+$ molecules with lengths between ~3.72 Å and ~3.88 Å llinking the $DMANH^+$ molecules side by side through the surrounding $DIMER^-$s (*Figure 5-38, right*).

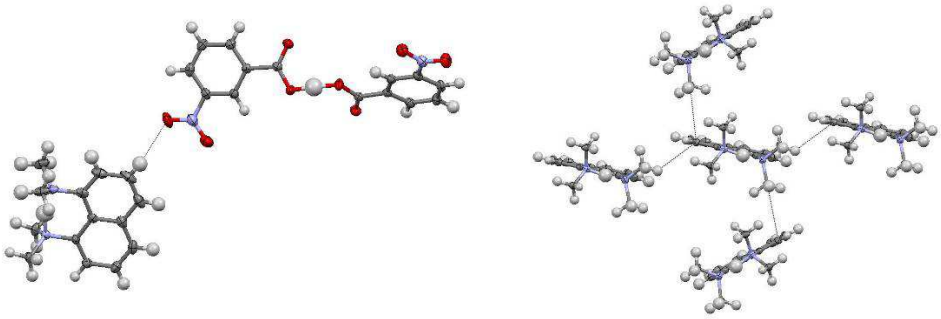

Figure 5-38. C–H···O interaction between the $DIMER^-$ below the $DMANH^+$ (left) and C–H···π weak HBs between the $DMANH^+$ molecules.

The two $DIMER^-$s connected from above the methyl group of the $DMANH^+$ molecule the one below the $DMANH^+$ moleucule, play the linking role between the $DMANH^+$ molecules surrounded by the $DIMER^-$s, forming the structure as whole (*Figure 5-39*).

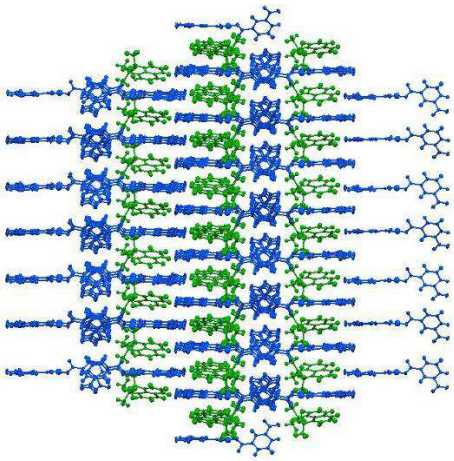

Figure 5-39. The structure of the DMAN : 3NBA molecular complex as a whole showing the $DMANH^+$ (green) surrounded by the 3NBA $DIMER^-$s (blue), linked together through the C–H···O intermolecular interactions between the $DIMER^-$s.

The charge assisted SSHB forming the 3NBA DIMER$^-$ has a length of 2.462(2) Å with asymmetric hydrogen bonding, O–H = 1.16(3) Å and H····O = 1.30(3) Å. The intramolecular hydrogen bond bridge, with N···N distance of 2.555(2) Å, is also asymmetric with N–H = 1.22(3) Å and H····N = 1.37(3) Å. The C–N bond lengths show no difference between the donor and acceptor side, but as the N–H···N bond is quite symmetric, this is not surprising (*Table 5-1*). There is no significant difference between the C–O and the C=O bond lengths in the two carboxyl groups of the DIMER$^-$ on the donor and acceptor side of the O–H···O HB (*Table 5-9*), but again neutron diffraction data would be required for further discussion. The thermal parameters of both hydrogen-bonded hydrogen atoms are larger than those of the other hydrogen atoms within the structure and a further discussion of the bonding has not been undertaken, in the absence of neutron diffraction data. There are also no further nitro-substituted benzoic acid : DMAN complexes yet available for comparison.

5.4 Conclusions

In this chapter eight non-halogen substituted benzoic acids complexes with DMAN have been presented. By introducing a hydrogen bond donor substituent in the molecular complex in the form of the hydroxyl-substituted benzoic acid, the bonding motif of the DIMER$^-$ connected through a single charge-assisted SSHB is changed compared to the halogen substituted benzoic acid DMAN complexes (Chapter 4). Instead, the deprotonated 3OHBA$^-$ is stabilised through a hydrogen bond between the deprotonated carboxyl group and the hydroxyl group of the next 3OHBA$^-$ molecules, however, this hydrogen bond is longer than those charge assisted SSHBs found in the DIMER$^-$s. The different bonding motif also changes the co-crystallisation ratio and the packing of the structure as a whole with the inclusion of a water molecule. In the 4OHBA complex, there are two different protonated molecules, which give a greater insight into the possible source of the influence causing the discrepancy of the hydrogen atoms electron distribution across the series of DMAN and benzoic acid complexes.

With two additional hydrogen bond donors introduced on the benzoic acid (dihydroxy-substituted benzoic acids) the hydrogen bonding motifs show different behaviour in all three cases. While in the case of the 24DOHBA : DMAN complex the hydrogen bonding of the deprotonated $24DOHBA^-$ is similar to that found in the hydroxy-substituted benzoic acid and DMAN complexes, it has no water in the structure. As a consequence it also shows very different packing. The comparison of variable temperature neutron and X-ray diffraction data collected on the DMAN : 26DOHBA complex shows that there are cases where the electron density might show an elongation along the hydrogen bond but the collection of neutron diffraction data is still essential to reveal any anomalous behaviour in the nature of the hydrogen bond.

The two methyl-substituted benzoic acid molecular complexes show similar behaviour and bonding motifs to those found in the majority of the DMAN and halogen-substituted benzoic acids with a 1:2 co-crystallisation ratio. The benzoic acids are connected through a single charge-assisted SSHB and a carboxyl group positioned above the $DMANH^+$, connecting them together through C–H···O weak hydrogen bonds. The DMAN : 4TOLA complex is isomorphous with the DMAN : 4BBA and DMAN : 4IBA molecular complexes, suggesting that the cause of the bending of the $DIMER^-$ might be the due to the size and position of the substituent of the benzoic acid rather than the halogen-halogen interactions. The very asymmetric nature of the N–H···N intramolecular HB of the DMAN in all three molecular complexes, also suggests that the asymmetry appearing in the hydrogen atom positions within the hydrogen bonds might be due to the weaker interactions within the complexes.

The $DIMER^-$ is also present in the structure of the DMAN : 3NBA molecular complex with the 1:2 co-crystallisation ratio, however, the introduction of a hydrogen acceptor group in the complex changes the overall packing of the structure.

The relation between the very asymmetric N–H···N bond and the C–N bond length discussed in the previous chapter (Chapter 4) shows the same behaviour in the molecular complexes presented in this chapter, showing a longer length of

the C–N bond at the donor side of the N–H···N intramolecular HB of the protonated $DMANH^+$. The difference appearing between the deprotonated carboxyl groups C–O and C=O bond lengths become less distinguishable where the carboxyl group is involved in a longer HB than the charge-assisted SSHBs seen between the $DIMER^-$s of the substituted benzoic acids.

Chapter 6

6. Molecular complexes of DMAN with other organic acids

Experimental

(1:1:2) DMAN : oxalic acid (OA) dihydrate: 1:1 molar ratio of DMAN and OA were dissolved in acetonitrile and evaporated at room temperature, slowing the evaporation by closing the vial with a small pierced lid. After the evaporation of the solvent, pale purple blocks were formed. Single crystal X-ray diffraction data were collected on a Bruker Nonius Kappa CCD diffractometer at 150K (*Table 6-1*). The data were solved with SHELXS97 and refined with SHELXL97, within the WinGX package.

(1:1) DMAN : chloranilic acid (ClA): 1:1 molar ratio of DMAN and ClA were dissolved in a 1:1 mixture of acetonitrile and methanol and evaporated at constant temperature of 4˚C, slowing the evaporation by closing the vial with a small pierced lid. After the evaporation of the solvent, dark red blocks were formed. Single crystal X-ray diffraction data were collected on a Bruker Nonius Kappa CCD diffractometer at 100K (*Table 6-1*). The data were solved with SIR-92[164] and refined with SHELXL97, within the WinGX package.

(2:1:2) DMAN : chloranilic acid (ClA) dihydrate: 1:1 molar ratio of DMAN and ClA were dissolved in methanol and evaporated at constant temperature of 4˚C, slowing the evaporation by closing the vial with a small pierced lid. After the evaporation of the solvent, pale red blocks were formed. Single crystal X-ray diffraction data were collected on a Bruker Nonius Kappa CCD diffractometer at 100K (*Table 6-1*). The data were solved with SHELXS97 and refined with SHELXL97, within the WinGX package.

(1:1) DMAN : bromanilic acid (BrA): 1:1 molar ratio of DMAN and BrA were dissolved in methanol and evaporated at constant temperature of 30˚C, slowing the evaporation by closing the vial with a small pierced lid. After the evaporation of the solvent, purple-red blocks were formed. Single crystal X-ray

diffraction data were collected on a Rigaku R-AXIS/RAPID diffractometer at 100K (*Table 6-1*). The data were solved with SHELXS97 and refined with SHELXL97, within the WinGX package.

Table 6-1. X-ray data refinement details of DMAN : OA dihydrate, DMAN : ClA, DMAN : ClA dihydrate, DMAN :BrA.

Compound	1:1:2 DMAN : OA dihydrate	1:1 DMAN : ClA	2:1:2 DMAN : ClA dihydrate	1:1 DMAN : BrA
Diffractometer	Nonius Kappa CCD	Nonius Kappa CCD	Nonius Kappa CCD	Rigaku R-Axis RAPID
Formula	C_{16} H_{24} N_2 O_6	C_{20} H_{20} Cl_2 N_2 O4	C_{34} H_{42} Cl_2 N_4 O_6	C_{20} H_{20} Br_2 N_2 O_4
Molecular weight / gmol^{-1}	340.37	423.28	673.625	512.2
Temperature (K)	150	100	100	100
Space Group	$P2_1/n$	$P\bar{1}$	$P\bar{1}$	$P\bar{1}$
a (Å)	9.9814(2)	9.7509(3)	9.3088(3)	9.8207(12)
b (Å)	9.2715(2)	10.9332(3)	9.3320(3)	11.0159(17)
c (Å)	18.4258(4)	11.0068(3)	9.5855(2)	11.1360(16)
α (°)	90	111.164(2)	104.681(2)	110.758(4)
β (°)	100.7950(10)	98.2410(10)	98.4570(10)	113.102(4)
γ (°)	90	113.7750(10)	92.9150(10)	99.255(4)
Volume (Å^3)	1674.99(6)	942.29(5)	793.36(4)	971.2(2)
Z	4	2	1	2
***θ* range/°**	2.17 – 27.48	2.11 – 30.05	2.22 – 30	3.03 – 27.48
Completeness (%)	99.8	99.9	99.8	99.2
Reflections Collected	31888	24506	24503	22698
Independent	3819	5513	4619	4416
Refln (obs.I>2theta(I))	3234	4291	3779	3926
R_{int}	0.0505	0.0439	0.037	0.0223
Data/Rest./Param.	3819/0/313	5513/0/333	4619/0/292	4416/0/333
GooF on F^2	1.042	0.995	0.958	1.047
R_1 (Observed)	0.0327	0.0316	0.0358	0.0223
R_1 (all)	0.0409	0.0466	0.0479	0.0275
wR_2 (all)	0.0872	0.0821	0.1028	0.0517
***ρ* (max / min) / e-Å^{-3}**	0.209 / -0.182	0.478 / -0.232	0.52 / -0.227	0.468 / -0.317
RMS / eÅ^{-3}	0.036	0.052	0.063	0.07

6.1 DMAN : oxalic acid dihydrate (1:1:2)

The structure of oxalic acid (OA) has been extensively studied and five different crystal forms have been published, including two anhydrous (α,β)[165] one dihydrate form[166] and two sesquihydrates produced serendipitously from co-crystallisations[167]. In many cases where OA is present in co-crystals[168-171], the OA appears in one protonated and one deprotonated form with a single hydrogen bond between the OA molecules. It might therefore be expected that upon co-crystallisation with DMAN this single hydrogen bonded OA-OA$^-$ dimer motif should

be present. However, the co-crystallisation of DMAN and OA produces a 1:1 dihydrate complex, and although the DMAN acts to deprotonate one of the carboxylic groups on the OA molecules as expected, the presence of the water molecules disrupts the anticipated hydrogen bonding scheme, with the OA-OA^- dimer not formed in this case.

In addition, the structure of the molecular complex does not show similarities to that of the dihydrate form of OA itself, since in this case the deprotonation of the OA by the DMAN changes the hydrogen bond motif as the OA molecule becomes charged. The deprotonated carboxylate group of the oxalic acid is connected through intermolecular C–H···O weak HBs to the methyl groups of the $DMANH^+$ molecule (*Figure 6-1*). These C–H···O interactions have lengths between 3.199(2) Å and 3.552(1) Å.

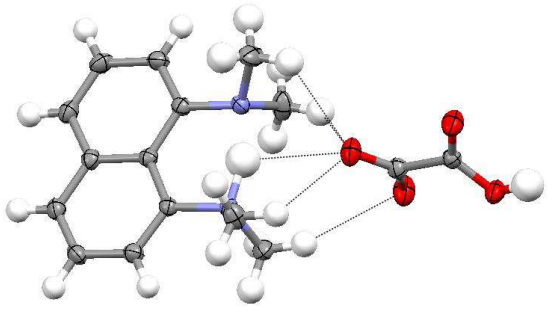

Figure 6-1. Intermolecular interactions between the deprotonated carboxylate group of the OA and the methyl groups of the $DMANH^+$ in the molecular complex of DMAN : OA dihydrate.

The OA^- molecules are connected to each other through intermolecular interactions between themselves and the water molecules forming a ribbon within the structure (Figure 6-2). There are two water molecules connecting two OA^- molecules together through O–H···O hydrogen bonds. One water molecule connects two OA^- molecules through the deprotonated oxygen atom of the carboxylate group of one molecule and the O–H of the carboxyl group of the other OA^- molecules with lengths of 2.661(1) Å and 2.538(1) Å, respectively (*Figure 6-2, marked in blue*). The other water molecule connects the carbonyl oxygen atom of the carboxyl group with an O–H···O hydrogen bond length of

2.905(1) Å and the other oxygen of the carboxylate group with an O–H···O bond length of 2.732(1) Å (*Figure 6-2, marked in green*).

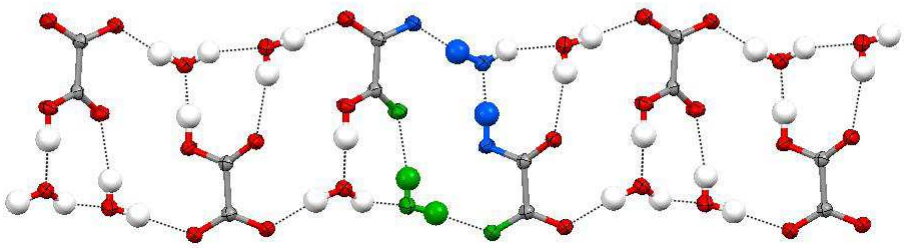

Figure 6-2. Ribbon formed from the OA^- and water molecules in the molecular complex of DMAN : OA dihydrate, showing the intermolecular interactions.

The chains of OA^- and water molecules are surrounded by the $DMANH^+$ molecules connected above and below through intermolecular interactions between the methyl groups of $DMANH^+$ and the deprotonated carboxyl group of the OA^- and on the sides through further C–H···O weak hydrogen bonds with lengths between 3.364(2) Å and 3.619(2) Å. There is a stacking arrangement of the $DMANH^+$ clearly visible on *Figure 6-3*.

The intramolecular N–H···N hydrogen bond within the $DMANH^+$ molecule, of length N···N = 2.581(1) Å, is asymmetric with N–H = 1.19(2) Å and H···N = 1.43(2) Å, with a longer C–N bond length on the donor and shorter on the acceptor side of the hydrogen bond bridge with lengths of 1.460(1) Å and 1.473(1) Å, respectively. The hydrogen atom has a large isotropic thermal parameter with the corresponding electron density elongated along the hydrogen bridge from the difference Fourier map, as observed frequently in such systems. The shortest O–H···O hydrogen bond surprisingly is between the carboxyl group of the OA^- molecule and the oxygen atom of the water molecule, which is not charge assisted and is just above distance limit normally expected for a SSHB, with a length of O···O = 2.538(1) Å. The hydrogen bond is very asymmetric, with O–H = 0.97(2) Å and H···O = 1.57(2) Å, with similarly large isotropic thermal parameters for the hydrogen atom as observed for the intramolecular bridge.

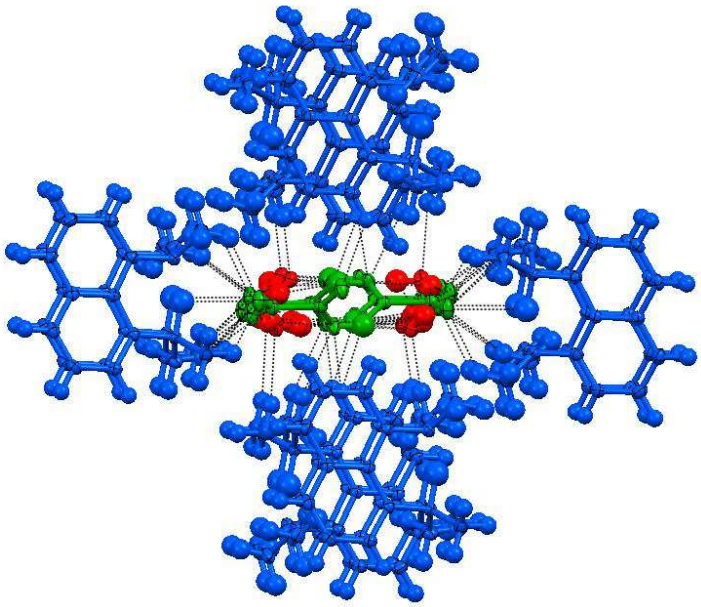

Figure 6-3. The ribbon of the OA^- (green) and water molecules (red) in the molecular complex of DMAN : OA dihydrate are surrounded by the $DMANH^+$ molecules (blue), linked by weak intermolecular interactions.

6.2 DMAN : chloranilic Acid (1:1) and DMAN : chloranilic acid dihydrate (2:1:2)

The crystal structure of the hydrated structure of the DMAN : ClA complex was previously reported in 1991 by Kanters et al., highlighting the asymmetric N–H···N hydrogen bonding within the $DMANH^+$ and the change of this asymmetric hydrogen position as a function of temperature[172]. These observations were made based on measurements of the donor acceptor distances from X-ray diffraction data. The structure has been re-determined in this work, with the aim of enabling comparison with the anhydrous form and related bromanilic acid complexes. All geometry values quoted below are from the present re-determination of the structure.

The chloranilic acid is in the doubly deprotonated form ClA^{2-}, with the asymmetric unit containing one protonated $DMANH^+$, a half of the ClA^{2-} and one water molecule. The N–H···N intramolecular hydrogen bond is asymmetric with N···N = 2590(1) Å, N–H = 1.08(2) Å and H···N = 1.58(2) Å. The ClA^{2-} molecules

are connected through two water molecules to the next ClA^{2-} molecule by O–H···O intermolecular hydrogen bonds (*Figure 6-4*). As can be seen, from one side of the water molecules there is a single O–H···O hydrogen bond to the ClA^{2-} molecule with a length of 2.965(1) Å while the other side is connected through a bifurcated hydrogen bond with lengths of 2.917(1) Å and 3.181(1) Å. On the side linked through the single HB, there is a weak O–H···Cl weak hydrogen bond with a O···Cl distance of 3.321(1) Å.

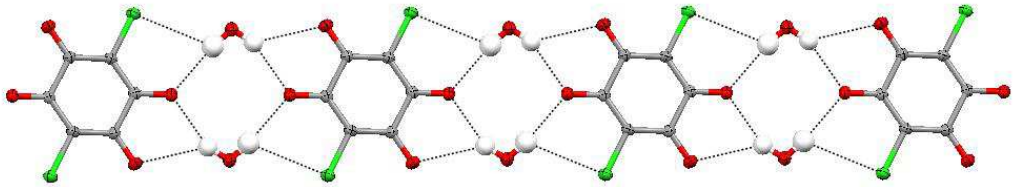

Figure 6-4. Chain formed of ClA^{2-} molecules connected through water molecules in the molecular complex of DMAN : ClA dihydrate

The chain formed of ClA^{2-} and water molecules is surrounded by DMANH+ molecules. The chain is connected to the $DMANH^{+}$ through C–H···O weak hydrogen bonds between the methyl group of the $DMANH^{+}$ and the oxygen atoms of the ClA^{2-} with lengths of 3.083(2) Å and 3.171(2) Å and also between the naphthalene ring and the oxygen atom with lengths of 3.320(1) Å and 3.392(1) Å. There are further weak C–H···π weak hydrogen bond involving the methyl groups of the DMANH+ molecules and the CA^{2-} molecule with a length of ~3.85 Å and from the naphthalene ring C–H to the ClA^{2-} with distances of ~3.45 Å. These interactions create a set of $DMANH^{+}$ molecules surrounding the chain (*Figure 6-5*).

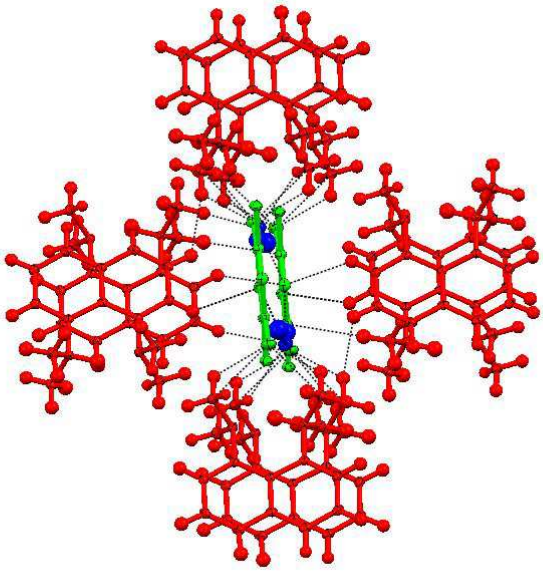

Figure 6-5. The chain of ClA^{2-} (green) and water molecules (blue) surrounded by the $DMANH^{+}$ molecules (red). The stacking of the DMAN molecules is also evident.

The hydrogen bonding motif connecting the two ClA^{2-} molecules through a link of two water molecules is similar to the motif that links the benzoic acid molecules in the DMAN : 3FBA hydrate complex (Chapter 4) (*Figure 6-6*).

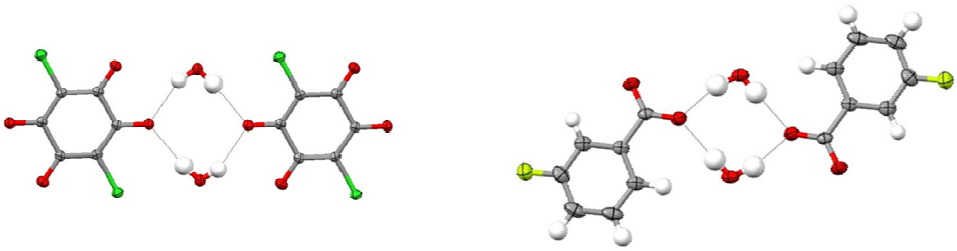

Figure 6-6. The ClA^{2-} (left) and $3FB^{-}$ molecules connected through a similar hydrogen bonded linkage involving two water molecules in their molecular complexes with DMAN.

It is of interest that the bonding motif linking the two ClA^{2-} and $3FBA^{-}$ through a double water link shows similarities given that the ClA^{2-} molecule has two potential hydrogen bond acceptors, resulting in the bifurcated hydrogen bonding in the structure. This is in contrast to the $3FBA^{-}$, which has one potential

hydrogen bond acceptor and so in this case, the two $3FBA^-$ molecules are connected through two single hydrogen bonds with the water molecules. This consistency of motif is worthy of note as also is the fact that its nature depends on the deprotonation of the acid molecules involved by the $DMANH^+$.

As discussed in Chapter 4, an anhydrous 2:1 molecular complex of 3FBA with DMAN, where just one of the two 3FBA molecules is deprotonated by the DMAN, and these form a $DIMER^-$ connected through a single charge-assisted hydrogen bond has also been characterised. From the crystallisations setup between DMAN and ClA, an anhydrous form of DMAN : ClA has also been obtained. In this 1:1 complex, the ClA is singly deprotonated by the DMAN and forms a $DIMER^{2-}$ unit with the two ClA^- molecules connected through a symmetry-related pair of O–H···O hydrogen bonds (*Figure 6-7*).

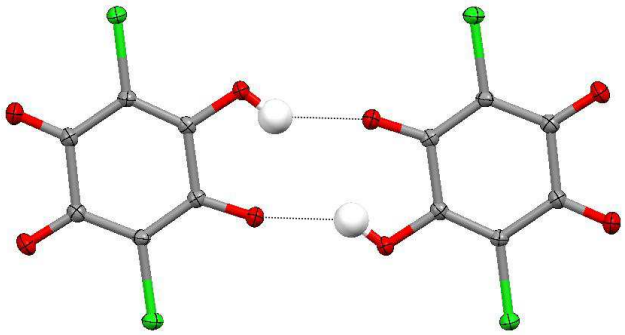

Figure 6-7. $DIMER^{2-}$ formed from the ClA^- connected through two O–H···O hydrogen bonds in the molecular complex of the DMAN : ClA.

The hydrogen bonds have a length of 2.748(1) Å with O–H = 0.88(2) Å and H···O = 1.98(2) Å. The thermal parameters of the hydrogen atom within the intermolecular O–H···O, as well as that in the intramolecular N–H···N hydrogen bond within the $DMANH^+$ is very large compared to those of the other hydrogen atoms in the structure. In the case of the intermolecular HB, the difference Fourier map shows a slightly larger spread of electron density in the hydrogen atom location, while in the case of the hydrogen within the N–H···N bridging bond (N···N = 2.610(2) Å) in the $DMANH^+$, the electron density shows a small elongation along the bonding direction, in an asymmetric position (*Figure 6-8*).

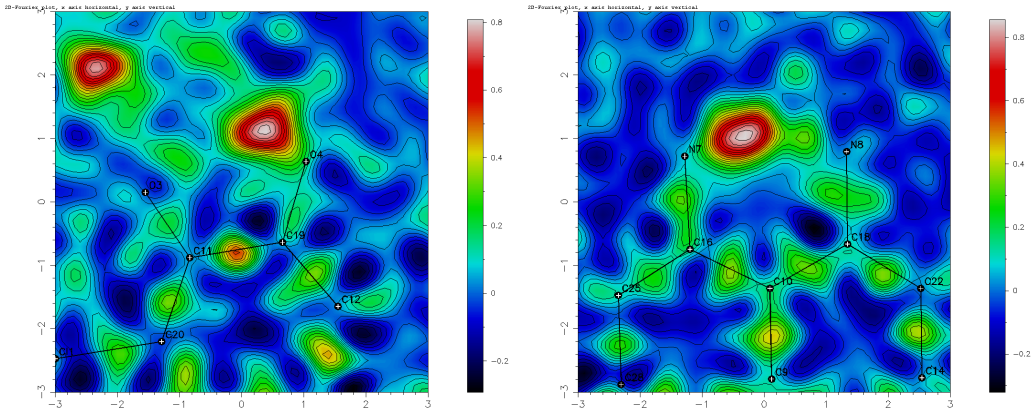

Figure 6-8. The difference Fourier map of the hydrogen atoms electron density within the intermolecular O–H···O(left) and intramolecular N–H···N (right) HB.

This is in agreement with the determined distances, N–H = 1.02(2) Å and H···N = 1.64(2) Å, from the X-ray diffraction measurements. The $DIMER^{2-}$ has no intermolecular interaction with other $DIMER^{2-}$ units and is surrounded by $DMANH^{+}$ molecules connected through a series of intermolecular interactions. The unprotonated sides of the $DIMER^{2-}$ are connected through C–H···O interactions to the methyl groups of the $DMANH^{+}$ molecule with lengths between 3.110(2) Å and 3.367(2) Å. There are two further halogen interactions between the chlorine atom and the naphthalene group with Cl···π distances of ~3.37 Å on one side and ~3.49 on the other and the chloranilic acid molecules show a displaced stacking arrangement and pairs of $DMANH^{+}$ molecules are held together through a C–H···π weak hydrogen bond with a distance ~3.69 Å (*Figure 6-9*).

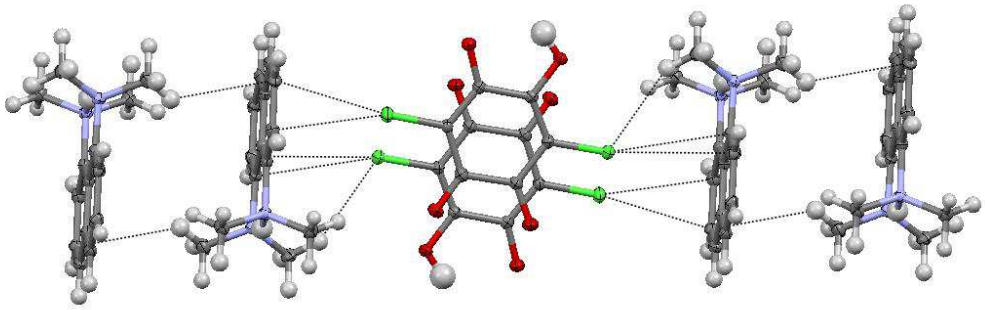

Figure 6-9. Intermolecular Cl···π between the ClA^{-} and $DMANH^{+}$ molecules and C–H···π interactions between the pairs of $DMANH^{+}$ molecules.

The packing as whole shows a stacking arrangement of pairs of $DMANH^+$ with a perpendicular position to the infinite stack of ClA^- molecules (*Figure 6-10*).

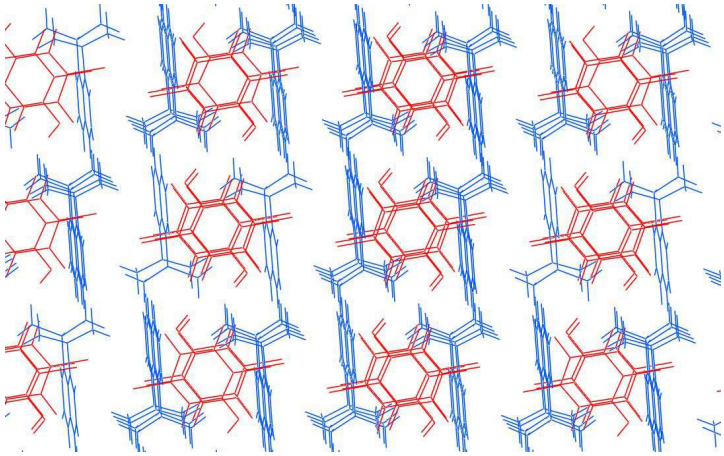

Figure 6-10. The packing as a whole with the stacked arrangement of the $DMANH^+$ and the ClA^- molecules.

In both the dihydrate and anhydrous complexes of DMAN : Chloranilic acid, the donor side methyl groups of $DMANH^+$ molecule are involved in a higher number and relatively stronger intermolecular interactions along the direction of the hydrogen bridge (*Figure 6-11*), discussed below.

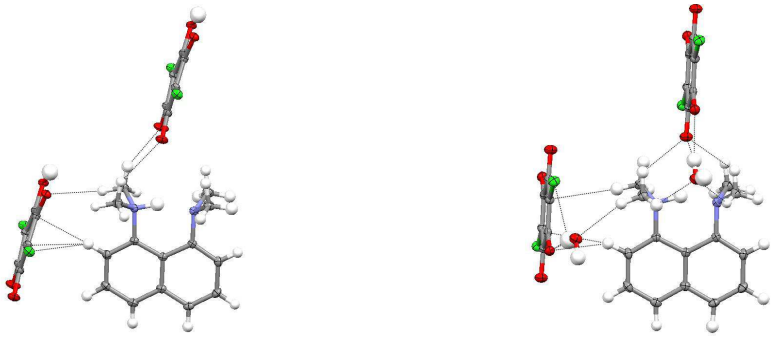

Figure 6-11. Intramolecular interactions between the $DMANH^+$ and its environment along the N–H···N hydrogen bridge in the anhydrous (left) and hydrated (right) form of DMAN : chloranilic acid complex.

DMAN : CA (1:1) (*Figure 6-11, left*): The proton side along the N–H···N HB is connected through two C–H···O interactions between the oxygen from the ClA^-

and the methyl group of the $DMANH^+$ with lengths of 3.110(2) Å and 3.367(2) Å, and a C–H···O weak hydrogen bond between the oxygen of the other ClA^- molecule and the methyl group with a length of 3.429(2) Å. The acceptor side has no significant intermolecular interaction along the N–H···N HB. The N–C bond lengths are 1.459(2) Å on the donor side and 1.470(2) Å on the acceptor side.

DMAN : CA dihydrate (2:1:2) (*Figure 6-11, right*): The proton side of the methyl group is involved in C–H···O weak hydrogen bonds along the N–H···N hydrogen bridge with the ClA^{2-} positioned above the methyl group with a length of 3.083(2) Å and the water molecule with a length of 3.390(2) Å. There is a further C–H···O weak hydrogen bond with the water molecule positioned on the side of the methyl group with a length of 3.541(1) Å, and a C–H···π interaction of the ClA^{2-} also positioned above on the side of methyl group, with a length of ~3.85 Å. On the other hand, the methyl groups on the acceptor side of the N–H··N are involved in just two C–H···O weak hydrogen bonds along the hydrogen bridge, with the oxygen atom of the ClA^{2-} and the water molecule, with lengths of 3.171(2) Å and 3.371(2) Å, respectively. The N–C bond lengths are 1.461(2) on the donor side and 1.475(2) on the acceptor side.

A comparison of these intermolecular interactions with those of the DMAN : 4OHBA complexes suggests that the number of intermolecular interactions might influence the electron density distribution of the intramolecular N–H···N hydrogen bond in these DMAN complexes. The C–N bond lengths are longer in both cases on the donor than on the acceptor side of the N–H···N hydrogen bond as in the other discussed cases where the hydrogen occupies a similar asymmetric position.

6.3 DMAN : bromanilic acid (1:1)

The molecular complex of DMAN : BrA is isostructural with the 1:1 anhydrous molecular complex of DMAN : ClA. The overlay of the asymmetric unit shows a very good agreement between the structures (*Figure 6-12*).

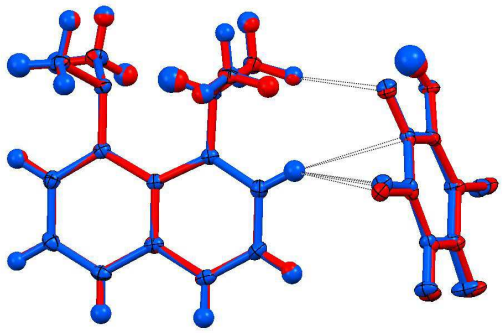

Figure 6-12. Overlay of the asymmetric unit of the molecular complexes of DMAN : BrA (red) and DMAN : ClA (blue).

The unit cell is slightly larger in the case of the DMAN : BrA as expected from the larger volume of the bromine atom. The longer C–Br bond length also introduces a slight shortening of the C–halogen···π intermolecular interactions present in both structures. These are between the BrA^- and the $DMANH^+$ molecules with Br···π distances of ~3.44 Å on one side and ~3.47 Å on the other. However, the details of whether a halogen interaction is significant or not is less important in this case, where it is more significant that the two structures adopt the same packing arrangement.

The N–H···N intramolecular hydrogen bond has the same length in the two complexes within the standard uncertainties, with a N···N distance of 2.612(2) in the BrA complex, but shows an even more asymmetric position from the X-ray diffraction measurement, with N–H = 0.89(3) Å and H···N = 1.77(3) Å, although in the presence of the heavy atom (bromine) in the structure these hydrogen bond length measurements are less reliable. The intermolecular interactions along the hydrogen bridge also show a more asymmetric nature. There are two C–H···O weak hydrogen bonds on the donor side between an oxygen atom of the BrA^- (positioned above the $DMANH^+$) and methyl groups with lengths of 3.106(3) Å and 3.316(3) Å and a C–H···O interaction between the other BrA^- molecule (positioned on the side of the $DMANH^+$) with a length of 3.441(3) Å. This could lead to the more asymmetric position of the hydrogen atom within the hydrogen bridge and it also show the difference between the N-C bonds with a distance of 1.472(3) Å on the donor and 1.462(3) Å on the acceptor side of the

N–H···N bridge. The difference Fourier map of the electron density in the region of the hydrogen atom within the N–H···N hydrogen bridge in the DMAN : BrA complex shows a similar slightly elongated contour as in the case of DMAN : ClA (*Figure 6-13*).

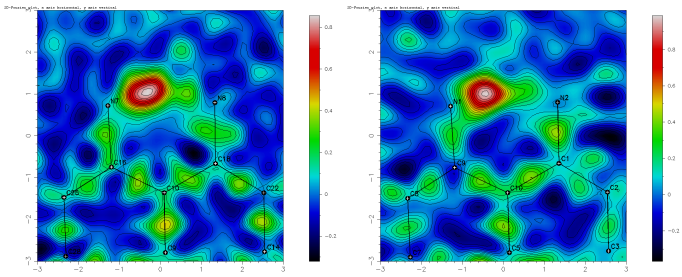

Figure 6-13. Difference Fourier map of the electron density in the region of the hydrogen atom within the N–H···N intramolecular hydrogen bond in the molecular complexes of DMAN : ClA (left) and DMAN : BrA (right).

The intermolecular hydrogen bond is slightly shorter in the case of the DMAN : BrA complex, with a length of 2.719(2) Å. The D–H and H···A distances are more different in their lengths, with O–H = 0.77(2) Å and H···O = 2.03(3) Å, but this difference is partly a result of the difference in the O-H-O bond angle, which is 149(3)˚ in DMAN : BrA and 144(2)˚ in DMAN : ClA.

The differences in the intermolecular interactions in the two complexes appears more noticeably in the halogen bonding; since the bromine atom is larger the structure is slightly expanded in the C–Br direction (*Figure 6-14*).

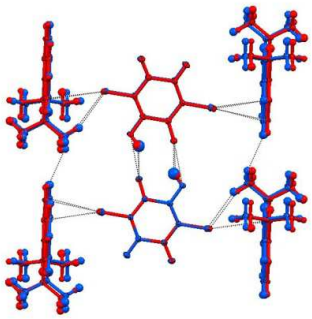

Figure 6-14. Overlay of the DMAN : BrA (red) and DMAN : ClA (blue) complexes, generated in the best fit plane of the ClA and BrA molecules.

A range of crystallisations have been set up in attempts to obtain the hydrated form of the DMAN : BrA complex, but none of the experiments set up have to date led to a successful crystallisation of this complex.

6.4 Conclusions

The four different molecular complexes of DMAN presented in this chapter complement the series of the substituted benzoic acid and DMAN complexes presented in the previous two chapters. The DMAN molecule deprotonates the organic acids in all four cases, as found in the substituted benzoic acid DMAN complexes, and forms an intramolecular N–H···N hydrogen bond. The comparison of hydrated and anhydrous forms of DMAN : ClA and the isomporhous structures of DMAN : BrA and the anhydrous DMAN :ClA complexes, provided another good opportunity to investigate the possible influence of the environment on the hydrogen atoms electron density distribution within the N–H···N hydrogen bond. The donor side in all three molecular complexes is on the side of the nitrogen atom where the methyl groups are involved a higher number of intermolecular interactions. The correlation between the N–C bond length in respect to the location of the donor side within the N–H···N asymmetric hydrogen bonds, shown in the substituted benzoic acid and DMAN complexes, shows similar conclusions here as well.

Chapter 7

7. Tuning proton behaviour in a ternary molecular complex

7.1 Introduction

The behaviour of the hydrogen atom within short, strong hydrogen bonds has been discussed in detail in a range of examples, as presented in Chapter 1. These examples include situations where the hydrogen atom behaviour changes significantly as a function of temperature, or sometimes of its environment in different molecular complexes, in which a full description of the hydrogen atom parameters often requires the use of neutron diffraction. These previous findings prompted the variable temperature examination of some of the molecular complex structures studied in earlier chapters, though there have been no significant examples found of such structure evolution with temperature in those. In this Chapter the structure of a rare example of a ternary molecular complex, of 3,5-dinitrobenzoic acid (35DNBA), 4-dimethylaminobenzoic acid(4DABA) and 4,4'-bipyridine (BIPY) will be presented. This complex has been studied with both X-ray and neutron diffraction methods, and is a good example of the observation and full characterisation of anomalous behaviour of a hydrogen atom within a hydrogen bond. This work has recently been published[173]. As a part of the work, I have carried out the experimental work, including crystal growth, variable X-ray and neutron diffraction data collection and structure solution as well as I contributed with a structural description report.

This investigation was part of a series of determinations of structures involving the 4DABA molecule. In the crystal structure of pure 4DABA the common motif of doubly hydrogen bonded dimers is formed between the carboxylic groups. Within the hydrogen bond between the dimers, clear evidence of disorder has been observed through difference Fourier maps of the electron density[174], and found to vary as a function of temperature. When 4DABA is co-crystallised with 35DNBA the $(4DABA)_2$ dimer still exists but in this case there are no signs of hydrogen disorder within the hydrogen bonds between the dimers at any of the measured

temperatures; instead there is disorder present in the dimer formed by the 35DNBA^2 components. This was postulated as being caused by the perturbation of the local environment, such as the charge transfer interactions between the 4DABA and the 35DNBA molecules, causing the pyramidalization of the nitrogen atom in the 4DABA molecule (*Figure 7-1*).

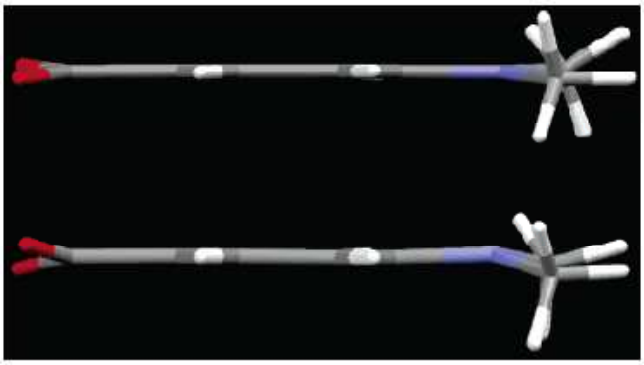

Figure 7-1. The 4DABA molecule in the native crystal structure of DABA (top) and in the molecular complex with 35DNBA. The increase in the degree of pyramidalization of nitrogen atom is clearly visible in the molecular complex with 35DNBA^2.

The ternary complex presented in the work herein represents a further perturbation of the local environment of the 4DABA molecule by introducing a third component in the molecular complex 4DABA and 35DNBA.

Ternary complexes are a less commonly studied branch of crystal engineering compared to the more easily formed binary complexes. It is also more difficult to predict the outcome of co-crystallisation experiments when ternary systems are formed[175-178], the variation of available hydrogen bonding motifs in a ternary complex have the potential significantly to modify the intermolecular interactions formed. However, in this case where the 4DABA dimer in its native crystal structure shows a very different behaviour of the hydrogen atom from that found in the molecular complex with 35DNBA, a further perturbation of the local environment could lead a better understanding of the phenomena of proton disorder in the molecular complexes.

To develop further the binary complex by introducing a third component in the molecular complex, the complementary possible intermolecular interactions have been identified between the different components. The 35DNBA is a stronger acid and thus a better hydrogen bond donor than the 4DABA, hence by introduction of a basic proton accepting molecule a selective bonding would be expected from the stronger acid to the proton acceptor site. 4,4'-bipyridine (BIPY) was chosen as being just such a good proton acceptor; the crystallisations set up resulted in the preparation of a 2:2:1 ternary complex of 4DABA : 35DNBA : BIPY, which has been studied by both X-ray and neutron diffraction methods.

7.2 Experimental data

The 4DABA, 3,5DNBA, BIPY ternary molecular complex was grown from methanol solution using the ReactArray Microvate for a programmed gradual cooling of the sample, in this way achieving a larger crystal size required for the neutron diffraction experiment in this case. The crystallization was setup with an equimolar quantity of the 4DABA (0.078 g) : 3,5DNBA (0.1 g) : BIPY (0.074 g). The components were dissolved in methanol at 50˚C and then cooled to 15˚C, decreasing the temperature by 1˚C every 90 minutes.

Figure 7-2. The two crystals mounted for the multiple crystal sample (left) and the vanadium can (right) used in the neutron diffraction experiment on SXD. Each interval on the ruler represents 1 mm.

Single crystal X-ray data were collected at 100, 200 and 300 K on a Bruker Nonius Kappa CCD diffractometer (*Table 7-1*). For the neutron experiment, a multiple single crystal sample was used to enable faster data collection in the

allocated neutron beam time. Due to uncertainties about the crystal stability under vacuum, the two crystals used in data collection were placed in a sealed Vanadium can (*Figure 7-2*). Neutron data sets were collected at four temperatures, 40, 100, 200 and 300 K at ISIS on the SXD instrument, although the 300 K data set was curtailed due to an unstable beam.

The X-ray diffraction data were solved with SHELXS97 and refined with SHELXL97 within the WinGX structure solution program suite. For the neutron diffraction data the initial atomic positions were taken from the refined X-ray diffraction structures. From these initial positions taken from the X-ray refinements, both the non-hydrogen and the hydrogen atoms were refined with anisotropic displacement parameters.

7.3 Results and discussion: structure of the ternary complex

The molecular complex of 4DABA:35DNAB:BIPY contains a dimer formed from pairs of 4DABA molecules connected through the carboxylic acid groups related to one another by an inversion centre, forming a $R_2^2(8)$ motif similarly to the dimer seen in the binary complex of 4DABA : 35DNBA. The hydrogen bond has a length of 2.652(5) Å with a O–H = 1.009(7)Å and H···O = 1.645(7) Å (neutron data, 40K). As a result of the introduction of a third component, the 35DNBA molecules no longer form a homo-dimer as in the binary complex but instead are connected though a short hydrogen bond to the nitrogen atom of the BIPY. This short hydrogen bond has a length of O···N = 2.551(3) Å, and is strongly asymmetric with O-H = 1.102(6) Å and H···N = 1.464(6) Å from the 40 K neutron data; the proton remains clearly located on the carboxylic acid group at all temperatures studied. The BIPY sits between two 35DNBA molecules, on the inversion centre located in the C–C bond linking the two pyridine rings (*Figure 7-3*).

Table 7-1. X-ray and neutron data refinement details for the ternary complex.

Compound	2:2:1 4DABA:35DNBA:BIPY			Compound	2:2:1 4DABA:35DNBA:BIPY			
Diffractometer	Nonius Kappa CCD	Nonius Kappa CCD	Nonius Kappa CCD	Diffractometer	SXD	SXD	SXD	SXD
Formula	$C_{21}H_{19}N_4O_8$	$C_{21}H_{19}N_4O_8$	$C_{21}H_{19}N_4O_8$	Formula	$C_{21}H_{19}N_4O_8$	$C_{21}H_{19}N_4O_8$	$C_{21}H_{19}N_4O_8$	$C_{21}H_{19}N_4O_8$
Molecular weight / $gmol^{-1}$	455.40	455.40	455.40	Molecular weight / $gmol^{-1}$	455.40	455.40	455.40	455.40
Temperature (K)	100	200	300	Temperature (K)	40	100	200	300
Space Group	$P\bar{1}$	$P\bar{1}$	$P\bar{1}$	Space Group	$P\bar{1}$	$P\bar{1}$	$P\bar{1}$	$P\bar{1}$
a (Å)	7.6431(3)	7.7483(3)	7.8659(3)	a (Å)	7.5996(13)	7.6442(14)	7.7483(19)	7.869(2)
b (Å)	8.6569(3)	8.6658(3)	8.6762(3)	b (Å)	8.6673(16)	8.6690(17)	8.670(2)	8.688(3)
c (Å)	15.4854(6)	15.5142(5)	15.5660(4)	c (Å)	15.484(3)	15.507(3)	15.523(4)	15.566(5)
α (°)	79.479(2)	79.804(2)	80.290(2)	α (°)	79.549(12)	79.544(12)	79.944(15)	80.49(2)
β (°)	82.732(3)	82.447(2)	81.985(2)	β (°)	82.855(12)	82.734(12)	82.471(16)	82.01(2)
γ (°)	87.277(2)	87.681(2)	88.252(2)	γ (°)	87.305(13)	87.262(14)	87.756(17)	88.30(2)
Volume ($Å^3$)	998.97(7)	1016.20(6)	1036.85(6)	Volume ($Å^3$)	994.9(3)	1002.1(3	1017.8(4)	1039.4(6)
Z	2	2	2	Z	2	2	2	2
θ range/°	2.39 -27.49	1.34 – 27.52	1.34 – 27.46	λ range (Å)	0.7 – 6.9	0.7 – 6.9	0.7 – 6.9	0.7 – 6.9
Completeness (%)	98.6	98.5	98.9	Completeness (%)	-	-	-	-
Reflections Collected	14014	14532	14987	Reflections Collected	11986	8695	5221	3283
Independent	4524	4611	4692	Independent	11986	8695	5221	3283
Refln (obs.I>2theta(I))	3794	3502	3016	Refln (obs.I>2theta(I))	9790	8695	4385	2840
R_{int}	0.0317	0.0285	0.0294	R_{int}	-	-	-	-
Data/Rest./Param.	4524/0/374	4611/0/374	4692/0/374	Data/Rest./Param.	11986/0/471	8695/0/471	5221/0/471	3283/0/471
GooF on F^2	1.045	1.017	1.02	GooF on F^2	1.337	1.866	1.347	1.634
R_1 (Observed)	0.0387	0.0439	0.0503	R_1 (Observed)	0.089	0.109	0.088	0.0971
R_1 (all)	0.0485	0.0622	0.0857	R_1 (all)	0.1031	0.109	0.1009	0.1104
wR_2 (all)	0.1096	0.134	0.1519	wR_2 (all)	0.2242	0.2721	0.2057	0.2308
ρ (max / min) / e-$Å^{-3}$	0.322 / -0.242	0.27 / -0.23	0.173 / -0193	ρ (max / min) / fm-$Å^{-3}$	3.199 / -2.854	2.475 / -2.084	1.027 / -1.103	0.794 / -0.943
RMS / e$Å^{-3}$	0.044	0.038	0.032	RMS / fm$Å^{-3}$	0.637	0.497	0.251	0.202

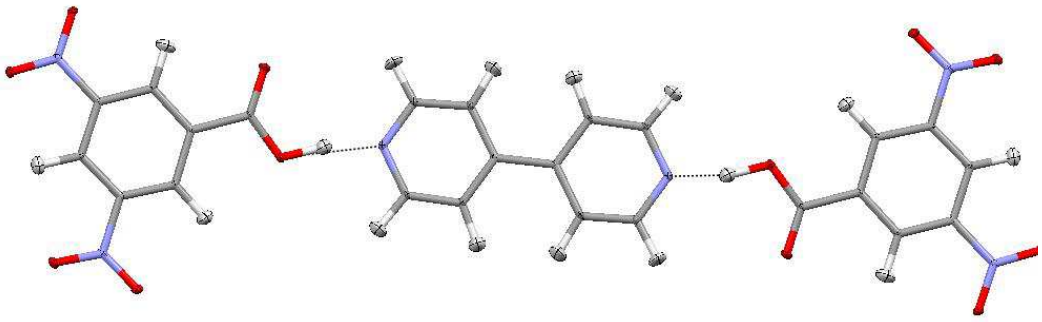

Figure 7-3. The BIPY is located on the inversion centre, between the two 35DNBA molecules in the ternary complex of 4DABA:35DNBA:BIPY (determined from the neutron, 40K data).

The 35DNBA and the BIPY molecules are almost co-planar with a ~5˚ tilt between the best planes (using all carbon atoms from the benzene and the pyridine rings, respectively) of the BIPY and 35DNBA molecules. The structure is layered, with each layer formed from all of the components of the molecular complex. The blocks of these three molecules (35DNAB-BiPY-35DNBA) are connected to each other side by side through C–H···O weak hydrogen bonds with C···O lengths between 3.366(3) Å and 3.377(3) Å (*Figure 7-4*).

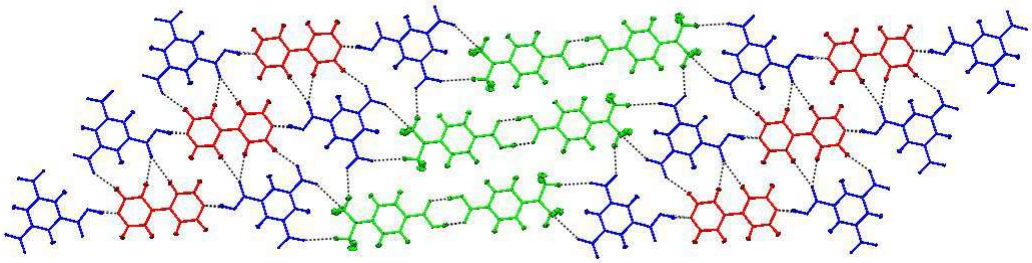

Figure 7-4. One layer of the ternary complex consisting of all three components of the complex: 4DABA (green), 35DNBA (blue) and BIPY (red).

Within the structure as a whole, the layers are positioned such that dimers of 4DABA and blocks of 35DNBA-BIPY-35DNBA are alternately stacked one above another (*Figure 7-5*). These layers are connected through C–H···O weak hydrogen bonds between the methyl groups of the 4DABA and the nitro group of the 35DNBA, with lengths between 3.219(3) Å and 3.467(3) Å, and through

C–H···π interactions between the methyl groups of 4DABA and the BIPY, of length ~3.56 Å. There are displaced π···π stacking interactions between 4DABA and 35DNBA with a distance of ~3.36 Å measured between the centroids of the aromatic rings.

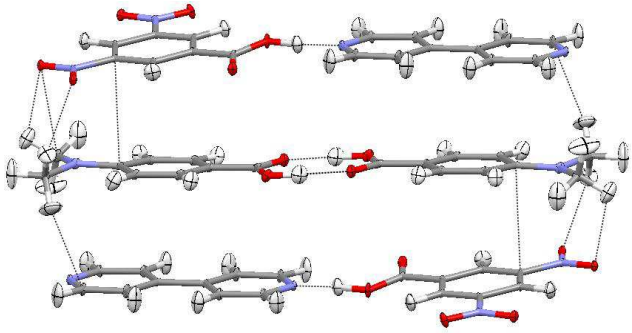

Figure 7-5. The intermolecular short contacts between the alternating layers of 4DABA dimers and 35DNBA-BIPY-35DNBA blocks.

The O–H···N hydrogen bond between the carboxyl group of the 35DNBA and the nitrogen atom from the pyridine ring does not show any significant change in length or donor-acceptor distances at any of the measured temperatures, from either neutron or from X-ray measurements. Both the isotropic thermal parameters refined from the X-ray diffraction experiment and the anisotropic parameters refined from the neutron diffraction data show a well-defined and well-localised hydrogen atom whose thermal motion is consistently increasing as a function of temperature, in line with the trends for the other hydrogen atoms present in the structure.

The hydrogen atom in the hydrogen bond between the 4DABA molecules forming the dimers, however, behaves very differently. The thermal parameters as a function of temperature show significant changes both from X-ray and from neutron diffraction. The anisotropic parameters of the hydrogen atom in the O–H···O hydrogen bond derived from the neutron diffraction data show a distinct elongation along the bonding direction at every temperature except at 40K (*Figure 7-6*). The isotropic thermal parameters of the hydrogen atom from the X-ray diffraction data shows similar changes, increasing significantly

compared to those of the rest of the hydrogen atoms as the temperature of the measurement increases.

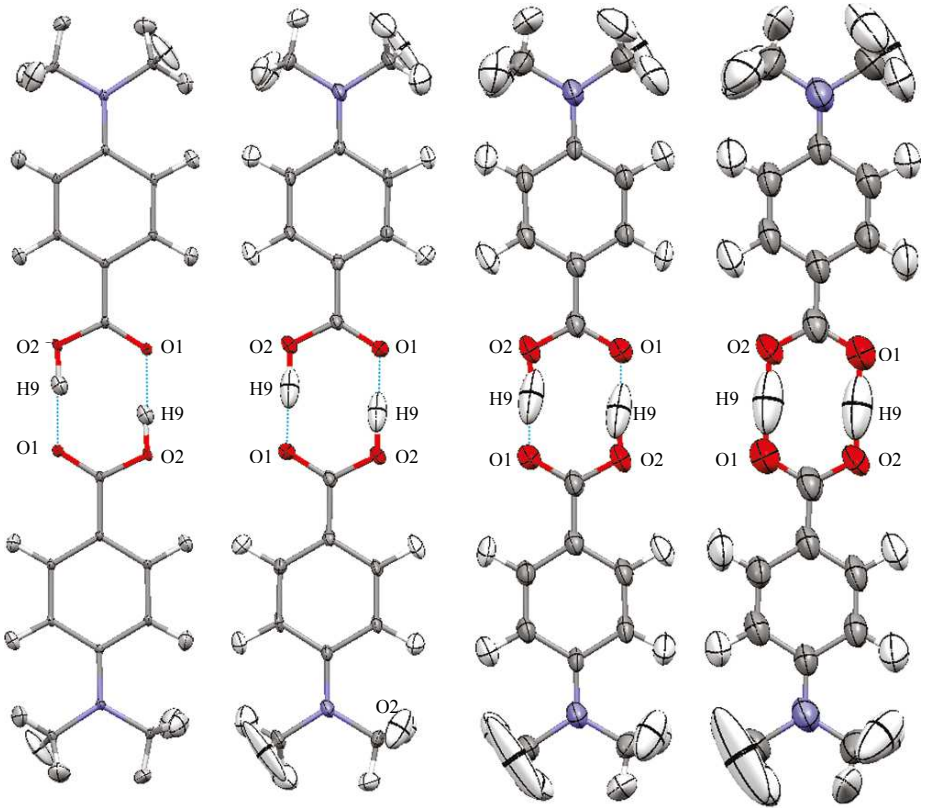

Figure 7-6. The 4DABA dimer showing the evolution of the intermolecular O–H··O hydrogen bond as a function of temperature: from left to right at 40, 100, 200 and 300 K (neutron data) with 50% probability of thermal ellipsoids presented.

The single, well-localised position at 40K and the increasing elongation of the hydrogen atoms anisotropic thermal parameter with the increase of temperature can often be a sign of one of two effects. The hydrogen atom may show disorder in a double well potential where the secondary position of the well is being occupied with the increase in temperature, or it may sit in an asymmetric flat single minimum potential (see Chapter 1.3). At low temperatures, from both neutron and X-ray diffraction data, the hydrogen atom is asymmetrically positioned, moving to a more centred position as the temperature increases, while the O···O distance does not change significantly across the measured temperatures (*Table 7-2)*. This trend can also be an indicator of either type of

behaviour, which can best be resolved by direct use of Fourier difference maps[179].

Table 7-2. Length of the intermolecular HB between the dimer of 4DABA within the ternary complex measured from neutron and X-ray diffraction data.

Temperature (K)	Data collection method	O2–H9 distance (Å)	H9···O1 distance (Å)	O2···O1 distance (Å)
100	neutron	1.08(1)	1.57(1)	2.642 (8)
	x-ray	1.10(3)	1.54(3)	2.637(1)
200	neutron	1.16(2)	1.48(2)	2.63(1)
	x-ray	1.21(3)	1.43(3)	2.632(2)
300	neutron	1.29(3)	1.33(3)	2.62(2)
	x-ray	1.24(3)	1.40(4)	2.633(2)

In order to obtain a greater insight into the hydrogen atom behaviour from the O–H···O intermolecular hydrogen bond between the 4DABA molecules, difference Fourier maps were generated from both X-ray and neutron diffraction data (*Figure 7-7*). The generated difference Fourier maps show a high consistency between the neutron and X-ray diffraction data. At 40K the hydrogen atom shows a well localised single position from the neutron diffraction data. As the temperature increases to 100K the first evidence appears of the secondary site; seen in both the nuclear and electron density belonging to the hydrogen atom. The appearance of a second peak from the nuclear density of the hydrogen atom is a clear indication of a secondary site of hydrogen atom and this is consistent with previously reported disordered hydrogen atom positions between carboxylic acid dimers (see Chapter 1.3). The size of the second peak increases with the temperature and at 300 K, as a result of the increased thermal motion, the two peaks are not clearly distinguishable. However, at 100 and 200 K the occupancy of the second site of the hydrogen atom can be refined from the neutron diffraction data (*Figure 7-8*). At 100K the freely-refined relative occupancy of the two sites shows a 75:25% ratio between the two positions when the isotropic parameters are restrained to take the same value. The separation of the two peaks is 0.68(5) Å with O–H lengths of 0.99(2) Å (75%) and 0.97(5) Å (25%).

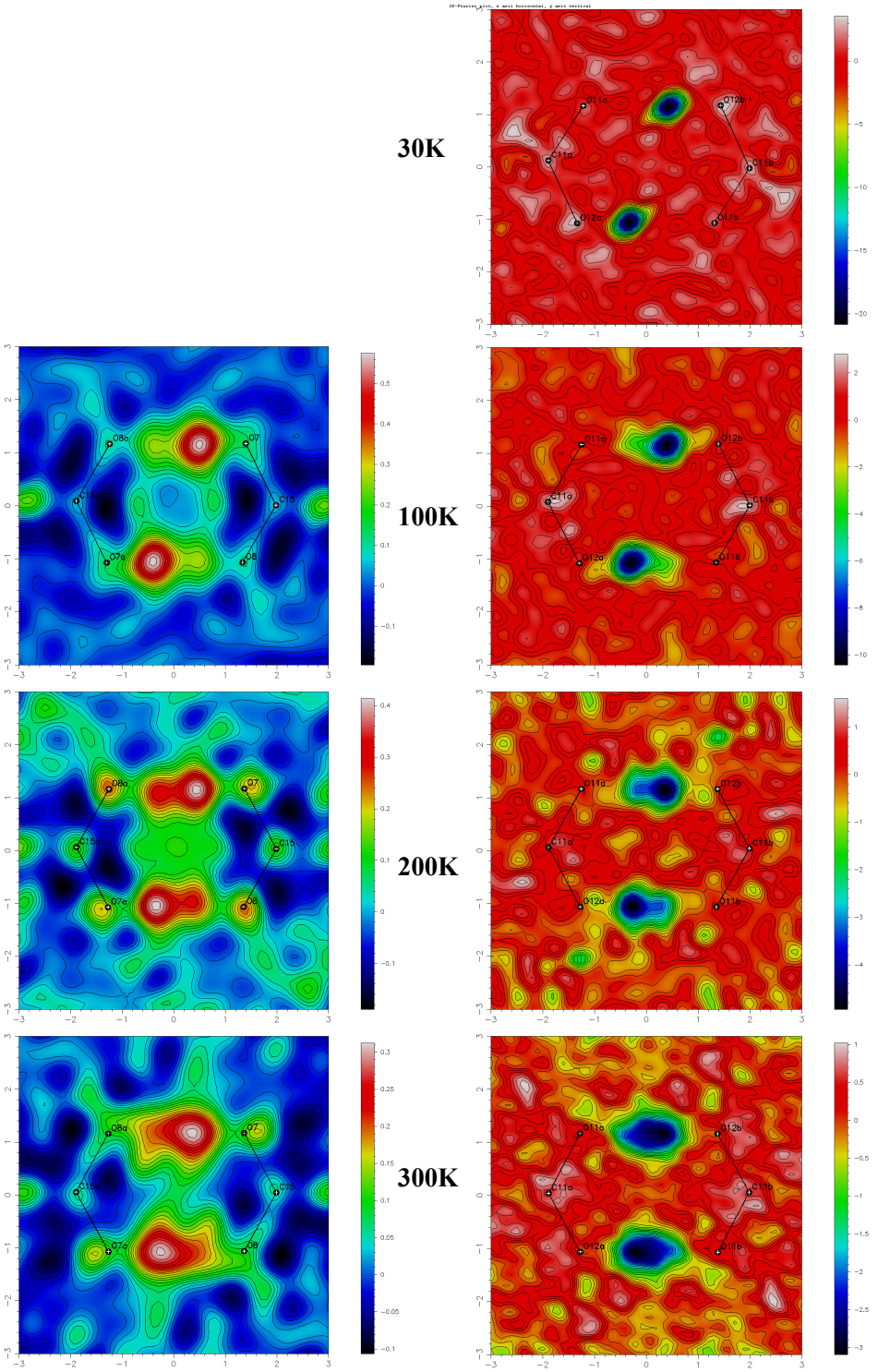

Figure 7-7. Difference Fourier maps of the electron density (left) and nuclear density (right) of the hydrogen atom within the intermolecular O–H···O hydrogen bridge between 4DABA molecules in the molecular complex of 4DABA : 35DNAB : BIPY at the marked temperatures.

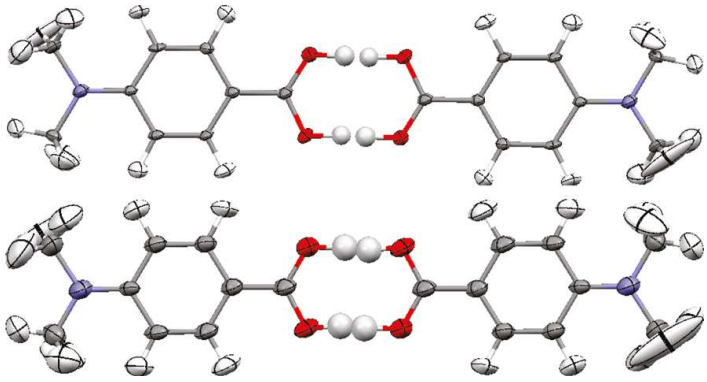

Figure 7-8. The 4DABA dimer in the ternary complex, showing the two refined sites of the hydrogen bonded hydrogen atom nuclear density derived from neutron data at 100K (top) and 200K (bottom).

With the increase of the temperature to 200 K the hydrogen atom nuclear density derived from the neutron diffraction data shows an increased relative occupancy of the second site, with a ratio of 60:40%. This change in the relative occupancy between the two sites is expected in a case of a double well potential, where the increase of the temperature allows the increase of occupancy of the higher energy (minor) configuration. As the thermal parameters increase with the temperature, the proximity of the refined two sites of the hydrogen atom allows a slight apparent overlap of the isotropic thermal parameters, though of course both sites cannot be occupied simultaneously. The O–H distances are 0.94(3) Å (60%) and 1.03(4) Å (40%), with a separation between the sites of 0.69(4) Å.

At 300K, as an effect of the thermal motion there is increased noise in the difference Fourier map and the lower quality of the neutron data set has compromised the refinement of the second position. However, the more centred position of the anisotropic thermal parameters of the hydrogen atoms strongly suggests an approximate 50:50% occupancy at this temperature, consistent with the observed trend.

The disorder observed in this complex can be related to the other two systems of the 4DABA where the degree of pyramidalisation at the nitrogen in the 4DABA molecule was postulated to be related to the observed proton disorder. In the binary complex of 4DABA : 35DNBA, the hydrogen atom is the only one of the

three complexes which shows no sign of disorder within the hydrogen bond between the 4DABA dimers. It is also the only structure of the three that does not have a layered structure. The methyl groups of the 4DABA are significantly pushed out of the plane of the molecules resulting in the pyramidalisation of the nitrogen atom (as shown in Figure 7-1). However, in the native crystal structure of 4DABA the hydrogen atom within the hydrogen bond between the dimer shows disorder of the hydrogen atom similarly to the present ternary complex. Both the native crystal structure of the 4DABA and the ternary complex have layered structures and there are fewer significant short contacts to pull the methyl groups out of the 4DABA plane, resulting in a more planar structure. The small deviation of this nitrogen from the plane of the molecule in the case of the ternary complex decreases with the increase of the temperature from a ring–N–C_{methyl} angle of ~9° at 40K to 3° at 300K. This would also support the observed increase in the relative occupancy of the disordered second site hydrogen atom at higher temperature.

7.4 Conclusion

The study of this ternary complex confirms the significant effect the local environment could have on the presence of disorder in the dimer of the 4DABA molecule. The systematic comparison with native 4DABA and the binary complex with 35DNBA systems suggests that where are significant interactions pulling the methyl group from the plane of the benzene ring, no disorder of the hydrogen atom is observed within O–H···O hydrogen bond of the 4DABA dimer. This is most likely caused by the disruption of the delocalising effect across the whole dimer as a result of the pyramidalisation of the N atom. In the case where are no such interactions, disorder is present as in the case the ternary complex herein presented.

The disorder has been observed by neutron diffraction and presented through difference Fourier maps of the nuclear density and by calculated relative site occupancies of the two hydrogen atom positions at 100 and 200 K. The refinement of the second site occupancy allowed the quantification of the disorder at different temperature showing an increasing ratio of the occupancy

with the increase of the temperature (from 75:25% at 100K to 60:40% at 200). However, the lower quality of the data set and the increased thermal motion compromised the refinement of the second site at 300 K, although the centred position of the nuclear density suggest a 50:50% occupancy which would be consistent with the 100 and 200 K data.

The observed increased planarity of the 4DABA with increasing temperature seems to be related to the increased occupancy of the second site. This is consistent with the findings from the 4DABA native and binary systems, suggesting that in the dimers of 4DABA, the disorder can be predicted from the heavy atom average structure through the observation of the degree of the pyramidalisation of the nitrogen atom.

Chapter 8

8. 4-phenoxyphenol: A porous molecular material

8.1 Introduction

Research into porous materials has gained a great deal of interest over the years, since cavities and pores within these structures can serve as potential storage spaces, with several possible applications across the sciences. Zeolites are one of the most well known naturally occurring porous materials. Since their discovery, the unique porous properties of zeolites have found a large variety of application across the sciences including in petrochemical cracking, water softening and purification, separation and storage of gases and nuclear waste treatment[180-189]. The potential functionality of such materials relies on the size and chemical functionality of the pores within the structure. Thus, to be able to tune these properties, a wide range of new materials have been synthesised with porous structures.

Families of structures such as metal-organic frameworks (MOFs) and covalent-organic frameworks (COFs) have recently become some of the most studied materials in the structural chemistry[190-193]. These newly developed structures contain large cavities with a wide range of chemical functionality and show a huge potential towards the development of gas storage materials, offering potential relevance in the management of greenhouse gases as well as in the storage of hydrogen. The development of these structures focuses on the production of system that are suitable for gas storage, ingress and egress under appropriate required conditions[194-196]. There are many of these structures present in the literature, largely involving inorganic or metal-organic systems with large cavities in their molecular structure. However, the number of purely molecular porous systems remains rather low, which is due to the fact that in purely molecular systems the molecules tend to pack in the most efficient manner which then also prevents the manifestation of porous structures with large cavities. Nonetheless, when such structures are successfully formed, the purely molecular porous systems have a potential advantages, in their low

density and lack of possible toxicity associated with the metal-containing porous materials.

These materials are differentiated by the type of porosity in their structure. This can be placed into two categories[197]: intrinsically porous materials, where the molecules forming the structure are porous themselves and the properties of the pores in the structure rely on covalent bond formation; or extrinsic porous materials, where the molecules themselves are not porous but self-assemble in a solid state in a way that develops pores in their structure. The prediction or design of the last obviously is more unpredictable and challenging[198-199].

There are a few examples in the literature of extrinsically porous materials, of which one of the earliest discovered is 4-(*p*-hydroxyphenyl)-2,2,4-trimethylchroman, commonly known as Dianin's compound. This forms a channel in the structure through a hexagonal shaped hydrogen bonded ring[200]. Since then the structure of Dianin's compound and its relation to the inclusion of guest molecule have been extensively studied and a large number of structures have been produced by re-crystallisation with various guest molecules[201-202]. The relation between the size of the pores and the host molecules has been highlighted, showing that where the guest molecules has a larger size it results in the slight increase of the pore size, which is explained in the terms of the greater steric stress on the molecules. Variable temperature studies have shown that in the case where isopropanol is the guest molecule in the pores, the clathrate undergoes a phase transition below 180K. This results in a doubling of the unit cell to a type II cage (as found in the case of ethylenediamine host molecule) where the length of the *a* and *b* axis doubles and the *c* axis shows a significant lengthening[203]. There are several other studies of the host guest interactions of Dianin's compound as well as on their derivatives[204-207] . The breaking of the trigonal host packing by co-crystallisation has also been investigated[208]. The guest free structure of Dianin's compound has been obtained from re-crystallisation from dodecane[209].

Another extrinsic porous material is β-hydroquinone, which also forms a hexagonal hydrogen-bonded ring adopting a similar trigonal structure, first determined from the SO_2 clathrate[210]. There are several published works on the

clathrate structure of β-hydroquinone, investigating various gas and solvent inclusion and trapping within the channels by both experimental and computational methods[211-215]. However, two other known non-porous polymorphs of hydroquinone exist and upon solvent removal from the channels the structure reverts to the more stable of the other two polymorphs[216].

Here will be presented the structure of 4-phenoxyphenol, a new extrinsically porous organic material extensively studied by X-ray and neutron diffraction with several solvent guests within the pores.

8.2 Experimental data

Crystals of 4-phenoxyphenol were grown by solvent evaporation from acetone, methanol, diethyl ether and acetonitrile by dissolving typically 0.05 g 4-phenoxyphenol in the solvent and evaporating at room temperature, slowing the evaporation by closing the vial with a pierced small clipped lid. After evaporation of the solvents colourless blocks were formed. The neutron size crystal was grown from acetonitrile in a 100 mL beaker, dissolving 5 g of 4-phenoxyphenol in ~20 mL solvent, slowing down the evaporation by closing the beaker with pierced parafilm, further slowing the evaporation of the solvent. Single crystal X-ray diffraction data were collected on the Nonius Kappa CCD at a 100 K from the crystals grown from methanol, deiethyl ether and acetonitrile and on the Bruker Apex II CCD at 100K from the crystal grown from acetone. Neutron diffraction data were collected at 30, 100, 200 and 300 K on the VIVALDI single crystal Laue diffractometer at the Institut Laue–Langevin in Grenoble, France. The X-ray diffraction data were solved with SHELXS97 and refined with SHELXL97 within the WinGX package. For the neutron diffraction data the initial atomic positions were taken from the refined X-ray diffractions structures. From these initial positions taken from the X-ray refinements, both the non-hydrogen and the hydrogen atoms were refined with anisotropic displacement parameters. The data collection and refinement details are listed in *Table 8-1*.

Table 8-1. X-ray and neutron diffraction data refinement details for 4-phenoxyphenol.

Compound	4-phenoxyphenol				Compound	4-phenoxyphenol			
Solvent used for cryst.	Acetone	Methanol	Diethyl Ether	Acetonitrile	Solvent used for cryst.	Acetonitrile	Acetonitrile	Acetonitrile	Acetonitrile
Diffractometer	Bruker Apex II	Nonius Kappa	Nonius Kappa	Nonius Kappa	Diffractometer	VIVALDI	VIVALDI	VIVALDI	VIVALDI
Formula	$C_{12}H_{10}O_2$	$C_{12}H_{10}O_2$	$C_{12}H_{10}O_2$	$C_{12}H_{10}O_2$	Formula	$C_{14}H_{13}O_2N_1$	$C_{14}H_{13}O_2N_1$	$C_{14}H_{13}O_2N_1$	$C_{14}H_{13}O_2N_1$
Molecular weight / $gmol^{-1}$	186.20	186.20	186.20	186.20	Molecular weight / $gmol^{-1}$	127.25	127.25	127.25	127.25
Temperature (K)	100	100	100	100	Temperature (K)	30	100	200	300
Space Group	$R\bar{3}$	$R\bar{3}$	$R\bar{3}$	$R\bar{3}$	Space Group	$R\bar{3}$	$R\bar{3}$	$R\bar{3}$	$R\bar{3}$
a (Å)	28.995(5)	29.0220(12)	29.0335(13)	28.7848(6)	a (Å)	28.890(5)	29.020(5)	29.070(5)	29.110(5)
b (Å)	28.995(5)	29.0220(12)	29.0335(13)	28.7848(6)	b (Å)	28.890(5)	29.020(5)	29.070(5)	29.110(5)
c (Å)	5.945(5)	5.8586(12)	5.8410(2)	5.9868(6)	c (Å)	6.000(5)	6.040(5)	6.050(5)	6.070(5)
α (°)	90	90	90	90	α (°)	90	90	90	90
β (°)	90	90	90	90	β (°)	90	90	90	90
γ (°)	120	120	120	120	γ (°)	120	120	120	120
Volume ($Å^3$)	4328(4)	4273.5(9)	4264.0(3)	4295.9(4)	Volume ($Å^3$)	4337(4)	4405(4)	4428(4)	4455(4)
Z	18	18	18	18	Z	18	18	18	18
θ range/°	1.4 – 29.56	1.4 – 30.05	1.4 – 30.02	1.41 – 30.01	$sin\theta/\lambda_{min}$ - $sin\theta/\lambda_{max}$	0.03 -0.89	0.03 – 0.82	0.03 – 0.64	0.03 – 0.56
Completeness (%)	100	99.9	0.991	100	Completeness (%)	-	-	-	-
Reflections Collected	17956	19415	19751	24414	Reflections Collected	16654	13917	9756	7102
Independent	2693	2781	2741	2799	Independent	3459	2525	1658	1179
Refln (obs.I>2theta(I))	2239	1700	1566	2257	Refln (obs.I>2theta(I))	2584	1905	1261	866
R_{int}	0.0376	0.082	0.1254	0.0518	R_{int}	0.1499	0.1321	0.132	0.1414
Data/Rest./Param.	2693/0/167	2781/0/167	2741/0/167	2799/0/167	Data/Rest./Param.	3459/0/233	2525/0/233	1658/0/233	1179/0/233
GooF on F^2	1.07	1.055	1.007	1.005	GooF on F^2	1.29	1.342	1.223	1.29
R_1 (Observed)	0.0455	0.0643	0.0742	0.0482	R_1 (Observed)	0.0627	0.0532	0.0503	0.0489
R_1 (all)	0.0534	0.1265	0.1527	0.0615	R_1 (all)	0.1062	0.0874	0.0806	0.0803
wR_2 (all)	0.1338	0.1242	0.1454	0.1221	wR_2 (all)	0.1125	0.098	1.012	0.0829
ρ (max / min) / e-$Å^{-3}$	0.407/-0.211	0.222 / -0.25	0.236 / -0.254	0.225 / -0.235	ρ (max / min) / fm-$Å^{-3}$	0.1 / -0.114	0.059 / -0.065	0.051 / -0.048	0.024/ -0.031
RMS / e$Å^{-3}$	0.053	0.049	0.054	0.048	RMS / fm$Å^{-3}$	0.024	0.014	0.01	0.006

8.3 Results and discussion: structure of 4-phenoxyphenol

4-phenoxyphenol crystallises in a porous crystal structure, with channels running along the crystallographic *c*-axis. It was re-crystallised from a large variety of solvents, at varying temperature, pH and solvent mixtures. The crystal structure shows no evidence of polymorphism from the large number of crystallisations carried out to date. Within the structures six molecules form a hydrogen bonded ring, graph set motif $R_6^6(12)$, connected through the hydroxyl groups forming a channel with an aperture of 5.8 - 6.0 Å (*Figure 8-1*). The hydrogen bond within the ring is of moderate strength with lengths listed *Table 8-2*.

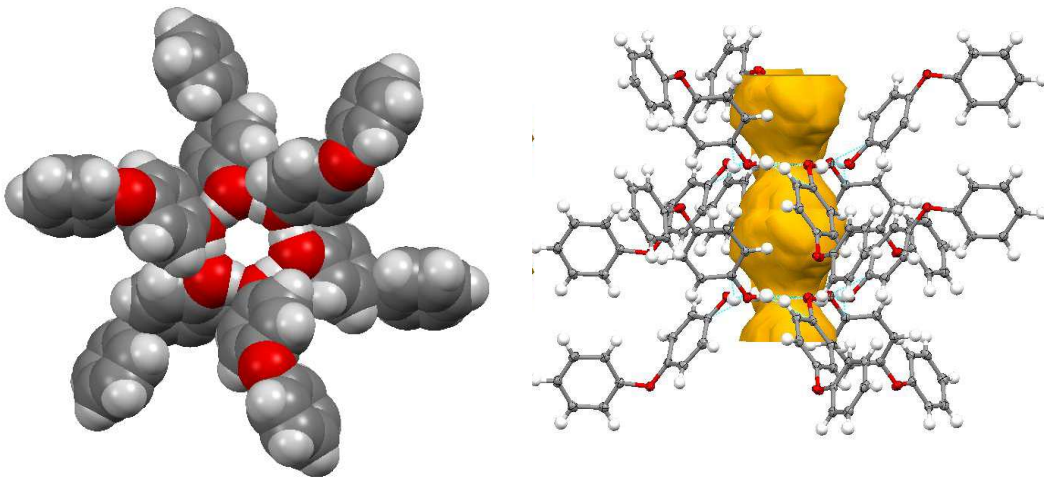

Figure 8-1. The O–H···O ring formed between the 4-phenoxyphenol molecules, viewed along the crystallographic c-axis (left), and the hour-glass shaped channel formed within the structure (right).

The channel forms an hour-glass shape within the crystal structure and generally incorporates the different solvents from which the crystal has been grown, as a guest molecule. The hydrogen bonded ring represents the narrowest part of the channel. The structure of the $R_6^6(12)$ ring is very similar to the channels seen in the crystal structure of Dianin's compound and of β-hydroquinone, which crystallise in the same $\bar{R}3$ space group. The O–H···O intermolecular interactions forming the hydrogen bonded ring are the only strong interactions within the structure. The 4-phenoxyphenol molecules forming the channels are interlocked

through C–H···π weak HBs with lengths between ~3.48 Å and π···π interactions with a length ~3.31 Å (*Figure 8-2* (distances from the 30K neutron data)).

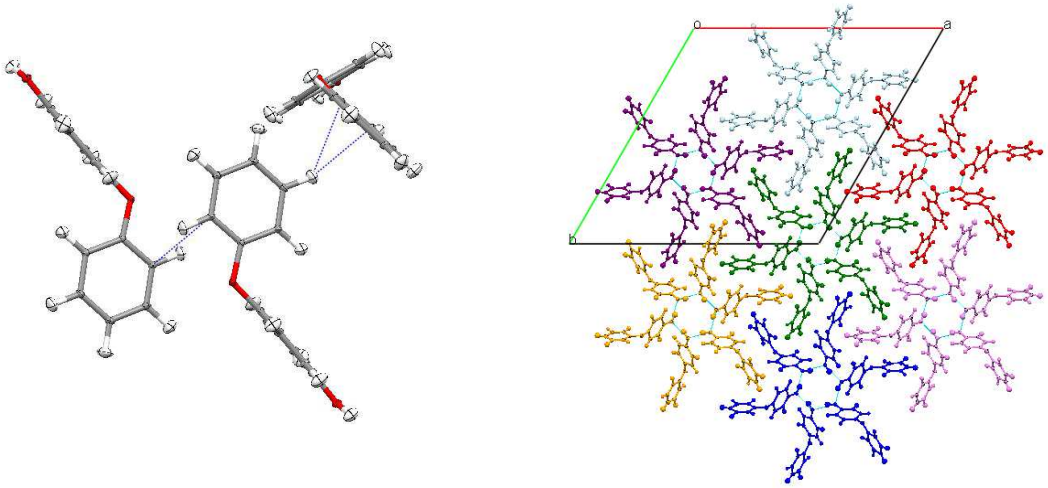

Figure 8-2. C–H···π and π···π intermolecular interactions between the 4-phenoxyphenol molecules (left), interlocking the formed hydrogen bonded rings (right).

4-phenoxyphenol has been successfully crystallised from four different solvents. The non-hydrogen atoms in the structure of 4-phenoxyphenol have been refined anisotropically from all four crystal structures grown from the four different solvents, while the hydrogen atoms have been determined isotropically in every case. A large amount of residual electron density has been found within the channel from the crystals grown from acetone, methanol and acetonitrile. From the residual electron density found in the channels, no molecules could be refined, except in the case of the crystal grown from acetonitrile. An estimation of the residual electron density in the channels has thus been calculated using SQUEEZE within the PLATON structure validation program[217], to allow a direct comparison between the amount of solvent included within the channels (Table 8-2). From the number of electrons found in the channels an estimation of the amount of the respective solvent can be calculated. In the case of the crystals grown from methanol and acetonitrile, the amount of the residual electron density corresponds to three solvent molecules per unit cell, amounting to one molecule per channel. In the case of the crystal grown from acetone, the number of electrons found in the residual electron density corresponds to approximately two molecules per unit cell, i.e. two molecules per three

channels. This suggests a disorder of the acetone not just occupying different orientations within the channel, but across the channels, with some including an acetone and others being empty. The crystal structure of 4-phenoxyphenol grown from diethyl ether, the largest solvent molecule of the four, contains just a very small amount of residual electron density, therefore the pore is essentially empty. In this case, the solvent molecule might be too large to be incorporated within the pore. The crystal structure of 4-phenoxyphenol grown from diethyl ether, together with the results that will be presented of attempts at solvent extraction, will show that the solvent does not show evidence of templating the assembly of the structure to its porous nature.

Table 8-2. Summary of the data on the effect of solvent and temperature on the hydrogen bonded channel within the structure.

	1A	1B	1C	2	3	4	Neutron
Solvent used in the crystallisation	Methanol	Methanol	Recrystal-lised from melt	Diethyl ether	Acetone	Acetonitrile	Acetonitrile
Dried at (°C)	-	75	90	-	-	-	-
a (Å)	29.0220(12)	29.0154(18)	29.0243(19)	29.0335(13)	28.995(5)	28.7848(6)	28.890(5)
c (Å)	5.8586(12)	5.8446(18)	5.8381(19)	5.8410(2)	5.945(5)	5.9868(6)	6.000(5)
Potential solvent area volume ($Å^3$)	194.5 (4.6% of unit cell)	192.0 (4.5% of unit cell)	190.0 (4.5% of unit cell)	190.2 (4.5% of unit cell)	212.9 (4.9% of unit cell)	208.0 (4.8% of unit cell)	-
Electron density in pores	55	53	15	20	70	67	-
Solvent molecules per channel	1	1	-	-	2	1	1
Max.. Channel diameter (Å)	5.4205(3)	5.412(2)	5.389(3)	5.388(4)	5.569(1)	5.536(2)	5.553(4)
O–H···O (Å)	2.712(2)	2.706(2)	2.695(2)	2.695(3)	2.784(1)	2.76821)	2.777(4)

To try to gain an explanation of the "guest-free" result of the crystallisation from diethyl ether, the extraction of the solvent from the channels of solvent-containing crystal structures was attempted. Single crystals grown from methanol were heated up to 75 and 90˚C and left "drying" for up to four days. After the heating process, the crystals remained of a good quality and single crystal X-ray diffraction data were collected from the "dried" samples of every heating process. The refined structures from the sample heated to 75˚C and the non-heated sample have approximately the same amount of residual electron density left within the channel. The sample left at 90˚C has significantly less residual electron density left in the channel, corresponding to less than one solvent molecule per pores and comparable to the sample crystallised from diethyl ether; this sample is essentially empty of solvent. However, the DSC (*Figure 8-3*) and TGA (*Figure 8-4*) measurements shows that while the drying of the sample at 90˚C succeeded, the sample in fact melted and then re-crystallised in the cooling process. Fundamentally, therefore, it has been re-grown from melt rather than the solvent having been driven from the channels.

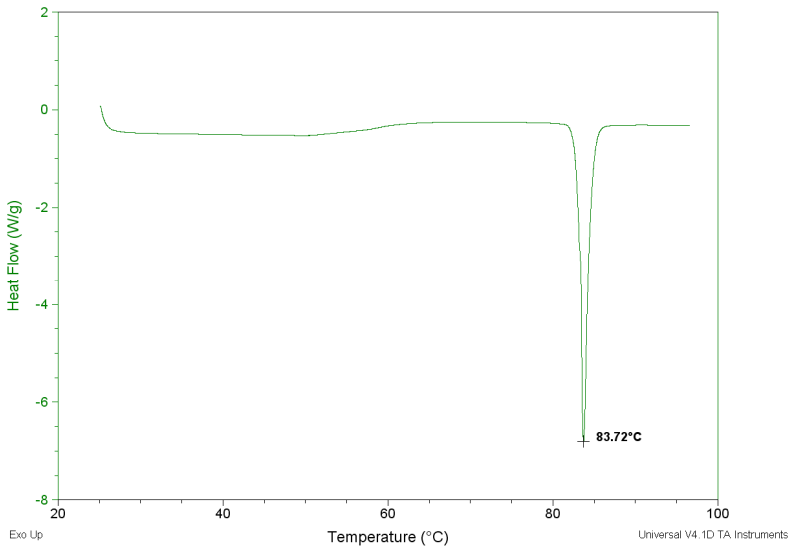

Figure 8-3. DSC plot of the sample grown from methanol, showing the melting at 83.72˚C. Measurement details: 3˚C/min heating rate.

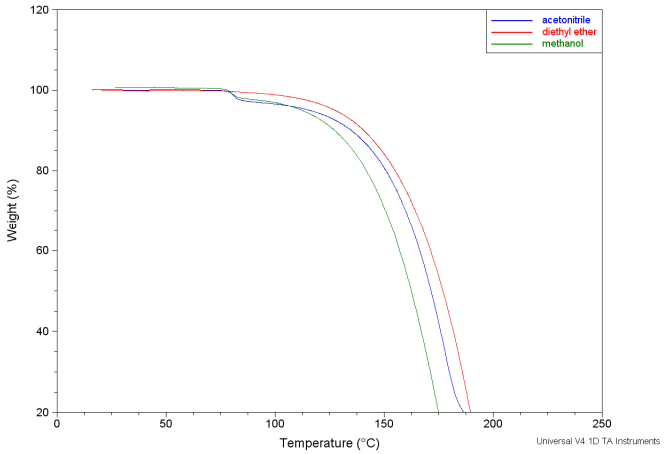

Figure 8-4. TGA plot of the samples grown from the solvents marked in the legend. Measurement method: 5˚C/min heating rate.

The TGA plot also contains the overlay of the measurements of the samples grown from diethyl ether and acetonitrile. While both the methanol and acetonitrile-grown samples lose ~3% of their mass between 75-83˚C, the sample grown from diethyl ether does not, in agreement with the lack of solvent content in this crystal. Both samples grown from diethyl ether and re-crystallised from the melt, with the essentially empty channels, show a contraction of the structure along the channel as well as in the lengths of the hydrogen bonds within the hydrogen bonded ring compared to the structures where the channels are filled by the solvent molecules (*Table 8-2*).

The only case where the solvent molecule found within the channel could be resolved is the sample grown from acetonitrile. From the neutron diffraction data, the solvent is found to lie in the centre of the pore with the 3-fold axis of the CH_3 group aligned along the crystallographic *c*-axis of the crystal structure. The solvent molecule is disordered across the inversion centre of the acetonitrile (*Figure 8-5*).

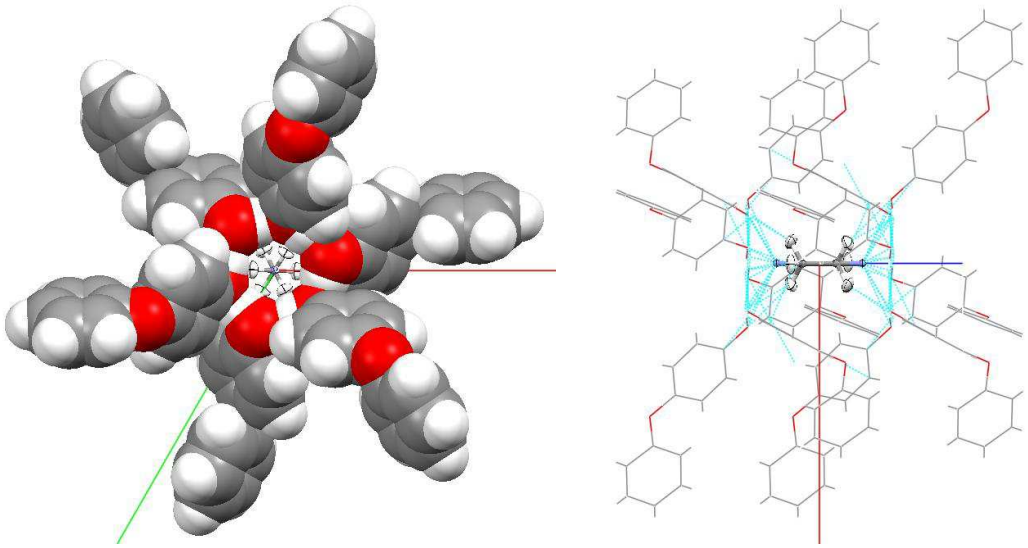

Figure 8-5. The crystal structure of 4-phenoxyphenol (grown from acetonitrile) from the 30 K neutron diffraction data, showing the position of disordered solvent within the channel from a view along (left) and perpendicular (right) to the crystallographic c-axis.

As neutron diffraction data is available in the case of the sample grown from acetonitrile, this allows the unambiguous determination of the hydrogen atom positions and their anisotropic displacement parameters. The determination of these accurate hydrogen positions becomes very important in order to understand the role of the weaker interactions holding the solvent within the channels of the structure.

While the oxygen atoms of the hydrogen bonded ring all lie in the same plane, the hydrogen atoms are positioned alternately below or above this plane (*Figure 8-6*). The acetonitrile is disordered across the inversion centre of the crystal structure and the methyl group shows a well-defined position with no disorder about the three-fold axis of the methyl group. C–H···O intermolecular interactions are present between the methyl group of the acetonitrile and the oxygen atom of the hydroxyl group of the 4-phenoxyohenol molecule, with a C···O length of 3.619(3) Å. These C–H···O interaction are formed between acetonitrile methyl groups and the oxygen atoms of the hydroxyl groups in which the hydrogen atom is alternated above the plane of the hydrogen bonded ring

while, this most probably creates an energetically more favourable orientation for the acetonitrile within the channel.

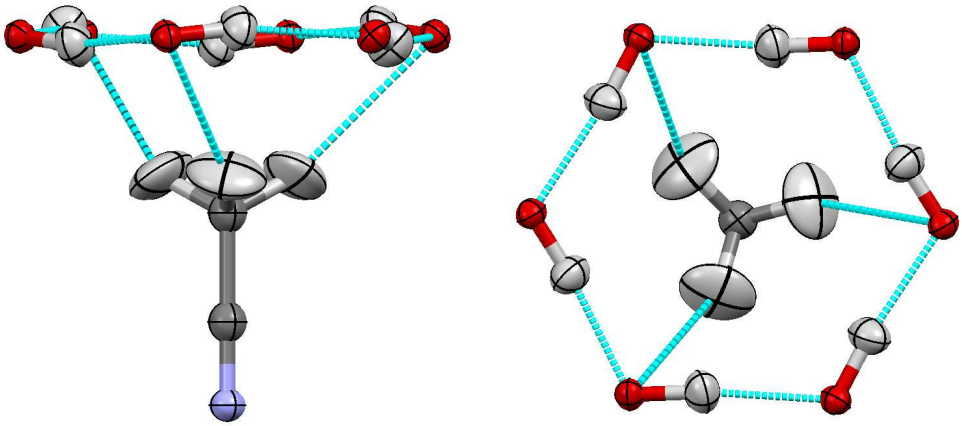

Figure 8-6. The C-H···O intermolecular interaction between the hydrogen bonded ring formed from the hydroxyl group of the 4-phenoxyohenol molecules and the included acetonitrile solvent molecule. For clarity the disordered part of the acetonitrile and the rest of the 4-phenoxyphenol have been removed (100K neutron).

From the variable temperature neutron diffraction data collected at 30, 100, 200 and 300 K, the position of the solvent could only be resolved fully, with anisotropic thermal parameters for all hydrogen atoms, in the case of the 30 and 100 K data. For the 200 and 300 K collections, due to the lower data parameter ratio of the data collection and the disorder within the solvent molecules could not be refined with sensible parameters. There are no changes in the structural framework with the increase of the temperature, apart from the expected larger thermal parameters at higher temperature measurements, in the structures determined with the refined acetonitrile at 30 and 100 K and with the solvent omitted at 200 and 300 K (*Figure 8-7*).

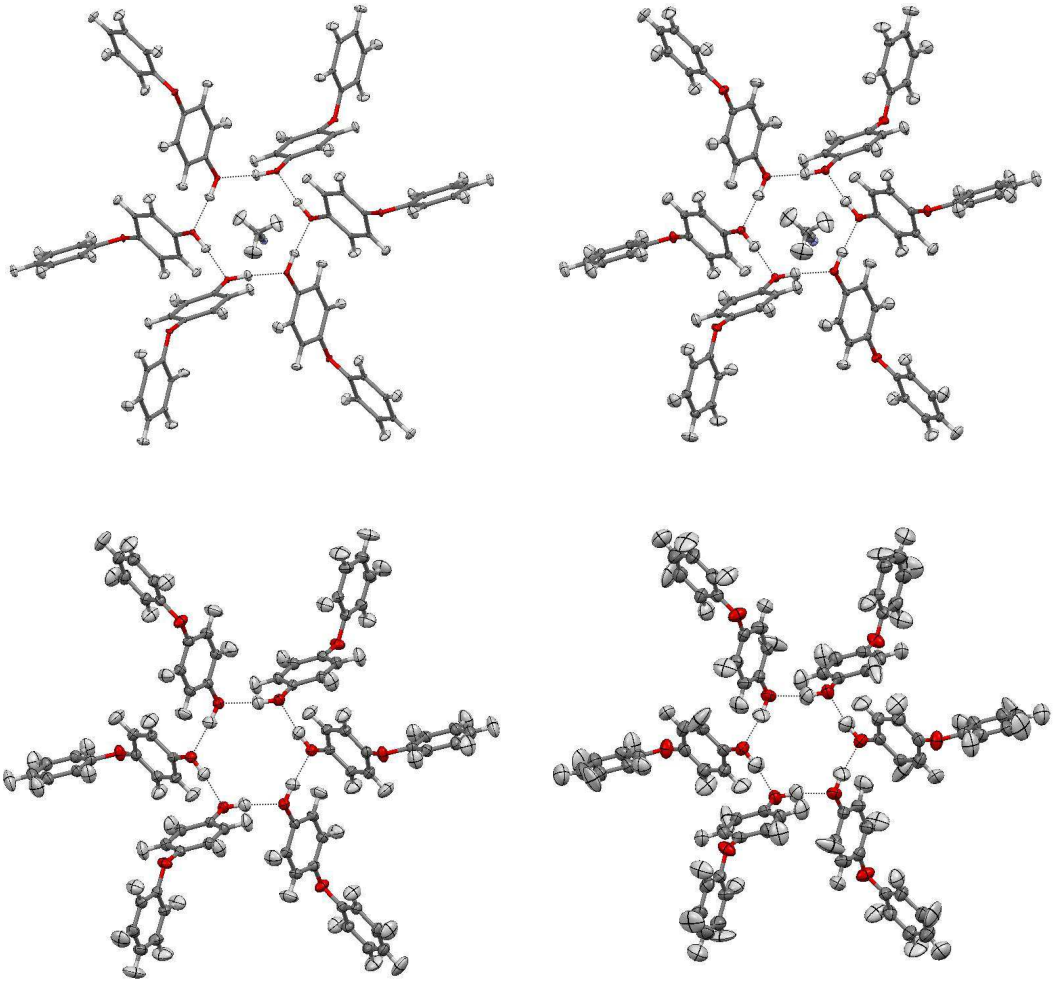

Figure 8-7. The evolution of the structure as a function of temperature from left to right; at 30K (top left) and 100K (top right), at 200K (bottom left) and 300K (bottom right). The solvent could only be modelled reliably at the two lower temperatures, and is omitted from the plots at 200 and 300 K.

8.4 Conclusions

The structure of 4-phenoxyphenol has been presented as a new example of an extrinsically porous molecular material. The structure can be crystallised from a wide range of solvents, and can be grown both as a clathrate with solvent within the channels in the case of the crystals grown from acetone, acetonitrile and methanol, or with essentially empty pores when grown from diethyl ether or re-

crystallised from the melt. There are no other polymorphs of 4-phenoxyphenol observed from the large number of crystallisations set up.

The solvent included within the channels could not be refined apart from the sample crystallised from acetonitrile, for which neutron data were obtained. However, the number of solvent molecules in the channel has been estimated from the residual electron density found within the pores using SQUEEZE. A flexibility of the system of six moderate hydrogen bonds forming the $R_6^6(12)$ ring has been observed from the different solvent clathrates, enabling a slight enlargement of the pores upon accommodation of larger solvent molecules. The neutron diffraction data from the acetonitrile solvate has highlighted the C–H··O interaction responsible for the orientation of the solvent molecule within the channel.

Chapter 9

9. Conclusions and forward look

9.1 Proton transfer in DMAN complexes

By using DMAN as a crystal engineering tool 26 different structures of DMAN have been successfully co-crystallised comprising a series of four halogen-substituted benzoic acids, two hydroxy-, three dihydroxy-, two methyl- and one nitro benzoic acid as well as three other organic acids. In every structure presented a proton is transferred from the acids in the molecular complex to the DMAN, resulting in the generation of a modified hydrogen bonding motif between the acids. A protonated $DMANH^+$ molecule is produced by the creation of a charge assisted intramolecular hydrogen bond between the two nitrogen atoms (*Figure 9-1*).

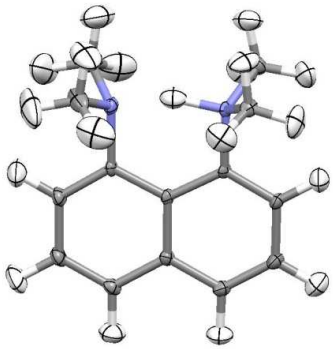

Figure 9-1. The protonated $DMANH^+$ molecule from the molecular complex of DMAN: 2IBA, from the neutron diffraction data collected at 100K.

However, while in every molecular complex the DMAN molecules is protonated, the first example has been found within the molecular complexes of DMAN where this molecule is present in both its protonated ($DMANH^+$) and its unprotonated form in the same time. While in these four complexes (3FBA hydrate, 3CBA, 3BBA and 4CBA with DMAN) both forms are of DMAN is present, the presence of the unprotonated form does not cause modification in the protonated form of DMAN, which has similar bond lengths and bond angles to

those found in the $DMANH^+$ found in other complexes. However, the unprotonated form of DMAN in two out of four complexes is disordered. In the DMAN : 4CBA the disorder appears just in the position of the methyl group while in the DMAN : 3CBA the whole DMAN molecule is disordered across two positions. The geometry of the unprotonated DMAN fits well in all three complexes with that of the unprotonated form found in the CSD.

9.2 Benzoic acid $DIMER^-$s

The proton transfer described above also has modified the bonding motif between the acids in the complexes. The well known double hydrogen-bonded dimer form found in benzoic acids has broken; as a result of the deprotonation the benzoic acid bonds to another benzoic acid through a single charge-assisted SSHB forming a $DIMER^-$ unit (*Figure 9-2*). This stabilises the lost hydrogen atom from its carboxyl group. In this way DMAN has been used as a tool in the co-crystallisations to deprotonate the benzoic acid, consistently producing the $DIMER^-$ form of the halogen substituted benzoic acid across the whole series of halogen substituted benzoic acids, two methyl- and a nitro- substituted benzoic acid complex with DMAN. The hydrogen bond between the $DIMER^-$s in every case is in the distance range of SSHB hydrogen bonds.

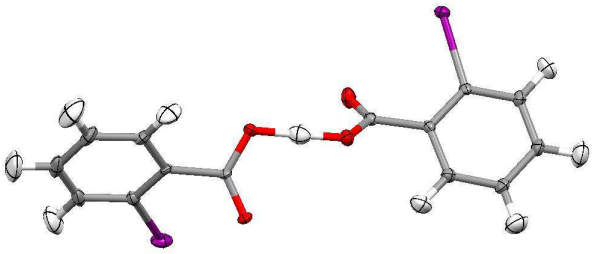

Figure 9-2. The $DIMER^-$ of the 2IBA molecule connected through a single charge-assisted SSHB in the molecular complex of DMAN: 2IBA, from the neutron diffraction data collected at 100K.

Where the $DIMER^-$ is present in the DMAN complex, in the majority of the above described complexes (1:2 co-crystallisation ratio) it is positioned above the DMAN molecule such that one or both of the oxygen atoms not involved in the SSHB between the $DIMER^-$ are connected to the methyl group of the $DMANH^+$

molecule, through C–H···O weak hydrogen bonds (*Figure 9-3*). The relative orientation of the $DIMER^{-}$s, however, are different in the complexes from one to another and is determined by the weaker interactions within the molecular complex and thus the overall packing across these complexes.

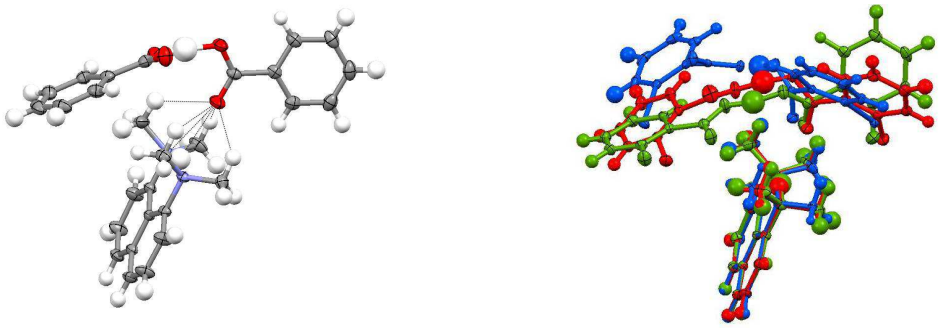

Figure 9-3. The intermolecular interactions between the carboxyl group of the $DIMER^{-}$ and the methyl group of the $DMANH^{+}$ molecule(left) and (right) the different orientations of the $DIMER^{-}$ with overlaid structures of the DMAN : 2FBA (green), DMAN : 2CBA (red) and DMAN : 2IBA (blue).

The formation of the $DIMER^{-}$ motifs present in the large majority of the $DMANH^{+}$ and substituted benzoic acid complexes does not happen in every case when a DMAN molecule deprotonates the acid. With the introduction of a competing hydrogen bond donor (hydroxy- and dihydroxy- benzoic acids) the $DIMER^{-}$ motif is no longer present. Instead, the hydroxyl group bonds to the deprotonated carboxylate group to stabilise the lost hydrogen with a slightly longer intermolecular O–H···O bond, creating a chain. However, in the molecular complex DMAN : 23DOHBA and DMAN : 26DOHBA, the two dihydroxyl substituted benzoic acids shows a different behaviour. In the former, the pair of 23DOHBA molecules are paired side by side connected through their hydroxyl groups, while in the latter, the two intramolecular hydrogen bonds are created between the hydroxyl groups and the oxygen atoms of the carboxylate group. As the hydroxyl- and dihydroxyl- substituted benzoic acids do not have the $DIMER^{-}$ motif found in the other substituted benzoic acids in this work, they pack differently. While the hydroxyl- substituted benzoic acid complexes shows a very similar packing arrangement, forming a layered structure with the water molecules and holding

the $DMANH^+$ molecules in pockets, the dihydroxy- substituted benzoic acids shows different packing with different motifs in all three presented cases.

The hydrogen bond $DIMER^-$ is also missing from the DMAN : 3FBA hydrate structure, where both $3FBA^-$ molecules are deprotonated and the water molecules introduced in this complex replace the charge-assisted SSHB between the $DIMER^-$. In this case the water molecules connect the two $3FBA^-$ molecules together through medium strength O–H···O bonds. This is the only water-containing structure yet found in the molecular complexes of halogen substituted benzoic acid where the water molecule breaks up the bonding $DIMER^-$ motif. While in the molecular complex of the 4FBA : DMAN hydrate the water molecule slightly shortens the O-H···O bond in the $DIMER^-$ creating the shortest O-H···O found in the herein studied DMAN complexes.However, the presence of the hydrate and anhydrous form of the DMAN : 3FBA complex and the hydrated and anhydrous form of the DMAN : ClA complex suggests that it might be possible to control the hydrogen bonding through the introduction of water into the structure.

9.3 Anomalous proton behaviour

Most of the molecular complex of DMAN presented here have been determined from single crystal X-ray diffraction data and for unambiguous determination of the hydrogen atom positions and behaviour neutron diffraction experiment is required. Nonetheless, by being able to compare a large number of similar structures, as the series of the DMAN complexes presented here, when good quality X-ray data are available, gives the possibility to reveal particularly interesting relationships between the hydrogen position within the hydrogen bond and its environment.

By determining the C–N bond lengths and the donor-acceptor distances of the intramolecular N–H···N hydrogen bond within the $DMANH^+$ showed that C–N bond length is longer on the donor side of the hydrogen bond than the acceptor side. However, this length difference appears only in the cases where the hydrogen bond shows a significant difference in the donor-acceptor hydrogen bond

distances, confirmed from observations in the two structures DMAN : 2IBA and DMAN : 26DOHBA. This correlation can be examined in more detail by comparing two $DMANH^+$ molecules, one with asymmetric and one with symmetric hydrogen bond, within the same structure but different environment (the number and the position of intermolecular interactions). This is found in the DMAN : 4OHBA complex, and the correlation has also been observed on comparison of the two isomorphous complex of DMAN : ClA and DMAN : BrA and the DMAN : ClA hydrate.

Other bond length relationships have been found within the charge-assisted SSHB of the $DIMER^-$s and between the C–O (hydrogen bonded oxygen atom) and C=O (non-hydrogen bonded oxygen atom) distances. A larger difference is found between these bond lengths in the case of the carboxyl group on the donor side of the O–H···O than the acceptor side. However, these hydrogen bonds are within the range of SSHB with lengths well under 2.5 Å and the deviation of the donor-acceptor hydrogen bond distances is not as large as in the case of the intramolecular N–H···N HBs. In some cases, therefore, these differences are not clearly distinguishable.

9.4 The role of halogen bonding and weaker interactions

As described in Chapter 4, co-crystallisation is a one step "reaction" and changing a single variable of the structure could lead to a better understanding of the significance and robustness of the interactions present. In the synthesis of a series of DMAN and substituted benzoic acid complexes the significance of the stronger interaction has been shown. However to get a full picture we have to take a closer look at the weaker interactions in cases where the stronger motifs are similar.

In the series of the DMAN : halogen substituted benzoic acid complexes the majority of the structure co-crystallise in 1:2 ratio. But even in these cases the weaker interactions such as halogen bonding introduce changes in the packing. A good example is found in the *ortho*- halogen substituted benzoic acid structures. In the case of the fluorine substitution the main changes are found in the

orientation of the $DIMER^-$ above the $DMANH^+$ molecule and the dihedral angle of the benzene ring and carboxyl group. These changes are influenced by the F···H interaction with the methyl group of the $DMANH^+$, while in the iodo-substitted case DMAN : 2IBA, the most influential weaker interaction is of I····π type. In the case of DMAN : 2CBA and DMAN : 2BBA the different weaker interactions of type Cl···Cl and Br···Br, respectively, introduce a disorder in the structure in addition to the above mentioned changes. There is also a consistent presence of stacking of $DMANH^+$ molecules across the full range of complexes studied. While these show substantial variations in both stacking distance and in offset of parallel planes with respect to each other, these stacking patterns clearly play a role in the overall organisation of these structures.

The effect of the substituent atom and its position can also change the co-crystallisation ratio of the complex even in the presence of the strong hydrogen bonding motif of $DIMER^-$. This is exemplified in the case of the DMAN : 3BBA and DMAN : 4CBA where the co-crystallisation ratio is 1:1, or the DMAN : 3CBA which has a co-crystallisation ratio of 3:4. These complexes all include both a protonated and an unprotonated DMAN in their structure. Although hydrated complexes can interrupt the commonly induced hydrogen binding patterns in the DMAN complexes studied, in the molecular complex of the DMAN : 4FBA hydrate, the introduction of the water does not break the $DIMER^-$ motif, although an additional component is also introduced in the complex, also changing the co-crystallisation ratio. As another effect of the substituent atom a change is observed in the linearity of the $DIMER^-$ in the case of the DMAN : 4BBA and DMAN : 4IBA complexes.

In all of the halogen (X) substituted benzoic acid and DMAN complexes apart from the DMAN:3CBA complex, there is a X····X, X····H or X····π interaction present in the structure. This would suggest that these interactions play a significant role in the packing of the structures. However, the methyl-substituted benzoic acid and DMAN complexes tell a different story.

The volume of a methyl group has a comparable volume to that of the chlorine atom, and a large number of the isostructural complexes found in the CSD are

between pairs of complexes where the chlorine atom has been interchanged with a methyl group[163]. However, the pairs of complexes DMAN :3CBA / DMAN : 3TOLA and DMAN :4TOLA / DMAN : 4CBA are very different, although both methyl- substituted benzoic acid complexes emulate the 1:2 co-crystallisation ratio of chloro- substituted benzoic acids. On the other hand the structure of DMAN : 4TOLA is isomorphous with the structures of DMAN : 4BBA and DMAN : 4IBA, containing the $DIMER^{-}$ with a bent arrangement, although the methyl group of DMAN : 4TOLA complex has no intermolecular short contacts within the sums of van der Waals radii.

These results suggest that, while halogen interactions can have a stabilising role in the structure, sometimes even leading to a modified co-crystallisation ratio and other structural behaviour, the size and the position of the substituent also plays a significant role, and there is no completely consistent pattern.

9.5 Neutron diffraction

The two DMAN complexes (DMAN : 2IBA, DMAN : 26DOHBA) studied by neutron justifies how valuable is the method in determining accurate hydrogen atom positions. In the case of the DMAN : 2IBA complex the difference Fourier map of both the intra- and intermolecular hydrogen bonds shows an elongated shape of the electron density along the bonding. However with neutron diffraction data the hydrogen atom could be accurately determined and show a single, well-defined nuclear density on the difference map. In this case the hydrogen atom determination from the X-ray diffraction data is more ambiguous as the molecular complex contains a heavy atom. In the case of the DMAN : 26DOHBA complex, a slight elongation of the electron density distribution is again observed in one of the O–H···O intramolecular hydrogen bonds, although considerably less than in the case of the DMAN : 2IBA complex. Once again, the neutron diffraction data does not show any anomalous behaviour of the hydrogen atom.

While these neutron studies of the DMAN complexes have resolved possible ambiguities in X-ray determinations by suggesting subtle features are not

significant, a more positive result of the neutron diffraction experiments is found in the case of the ternary complex (Chapter 7). Good quality X-ray diffraction data have been collected on the complex and the difference Fourier map of the electron density distribution of the hydrogen atom in the HB between the 4DABA carboxyl groups showed a possible second position of the hydrogen atom. These findings, togegher with previously published results, justified the collection of the neutron diffraction data. Variable temperature neutron diffraction data were collected, from which the difference map of the nuclear density confirmed temperature dependent disorder of the hydrogen atom across two positions, showing a single well-defined position at 30 K with an increasing occupancy of a secondary position as a function of temperature. The hydrogen atom occupancy has been refined from the neutron diffraction data at 100 and 200 K showing a approximately 25:75 and 40:60% occupancy of the two positions when the isotropic parameters are restrained to take the same value. At 300 K, however, as a result of the increased thermal motion, the two positions are not clearly distinguishable.

The significant importance of the neutron diffraction data has been also shown in the porous structure of 4-phenoxyphenol. The structure has been determined from X-ray diffraction data in every solvent guest case. However, without neutron diffraction data available, the disorder of the solvent guest molecule did not allow for a full determination of the solvent within the channels. The structure determined from neutron diffraction data with the acetonitrile guest molecule in the pore allowed this to be resolved and led to the understanding of the weaker interactions (C–H···O hydrogen bonds) that play a role in the orientation of the solvent molecule within the pore. This also helped understand the possible cause of increase in the size of the pore-forming $R_6^6(12)$ hydrogen-bonded ring formed from the hydroxyl groups of six related molecules.

9.6 Forward look

Variable temperature X-ray diffraction data has been collected on large number of the DMAN and substituted benzoic acids. This reveals possible discrepancies in the electron density distribution within the intra- and intermolecular HBs. The

neutron diffraction data in case of the two DMAN complexes studied to date show a well defined nuclear density. However, the hydrogen bonds involved are all very short, and further investigation of DMAN and substituted benzoic acids complexes with variable temperature neutron diffraction data collection are justified.

There is also a further opportunity for the contribution of neutron diffraction in this area. Low temperature neutron diffraction data collection on the whole series of the DMAN complexes would help rationalize correlations observed in the structure: the correlation between the donor side of the intramolecular N–H···N HB and the C–N bond length, and that between the C–O and C=O bond lengths and the donor side of the O–H···O bond. This also could lead to unambiguous determination of the relation between the very asymmetric intramolecular hydrogen position within the N–H···N bond and the asymmetry in the intermolecular short contacts between the two sides of these bonds.

The series of DMAN and substituted benzoic acid complexes is a good example of crystal engineering, showing a series of molecular complexes where the stronger interaction within the complexes can be controlled, leading to predictable building blocks such as the $DIMER^{-}$ or the chain of hydroxyl- substituted benzoic acids. However, to take this control over the stronger interaction to the next level, and to be able to fully understand and control weaker intermolecular interactions such as C–H···O, C–H···π, etc., further research on the complexes of DMAN and other series of carboxylic acids would be required.

The further study of the 4-phenoxyphenol is justified as well. To understand fully the behaviour of a purely organic, self-assembling porous material could lead one step forward to a creation of materials with potential gas storage. It would be ideal to attempt the crystal growth from a series of other solvents and their further study with neutron diffraction as well as the study of possible gas capture. Another possibility would be to attempt to modify the channel size by coordinating the 4-phenoxyphenol molecule to metals.

References

1. C. C. Wilson, *Crystallography Reviews*, 2007, **13**, 143 - 198.
2. A. Parkin, C. C. Seaton, N. Blagden and C. C. Wilson, *Crystal Growth & Design*, 2007, **7**, 531-534.
3. M. S. Adam, M. J. Gutmann, C. K. Leech, D. S. Middlemiss, A. Parkin, L. H. Thomas and C. C. Wilson, *New J. Chem.*, 2010, **34**, 85-91.
4. L. H. Thomas, A. J. Florence and C. C. Wilson, *New J. Chem.*, 2009, **33**, 2486-2490.
5. G. A. Craig, L. H. Thomas, M. S. Adam, A. Ballantyne, A. Cairns, S. C. Cairns, G. Copeland, C. Harris, E. McCalmont, R. McTaggart, A. R. G. Martin, S. Palmer, J. Quail, H. Saxby, D. J. Sneddon, G. Stewart, N. Thomson, A. Whyte, C. C. Wilson and A. Parkin, *Acta Crystallographica Section E*, 2009, **65**, o380.
6. C. C. Wilson, X. Xu, A. J. Florence and N. Shankland, *New J. Chem.*, 2006, **30**, 979-981.
7. C. A. Morrison, M. M. Siddick, P. J. Camp and C. C. Wilson, *J. Am. Chem. Soc.*, 2005, **127**, 4042-4048.
8. G. A. Jeffrey, *An Introduction to Hydrogen Bonding*, Oxford University Press, Oxford, 1997.
9. G. R. Desiraju, *Crystal Growth & Design*, 2011, **11**, 896-898.
10. G. R. Desiraju, *Angew. Chem. Int. Ed.*, 2011, **50**, 52-59.
11. I. C. b. A. D. M. a. A. W.), *Compendium of Chemical Terminology (the "Gold Book")*, 2nd edn., Blackwell Scientific Publications, Oxford, 1997.
12. http://www.iupac.org/web/nt/2010-10-25_hydrogen_bond, *Provisional Recommendation - Definition of the Hydrogen Bond*, 2011.
13. S. Goswami, S. Jana, A. Hazra, H.-K. Fun and S. Chantrapromma, *Supramol. Chem.*, 2008, **20**, 495 - 500.
14. J.-P. Bideau, G. Bravic and A. Filhol, *Acta Crystallographica Section B*, 1977, **33**, 3847-3849.
15. E. O. Schlemper, R. K. Murmann and M. S. Hussain, *Acta Crystallographica Section C*, 1986, **42**, 1739-1743.
16. M. S. Hussain, E. O. Schlemper and W. B. Yelon, *Acta Crystallographica Section B*, 1981, **37**, 347-351.
17. E. O. Schlemper, W. C. Hamilton and S. J. La Placa, *The Journal of Chemical Physics*, 1971, **54**, 3990-4000.

18. E. O. Schlemper and C. K. Fair, *Acta Crystallographica Section B*, 1977, **33**, 2482-2489.
19. A. Kvick, T. F. Koetzle, R. Thomas and F. Takusagawa, *The Journal of Chemical Physics*, 1974, **60**, 3866-3874.
20. D. Pyżalska, R. Pyżalski and T. Borowiak, *J. Chem. Crystallogr.*, 1983, **13**, 211-220.
21. Z. Malarski, T. Lis, E. Grech, J. Nowicka-Scheibe and K. Majewska, *J. Mol. Struct.*, 1990, **221**, 227-238.
22. O. Grineva, P. Zorky and E. Rostov, *Struct. Chem.*, 2007, **18**, 443-448.
23. M. Palusiak, I. Janowska, J. Zakrzewski and S. J. Grabowski, *Acta Crystallographica Section C*, 2005, **61**, m55-m57.
24. P. Gilli, V. Bertolasi, V. Ferretti and G. Gilli, *J. Am. Chem. Soc.*, 1994, **116**, 909-915.
25. P. G. G. Gilli, *The Nature of the Hydrogen Bond: Outline of a Comprehensive Hydrogen Bond Theory*, Oxford University Press, Oxford, 2009.
26. J. Stare, M. Hartl, L. Daemen and J. Eckert, *Acta Chim. Slov.*, 2011, **58**, 521-527.
27. M. W. Johnson, E. Sandor and E. Arzi, *Acta Crystallographica Section B*, 1975, **31**, 1998-2003.
28. G. S. Denisov, A. Koll, V. I. Lobadyuk, V. M. Schreiber, A. V. Shurukhina and V. N. Spevak, *J. Mol. Struct.*, 2002, **605**, 221-226.
29. D. Williams, *Acta Crystallographica*, 1966, **21**, 340-349.
30. P. Gilli, L. Pretto, V. Bertolasi and G. Gilli, *Acc. Chem. Res.*, 2008, **42**, 33-44.
31. G. Gilli and P. Gilli, *J. Mol. Struct.*, 2000, **552**, 1-15.
32. P. Gilli, V. Bertolasi, V. Ferretti and G. Gilli, *J. Am. Chem. Soc.*, 2000, **122**, 10405-10417.
33. G. R. Desiraju, *Acc. Chem. Res.*, 2002, **35**, 565-573.
34. T. Steiner and G. R. Desiraju, *Chem. Commun.*, 1998, 891-892.
35. R. Thaimattam, D. Shekhar Reddy, F. Xue, T. C. W. Mak, A. Nangia and G. R. Desiraju, *J. Chem. Soc., Perkin Trans. 2*, 1998, 1783-1790.
36. I. Mata, E. Molins, I. Alkorta and E. Espinosa, *The Journal of Physical Chemistry A*, 2007, **111**, 6425-6433.
37. C. C. Wilson, N. Shankland and A. J. Florence, *J. Chem. Soc., Faraday Trans.*, 1996, **92**, 5051-5057.
38. C. C. Wilson and A. E. Goeta, *Angew. Chem. Int. Ed.*, 2004, **43**, 2095-2099.

39. A. Parkin, K. Wozniak and C. C. Wilson, *Crystal Growth & Design*, 2007, **7**, 1393-1398.
40. J. A. Kanters, G. Roelofsen and J. Kroon, *Nature*, 1975, **257**, 625-626.
41. C. L. Nygren, C. C. Wilson and J. F. C. Turner, *The Journal of Physical Chemistry A*, 2005, **109**, 2586-2593.
42. G. Wojciechowski, M. Ratajczak-Sitarz, A. Katrusiak and B. Brzezinski, *J. Mol. Struct.*, 2002, **612**, 59-64.
43. G. Wojciechowski and B. Brzezinski, *J. Mol. Struct.*, 2001, **595**, 195-199.
44. C. C. Wilson, N. Shankland and A. J. Florence, *Chem. Phys. Lett.*, 1996, **253**, 103-107.
45. Macdonal.Al, J. C. Speakman and D. Hadzi, *J. Chem. Soc.-Perkin Trans. 2*, 1972, 825-&.
46. C. L. Perrin, *Acc. Chem. Res.*, 2010, **43**, 1550-1557.
47. D. F. Brougham, A. J. Horsewill and R. I. Jenkinson, *Chem. Phys. Lett.*, 1997, **272**, 69-74.
48. M. Neumann, D. F. Brougham, C. J. McGloin, M. R. Johnson, A. J. Horsewill and H. P. Trommsdorff, *The Journal of Chemical Physics*, 1998, **109**, 7300-7311.
49. M. A. Neumann, S. Craciun, A. Corval, M. R. Johnson, A. J. Horsewill, V. A. Benderskii and H. P. Trommsdorff, *J. Lumin.*, 1998, **76-77**, 56-59.
50. C. L. Perrin and B. K. Ohta, *Bioorg. Chem.*, 2002, **30**, 3-15.
51. G. K. H. Madsen, G. J. McIntyre, B. Schiøtt and F. K. Larsen, *Chemistry – A European Journal*, 2007, **13**, 5539-5547.
52. R. Boese, M. Y. Antipin, D. Blaser and K. A. Lyssenko, *J. Phys. Chem. B*, 1998, **102**, 8654-8660.
53. D. S. Middlemiss, M. Facchini, C. A. Morrison and C. C. Wilson, *CrystEngComm*, 2007, **9**, 777-785.
54. T. Steiner, I. Majerz and C. C. Wilson, *Angew. Chem.-Int. Edit.*, 2001, **40**, 2651-2654.
55. A. Parkin, S. M. Harte, A. E. Goeta and C. C. Wilson, *New Journal of Chemistry*, 2004, **28**, 718-721.
56. C. C. Wilson, *Acta Crystallogr. Sect. B-Struct. Sci.*, 2001, **57**, 435-439.
57. J. A. Cowan, J. A. K. Howard, G. J. McIntyre, S. M.-F. Lo and I. D. Williams, *Acta Crystallographica Section B*, 2003, **59**, 794-801.
58. J. A. Cowan, J. A. K. Howard, G. McIntyre, J.,, S. M.-F. Lo and I. D. Williams, *Acta Crystallographica Section B*, 2005, **61**, 724-730.

59. N. Casati, P. Macchi and A. Sironi, *Chem. Commun.*, 2009, 2679-2681.
60. P. Macchi, N. Casati, W. G. Marshall and A. Sironi, *CrystEngComm*, 2010, **12**, 2596-2603.
61. G. Smith, U. D. Wermuth and J. M. White, *Acta Crystallographica Section C*, 2008, **64**, o180-o183.
62. C. B. Aakeroey and M. Nieuwenhuyzen, *J. Am. Chem. Soc.*, 1994, **116**, 10983-10991.
63. M. Kamiya, S. Saito and I. Ohmine, *The Journal of Physical Chemistry B*, 2007, **111**, 2948-2956.
64. A. Jacobs, L. R. Nassimbeni, G. l. Ramon and B. K. Sebogisi, *CrystEngComm*, 2010, **12**, 3065-3070.
65. J. S. Stevens, S. J. Byard and S. L. M. Schroeder, *J. Pharm. Sci.*, 2010, **99**, 4453-4457.
66. G. R. Desiraju, *Science*, 1997, **278**, 404-405.
67. M. Schmidtmann, M. J. Gutmann, D. S. Middlemiss and C. C. Wilson, *CrystEngComm*, 2007, **9**, 743-745.
68. G. R. Desiraju, *J. Chem. Soc., Perkin Trans. 2*, 1983, 1025-1030.
69. K.-S. Huang, D. Britton, t. late Margaret C. Etter and S. R. Byrn, *Journal of Materials Chemistry*, 1997, **7**, 713-720.
70. S. Kawata, K. Adachi, Y. Sugiyama, M. K. Kabir and S. Kaizaki, *CrystEngComm*, 2002, **4**, 496-498.
71. M. Schmidtmann and C. C. Wilson, *CrystEngComm*, 2008, **10**, 177-183.
72. M. N. G. James and G. J. B. Williams, *Acta Crystallographica Section B*, 1974, **30**, 1249-1257.
73. Z. M. Jin, Y. J. Pan, M. L. Hu and J. W. Zou, *J. Mol. Struct.*, 2002, **609**, 83-87.
74. T.-a. Nihei, S. Ishimaru, rsquo, ichi, H. Ishida, H. Ishihara and R. Ikeda, *Chem. Lett.*, 2000, **29**, 1346-1347.
75. H. Suzuki, H. Mori, J.-i. Yamaura, M. Matsuda, H. Tajima and T. Mochida, *Chem. Lett.*, 2007, **36**, 402-403.
76. K. Raatikainen, M. Cametti and K. Rissanen, *Beilstein Journal of Organic Chemistry*, 2010, **6**, 4.
77. H. A. Bent, *Chem. Rev.*, 1968, **68**, 587-648.
78. J. P. M. Lommerse, A. J. Stone, R. Taylor and F. H. Allen, *J. Am. Chem. Soc.*, 1996, **118**, 3108-3116.

79. T. Clark, M. Hennemann, J. Murray and P. Politzer, *J. Mol. Model.*, 2007, **13**, 291-296.
80. G. R. Desiraju and R. Parthasarathy, *J. Am. Chem. Soc.*, 1989, **111**, 8725-8726.
81. V. R. Pedireddi, D. S. Reddy, B. S. Goud, D. C. Craig, A. D. Rae and G. R. Desiraju, *J. Chem. Soc., Perkin Trans. 2*, 1994, 2353-2360.
82. P. Metrangolo and G. Resnati, *Science*, 2008, **321**, 918-919.
83. E. Corradi, S. V. Meille, M. T. Messina, P. Metrangolo and G. Resnati, *Angew. Chem. Int. Ed.*, 2000, **39**, 1782-1786.
84. B. K. Saha, A. Nangia and M. Jaskolski, *CrystEngComm*, 2005, **7**, 355-358.
85. C. Glidewell, J. N. Low, J. M. S. Skakle and J. L. Wardell, *Acta Crystallographica Section C*, 2003, **59**, o509-o511.
86. H. Ishida and T. Fukunaga, *Acta Crystallographica Section E*, 2004, **60**, o1664-o1665.
87. P. Jones, *Acta Crystallographica Section C*, 2001, **57**, 880-882.
88. N. J. Singh, S. K. Min, D. Y. Kim and K. S. Kim, *Journal of Chemical Theory and Computation*, 2009, **5**, 515-529.
89. S. L. Cockroft, C. A. Hunter, K. R. Lawson, J. Perkins and C. J. Urch, *J. Am. Chem. Soc.*, 2005, **127**, 8594-8595.
90. J. Ribas, E. Cubero, F. J. Luque and M. Orozco, *The Journal of Organic Chemistry*, 2002, **67**, 7057-7065.
91. K. Nakamura and K. N. Houk, *Org. Lett.*, 1999, **1**, 2049-2051.
92. M. O. Sinnokrot and C. D. Sherrill, *The Journal of Physical Chemistry A*, 2006, **110**, 10656-10668.
93. C. A. Hunter and J. K. M. Sanders, *J. Am. Chem. Soc.*, 1990, **112**, 5525-5534.
94. S. Tsuzuki, T. Uchimaru and M. Mikami, *The Journal of Physical Chemistry A*, 2006, **110**, 2027-2033.
95. R. W. Alder, P. S. Bowman, W. R. S. Steele and D. R. Winterman, *Chemical Communications (London)*, 1968, 723-724.
96. O. Kazheva, G. Shilov, O. Dyachenko, M. Mekh, V. Sorokin, V. Ozeryanskii and A. Pozharskii, *Russ. Chem. Bull.*, 2005, **54**, 2492-2495.
97. A. F. Pozharskii, *Russian Chemical Reviews*, 1998, **67**, 1.
98. L. Sobczyk, *J. Mol. Struct.*, 2010, **972**, 59-63.
99. Z. Glasovac, M. Eckert-Maksic and Z. B. Maksic, *New J. Chem.*, 2009, **33**, 588-597.

100. V. Raab, E. Gauchenova, A. Merkoulov, K. Harms, J. Sundermeyer, B. Kovačević and Z. B. Maksić, *J. Am. Chem. Soc.*, 2005, **127**, 15738-15743.
101. A. F. Pozharskii, M. A. Povalyakhina, A. V. Degtyarev, O. V. Ryabtsova, V. A. Ozeryanskii, O. V. Dyablo, A. V. Tkachuk, O. N. Kazheva, A. N. Chekhlov and O. A. Dyachenko, *Organic & Biomolecular Chemistry*, 2011, **9**, 1887-1900.
102. G. Paolucci, P. A. Vigato, G. Rossetto, U. Casellato and M. Vidali, *Inorg. Chim. Acta*, 1982, **65**, L71-L73.
103. K. Nagasawa, *Related Organocatalysts (1): A Proton Sponge*, John Wiley & Sons, Ltd, 2009.
104. J. W. Gilman and Y. A. Otonari, *Synthetic Communications: An International Journal for Rapid Communication of Synthetic Organic Chemistry*, 1993, **23**, 335 - 341.
105. P. R. Mallinson, G. T. Smith, C. C. Wilson, E. Grech and K. Wozniak, *J. Am. Chem. Soc.*, 2003, **125**, 4259-4270.
106. T. Glowiak, E. Grech, Z. Malarski, J. Nowicka-Scheibe and L. Sobczyk, *J. Mol. Struct.*, 1996, **381**, 169-175.
107. R. Coult, M. A. Fox, W. R. Gill, K. Wade and W. Clegg, *Polyhedron*, 1992, **11**, 2717-2721.
108. V. A. Ozeryanskii, A. F. Pozharskii, A. J. Bieńko, W. Sawka-Dobrowolska and L. Sobczyk, *The Journal of Physical Chemistry A*, 2005, **109**, 1637-1642.
109. T. Glowiak, Z. Malarski, L. Sobczyk and E. Grech, *J. Mol. Struct.*, 1992, **270**, 441-447.
110. K. Wozniak, C. C. Wilson, K. S. Knight, W. Jones and E. Grech, *Acta Crystallographica Section B*, 1996, **52**, 691-696.
111. P. R. Mallinson, K. Woźniak, C. C. Wilson, K. L. McCormack and D. S. Yufit, *J. Am. Chem. Soc.*, 1999, **121**, 4640-4646.
112. A. A. Hoser, Ł. Dobrzycki, M. J. Gutmann and K. Woźniak, *Crystal Growth & Design*, 2010, **10**, 5092-5104.
113. A. V. Degtyarev, O. V. Ryabtsova, A. F. Pozharskii, V. A. Ozeryanskii, Z. A. Starikova, L. Sobczyk and A. Filarowski, *Tetrahedron*, 2008, **64**, 6209-6214.
114. Y. Horbatenko and S. F. Vyboishchikov, *ChemPhysChem*, 2011, **12**, 1118-1129.
115. CSD search carried out using release V5.32, November 2010 on the structure of the benzoic acid, excluding structures from powder diffraction data.
116. L. Leiserowitz, *Acta Crystallographica Section B*, 1976, **32**, 775-802.
117. D. Das and G. R. Desiraju, *Chemistry – An Asian Journal*, 2006, **1**, 231-244.

118. T. Beyer and S. L. Price, *The Journal of Physical Chemistry B*, 2000, **104**, 2647-2655.
119. T. Steiner, *Acta Crystallographica Section B*, 2001, **57**, 103-106.
120. CSD search carried out using release V5.32, November 2010.
121. P. Rodríguez-Cuamatzi, O. I. Arillo-Flores, M. I. Bernal-Uruchurtu and H. Höpfl, *Supramol. Chem.*, 2007, **19**, 559 - 578.
122. N. Kobayashi, T. Naito and T. Inabe, *Bull. Chem. Soc. Jpn.*, 2003, **76**, 1351-1362.
123. H. Minemawari, T. Naito and T. Inabe, *Bull. Chem. Soc. Jpn.*, 2010, **83**, 505-513.
124. C. C. Wilson, *Single Crystal Neutron Diffraction from Molecular Materials*, World Scientific Publishing Co. Pte. Ltd. , London, 2001.
125. R. M. Glaeser, *Journal of Structural Biology*, 1999, **128**, 3-14.
126. IUCr, Crystallography, Kluwer Academic Publisher, Dodrecht, 1993, vol. A, p. 45.
127. X-ray structure analysis notes, Trevelyan College, University of Durham, 2009, pp. 5-2.
128. H. L. M. C. Giacovazzo, G. Artioli, D. Viterbo, G. Ferraris, G. Gilli, G. Zanotti, M. Catti, *Fundamentals of Crystallography*, 2002.
129. C. C. Wilson and L. H. Thomas, *Comptes Rendus Chimie*, **8**, 1434-1443.
130. C. C. Wilson, L. H. Thomas and C. A. Morrison, *Chem. Phys. Lett.*, 2003, **381**, 102-108.
131. D. A. Keen, M. J. Gutmann and C. C. Wilson, *J. Appl. Crystallogr.*, 2006, **39**, 714-722.
132. T. A. A. - TA Instrument, http://www.tainstruments.com/.
133. N. Kappa-CCD Four circle diffractometer. Nonius BV, Delft, The Netherlands. http://www.nonius.nl/products/sms/kappa/.
134. S. Mackay, Dong, W. , Edwards, C. , Henderson, A. Gilmore, C.J. Stewart, N. Shankland, K. Donald, A. Bruker-Nonius and University of Glasgow, 2003.
135. S. Area-Detector Absorption Correction. (1996) Siemens Industrial Automation, Inc.: Madison, WI.
136. Z. Otwinowski, M. Winor, *Methods Enzymol.*, 1997, 307-326.
137. A. B. A. 2007., Editon edn.
138. A. s. f. c. s. http://www.bruker-axs.com/software_apex2.html.
139. R. C. CrystalClear Version 1.4.0: An Integrated Program for the Collection and Processing of Area Detector Data, © 1997-2011.
140. L. Farrugia, *J. Appl. Crystallogr.*, 1999, **32**, 837-838.

141. S. [Includes SHELXS97, SHELXL97] - Sheldrick, G. M. (1997). SHELX97. Programs for Crystal Structure Analysis (Release 97-2). University of Göttingen, Germany. .
142. G. Sheldrick, *Acta Crystallographica Section A*, 2008, **64**, 112-122.
143. A. Altomare, G. Cascarano, C. Giacovazzo and A. Guagliardi, *J. Appl. Crystallogr.*, 1993, **26**, 343-350.
144. C. F. Macrae, P. R. Edgington, P. McCabe, E. Pidcock, G. P. Shields, R. Taylor, M. Towler and J. van de Streek, *J. Appl. Crystallogr.*, 2006, **39**, 453-457.
145. L. Farrugia, *J. Appl. Crystallogr.*, 1997, **30**, 565.
146. J. Rohlicek and M. Husak, *J. Appl. Crystallogr.*, 2007, **40**, 600-601.
147. F. H. Allen, O. Johnson, G. P. Shields, B. R. Smith and M. Towler, *J. Appl. Crystallogr.*, 2004, **37**, 335-338.
148. M. J. O'Neill, *Anal. Chem.*, 1964, **36**, 1238-1245.
149. T. I. http://www.tainstruments.com.
150. http://www.isis.stfc.ac.uk/.
151. C. Wilson, *J. Appl. Crystallogr.*, 1997, **30**, 184-189.
152. http://www.ill.eu/.
153. H. Einspahr, J.-B. Robert, R. E. Marsh and J. D. Roberts, *Acta Crystallographica Section B*, 1973, **29**, 1611-1617.
154. P. Hodgson, G. C. Lloyd-Jones, M. Murray, T. M. Peakman and R. L. Woodward, *Chemistry – A European Journal*, 2000, **6**, 4451-4460.
155. G. S. Nichol and W. Clegg, *Crystal Growth & Design*, 2005, **6**, 451-460.
156. M. O. Sinnokrot, E. F. Valeev and C. D. Sherrill, *J. Am. Chem. Soc.*, 2002, **124**, 10887-10893.
157. J. Krausse and H. Dunken, *Acta Crystallographica*, 1966, **20**, 67-73.
158. G. Ferguson and G. A. Sim, *Acta Crystallographica*, 1961, **14**, 1262-1270.
159. T. Liwporncharoenvong and R. L. Luck, *Inorg. Chim. Acta*, 2002, **340**, 147-154.
160. G. Ferguson and G. A. Sim, *Acta Crystallographica*, 1962, **15**, 346-350.
161. CSD search carried out using release V5.32, November 2010 on the structure of 1,8-Bis(dimethylamino)naphthalene, excluding structures from powder diffraction experiments CSD.
162. N. Okabe and H. Kyoyama, *Acta Crystallographica Section E*, 2001, **57**, o1224-o1226.
163. S. Ebenezer, P. T. Muthiah and R. J. Butcher, *Crystal Growth & Design*, 2011, **11**, 3579-3592.

164. A. Altomare, G. Cascarano, C. Giacovazzo, A. Guagliardi, M. C. Burla, G. Polidori and M. Camalli, *J. Appl. Crystallogr.*, 1994, **27**, 435-436.

165. J. L. Derissen and P. H. Smith, *Acta Crystallographica Section B*, 1974, **30**, 2240-2242.

166. F. R. Ahmed and D. W. J. Cruickshank, *Acta Crystallographica*, 1953, **6**, 385-392.

167. M. Wenger and J. Bernstein, *Molecular Pharmaceutics*, 2007, **4**, 355-359.

168. D. Braga, M. Eckert, M. Fraccastoro, L. Maini, F. Grepioni, A. Caneschi and R. Sessoli, *New J. Chem.*, 2002, **26**, 1280-1286.

169. N. G. Fernandes and R. Tellgren, *Acta Crystallographica Section C*, 1989, **45**, 499-504.

170. B. Koleva, R. W. Seidel, T. Kolev, S. Zareva, H. Mayer-Figge, I. M. Oppel and W. S. Sheldrick, *J. Mol. Struct.*, 2009, **921**, 163-171.

171. S. Athimoolam and S. Natarajan, *Acta Crystallographica Section C*, 2007, **63**, o263-o266.

172. J. A. Kanters, A. Schouten, A. J. M. Duisenberg, T. Glowiak, Z. Malarski, L. Sobczyk and E. Grech, *Acta Crystallographica Section C*, 1991, **47**, 2148-2151.

173. L. H. Thomas, N. Blagden, M. J. Gutmann, A. A. Kallay, A. Parkin, C. C. Seaton and C. C. Wilson, *Crystal Growth & Design*, 2010, **10**, 2770-2774.

174. C. B. Aakeroy, J. Desper and B. Levin, *Acta Crystallographica Section C*, 2005, **61**, o702-o704.

175. C. B. Aakeroy, J. Desper and J. F. Urbina, *Chem. Commun.*, 2005, 2820-2822.

176. T. Friščić, A. V. Trask, W. Jones and W. D. S. Motherwell, *Angew. Chem. Int. Ed.*, 2006, **45**, 7546-7550.

177. B. R. Bhogala, S. Basavoju and A. Nangia, *CrystEngComm*, 2005, **7**, 551-562.

178. C. B. Aakeroy and D. J. Salmon, *CrystEngComm*, 2005, **7**, 439-448.

179. C. C. Wilson, *Crystallography Reviews*, 2007, **13**, 143-198.

180. R. Leyva-Ramos, A. Jacobo-Azuara, P. E. Diaz-Flores, R. M. Guerrero-Coronado, J. Mendoza-Barron and M. S. Berber-Mendoza, *Colloids and Surfaces A: Physicochemical and Engineering Aspects*, 2008, **330**, 35-41.

181. P. Baltrënas and E. Brannvall, *Journal of Environmental Engineering and Landscape Management*, 2006, **14**, 31-36.

182. N. Widiastuti, H. Wu, M. Ang and D.-k. Zhang, *Desalination*, 2008, **218**, 271-280.

183. T. Motsi, N. A. Rowson and M. J. H. Simmons, *Int. J. Miner. Process.*, 2009, **92**, 42-48.

184. L. Y. Li, K. Tazaki, R. Lai, K. Shiraki, R. Asada, H. Watanabe and M. Chen, *Applied Clay Science*, 2008, **39**, 1-9.
185. W. Xu, L. Y. Li and J. R. Grace, *Applied Clay Science*, 2010, **50**, 158-163.
186. H. Li, W.-y. Shi, H.-b. Shao and M.-a. Shao, *J. Hazard. Mater.*, 2009, **169**, 1106-1111.
187. Z. Ya-ping, G. A. O. Ting-yao, J. Shang-ying and C. A. O. Da-wen, *Journal of Environmental Sciences*, 2004, **16**, 1001-1004.
188. M. J. Harbottle, M. D. Mantle, M. L. Johns, R. van Herwijnen, A. Al-Tabbaa, T. R. Hutchings, A. J. Moffat and S. K. Ouki, *Environmental Science & Technology*, 2007, **41**, 3444-3448.
189. P. J. Leggo, B. Ledésert and G. Christie, *Sci. Total Environ.*, 2006, **363**, 1-10.
190. S. Kitagawa, R. Kitaura and S.-i. Noro, *Angew. Chem. Int. Ed.*, 2004, **43**, 2334-2375.
191. J. L. C. Rowsell and O. M. Yaghi, *Microporous Mesoporous Mater.*, 2004, **73**, 3-14.
192. M. O'Keeffe, *Chem. Soc. Rev.*, 2009, **38**, 1215-1217.
193. O. M. Y. a. Q. Li., *MRS Bull.*, 2009, **34**, 682-690.
194. Z. Wang and S. M. Cohen, *J. Am. Chem. Soc.*, 2009, **131**, 16675-16677.
195. K. Hirai, S. Furukawa, M. Kondo, H. Uehara, O. Sakata and S. Kitagawa, *Angew. Chem. Int. Ed.*, 2011, **50**, 8057-8061.
196. A. R. Millward and O. M. Yaghi, *J. Am. Chem. Soc.*, 2005, **127**, 17998-17999.
197. J. R. Holst, A. Trewin and A. I. Cooper, *Nat Chem*, 2010, **2**, 915-920.
198. A. J. Cruz-Cabeza, G. M. Day and W. Jones, *Chemistry – A European Journal*, 2009, **15**, 13033-13040.
199. D. D. MacNicol, J. J. McKendrick and D. R. Wilson, *Chem. Soc. Rev.*, 1978, **7**, 65-87.
200. W. Baker, A. J. Floyd, J. F. W. McOmie, G. Pope, A. S. Weaving and J. H. Wild, *Journal of the Chemical Society (Resumed)*, 1956, 2010-2017.
201. R. Small, *Acta Crystallographica Section B*, 2003, **59**, 141-148.
202. G. O. Lloyd, M. W. Bredenkamp and L. J. Barbour, *Chem. Commun.*, 2005, 4053-4055.
203. J. J. Lee, R. O. Fuller, A. N. Sobolev, H. F. Clausen, J. Overgaard, G. A. Koutsantonis, B. B. Iversen and M. A. Spackman, *Chem. Commun.*, 2011, **47**, 2029-2031.

204. D. D. MacNicol, *Journal of the Chemical Society D: Chemical Communications*, 1969, 836-836.

205. D. D. Macnicol and F. B. Wilson, *Journal of the Chemical Society D-Chemical Communications*, 1971, 786-&.

206. D. D. MacNicol, *J. Chem. Soc., Chem. Commun.*, 1973, 621-622.

207. J. G. Selbo, J. M. Desper and C. J. Eckhardt, *Journal of Inclusion Phenomena and Macrocyclic Chemistry*, 2003, **45**, 73-78.

208. T. Jacobs, G. O. Lloyd, M. W. Bredenkamp and L. J. Barbour, *CrystEngComm*, 2009, **11**, 1545-1548.

209. F. Imashiro, *J. Am. Chem. Soc.*, 1993, **115**, 2231-2235.

210. D. E. Palin and H. M. Powell, *Journal of the Chemical Society (Resumed)*, 1947, 208-221.

211. J. L. Daschbach, T.-M. Chang, L. R. Corrales, L. X. Dang and P. McGrail, *The Journal of Physical Chemistry B*, 2006, **110**, 17291-17295.

212. J. Kundin, C. Yurudu, J. Ulrich and H. Emmerich, *Eur. Phys. J. B*, 2009, **70**, 403-412.

213. Y.-J. Lee, K. W. Han, J. S. Jang, T.-I. Jeon, J. Park, T. Kawamura, Y. Yamamoto, T. Sugahara, T. Vogt, J.-W. Lee, Y. Lee and J.-H. Yoon, *ChemPhysChem*, 2011, **12**, 1056-1059.

214. T. C. W. Mak, J. S. Tse, C.-S. Tse, K.-S. Lee and Y.-H. Chong, *J. Chem. Soc., Perkin Trans. 2*, 1976, 1169-1172.

215. T. Birchall, C. S. Frampton, G. J. Schrobilgen and J. Valsdottir, *Acta Crystallographica Section C*, 1989, **45**, 944-946.

216. K. Maartmann-Moe, *Acta Crystallographica*, 1966, **21**, 979-982.

217. A. Spek, *J. Appl. Crystallogr.*, 2003, **36**, 7-13.